THE CRYSTALLISATION OF CITRIC ACID AND METAL CITRATE DURING BLEACHING AND DRYING, AND THEIR IMPACT ON FILTRATION

Lappeenranta–Lahti University of Technology LUT

Master's Programme in Biorefinery Programme

2023

Mirka Notkonen

Examiners: Professor Tuomas Koiranen

Teemu Kinnarinen, D.Sc

Advisors: Ronny Walhström, D.Sc

Tuomas Kulomaa, M.Sc

ABSTRACT

Lappeenranta–Lahti University of Technology LUT

LUT School of Engineering Science

Chemical engineering

Mirka Notkonen

The crystallisation of citric acid and metal citrate during bleaching and drying, and their impact on filtration

Master's thesis

2023

162 pages, 107 figures, 16 tables and 7 appendices

Examiners: Professor Tuomas Koiranen & Teemu Kinnarinen, D.Sc

Keywords: Pretreatment process, bleaching, filtration, citric acid, metal citrates, oil purification, Pixact measurement, dynamic image analysis.

Bio-oils require multiple purification steps before they can be used for the biofuel production or for other suitable purposes. The feedstock often contains several types of impurities, e.g. trace metals, pigments, and phospholipids. The pretreatment process for removal of the impurities consists of several individual process steps, from which the main ones are presented in this thesis.

The aim of this study was to focus on the behaviour of citric acid used in the bleaching process, and how it affects trace metals in the solution during the pretreatment including bleaching, drying and filtration. It has been noticed earlier that citric acid crystallizes in the bio-oils during the pretreatment process, but the effect of these particles has still remained unclear.

In this work, crystallisation of citric acid in purified and bleached palm oil was studied with different process conditions and during different process steps, and the samples were monitored via Pixact dynamic image analysis. To investigate the effect of trace metals more deeply, metal components were added to the solution as salts and their impact on the filtration was studied. Finally, the experiments included the use of two technical feedstock for confirming the behaviour of citric acid and metal salts in the pretreatment process.

TIIVISTELMÄ

Lappeenrannan–Lahden teknillinen yliopisto LUT

LUTin insinööritieteiden tiedekunta

Kemiantekniikka

Mirka Notkonen

Sitruunahapon ja metallisitraattien kiteytyminen valkaisun ja kuivauksen yhteydessä, ja niiden vaikutus suodatukseen

Kemiantekniikan diplomityö

2023

162 sivua, 107 kuvaa, 6 taulukkoa ja 7 liitettä

Tarkastajat: Professori Tuomas Koiranen ja tekniikan tohtori Teemu Kinnarinen

Avainsanat: Esikäsittelyprosessi, valkaisu, suodatus, sitruunahappo, metallisitraatti, öljyn puhdistus, Pixact-mittaus, dynaaminen kuva-analyysi.

Biopohjaiset öljyt vaativat useita puhdistusvaiheita ennen kuin niitä on mahdollista käyttää polttoaineiden valmistukseen tai muihin tarkoituksiin. Biopohjaiset syöttöaineet sisältävät usein erilaisia epäpuhtauksia, kuten metalleja, pigmenttejä ja fosfolipidejä. Esikäsittelyprosessiin kuuluu useita eri vaiheita, joista päävaiheet on esitelty tässä diplomityössä.

Työn tarkoitus oli keskittyä tutkimaan sitruunahapon käyttäytymistä valkaisuprosessissa, ja sitä miten se vaikuttaa öljyssä oleviin metallikomponentteihin esikäsittelyn aikana (valkaisu, kuivaus ja suodatus). Aikaisemmin on huomattu, että sitruunahappo kristallisoituu esikäsittelyn aikana, mutta syntyneiden partikkeleiden vaikutus prosessiin on tuntematon.

Sitruunahapon kristallisoitumista puhdistetussa ja valkaistussa palmuöljyssä tutkittiin tässä diplomityössä erilaisissa prosessiolosuhteissa ja prosessivaiheissa. Kristallisoitumisen seuraamisessa käytettiin Pixact-laitteistoa, joka perustuu dynaamiseen kuva-analyysiin. Metallien käyttäytymistä tutkittiin lisäämällä biopohjaiseen öljyyn metallisuoloja, ja seuraamalla niiden vaikutusta valkaisuun ja suodatukseen. Työn lopuksi myös kahta teknistä syötettä testattiin vahvistamaan hypoteesia partikkelien vaikutuksista.

ACKNOWLEDGEMENTS

I want to thank my advisors Ronny Wahlström and Tuomas Kulomaa for all their help, time and shared knowledge in this thesis, and Joanna Johnsson for reading and commenting despite her own work. Without your effort the content of this thesis would be much poorer. Thank you, Ronny, for all the excellent comments in the literature part, and to the results despite your own work. I want to thank Tuomas, who put his vacation aside for a couple of days to comment the results, so I could keep up with my schedule, helped with Pixact measurement results anytime I needed. I also want to thank my examiners Tuomas Koiranen and Teemu Kinnarinen at LUT University, who helped me a lot with the thesis, especially with particles and crystallisation.

Big thanks to the pretreatment lab staff, who guided me with the equipment and practicalities of the lab and helped me anytime any assistance was needed. The work would not have been that fun without you enlightening the lab.

Another big thanks to my teams in the piloting and refining research and separation and fractionation, who took excellent care of my tasks while I was busy with my thesis. Could not thank you more.

Finally, I want to thank my family and friends, who supported me during my study years and thesis process and tolerated my lack of time to spare on other things.

In Tuusula 28.10.2023

Mirka Notkonen

SYMBOLS AND ABBREVIATIONS

Roman characters

A	area of the filter	[m^2]
A_p	external surface area of the particle	[m^2]
c	filtration concentration	[kg d.s./m^3]
d	particle diameter	[m]
d_s	diameter of a sphere having the same surface area	[ ]
d_v	diameter of a sphere having the same volume	[ ]
k	the permeability of filter	[m^2]
m_c	mass of cake	[kg]
$\bar{m}$	cake mass ratio	[ ]
n	compressibility coefficient	[ ]
L	thickness of the filter media	[m]
p	pressure	[bar, Pa]
P	permeability of the filter cake	[m^2]
Q	filtrate flow rate	[m/s]
R_m	filter medium resistance	[1/m]
R_c	cake resistance	[kg/m^2]
T	temperature	[ºC, K]
V	volume	[m^3]
V_p	external volume of the particle	[ ]

Greek characters

α	specific resistance	[m/kg]
α_0	specific cake resistance reference at 1 bar	[m/kg]
$\bar{\varepsilon}$	average cake porosity	[ ]
ε	porosity of the cake	[ ]
ρ	density of the filtrate	[kg/m^3]
ρ_p	density of the particle	[kg/m^3]
ρ_s	density of the solids	[kg/m^3]
Δp	pressure difference	[bar, Pa]
Δp_c	pressure difference in the cake	[bar, Pa]
Δp_0	local scaling pressure	[bar, Pa]
Δt	time change	[s]
ΔV	change of the filtrate volume	[m^3]
μ	viscosity	[Pa*s]

Abbreviations

AF	Animal fat
BG	Brown grease
CA	Citric acid
Ca-stearate	Calcium stearate
CCD	Charge-coupled device
FAME	Fatty acid methyl ester
FFA	Free fatty acid
HSM	High-shear mixer
HVO	Hydrogenated vegetable oil

MSS	Municipal sewage sludge
Na-oleate	Sodium oleate
Na-stearate	Sodium stearate
PSD	Particle size distribution
RBDPO	Refined, bleached and deodorized palm oil
RO	Reverse osmosis
SEM	Scanning electron microscope
TAG	Triacylglyceride
UCO	Used cooking oil
WCO	Waste cooking oil
XRDP	X-ray diffraction pattern

Table of contents

Appendices

1 Introduction

Sustainable thinking has led to the path where waste valorisation has become an attractive research area. Organic waste (agricultural, industrial, food, etc.) is generated every day in extensive quantities creating a significant problem. From an environmental point of view, old-fashioned ways using waste as landfill or composting are not satisfactory ways anymore to dispose organic waste or biomass. Additionally, the disposal methods might create toxic emissions and other harms to the environment and living things. (Arancon et al, 2013)

Demand for renewable fuels and chemicals, tightening organic waste regulations, and the sustainable way to use land and crops are pushing manufacturers and industry toward higher sustainability in the production level but also in feedstock selection. Biobased diesel has been produced earlier from the edible oil sources, for example rape seed, which then created an ethical problem for land use and food production, while a part of the world's population is famishing. (Adewale et al, 2015; Gupta, 2017)

Fuel production from biobased feedstock considered as waste gear toward a more benign and sustainable fuel, as decreasing sources of fossil-based fuels is clearly visible. Fossil-based fuels have caused environmental concerns all around the world due to greenhouse gas emissions (Arancon et al, 2013). The renewable energy directive (RED II) of EU (European Union) is forcing corporations to move toward renewable and sustainable products and production to reduce GHG (Green House Gas) emissions. Transportation is one of the biggest emission sources, and reducing those has a profound impact on the atmosphere. Biobased fuel production plays quite a remarkable role in that, and the market is researching to find not only sustainable technology but a sustainable feedstock pool as well (Chiaramonti et Goumas, 2019). Using waste biomass maximizes the use of resources and minimizes waste generation while decreasing the competition with food production or land use. (Morales et al, 2011)

Raw material prices are driven up by the interest rate shown by different companies competing for waste fats and oils. To maintain an adequate feedstock pool, searching for affordable raw material is necessary, leading to lower quality waste and residue streams, i.e., used cooking oil and palm mill effluent sludge. Lower quality feedstock requires significantly more purification before refining to high-value end-products, due to the

contaminants (soluble and solid impurities) (Chiaramonti et Goumas, 2019). Alongside the waste oils obtained from vegetable origin, waste animal fats have gained attention as a feedstock. Non-edible animal fats, known as waste animal fats, are by-products from the food industry. Some of the lower-grade waste streams can be obtained from expired food products, catering waste, and dead livestock. (Morales et al, 2011; Adewale et al, 2015; Bondioli et al., 2019)

Oils and fats from waste streams contain different impurities, like phospholipids, pigment and a certain amount of trace metals that might cause harm to the oil stability. Trace metals can catalyse autoxidation, which is a radical reaction where the alkyl group is attacked, followed by a chain reaction, and leading to the formation of a hydroperoxide group (-OOH) into the molecule. The hydroperoxide group continues the reaction by forming aldehydes, ketones, and free fatty acids. The reaction is promoted by light and heat, along with the trace metal catalyst, and might occur fast, decreasing the stable storage time. Polyunsaturated oils are principally sensitive to the reaction described. Naturally occurring antioxidants and chelate-building additives, such as citric acid, can secure metal impurities and help to avoid oxidation. Bleaching is usually used as a removal process for trace metals, with the help of acid. (Bockisch, 1998; Gupta, 2017)

Purification process consists of several individual parts targeting the removal of different impurities. Colour components, FFA (Free Fatty Acids), phospholipids, metals and other minor impurities can be removed through chemical purification, which includes degumming, neutralizing, washing, bleaching, hydrogenation, and deodorization. (Jayasinghe, P. et Hawboldt, K., 2012; Gharby, 2022)

The target of the degumming process is to remove phospholipids, often referred to as gums, from the feedstock. Phospholipids are naturally present in the oil, but cause problems later in the process and give unsatisfactory performance of the oil in many applications (Chen et al, 2014). Citric acid is suitable for the process, due to its ability to decompose the phospholipid molecules and its ability to act as a chelating agent to maintain the metal components in a water-soluble mode (Zufarov et al, 2009). Bleaching is classified as a physical process, where the metal impurities present in the oil are eliminated with the help of an adsorbent (List, 2009; Gupta, 2017). The porous structure of bleaching earth retains the impurities from the oil. Bleaching reduces the colour bodies, and the amount of trace metals present in the bio-oil. A certain amount of acid (citric acid, or phosphoric acid) can

be added to the bleaching process to improve the removal of trace metals (Gupta, 2017; Gharby, 2022).

After bleaching, the solids are separated from the suspension by filtration. In general, filtration is a physical process, where solids are removed from the liquids by passing a suspension through a permeable media. After the bleaching adsorbent is added to the liquid, it adsorbs the impurities, and is then retained by the filter media (Gupta, 2017). The surface of the filter will retain the particles that are larger than its pores and ideally allow only the liquid to pass through the filter. The formed cake is normally highly effective at capturing solids and starts acting like a filter in the initial stages of formation (Svarovsky, 2000; Sparks et Chase, 2016). The success of the filtration is affected by particle size distribution, fluid and media properties, and the state of the system, i.e., porosity and the solids concentration (Gupta, 2017). The filtration process is highly affected by the particles present in the bio-oil, so the quality and quantity of the particles are keen parameters as a research point of view to improve filterability of the bio-oil. For example, particles presenting needle-like characteristics often present a much higher compressibility compared to spherical particles, and therefore can affect the mean pore size of the cake. (Bouncier et al, 2016)

As mentioned above, different trace metals such as calcium, magnesium, sodium, and potassium are present in the feedstock. In several cases, the metals are in the form of fatty acid soaps and need to be separated to free fatty acids and metal ions, carried out with the help of phosphoric acid or citric acid in an aqueous liquor. Citric acid is preferred in acid addition due to its useful property to also act as a sequestrant, allowing the metal ions to transfer to the water phase in the solution (Bondioli et al, 2019). However, the effect of citric acid precipitates on filtration has not been studied. A master's thesis done by Ida Laaksonen (2022) recently showed that the concentration of citric acid had a remarkable effect on the formation of precipitates, also affecting the particle properties in the bio-oil. Citric acid seems to form metal citrates with the trace metals present in the bio-oil, and the particle size was seen to vary according to the concentration of citric acid in the solution.

The aim is to continue this work, to study further how the precipitated particles affect the filtration process and what is the connection between the citric acid addition and particle formation.

The thesis is focusing on following research questions:

How does citric acid affect metal citrate formation?

What is the effect of citric acid concentration change?

How do metal citrates affect filtration with different citric acid dosages?

Do different bleaching procedures affect the formation of metal citrates?

- How does the mixing (high-shear mixer + citric acid) affect metal citrate formation?
- How does the drying procedure affect metal citrate formation?

2 Oils and fats feedstock and chemicals

To meet the target for reducing greenhouse gas emissions and improve the use of renewable fuels, the interest in biofuels and their production is growing fast. So-called first-generation biofuels are obtained for example from palm oil, canola and soya oil, which has created a new problem: The source of renewable fuel competes with food production and land use. To tackle this problem, waste and residue recycling has taken over and low-quality waste streams are becoming more and more interesting. (Morales. et al 2011; Jayasinghe et Hawboldt, 2012)

Waste fats and oils contain mostly triglycerides (Figure 1), also known as TAGs (triacylglycerols) or triglycerides, free fatty acids (FFA), and impurities like metals, and phospholipids. The fatty acids connected to the glycerol molecules define the most of the properties of the triglycerides via their moieties. The fatty acids form ester bonds with the glycerol molecule. Fatty acid moieties differ depending on carbon chain length and on the type (cis or trans), position, and number of double bonds. The carbon chain can contain 4-24 carbon atoms and zero, one or more double bonds (Hirata, G., et al, 2013). Triglyceride is formed from one glycerol unit and three fatty acid units, forming water as a side product in the reaction. The compounds can be divided into monoglycerides, diglycerides and triglycerides based on the number of FFA units in the molecule. When speaking of oils and fats, triglyceride molecules are called “oil” if it is liquid at room temperature (approx. 20 °C), and “fat” if it is solid at room temperature. (Gupta, 2017)

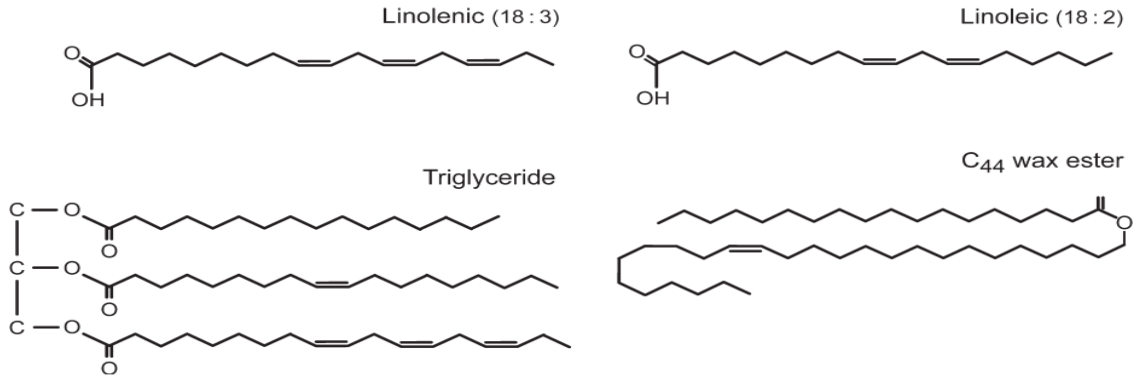

Figure 1 Structures of common FFAs Linolenic and Linoleic on the top, and at the bottom, structures of triglyceride and was ester (Vanhercke et al, 2013)

Different type of waxes may also be present in the oil feedstock. Waxes have typically a carbon chain length of 40 to 60 carbon atoms and have a structure of a fatty acid esterified to an alcohol. The properties of waxes depend heavily on the structure and may cause problems to the product quality (high pour point for example). From a process point of view, the removal of waxes from the feedstock is not often necessary. Waxes (also called wax esters, Figure 1) present in the vegetable oil acted as a component in a plant's surface lipid layer. Some of the waxes can be used as bio-based lubricants, as they have excellent resistance to hydrolysis and good oxidative stability. (Vanhercke et al, 2013; Lusas et al, 2017)

2.1 Chemical composition of fatty acids and triglycerides

Oils and fats are known as lipids. Crude oils and fats contain mainly triglycerides, small amounts of free fatty acids and some other compounds, like trace metals. (Jayasinghe et Hawboldt, 2012; Hirata et al, 2013)

Triglycerides are esters of three fatty acids with the trihydric alcohol glycerol. The main qualities presented shortly: fats and oils have a low vapour pressure, and their boiling point is high. Density is normally around 900-950 kg/m^3, and the solubility is good in nonpolar solvents. (Bockisch, 1998)

Mono- and diglycerides present in the fat or oil are a result from partially hydrolyzation of triglyceride. (List, 2009) In monoglycerides, only one OH group in the molecule is esterified with a fatty acid, and therefore diglycerides include two fatty acids. Monoglycerides are common emulsifiers in the food industry and have a stronger lipophilic nature due to their molecular structure: the hydroxyl micelle head components are relatively small and non-ionic. Monoglycerides present naturally in the oil at very low levels (<2 %) but can be manufactured via enzymatic hydrolysis of triglycerides (Msagati, 2012). Due to the presence of the hydrophilic group in the structure, diglycerides can also be used as an emulsifier or surfactant, and have lately been studied as a fat substituent, as they seem to have a beneficial impact on the suppression of the body fat accumulation. Diglycerides are naturally present in oil at a maximum level of 10 %. (Phuah et al, 2015)

2.1.1 Triglycerides

Triacylglycerols (TAGs), also known as triglycerides are the most interesting lipid fraction for the biofuel production. A TAG molecule consists of three fatty acids with a glycerol as a skeleton of the molecule, connected by ester bonds, as can be seen from the Figure 2. The structure of the molecule is important due to its effect on the physical properties of TAG. Fatty acid forms a major part of TAG molecules, up to 94-96 w-%, the rest being the glycerol backbone (Jayasinghe et Hawboldt, 2012; Bockisch, 1998; Hirata et al, 2013). The fatty acids existing in a TAG molecule can be the same type, or they can vary, influencing the characteristics of TAG molecule (List, 2009). Even-numbered chain length from 4 to 26 carbon atoms is the most common for TAGs found from animal fat and vegetable oil (Bockisch, 1998).

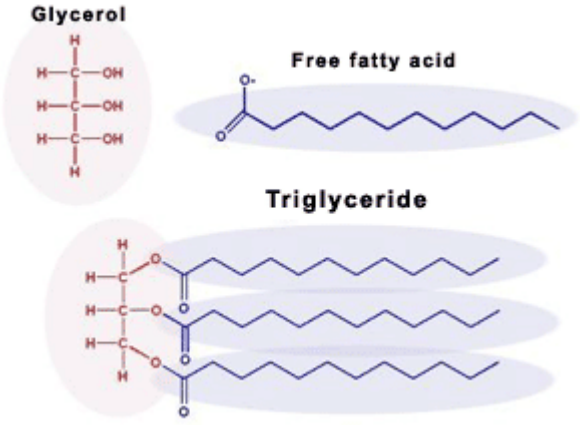

Figure 2 TAG molecule contains glycerol molecule and three free fatty acids. (Clínica Diabetológica)

Lipid feedstock varies the TAG composition. Animal fat is rich in palmitic, stearic and oleic acids, which are the main contributors to the triglyceride composition of lipid feedstock. Fish oil consists of a large number of fatty acids with equal number of carbon atoms, while the amount of double bonds varies in the oil. (Bockisch, 1998; Bondioli et al., 2019)

Vegetable oils can be categorized by their TAG composition:

- Pulp oils (e.g., palm oil)

- Lauric oils (e.g., coconut oil)
- Fats (e.g., shea butter, rich in palmitic and stearic acids)
- Seed oils rich in palmitic acid (e.g., corn oil)
- Seed oil rich in oleic and linoleic acids (e.g., sesame oil and sunflower oil)
- Oils of Fabaceae family (e.g., peanut oil, soybean oil, lentil oil)
- Oils of Brassicaceae family (e.g., rapeseed oil)

Palm oil contains mostly palmitic and oleic acid. Seed oils mostly have a similar type of fatty acid composition, consisting mainly of five fatty acids (myristic, palmitic, stearic, oleic, and linoleic acids). Seeds often contain by-products, which need to be separated from the oils and fats. (Bockisch, 1998)

Oil from fish waste contains TAG with fatty acids with carbon chain varying from 14 to 22 with several double bonds. Other lipids, such as FFA, waxes and alcohols can also be present in the oil. The fish oil usually contains stearic, palmitic, and myristic acids. (Jayasinghe et Hawboldt., 2012; Bockisch, 1998)

2.1.2 Fatty acids

Term fatty acids covers hundreds of identified compounds. Not all of them are found from triglycerides. Fatty acids that appear in natural sources are usually monobasic (one carboxylic acid group presented in the molecule) and unbranched, aliphatic monocarbonic acids are mainly saturated or mono- or biunsaturated. (Bockisch, 1998; Jayasinghe et Hawboldt, 2012)

The structure of fatty acids affects their properties and therefore also the properties of triglyceride molecule. Based on the fatty acid structure (Figure 3), they can be categorised as: (Bockisch, 1998; Jayasinghe et Hawboldt, 2012)

- saturated fatty acids (SFA) (the most common are palmitic and stearic acids)
- monounsaturated fatty acids (MUFA) (the most common is oleic acid)

- polyunsaturated fatty acids (PUFA) (the most important are linoleic and linolenic acids)

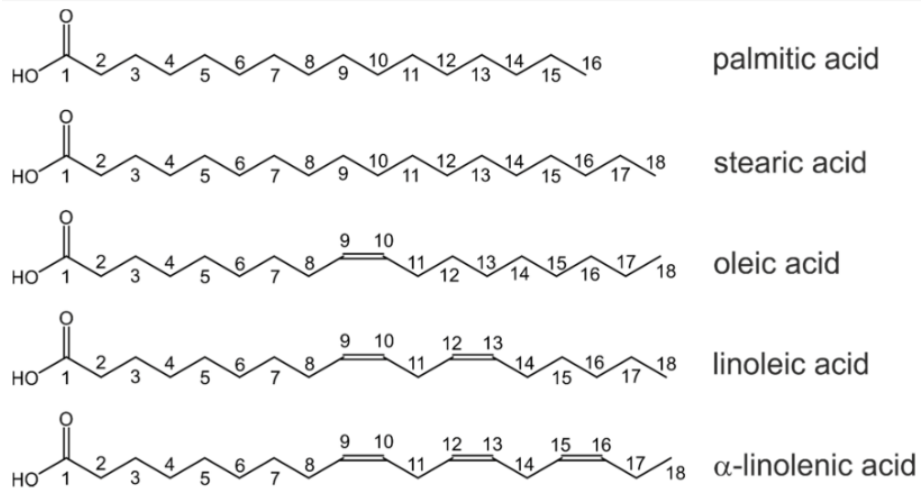

Figure 3 Structures of fatty acids presented in the oils and fats feedstock (Di Pietro et al, 2020)

Only single bonds are present in saturated fatty acids, when in monounsaturated fatty acids one double bond is present, and polyunsaturated fatty acids contain multiple double bonds. (Jayasinghe et Hawboldt, 2012)

From all fatty acids, (poly)unsaturated fatty acids have further potential for isomerization, such as cis and trans-configuration in one molecule, and for isolated or conjugated double bonds. The fuel properties of bio-oil depend on the fatty acid combination, its chain length and degree of unsaturated and saturated bonds. (Bockisch, 1998; Jayasinghe et Hawboldt, 2012)

Oils and fats are soluble in nonpolar solvents, but fatty acids have a high solubility in polar solvents. This creates the possibility to separate them from fats and oils by washing, as the free fatty acids that can be formed in the oil might cause harm later in the process. Free fatty acids (FFA) for example increase the solubility of oxygen into the oil. The solubility of fatty acids and triglycerides increases with temperature and decreases when the chain length is increased. (Bockisch, 1998)

2.2 Production of biodiesel from biobased feedstock

There are two common ways to produce biodiesel from biobased feedstocks. In the FAME process (Fatty Acid Methyl Esters process), the oils and fats feedstock is processed via transesterification, where glyceride reacts with an alcohol in the presence of a catalyst. The formed products in this reaction are fatty acid esters and alcohol. The FAME process is delicate to the amount of FFA due to the soap formation with an alkaline catalyst. Often a preliminary esterification treatment with alcohol and acid is required before the FAME process to reduce the FFA content below 0.5 w%. The transesterification reaction from triglycerides leads to a glycerol rich phase and an ester rich phase (biodiesel), as the reaction is an equilibrium reaction. The reaction conditions and the addition of reagents can affect the product yields. After the transesterification process, the products are separated and cleaned for further use. (Santori et al, 2012; European Biofuels fact sheet; Buchori et al, 2016) The use of FAME diesel is limited, as the common diesel engines can handle the FAME biodiesel only as blended in a fossil-based diesel. Common challenges are poor cold characteristics (affected by the FFA content) and oxygen content of the fuel. (Buchori et al, 2016)

Hydrogenated vegetable oil (HVO) is a biobased diesel product manufactured from triglycerides and fatty acids. After the FAME process, it is the second largest biobased diesel product globally. The production of HVO includes hydrogenation (hydrotreatment) and hydrocracking/isomerization steps in the presence of a catalyst in a high pressure and temperature. The process itself is more expensive compared to the FAME process, but the product obtained is similar compared to fossil diesel and is free from sulphur, oxygen and aromatic hydrocarbons, and has better cold properties. The product qualities are slightly affected by the carbon chain length of the feedstock and process conditions, but there are no exact limitations for the triglyceride and fatty acid feedstock and the process is very flexible. (Shukla et al, 2018; European Biofuels fact sheet)

2.3 Feedstock pool

Traditionally biodiesel has been produced from edible vegetable oils, like rapeseed oil or soybean or canola oil, which leads to food insecurity and ethical issues (Adewale et al, 2015).

There are several waste stream options for bio-oil production, which can then be processed into valuable products, such as fuels and chemicals. Some examples of the possible feedstock are plant matter, agricultural matter, animal waste, municipal waste, and industrial effluent. Bio-oils can be obtained in several processes, possible treating methods for biomass conversion can be thermochemical, biochemical, physical and/or chemical processes, such as hydrolysis, physical/chemical extraction, fermentation, and pyrolysis. (Jayasinghe et Hawboldt, 2012)

Bio-oils obtained from waste biomass or other waste streams have the advantage of recovering high-value by-products, decreasing the volume of waste discharged to landfill and environment (Jayasinghe et Hawboldt, 2012). Animal waste feedstock is one of the waste streams lately gained attraction as an alternative to vegetable oils conventionally used for bio-oil production. Animal fats are low cost due to their classification as feeds, mitigate environmental damage, and have a favourable effect on the biodiesel quality. Animal fat waste is rich in saturated fatty acids, improving the cetane number compared to vegetable oils. A high cetane number is connected to lower NO_x emissions, as it lowers the temperature during the critical part of combustion process in the engines. Saturated fatty acids are also increasing oxidative stability, as they lack double bonds in the chain structure which decrease the amount of oxidative reactions in the oil. Better oxidative stability leads to better storability before processing. (Adewale et al, 2015).

2.3.1 Vegetable oils

Vegetable oils are often categorised into edible and non-edible oil. The vegetable oil categorised as non-edible often contains too high free fatty acid content or has toxic content making it unsuitable for human or animal consumption. (Adewale et al, 2015; Gupta, 2017) From the biodiesel production point of view, non-edible oil is an interesting category.

Majority of the plants used for the oil production contain the oil in their seeds or fruits and are therefore referred as oilseeds or oleaginous fruits. Some of the most common oilseeds are soybean, rapeseed, and sunflower; oleaginous fruits are for example palm and olive. Breeding has improved the quality of the oil obtained from oilseeds. (Bockisch, 1998; Gharby, 2022)

Vegetable oils consist mostly of triglycerides (about 98 g/100 g), the rest of vegetable oil contains other substances in a minority proportion, for example compounds such as diglycerides, vitamins and polyphenols. (Gharby, 2022)

Bio-oils can be derived from those edible and non-edible oilseed crops, as well as from wood or lignocellulosic biomass. The sustainable crop-based or wood-based biomass is obtained as a by-product of forest industry or food production. The upgrading process for waste streams is more difficult and requires more advanced technology. The conversion of wood residues or lignocellulosic matter into bio-oil is quite challenging due to their complex composition. (Jayasinghe et Hawboldt, 2012)

2.3.2 Animal fat

Non-edible animal fats, known as waste animal fats, are mainly by-products from the food industry. Some of the lower grade waste streams can be obtained also from expired food products or from catering waste, as well as from the deceased livestock. (Morales et al, 2011; Adewale et al, 2015; Bondioli et al., 2019)

In 2019, a total annual amount of slaughtered animals sent to rendering units was 12 million tonnes, meaning eight billion animals were slaughtered worldwide for the food industry in a year. The meat consumption of humans is approximately 60 % of the animal weight, where the rest is left behind as by-products and waste. (Bondioli et al., 2019; Müller et al, 2023)

Waste animal fats can be categorised in three different classes:

- Category 1: Material with maximum health risk, usually incinerated.
- Category 2: Material from deceased or diseased stock.
- Category 3: Butchery waste originating from healthy animals slaughtered for human consumption (Morales et al, 2011; Bondioli et al., 2019).

Animal fats, both edible and non-edible can be obtained from several sources:

Rendered fats are obtained from meat production as a by-product, these fats are not produced just for fat. Rendering process includes cooking, the material is either processed as it is (wet processing) or dried at first before cooking (dry processing). When the cooking is finished, bones and other parts are removed. Fat, solid fraction and water phase are separated by

centrifuges and decanters in the wet process, while in the dry process the fat is separated from tissue and other material by water evaporation and pressing of dried feedstock. After the wet process, the crude animal fat is filtered and dried, in the dry process the separation of fat and solids are carried out in a screw press. For energy purposes, the wet process provides better final product quality. (Bockisch, 1998; Adewale et al, 2015; Bondioli et al., 2019)

The amount of fats that can be collected depends on the animal, and the breeding of more low-fat meat has decreased the amount of fat that can be obtained from one animal, although the meat consumption is still increasing. Rendered fats can be categorised by the species it is originally from, as tallow (beef), lard (pork), chicken (poultry) or other animals (Bockisch, 1998; Bondioli et al., 2019)

Fish processing industry creates a notable amount of oil-rich waste, which is suitable for bio-oil production. Although the fish oil as feedstock provides its own challenges: the high levels of proteins, fats, and enzymes present in fish waste can cause enzymatic hydrolysis and microbial degradation, leading to the poor quality of the oil. The moisture content in the fish waste enhances the hydrolysis, as well as enzymes, such as lipases, cause the formation of free fatty acids (FFA). The recovered oil from fish waste may be highly reactive and unstable, due to polyunsaturated fatty acids in the oil, and the stabilisation of the oil is necessary, quite usual methods are chilling or freezing. (Jayasinghe et Hawboldt, 2012; Adewale et al, 2015)

Fish waste for bio-oil production can be collected from the waste effluent, which contains all sorts of fish parts and matter mixed with wastewater. The oil phase can be collected from the wastewater by grinding or homogenising the waste, heating it to 95-100 °C for 20 mins. After that the effluent is run to the screw process for solid removal, and then centrifuged to remove the water from the oil phase. The obtained oil is later polished, collected yield varies between 6 and 11 wt% from the total effluent. (Adewale et al, 2015)

The composition of fatty acids varies according to the source of fat. For example rendered fats contain mostly saturated fatty acids and fish oil polyunsaturated fatty acids. The composition of fatty acids can be affected by the feeding of the animals, but the real benefit is usually insignificant. The quality of the waste animal fat differs remarkably according to

the source, storage conditions and time, the presence of insects or microorganisms etc. (Bockisch, 1998; Bondioli et al., 2019)

2.3.3 Waste lipid oils

This chapter and its subchapters present several possible feedstock options for fuel production that are categorised as waste lipid oils. Some are more commonly used already, as others are possibly used more widely in the future.

Used cooking oil

Used cooking oil or waste cooking oil (UCO or WCO) is considered as economic feedstock for fuel production, as it does not compete with food availability and land usage. Used cooking oil can be either vegetable or animal based oil used for cooking various range of different food products, e.g., fried foods, and can therefore also include grease from the food. UCO can be categorised into yellow grease and brown grease. Yellow grease is obtained from the restaurants or cooking industry, while brown grease, as known as trap grease, is collected from grease traps installed in restaurant, urban or industrial sewage facilities. The brown grease requires a more detailed purification process due to its high water and FFA (>15 %) content, which have a negative effect on biodiesel conversion. The availability of UCO has been increasing while the waste circulation processes have developed. A major part of UCO is still disposed into the environment, causing major problems, and the valorisation of UCO through the production of renewable fuel could increase the recovery rate from the waste cycle. (Morales et al, 2011; Adewale et al, 2015)

Municipal sewage sludge

One possible feedstock has received increasing attention during recent years, due to its massive amount in society and its harmful nature to the environment, if not treated properly. Municipal sewage sludge (MSS) exists all around the world and has gained attention as it contains a remarkably amount of lipids . (Morales et al, 2011)

Roughly 6.2 million dry metric tons of MSS is generated by wastewater treatment plants annually in the US alone (situation in 2010). It can be said that the amount of MSS is abundant worldwide and consist of significant amounts of lipids derived from the source of wastewater (households, industries i.e., food processing, rendering) and from the microbial

activity. Sondhi et Kumar (2020) present that the oil content suitable for diesel production is approximately 30 w%, where in study in China, Liu et al (2021) found that the average lipid concentration of sludge is 10-20 %. Primary sludge from wastewater treatment plant consists mainly of grease and solids from primary clarifier. Secondary sludge contains more cell material from bacteria and other microorganisms. Microorganisms used in the wastewater treatment facilities stay in the produced sludge, and their cell membrane is a major component of MSS, containing mostly lipids, including for example triglycerides, phospholipids and free fatty acids. (Kargbo, 2010; Sondhi et Kumar, 2020)

Disposal of MSS has faced some challenges. MSS has tried to be used for land and agricultural applications, but the heavy metal content, odour and possibility of exposure to pharmaceutical chemicals creates more harm than useful solutions. Incineration of MSS results in harmful emissions containing dioxins and heavy metals. Diesel production from MSS has been studied recently due to its disposal challenges and high lipid concentration. The main challenges in the diesel production via the FAME process were the variety of feedstock, as the primary and secondary sludge already presents different kinds of lipid composition, which might create challenges on the process conditions and catalyst selection (Kargbo, 2010; Sondhi et Kumar, 2020). With suitable process conditions, produced biodiesel contains mainly palmitoleic acid, palmitic acid, oleic acid, and stearic acid (C18:0), which account for approximately 70–80% of the amount of the biodiesel (Liu et al, 2021).

Leather industry waste

Waste from the leather industry is an understudied field of waste feedstock, even though it is one of the considerably polluting industries. The waste stream from the leather industry contains fat-originated liquid and solid wastes originating from processing hides and skins. The solid waste is obtained from the fleshing procedure where flesh and natural fats are removed from the hides and skins. Around 10 million animal skins were processed during 2013, the Turkish leather industry in the prominent place with high export productivity, creating a notable waste stream with fat content. Industrial or even pilot scale applications for fat collection from leather industry waste lack in existence. (Alptekin et al, 2014; Adewale et al, 2015)

Pyrolysis oil

Pyrolysis oil presents a sustainable and renewable feedstock for bio-oil production, when the biomass for pyrolysis is from sustainable origin. Pyrolysis oil is liquid produced by the pyrolysis of a biomass by a thermal decomposition, and it can be used for producing multiple high-value compounds, such as fuels and chemicals. Typically, pyrolysis oil has high content of water and oxygen, causing undesirable properties such as instability while storing, leading to the situation where an efficient upgrading process is usually needed. Pyrolysis process includes thermal breakdown of the components at high temperatures in the absence of oxygen. Sometimes a catalyst is used in the process. Products obtained are bio-oil (containing organic acids, esters, ketones furans etc.), biochar and biogas. (Jayasinghe et Hawboldt, 2012; Adewale et al, 2015; Staš et al, 2017)

The conventional pyrolysis processes can be divided into fast or slow pyrolysis, based on the heating rate and the residence time. In both, the final temperature is higher compared to the HTL process, from 350 to 700 °C. The residence time in slow pyrolysis can vary from several minutes to hours, compared to fast pyrolysis where the residence time is maximum of a few minutes. The fast pyrolysis process usually uses a fluidized bed, and the process has been tested with waste and biomass. The upgrading of the bio-oil from fast pyrolysis can be challenging due to the reactivity of the oil, although it has the advantage of providing larger bio-oil yield. Slow pyrolysis has been discovered to have lower mass yields but better product quality, with lower water and oxygen content and better thermal stability (Elliott, 2007; Jayasinghe et Hawboldt, 2012; Xia et al, 2022). One example of possible liquid product yield is mentioned by Adewale et al, 2015, where in fast pyrolysis the obtained liquid yield was 73 w %, when the operating conditions were 525 °C with 5 w % water content while the residence time was 17 s.

Typically bio-oils from the pyrolysis process need to be upgraded due to their high oxygen and water content. Upgrading process includes for example deoxygenation process (HDO process) before the bio-oil can be used for fuel production. (Elliott, 2007; Jayasinghe et Hawboldt, 2012)

2.4 Impurities

The amount and type of impurities is highly dependent on the source of the feedstock. Fats and oils contain some amounts of impurities, especially when the feedstock is obtained from

a waste stream. Common impurities are water, phospholipids, proteins, pigments and trace metals, such as sodium, calcium, potassium, and magnesium (Gharby, 2022). Physical and/or chemical purification processes, e.g., filtration and bleaching, are normally needed for feedstock to be used for fuel. Vegetable oils normally contain large amounts of phosphorus, whereas animal fats and fish oil have a higher metal content. (Jayasinghe et Hawboldt, 2012; Morales et al, 2011; Gharby, 2022)

Phosphorus is one of the most important impurities that need to be removed from the bio-oil. It is known for its ability to harm the catalyst used in the upgrading process by forming phosphorus oxide and different phosphates and causing decreasing of the surface area and pore volume in the catalyst (Wang et al, 2020). Phosphorus has a tendency to form insoluble precipitates when heated and existing in aqueous environment. The precipitates formed have a glue-like nature, creating multiple problems in pipes, filters, pumps and nozzles (Bondioli et al., 2019).

Oils and fats from waste streams may contain a certain amount of trace metals that might cause harm to the stability and quality of the oil. They can catalyse autoxidation, which is a radical reaction where the alkyl group is attacked, followed by a chain reaction and leading to a formation of a hydroperoxide group (-OOH) into the chain. The hydroperoxide group continues the reaction by forming aldehydes, ketones and free fatty acids. The reaction is promoted by light and heat, along with the trace metal catalyst, and might occur fast, decreasing the stable storage time. Polyunsaturated oils are more sensitive to this reaction. Naturally occurring antioxidants and chelate-building additives, such as citric acid, can bind the trace metals and prevent oxidation. Bleaching is usually used as a removal process for trace metals, with the help of acid. (Bockisch, 1998; Gupta, 2017)

Free fatty acids may be classified as impurities depending on the used process. Free fatty acids are problematic in the FAME process due to their nature to react with conventional alkaline catalysts such as potassium and sodium hydroxide, producing soaps in this reaction and decreasing biodiesel yield. The soaps formed in the reaction will then prevent the separation of esters from glycerine and wastewater (Wadumestrige et al, 2009; Alptekin et al, 2014; Nisar et al, 2021). FFAs are formed during the decomposition of TAG or other lipid molecules. High levels (>5%) limit the use of oil or fat in the fuel production when using the FAME process. Recycled oils and animal fats usually contain a high amount of

FFA, up to 15-20 %. For comparison, virgin soybean oil contains only 1.5 % of FFA. (Jayasinghe et Hawboldt, 2012; Hirata et al, 2013; Alptekin et al, 2014; Adewale et al, 2015)

The removal of impurities is significant due to their affect to the diesel quality in the end, leading to harmful situations with the diesel engines (Morales et al, 2011). The effect of small particles in the bio-oil are presented in more detail in chapter 4.

2.5 Citric acid

Citric acid (2-hydroxy-1,2,3-propanetricarboxylic acid) is a common compound that exists widely as a metabolic product of plants and animals. A molecule of citric acid (CA) consists of three carboxyl groups and one hydroxyl group (Figure 4). Its precipitate is white, translucent crystals of monoclinic form. CA is categorised as a polyprotic α-hydroxy acid, although it has a slightly different structure compared to other α-hydroxy acid, such as glycolic and lactic acids, by having three carboxylic acid functional groups instead of one. This means CA is triprotic and has three different pK_as, making it a prime buffer component. (Fiume et al, 2014; Li et al, 2019)

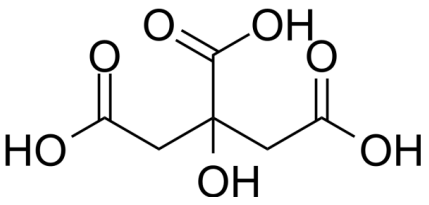

Figure 4 Citric acid (MedChemExpress)

CA is present in citrus fruits, but most of the world's CA production comes via mycological fermentation of crude sugar stocks, e.g., molasses. It is one of the most commonly used chemicals in the world, and is used e.g., in cosmetics as a chelating agent, as a pH adjuster, in food industry as a food additive, in pharmaceutical industry, in pesticide products, in manufacturing of ecologically compatible detergents and chemical cleaning products. It is a

normal metabolite, and orally dozed is completely metabolised and absorbed. CA is involved in the breakage of pyruvate, which is formed from glucose through glycolysis. The normal citrate level in human blood is approx. 25 mg/L. (Fiume et al, 2014)

CA is highly soluble in water due to its hydrophilic nature, and also soluble in some organic solvents. Most of its salts are also highly soluble in water (Fiume et al, 2014). At the pH below 7, the two out of three carboxyl groups in CA molecules are ionised, and hydrogen bonded to water molecules and often coordinated to metal ions, like Ca^{2+}. The third carboxyl group is only weak acid with a pK_a of 3.1. (Li et al, 2019; Fiume et al, 2014)

CA can form citrates with metal ions, with ionic/electrostatic bonding. The covalent character in the formed molecule is very small. In the solution, the terminal carboxyl groups are ionised first, as the centre remains to be the last. Three ionisation states of CA are presented in the Figure 5, as due to triprotic nature, citric acid can donate three protons. In aqueous environment, formed citrate ions can form citrates with alkalis. (Macarigue et al, 2020)

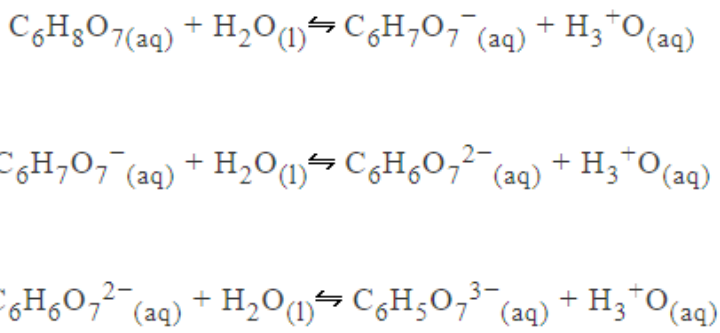

Figure 5 Three ionisation states of citric acid. Ionisation reaction to produce citrate ions and hydronium ions. This reaction occurs in aqueous solutions. (Macarigue et al, 2020)

The ionization of citric and formation of citrate are important to this thesis. Alongside citric acid can react in other ways. Under certain conditions, oxidation reactions are possible, e.g. in the citric acid cycle, which is an essential part of cellular respiration. Citric acid can also be involved in esterification reactions, where it reacts with alcohol to form esters. This type of reaction is common in food and beverage production. (Macarigue et al, 2020).

The first and second equations from the Figure 5 are favoured at the terminal carboxylic groups. (Macarigue et al, 2020) Citrates are well-known chelating agents, which is related to the ionisation of carboxyl groups: the molecule is bridging two or more metal ions, which increases the size of the cation. As the cation increases in size, chelation to a single metal ion becomes more frequent. (Kaduk et Rammohan, 2018)

As mentioned above, different trace metals such as calcium, magnesium, sodium and potassium are present in the feedstock. In several cases, the metals are in a form of fatty acid soaps and need to be separated to free fatty acids and metal ions, carried out with the help of aqueous solution of CA or phosphoric acid. CA is preferred in the acid addition due to its useful property to also act as a sequestrant, allowing the transfer of metal ions in the aqueous solution. The splitting of fatty acid soap to free fatty acid and metal ion can be performed e.g., during the pretreatment process. (Bondioli et al, 2019)

CA is an economically feasible chemical and involved in many development projects. Lately CA addition has been tested in the pyrolysis process for bio-oil production. It has been noticed that CA addition increased the bio-oil yield, as well as the yield of organics compared to raw samples (no acid addition) and water-leached samples. The acidic pretreatment was also found to be effective for removing alkali and alkaline earth metals from sugarcane residue. (Rodríguez-Machín et al, 2019)

3 Pretreatment process

Different processes are needed for removal of different impurities. Colour components, FFA, phospholipids, metals and other minor impurities can be removed through chemical purification, which includes e.g. degumming, neutralising, washing, bleaching and hydrogenation (Figure 6). Phospholipids, solids, gums and water are removed during degumming. A part of FFA can be removed during neutralisation, as well as phospholipids and chlorophylls. Washing and drying are used to remove soap residuals and water. Trace metals, aldehydes, residual free fatty acids and natural pigments can be removed by bleaching, in which the oil is mixed with bleaching clay or agent. To improve the bio-oil quality, hydrogenation can be used as a part of the pretreatment process. Deodorizing process is used for removing volatile compounds by vacuum steam distillation, resulting in the stabilising of odour. The membranes have also been studied for removal of impurities, but they are not so commonly used in industry. (Jayasinghe, P. et Hawboldt, K., 2012; Gharby, 2022)

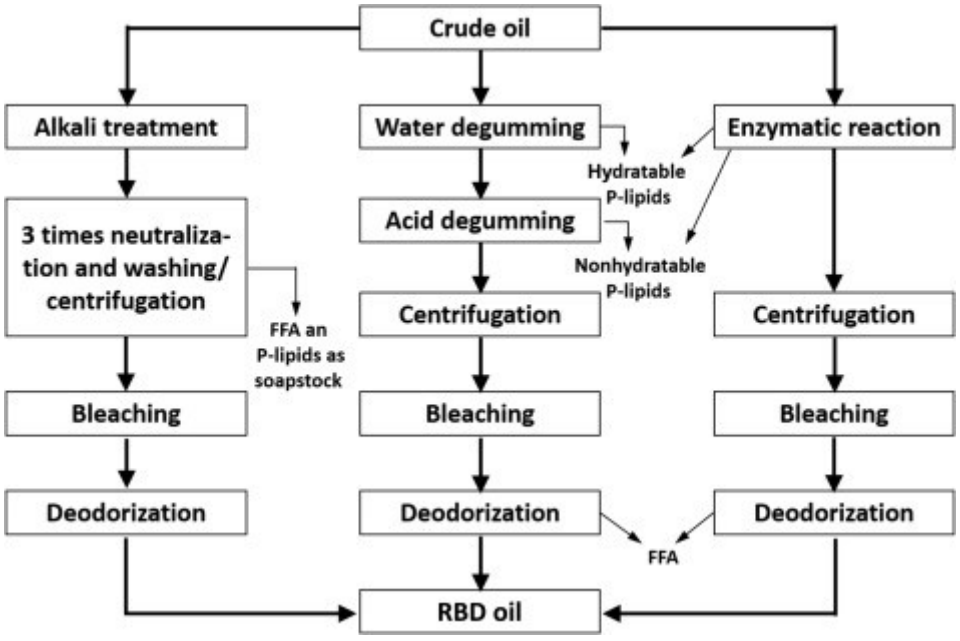

Figure 6 Possible pretreatment routes for crude bio-based oil. (Jiang, Y., 2019)

In this chapter, the pretreatment processes related to experimental work are presented in more detail.

3.1 Degumming

Phospholipids, often referred to as gums, are naturally present in bio-oil feedstock, but have been seen harmful in many processes. Phospholipids cause unsatisfactory performance of the oil in many applications: For example, in edible oils phospholipids affect the flavour stability, and in refining processes they can cause problems in the process. In cars, diesel engines and the emission control can be harmed by phospholipids and metal in the final product (Chen et al, 2014)

The phospholipid content in the feedstock differs according to the source, but overall crude oil contains both hydratable and non-hydratable phospholipids (Gupta, 2017). Phospholipid molecule consists of hydrophobic fatty acid chains and a hydrophilic head group (Figure 7) (Szydłowska-Czerniak et Łaszewska, 2017).

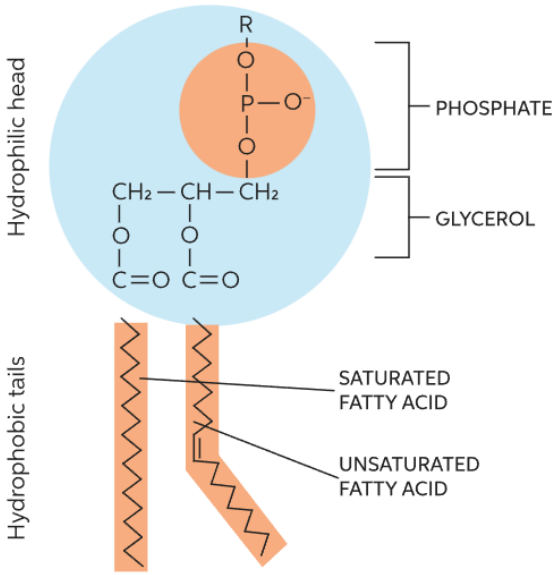

Figure 7 Structure of phospholipid molecule (Chegg)

There are several process options for phospholipid removal, or degumming process. The oldest degumming treatment is water degumming, which works for the hydratable phospholipids. In this process, deionized water is added to the oil. Phospholipids absorb water and settle out from the oil as a water phase, and therefore are easily separated from the oil. Water degumming removes most of the hydratable phospholipids but does not perform any effect on non-hydratable phospholipids. Oils or fats with a poor quality require acid treatment or degumming. (Dijkstra et al; Gupta, 2017)

The non-hydratable phospholipids are harder to remove and require acidic treatment. The phospholipid molecules are decomposed by the presence of acid (i.e., phosphoric acid or citric acid). After the decomposition, the hydration of phospholipids is carried out by the water molecules present in the oil, preventing the phosphatide part from migrating back to the oil. Citric acid can be chosen to be used in the process for two reasons: It detaches the metals bound to the phospholipid molecules, but also acts as a chelating agent to maintain the metal components in a water-soluble mode. (Zufarov et al, 2009)

The acid (400-1000 ppm) is mixed into the oil with a high shear mixer, due to the insolubility of the acid into the oil. With a high shear mixer, the acid is dispersed into the oil in micro size droplets to maximise the contact area between the acid and the oil. Incomplete mixing results in poor hydration of the non-hydratable phospholipids and may cause the acid to settle out from the oil. Precipitated salts and hydrated gums, that are insoluble in the oil, tend to blind the filter media, and are therefore removed e.g. by centrifugation after degumming. The acid dosage depends on the amount of metals in the feedstock and can be estimated based on metal analysis and calculation. At low dosage, some of the non-hydratable phospholipids may not be correctly hydrated, but with dosage too high some hydrolysis of the oil may occur. After acid treatment, the oil can be directly guided to bleaching. (Chen et al, 2014; Gupta, 2017)

Acid degumming is a more efficient process compared to acid treatment. This version combines both water degumming and acid treatment and provides more adequate phospholipid removal even from the most difficult oils. (Gupta, 2017) Acid degumming is commonly used in the oil refining industry (Chen et al, 2014; Szydłowska-Czerniak et Łaszewska, 2017).

Enzymatic degumming is taking advantage of a variety of enzymes to hydrolyse phospholipids. The gum products obtained from enzymatic degumming are often easily removed from the oil by centrifugation. Especially phospholipase C enzymes have lately gained attention, as it not only reduces the amount of phospholipids in the oil but generates TAGs in the process, improving the oil yield (Elena et al, 2017). Enzymatic degumming is considered as a more eco-friendly and cleaner process compared to acid degumming, but the industrial applications are currently quite limited due to the high price of enzymes and the lack of suitable process concepts. (Szydłowska-Czerniak et Łaszewska, 2017)

Alongside with the processes already mentioned, there are also other variations of the degumming process, mainly developed for a certain type of oil or product (Gupta, 2017).

3.2 Bleaching

Bleaching is defined as a physical pretreatment process in which the impurities present in the bio-oil are removed by the agency of an adsorbent. The process in a nutshell involves mixing the biobased oil with a porous solid material, adsorbent, and heating the mixture to a specific temperature while stirring it (Figure 8). After a certain time, the adsorbent is removed from the oil by filtration. To improve the efficiency of the bleaching, small addition of water and acid can be used. (List, 2009)

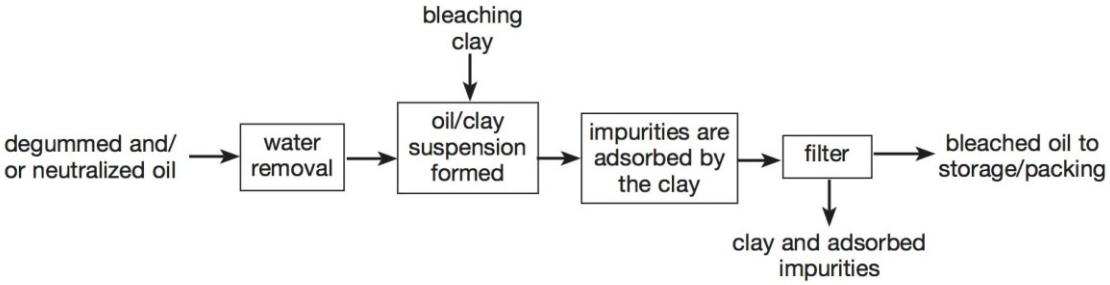

Figure 8 Bleaching process. The water removal is possible to perform before or after the bleaching earth/clay addition. (Silverson)

In early stages, bleaching was used for colour removal. The main procedure during that time was to add bentonite to the oil, stirred for a while until the colour of the oil has reached the

wanted stage, and then filter the bentonite out of the oil. Green colour caused by chlorophyll was an unwanted quality in the oil. After some time, it was also discovered that the amount of bleaching earth should be restricted, as excess amounts of adsorbent reduced the storage stability of the oil from vegetable origin. The amount of bleaching earth is often 0.1-2 w%. The fall of storage stability refers to poorer oxidative stability, which is caused by the excessive dosage of the bleaching clay. It diminishes the tocopherol content of the oil. Tocopherols are antioxidants, widely present in vegetable oils (e.g., soybean around 1000 pm) but lesser amounts found from animal fats. (List, 2009; Gupta, 2017)

3.2.1 Adsorbents

The most common adsorbent is bleaching earth, other options are also silica-based adsorbent and activated carbon products.

The adsorbents used in bleaching can be categorised as natural and acid activated. The natural bleaching earths are derived from clay-mineral deposits. The natural bleaching earth consists mostly of aluminium silicate and minor parts of different minerals. Following properties must be present in the adsorbent:

- High adsorption capacity with the correct porosity and numerous active sites
- Acidic pH for the acid-activated adsorbent
- Decent flow rate through the filter media. (Gupta, 2017)

Natural adsorbent is usually used for colour removal and is not effective enough for phospholipid or soap removal. Acid-activated adsorbent is suitable for the removal of soap and phospholipids but might increase the amount of FFAs (0.03-0.04 w %) via hydrolysis over the vacuum-dried oil. (Varzakas & Tzia, 2016; Gupta, 2017)

Acid-activated bleaching adsorbents have poor bleaching properties in its natural stage, and activation is needed to maximise their adsorption ability (Varzakas & Tzia, 2016). Activation is performed with an acid, and this chemical treatment changes its textural characteristics in prominent ways. In acid activation, acid is substituting cations with protons while increasing remarkably the adsorbing surface. The cation substitution level is affecting the bleaching properties and adsorbent structure. Acid used for activation is often HCl or

H_2SO_4, diluted into water. (List, 2009; Gharby, 2022) The chemical reaction is presented in Equation (1), as Gharby h.as it presented.

$$Cation - Adsorbent + 2H^+ \rightarrow H - Adsorbent + Cation \quad (1)$$

3.2.2 Removal of impurities

Impurities that might exist in the oil are for example trace metals, colour bodies, phospholipids, and oil decomposition products (Gupta, 2017; Gharby, 2022). The porous structure of bleaching earth retains the impurities from the oil. Often the adsorption of impurities is enhanced with a small amount of water added to the oil, although the oil cannot be so wet that it hinders the spreading of the clay. (List, 2009) It was reported by List (2009) that the amount of water can be as little as 0.1 w%, up to some w %. The adsorbent concentration is normally <1 % of the vacuum-dried oil (Gupta, 2017).

The impurities are attracted by the active sites of the adsorbent via multiple ways: van der Waal's force of attraction are present in the adsorption, and especially in acid-activated bleaching earth the cations at the strongly acidic sites are ready to donate a proton to the impurity, creating an electrostatic attraction (List, 2009; Gupta, 2017). Several factors affect the amount of attraction (adsorption capacity) between the impurities and the adsorbent: (Gupta, 2017)

- The size of the compounds participating (both the impurities and the adsorbent)
- The electrostatic force of each component
- The distance between the components, affected by the degree of mixing
- Porosity and the specific surface of the adsorbent

The benefits of bleaching are significant:

- Bleaching reduces the colour bodies present in the oil, e.g., like chlorophyll, that harm the photooxidative stability of the oil
- Bleaching reduces the trace metal ions such as Ca^{2+}, Mg^{2+}, Fe^{3+}, Na^+, etc.

- Reduces the amount of non-hydratable phospholipids in the oil
- Removes decomposition products, such as aldehydes, ketones, and polymers. (Gupta, 2017)

The effectiveness of the bleaching can be controlled by the mixing of the adsorbent and the oil (maximum contact between the oil and the adsorbent), temperature and time. Acid-activated bleaching earth is used for water-washed oil at medium temperature (60-100 °C), in atmospheric or vacuum conditions. Use of temperature above 150 °C should be avoided due to promotion of isomerization reaction (Varzakas & Tzia, 2016). It is preferable to use vacuum for avoiding oxidative side reactions in the oil (from contact with air oxygen). Mechanical mixing helps to provide intimate contact between the oil and the adsorbent, the contact is kept for 20-50 min. In addition to the adsorbent, a small amount of acid (CA, or phosphoric acid) can be added to the bleaching process to improve the removal of trace metals (Gupta, 2017; Gharby, 2022). The acid addition is done before the addition of the bleaching earth, to split the remaining traces of soap. The addition of acid also improved the adsorption of trace metals, which can otherwise cause harm to the oxidative stability of the oil. (List, 2009)

The acid in the solution forms chelate complexes with trace metals, which then can be adsorbed by activated bleaching earths. The meaning of acid addition is to hydrolyse the soap in the oil to enhance the efficiency of scavenging the trace metals from the oil by the adsorbent (Gupta, 2017). A typical acid addition can be e.g., 0.05 % w/w of citric acid /oil to be bleached, as a 50 % solution in water. The effect of acid varies according to the acid itself. Citric acid has the advantage of scavenging free oxygen, splitting the soap and converting nonhydratable phospholipids to hydratable phospholipids. (List, 2009)

Moisture can exist in the bleaching process from three sources: It can be present in the oil in the first place; the bleaching earth may naturally contain moisture; it can be added to the bleaching process. The presence of water enhances the removal of phospholipids, as during the degumming process. (List, 2009)

At the industrial level, modern plants are using vacuum bleaching units to avoid oxidation in the process. After the bleaching unit, the oil is filtered, cooled and stored, or directly sent to the following process unit, such as hydrogenation or deodorization. Some plants include a pretreatment unit using silica hydrogel before the bleaching unit. This procedure has been

seen to increase the effectiveness of trace metal and phospholipid removal from the oil. (Gupta, 2017)

3.3 Filtration

Filtration is thought to be a very important step in bio-oil pretreatment. In the filtration process, a mixture of liquids and solids is separated into individual phases; the process itself is also known as solid-liquid separation. It is often referred to as a mechanical separation due to its purely physical nature, where the separation is obtained generating a pressure difference through filter media. The pressure difference can be created either with gravity, pressure, vacuum or centrifugal force. The phase containing solid fraction is often referred to as mass recovery or retention, while the liquid phase is called the filtrate. (Svarovsky, 2000; Gupta, 2017; Sparks et Chase, 2016)

Filtration as a separation technology has a significant role in the chemical industry. Via separation process, product purity can be increased, and valuable material can be collected from the waste streams. Filtration-type of solid-liquid separation is used e.g., for a recovery and dewatering of the high-value solids from a slurry, a recovery and cleaning of the liquid, a separation of two phases from each other before recirculation of both, or before their disposal for environmental reasons. (Svarovsky, 2000)

Often the separation of two or more substances is done, because the components in the slurry or suspension are more valuable or less harmful as individual components than in a suspension. For example, bio-oils contain different impurities that are harmful either to the process or decrease the quality of the end-product. In the separation process, solids can be removed from a valuable fluid, or vice versa. In some cases, both products are valuable and need to be collected. (Sparks et Chase, 2016; Svarovsky, 2000)

According to Sparks et Chase, 2016, there are several capture mechanisms existing in filtration systems:

- Sedimentation/gravity: larger and thicker particles may settle out and accumulate during the filtration by themselves and might affect the process performance.

- Straining/sieving: The particle can be held back by the filter medium, when it is larger than the medium pores and does not have enough inertia to damage the filter media.
- Inertial impaction: The particle does not travel in the flow of solution but continues its existing route to intercept with the filter media. This mechanism might not always be important, but its effect can be seen on the number of solids passing the filter on different flow rates.
- Interception: The particle follows the flow and eventually contacts with the filter medium and is captured. The capture of the particle depends on the ratio of particle to pore size and the bonds formed between the particle and the pore/filter medium. In this case, the fluid flow is considered as laminar.
- Brownian motion: An arbitrary motion as a result of collision with smaller molecules in the stream. The motion of a small particle is influenced by the Brownian motion and the streamline, which can bring the particle to contact with the filter media. This capture mechanism is affected by the fluid and particle densities and particle size.
- Electrostatic deposition: The surface charge of the particle may affect its pathway to the medium where it remains. The charge of the particles is in this case opposite to that of a pore in the filter medium. The opposite process of magnetic deposition can also occur.

3.3.1 Types of filtrations

Three major types of filtrations occur, they can be categorised as depth filtration, surface filtration or bridging filtration. Depth filtration (Figure 9) traps the solid particles from the fluid into the pore structure of its filter medium. The particles are guided into the pores by hydraulic pressure of Brownian motion, in the presence of inertial force. Inside the pores, solid particles attach or agglomerate together by the affection of van der Waal's forces. The solid retention takes place inside the medium and cake deposition on the filter surface is undesirable. In industry, for example sand filters are common types of depth filters used. The filter media can also be made of fibrous material, like cellulose. (Svarovsky, 2000; Wakeman, 2007; Sparks et Chase, 2016)

Figure 9 the principle of surface filtration is presented on the left, and the principle of depth filtration on the right. (FDPP)

In surface and bridging filtration (Figures 9 and 10), a large number of particles arrive at the filter medium. When the size of pore is smaller than the particle size, the surface of the filter will retain the particles and ideally allow only the liquid to pass through the filter. There are several options that can be used as a filter media, but the most common solutions are fibrous material, granular beds or metal screens. In real life, the filtration is not totally completed and some of the fine particles might end up in the filtrate, especially in the beginning of the filtration. The retained larger particles form a deposit layer, or "the cake", on the medium surface. The bridging filtration occurs when a large number of particles, that could individually pass the filter medium, arrive at the filter surface and jam together to form a bridge-like structure over the pore. Therefore, the medium pore size does not essentially give direct information of the minimum particle size that can be retained. (Wakeman, 2007; Sparks et Chase, 2016)

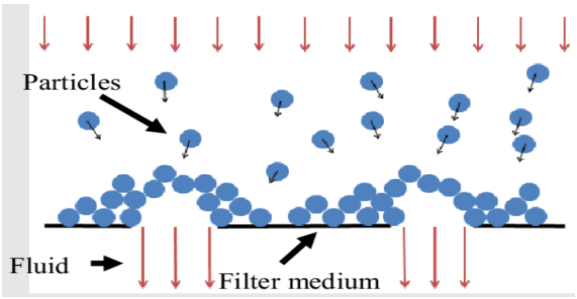

Figure 10 Bridging mechanism in filtration (Hund et al, 2017)

The formed cake is often very effective at capturing particles and starts acting like a filter in very early stages of formation. The thicker the cake is, the higher is the probability of retaining fine particles, therefore the effectiveness of the cake increases during time, which positively affects the filtrate clarity. The pressure in the filtration normally increases while the cake starts to build up. This process is generally called cake filtration, and in industry used for fluids containing at least 1 w % of solids. Cake filtration is a common process used in the chemical industry and is used in the experimental part in this thesis as it is often used for purification of oils and fats. (Svarovsky, 2000; Sparks et Chase, 2016)

After the bleaching process, filter precoat is needed for successful filtration. The suspended bleaching adsorbent tends to blind the filter screen, and the wanted filtration result cannot be achieved. (Gupta, 2017)

3.3.2 Filtration equations

The filtration flow can be calculated via Darcy's Law (Equation (2)), which is a fundamental equation in filtration (Holdich, 2002).

$$Q = \frac{kA\Delta p}{\mu L} \tag{2}$$

Where Q flow rate through the filter [m/s]

k the permeability of filter [m^2]

A filtration area [m^2]

Δp pressure drop before and after the filter [Pa]

μ fluid viscosity [Pa*s]

L thickness of the filter media [m]

During the cake build-up, the resistance to liquid flow through the cake increases. This factor is presented as a specific resistance (Equation (3)). The specific resistance is described as

the ability of the cake to resist the flow of filtrate through the cake and is one of the most important factors in the filtration process.

$$\alpha = \alpha_0(1-n)\left(\frac{\Delta p_c}{\Delta p_o}\right)^n \quad (3)$$

Where α specific resistance [m/kg]

α_0 specific cake resistance reference at 1 bar [m/kg]

Δp_c pressure change in the cake [Pa]

Δp_o local scaling pressure [Pa]

n compressibility coefficient

The specific resistance is affected by the compressibility of the cake, as the filtering pressure increases during the time pressing the particles tighter together so the voids among the particles decrease in size (Endo et Alonzo, 2001; Bouncier et al, 2016). In pressure filters, the increase of the pressure decreases the cake porosity, increasing the specific resistance the more dramatically the higher the pressure is, in cases where the material is compressible (Endo et Alonzo, 2001).

Cake resistance (Equation (4)) can be calculated via the specific cake resistance, mass of the cake and area of the filter (Holdich, 2002):

$$R_c = \alpha \frac{m_c}{A} \quad (4)$$

Where m_c mass of the cake kg

R_c cake resistance [kg/m^2]

The general filtration equation for the constant cake filtrations (Equation (5)) can be used for determining the resistance of the filter media (Holdich, 2002):

$$\frac{\Delta t}{\Delta V} = \frac{\mu \alpha_{av} c}{2A^2 \Delta p}(V + V_s) + \frac{\mu R_m}{A \Delta p} \quad (5)$$

where α_{av} average cake resistance [m/kg]

c filtration concentration [kg d.s./m^3]

R_m resistance of the filter media [1/m]

Δt time change [s]

ΔV change of the filtrate volume [m^3]

The filtration time reduction is smaller at high pressure, indicating that the effect of the pressure drop is reduced by the increase in the specific resistance. This was demonstrated by Bouncier et al (2016) in an experiment, where a higher filtration speed was achieved for spheres at the highest pressure drop (pressure used was between 1 and 5 bars). It should be noted that increasing the pressure increases the filtrate flow, unless the compressibility coefficient of the material is >1.

The simple version of porosity of cake and the amount of moisture can be determined from a mass balance after the filtration: The wet cake is weighted after draining, often with the help of compressed air, and dried after that. The dry cake is weighted and the difference between the weights before and after provides the amount of moisture. This type of calculation (Equation (6)) is suitable in a situation where all the pores of the cake are full of liquid i.e., the saturation of the cake is 100 % (Bouncier et al, 2016). The average porosity of the cake is traditionally determined by the wet to dry cake mass ratio shown in Equation (4) (Tien et Ramarao, 2013).

$$\bar{m} = 1 + \frac{\rho \bar{\varepsilon}}{\rho_p (1 - \bar{\varepsilon})} \quad (6)$$

where $\bar{\varepsilon}$ average cake porosity

$\bar{m}$ cake mass ratio

ρ	density of the filtrate [kg/m^3]
ρ_p	density of the particle [kg/m^3]

Sometimes in cake filtration filter aids are needed for successful filtration. Filter aids are porous, rigid, and highly permeable powders that can be used with very dilute or very fine and slimy suspensions. Some examples of possible filter aids are diatomaceous earth, perlite and cellulose. Some fluids are too problematic to be filtered by a cake filtration because they tend to blind the filter and cause fast pressure build-up. Filter aids can be used in two different techniques: They can be mixed with the fluid as a body feed, to increase the solid concentration and permeability of the resulting cake, or they can be used to form a precoat on a coarse support material. This precoat acts like a filter medium, allowing filtration of very fine particles. (Svarovsky, 2000)

Three main parameters define the solid-liquid separation process: the state of the system, primary properties and macroscopic properties. The state of the system includes the porosity of the cake/filter and concentration of solids in the suspension. Primary properties of the suspension are defined beforehand, and they include particle size, shape, and size distribution, and fluid properties i.e., density and viscosity. The particles are interacting with the environment constantly, and finer particles are especially affected by interparticle forces that can become as remarkable as gravitational or hydrodynamically induced forces. These interactions affect later the particle settling rate, filter cake consistency and captivity of the particles in the filter medium. The state of the system and the primary properties control the macroscopic filtration properties, including for example specific cake resistance and permeability of the cake. (Wakeman, 2007)

4 Particles

Particles may be present in fluid in very different shapes and sizes, from very fine colloidal material to harsh solids. The particles can be categorised based on their size, for example dissolved (< 0.001 μm), colloidal (0.001–1 μm), supra-colloidal (1–10^2 μm), and settleable (> 10^2 μm). The composition of particles may vary according to the feedstock composition. Their presence and size have a substantial consequence on the suspension properties and behaviour in a solid-liquid separation process. (Chaloupková et al, 2019; Cornacchia et al, 2022)

Four primary reasons to measure particle size in the suspension are presented as such by Wakeman (2007):

- Study of solids in the suspension can be used to foresee their behaviour in the separation process. The collected information can be used for selecting suitable processes or pretreatment methods. When the use of information is predictive, the measuring method must be selected cautiously.
- To characterise the suitable filter medium which retains the particles of different sizes from the suspension. This type of evaluation is commonly used in fluid polishing operations and the specification of a nominal pore size for a polishing medium.
- The specification of valuable filtrate product quality from a filtration process. This case is often associated with very dilute suspensions, from which the filtration of particles is difficult to perform. Often the total concentration of solids is the only needed information from the suspension, as it is in the water treatment process, but sometimes the size of remaining solids is also critical (hydraulic fluids for example).
- The solids can also be a valuable product, although the completely dry state is almost never accomplished and further processing is needed. The evaluation of the solid product is often related to the quality control, not solely to the separation process.

The most commonly required particle size value in filter cake formation, washing or deliquoring calculations is the surface-volume mean diameter, which is also known as Sauter diameter $d_{(32)}$ (Scala, 2013). The Sauter mean diameter is often expressed in terms of the

surface diameter given as the diameter of a sphere (Equation (7)) having the same surface area as the given particle (Equation (8)). Combined Equation (9) defines the Sauter mean diameter.

$$d_s = \sqrt{\frac{A_p}{\pi}} \tag{7}$$

$$d_v = \sqrt[3]{\frac{6V_p}{\pi}} \tag{8}$$

$$d_{32} = \frac{d_v^3}{d_s^2} \tag{9}$$

where d_s diameter of a sphere having the same surface area

d_v diameter of a sphere having the same volume

A_p external surface area of the particle

V_p external volume of the particle

Various types of particles are present in the bio-oils. Crude animal fats can contain plastic polymers originating from plastic bags or nylon food containers, in which the rendered fats were stored before recycling. Some of the crude animal fats can contain up to 500 mg/kg of polyethylene, which can be a major problem in filters and pumps in the refining process. Some companies have homemade solutions through a try and error method, mostly using acid degumming to reduce the polyethylene concentration in crude animal fats. (Bondioli et al, 2019)

4.1 Characteristics of a particle

Particles are characterised by their properties, such as size, density and shape, particle size distribution and surface properties, together with the properties of the liquid. Primary properties of the liquid are viscosity and density. Alongside these properties also the state of the solid-liquid suspension and concentration of solids are characterised to determine

secondary properties such as the specific resistance of a filter cake, settling velocities of the particles or permeability of the cake. (Svarosvky, 2000)

There are several reasons why particle characterisation can be challenging, but one major factor is their complexity and wide range of different chemical and physical properties. Particles come in all shapes, as discussed before, and their texture varies: They can be hollow, solid or filled with gas, with different surface structure and porosity, affecting their behaviour. The method chosen needs to tackle the upcoming challenges where the particles adhere to each other due to the chemical reactions, mechanical bonding or electrostatic interactions. The challenges are more frequent with smaller particles. (Snowsill, 2009)

4.1.1 Particle size distribution

Particle size distribution is an outstanding way to describe the particles in samples of no monodisperse size. Particle size distribution characterizes the number, volume or mass percentage of particles of various sizes in the sample (Doroszkowski, 1999). The size is an important factor, as it affects the chemical reactivity, electrical charge, optical properties as well as the behaviour of particles in the fluid or gas stream. (Snowsill, 2009) By determining the particle size distribution, the quality, safety and performance of the final product can be improved. Particle size distribution is one of the most important factors of particulate samples. (Swirniak et Mroczka, 2022)

Probably the most frequent graphical presentation of particle size distribution is a histogram. The histogram provides an easily readable vision of the particle size distribution (Cornacchia et al, 2022). Particle size distribution (PSD, Figure 11) is also often presented as differential distribution or as cumulative distribution. Differential distribution can be explained as a percent of the samples that are equivalent to the given function, such as volume or diameter. Differential distribution can be obtained from a histogram. Cumulative distribution expresses the probability of a sample to have a value lower or equal to the x-axis. (Xu, 2014)

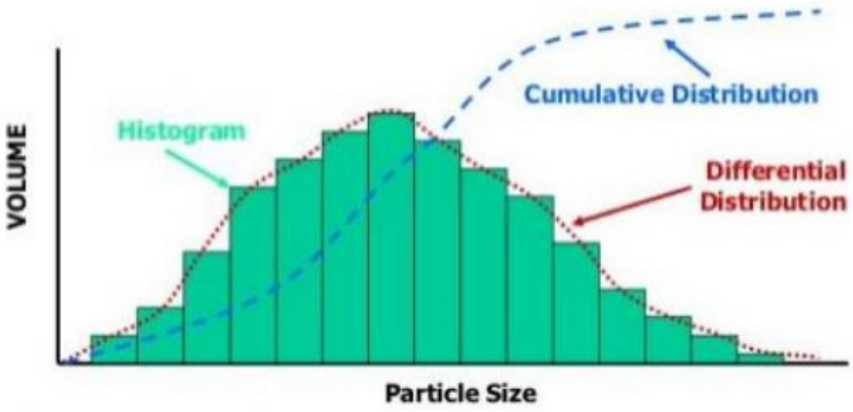

Figure 11 Different particle size distribution models presented by Treviranus (2011).

In practical applications, the particle size needs often to be characterised in terms of a single number. Some of the popular statistical numbers can be described as such (Rhodes, 2008):

- Mode: the most frequently occurring size in the sample
- Median: easily read from the cumulative distribution as the 50 % size, sharing the distribution into two equally sized parts.
- Mean: can be defined for a given size distribution. Several options such as arithmetic, geometric etc.

The use of statistical numbers as a description of particle size can be determined by the needed information.

4.1.2 Particle shape

Multiple filtration models make a presumption that the particles are spherical, although those kinds of particles are rarely found from industry. Particle shape can be described as asymmetrical, crystalline, snowflake-like, needle-like or plate-like. Alongside with the particle shape, the size and density are also important factors, which affect the interaction between the particles in the filtration process. (Sparks et Chase, 2016) Particles originating from biomass are irregular, and the assumption of spherical particles may result in large errors in the estimation of particle size distribution. (Chaloupková et al, 2019)

To describe irregular particles, at least two parameters are necessary. These parameters can be for example the length, width, diameter, surface area or volume of the particle. For now there is no universal consensus on how to describe the bio-based particles in detail (Chaloupková et al, 2019). The suitable dimensions for each particle analysis depend on the property or dimension that can be measured from the particle (Rhodes, 2008).

Some mean diameters commonly used to describe particles are shown in the Figure 12. Snowsill (2009) has describes the diameters as such:

> "Ferêt diameter: the mean of the overall width of a particle measured in all directions.
>
> Martin's diameter: the mean of the length of a chord bisecting the projected area of the particle, measured in all directions.
>
> Projected area diameter: the mean of the diameters of circles having the same area as the particle viewed in all directions.
>
> Image shear diameter: the mean of the distance that the image of a particle needs to be moved so that it does not overlap the original outline of the particle, measured in all directions."

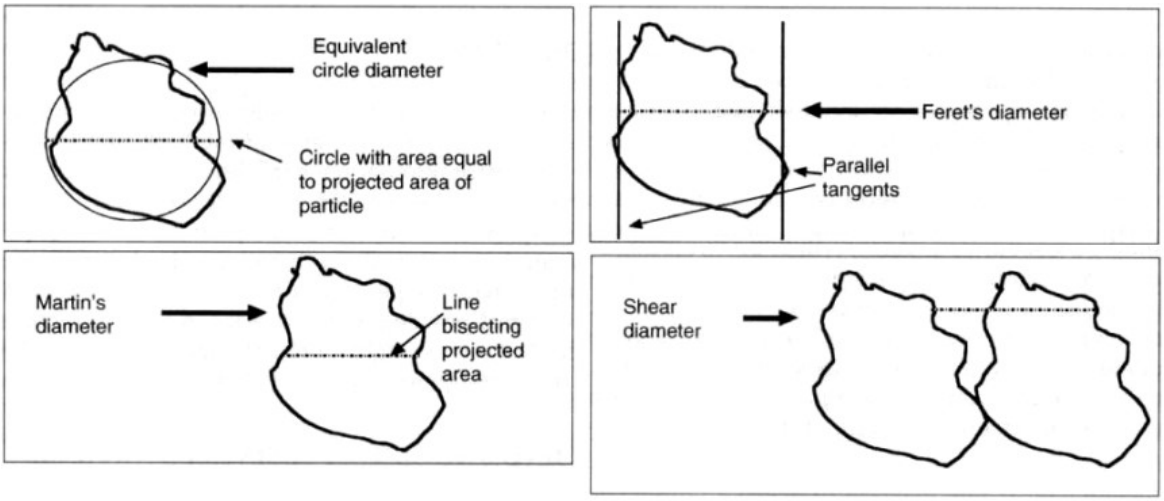

Figure 12 Different particle diameters presented by Rhodes (2008)

When the particles are irregularly shaped, two particles with the same diameter (Martin's for example) can greatly vary in shape. This has brought up a need for shape coefficients. The most common ones are volume shape coefficient α(V,F), which is based on Ferêt diameter,

surface coefficient α (S,F) and surface volume coefficient α (s)/ α (v) = α (s,v). These kinds of coefficients can provide a decent expression of particle shape in a quantified form, when used together. (Snowsill, 2009)

Particles can be described through several mathematical ways, from where the elongation of the particles can be investigated.

- Aspect ratio, which is often described by the ratio of the minimum to the maximum length and can be for example to Ferêt diameter $\psi A = x_{Feret\ min} / x_{Feret\ ma}$. From the aspect ratio, the elongation of the particle can be indicated. (Xu et Di Guida, 2003; Carter et Yan, 2005; Snowsill, 2009)

- Sphericity is defined as a measure of how spherical a particle is. It is calculated as the ratio of the surface area of a sphere to the actual surface area of the particle (Xu et Di Guida, 2003). Several equations can be found, the simplified sphericity index can be present as $\Psi = d_n/A$, where d_n is the diameter of the sphere having the same volume as the particle. The range of sphericity is from 0 (elongated shape) to 1 (perfect sphere) (Cruz-Matías et al, 2019).

- Circularity is described as a 2D version of sphericity. Circularity indicates the roundness of a particle, how closely it resembles a perfect circle. Circularity can be used to describe the regularity of a particle. The range of circularity is from 0 (elongated shape) to 1 (perfect circle). (Cruz-Matías et al, 2019)

The interaction of particles is also affected by the electrical charges on the surface of the particles, caused by repulsive and attractive forces between them. Forces present in the filtration system affect the motion of the particles, and therefore have an effect on settling properties. (Sparks et Chase, 2016)

4.1.3 Common methods

Size distribution of particles in a suspension can be measured in several ways. The results are often affected by the selected method and by the operator (human factor). The chosen method should represent the process under investigation, to provide sufficient data from irregularly shaped particles. For example, a projected area diameter is a suitable method for representing the size of pigments in paints, but when examining the effect of chemical

reaction of involved particles, an equivalent surface diameter would be more suitable. Particle size measurement is often practically challenging, unless a well-established laboratory resource is available. (Wakeman, 2007)

Traditional method for particle size distribution is sieving, which provides cumulative mass curve and overall particle size distribution. Harsh differential particle size distribution is also possible to accomplish. The accuracy of sieving results depends on the amount and size of used sieves during the sizing. Sieving is still one of the most popular methods, due to its cost-efficient nature and wide range of sieve sizes from about 20 μm to 125 mm, using standard woven wire sieves (Snowsill, 2009; Chaloupková et al, 2019). Sieving may not be the best option for all particle shapes, as the non-spherical and irregular-shaped particles may still pass, or the sieve holes may be blinded by larger particles. (Snowsill, 2009)

Sedimentation method is based on the sedimentation velocity of the particle, where the measured particle size is described as the diameter of a sphere having the same velocity under the same sedimentation circumstances. In sedimentation the suspension is dilute, and the particles can be presumed to fall at their individual terminal velocity in the fluid. The settling of the particles can be observed multiple ways, one of the most common is via a light source or x-ray passed through a narrow portion into the sample, and the results are obtained from the amount of light or x-ray absorbed to the sample. The method is suitable for small particles normally under 50 μm in diameter. The particle diameter is connected to the terminal velocity via the settling time and can be obtained as Stokes diameter. (Rhodes, 2008) The sedimentation can be enhanced by centrifugation. (Doroszkowski, 1999)

Computer vision based methods are a growing field of interest. They can provide more precise information with better efficiency, quality and performance. Better data quality may enhance the efficiency of processes leading to better product quality (Chaloupková et al, 2019).

Spectroscopic techniques, e.g., laser diffraction can be used to a wide range of particle sizes. Laser diffraction technique is based on the laser beam travelling through a suspended sample containing particles. Different types of particles diffract or scatter the light at various angles related to the particle characteristics. The diffracted beam is measured by detectors, and results calculated based on the Mie theory of light scattering. (Cornacchia et al, 2022)

Mie scattering theory is an inclusive mathematical solution to diffracting of incident light by spherical particles but can be extended to include also particles with varying shapes and aspect ratios. The Mie scattering theory points out the need for a precise knowledge of the real and imaginary components of the reflective index of the material under study, to be able to determine the size of the particles and PSD. The theory is widely used among the modern instruments for modelling diffraction patterns formed. The Mie theory is suitable for particles smaller than, or equal to, the wavelength of the incident light. (Jillavenkatesa et al, 2001)

Even more widely used theory for modelling the diffraction of light is Fraunhofer diffraction. Fraunhofer diffraction is a phenomenon that occurs when a coherent light source, such as a laser, passes through a small aperture or encounters an obstacle with a distinct edge. It leads to the bending and spreading of light waves, resulting in a pattern of light and dark regions known as a diffraction pattern. The main characteristic of Fraunhofer diffraction is that the source of light and the observation screen (where the diffraction pattern is observed) are at a considerable distance from the diffracting object. This distance ensures that the light waves coming from different parts of the aperture or obstacle arrive at the observation screen in a parallel fashion. The mathematical description of Fraunhofer diffraction involves the Fourier transform, which relates the spatial distribution of the diffracting object or aperture to the pattern observed on the screen. The resulting diffraction pattern depends on the size and shape of the aperture, the wavelength of light, and the distance between the object and the screen. Fraunhofer diffraction can be used for analysing particles, for example smaller particles produce broader diffraction patterns, while larger particles create narrower patterns. Analysing the diffraction pattern allows scientists to estimate the size of particles, and other properties. (University of Cambridge; Lambda Scientific; Picart et Jun-Chang, 2012)

As the particle technology develops, it has been recognised that irregular shapes particles can dramatically vary in scattering properties, while creating tiny connections between each other creating fractal-like aggregates. The shape of a particle has been overlooked and assumed to be spherical or related to that, which may cause errors in result handling. The interpretation of the chosen technique needs to be carried out with enough caution. (Swirniak et Mroczka, 2022)

4.1.4 Microscopy and image analysis

Microscopy is a common method for particle study, offering a possibility to examine particle shape, surface structure, and other properties like colour or texture. Optical microscopes can be used to study the small particles, whose size approaches the wavelength of light (Snowsill, 2009). A scanning electron microscope (SEM) can be used for characterising even smaller particles, often combined with image analysis software. With this combination, specific particle dimensions can be defined, e.g., volume and surface area (Bouncier et al, 2016). Microscopy offers a possibility to have a direct observation of the particles. The determination of particle size is based on a defined diameter. The calculated sizes are presented as the diameter of a sphere having the same projected area as the projected image of the particle (Jillavenkatesa et al, 2001; Rhodes, 2008). Disadvantage of microscopy lies in the restricted depth of focus, causing constant refocusing when analysing samples with a wide size range. There is also a possibility to miss particles during the scan that are placed outside the focus. (Snowsill, 2009)

Image analysis is a technique that is paying more attention to the geometrical shape of the particle. It includes more factors than just sphericity, offering more precise results (Chaloupková et al, 2019). In this analysis, the sample is placed on a flat surface under the focus of a CCD (charged-coupled device) camera. A CCD camera is more sensitive compared to regular camera equipment and can capture a high amount of incident light in all wavelengths. When the measurement light interacts with the sample, a digital detector collects the information and delivers it as an image. After placing the sample and picture taken, digital image processing techniques can be applied to deliver the information about particle characteristics, its aspect ratio, surface area, and shape factor. Working area is often about 150 µm to 25 mm, some equipment can measure particles from 0.5 µm. This analysis method can provide successfully reliable information about the particle characteristics, although it may be a bit insensitive to the particle size. Image analysis is often used as a static analysis, but some on-line measurement methods have also been developed. (Carter et Yan, 2005; Malvern Panalytical)

Image analysis can be divided into two categories: static image analysis and dynamic image analysis. The static image analysis is described only in a few sentences, as the equipment more valuable for this thesis is falling into the category of dynamic image analysis. In static

image analysis, the sample is placed on an object slide, and is combined with an optical microscopy or electron microscopy. The particle detection with electron microscopy has superior detection range compared to optical microscopy, due to its ability to use electrons as a light source. Optical microscopes can use only visible light (400-700 nm), which limits their capacity to detect small particles. (Ebnesajjad, 2011)

Dynamic image analysis is used for a moving fluid for particle detection. The method is software-based and highly automated microscopic analysis, where multiple images are taken from the sample in motion. Similarly to the static image analysis, this method also consists of a light source, lens and a CCD camera (Figure 13). The light source of this method is often a solid-state laser pulsing the light into the sample, transmitting illumination through the flow cell containing flowing particles. The particles can be seen as dark silhouettes on the camera lens, recorded and automatically analysed by the software. (Ulusoy et Igathinathane, 2016)

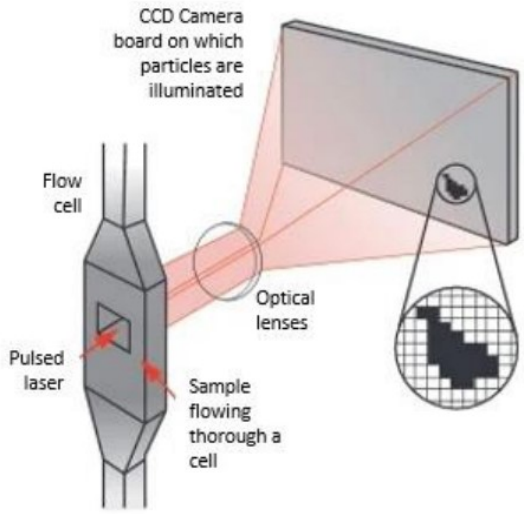

Figure 13 General principle of a dynamic image analysis (AZO Materials, 2019)

Dynamic image analysis can be used in industrial processes providing online measurement from the process, e.g., crystallization. The advantage of this method compared to the static image analysis is that the images are obtained from a sample in motion, providing a larger amount of sample to be measured. The method is highly automated, needing less operating during the measurement, and the results can be achieved in relatively short time. (Ulusoy et Igathinathane, 2016)

4.2 How particles affect the filtration

The performance of the separation process is highly affected by the particle properties, such as size distribution and shape. At plant scale solid-liquid separation is usually a time-consuming process, especially with small particles (<100 μm) having irregular shape and/or a wide size distribution affecting e.g., the cake filterability. Increasing the pressure is not always an option, due to its effect on cake compression. Filterability and compressibility need to be determined when a suitable solid-liquid separation process is chosen. (Bouncier et al, 2016)

The particle size and particle size distribution has been studied more extensively by Wakeman (2007), who suggested that the solid-liquid separation is significantly affected by these three parameters: the state of the system, primary properties and macroscopic properties.

The relation between particle size and specific resistance of a filter cake can be described as Wakeman (2007) has presented them in following Equations (10) and (11), from which one can notice that the permeability of the filter cake is inversely related to the resistance of a filter cake to allow the fluid flow through.

$$\alpha = \frac{1}{\rho_s(1-\varepsilon)P} \tag{10}$$

$$\alpha \propto \frac{1}{d^2} \tag{11}$$

Where α specific resistance [m/kg]

ρ_s density of the solids [kg/m^3]

ε porosity of the cake

P permeability of the filter cake [m^2]

d particle diameter [m]

The Equation (11) shows that the specific resistance increases while the particle size decreases; the specific resistance is therefore inversely related to the square of the particle size. Reducing the particle size by e.g., a factor of 10, the specific resistance increases by a factor of 100 (Wakeman, 2007; Haramkar et al, 2021). The specific resistance is also connected to the duration of filtration: The higher the specific resistance, the longer the duration of filtration, when performed in the same pressure. (Bouncier et al, 2016)

It can also be noticed that the shape of the particles influences the specific resistance, since the sphere particles have shown a lower resistance than platelets with a similar size. Particles exhibiting needle-like shape present often a much higher compressibility, it is assumed that this type of particles rearrange in each cake layer resulting in the decrease of mean pore size without disturbing the total porosity. (Bouncier et al, 2016)

Specific surface and the flow rate of liquid through formed filter cake are affected by the particle shape through their volume and surface area. Ideally, the suspended solids in the fluid are preferred to have large particle size, spherical shape and limited distribution. The challenges are formed when particles are more elongated than spherical, as they may travel through the filter more easily compared to spherical particles. (Wakeman, 2007)

The porosity of the formed cake is however not dependent on the particle size. The dependence can be seen to be more related to the particle distribution, meaning that the cake is packed more tightly with a wide range of particle distribution. With a wide range of particle sizes, the smaller particles are able to fill gaps created by the larger particles, and therefore decrease the porosity of the cake. Denser cake does not allow the filtrate flow through easily, resulting in an increased filtration time and decreased filtrate flow rate. (Haramkar et al, 2021)

The last step of filtration is cake washing and collecting, if necessary for the upcoming processes. Particle size has been seen to have an influence on cake washing as well: the specific resistance of the cake is reduced by larger particle sizes enabling higher wash liquid flow rates, which tend to enlarge pores in the cake increasing its porosity and therefore improving mass transfer coefficients when localised turbulence is promoted. In practical cases, for example on the industrial side, the Reynold Number is so small that mass transfer is decided by the rate of diffusion of the solute into the wash liquid. (Wakeman, 2007)

The filtration cycle is affected by the particle size distribution in multiple stages, and many of the filtration process stages affect the result gained from the next one. The change in some level affects multiple factors, making it difficult to estimate the result from one change. Especially the smallest size particles have the greatest impact throughout the filtration cycle: they can leak through the filter cloth and migrate through the voids in a forming cake, concentrating into the cake layer nearest to the filter cloth. Their behaviour affects the specific resistance of the filter cake, and slows the rates of filtration, increasing the moisture content in the cake and interacting more forcefully with ions or other substances in the fluid. (Wakeman, 2007)

5 Crystallisation

Crystallisation is a process where the liquid substance is solidified into a highly structured solid matter. In the formed crystal, atoms and/or molecules are forming an organised and regular three-dimensional crystal lattice. A crystal can consist of multiple numbers of unit cells, which creates one of the most important features of a crystal: the long-range order of these unit cells, which form symmetric solid matter. The symmetric arrangement of the crystal maximises the interactions between the unit cells leading to the stable solid. (Mullin, 2001; Beckmann, 2013)

The affecting forces in the crystal can be categorized into four different types according to the method of bonding: ionic, covalent, molecular and metallic. Hydrogen bonding may occur in the molecular crystals. Most of the crystals present predominantly one of these types, but intermediate materials also exist. Crystals classified as ionic are composed of changed ions that hold the lattice by electrostatic forces, for example sodium chloride. The crystals with covalent bonding hold the lattice via sharing their outer electrons. The most common example is a diamond. Weak attractive forces are present in molecular crystals, like organic compounds. Metallic crystals, like copper, share their outer electrons of constituent atoms but these are loosely held and allow to move in the lattice, creating metallic properties. (Mullin, 2001)

5.1 Formation of crystals

The crystal formation starts from the nucleation process. The environment of supersaturation or supercooling alone is often not strong enough to start the crystallisation process in the system. Before crystallisation, cell units, nuclei or seeds can exist in the system that act as the centre of crystallisation. Nucleation can occur spontaneously in the presence or absence of any foreign surface. In the absence of any foreign material, the occurrence is called primary nucleation as the crystalline material is considered as material de novo. Primary nucleation can be divided into homogeneous or heterogeneous types depending on the presence of a foreign surface or substance in the liquid. From these types, homogeneous

nucleation is rarely seen, as the solution often contains dust or impurities that cannot be detected. (Lee et Myerson, 2006; Mullin, 2001; Beckmann, 2013).

When already existing particles are involved in the nucleation, it is called secondary nucleation, and is often faster compared to primary nucleation. Nucleation can also be obtained artificially by mechanical shock, agitation, or temperature or pressure change. In cooling crystallisation, the saturation point of the system is crossed, leading to the supersaturation and formation of nuclei (Lee et Myerson, 2006; Mullin, 2001; Beckmann, 2013).

Recent studies have indicated that the nucleation of solute includes two steps instead of the classical nucleation theory, which has a weakness of creating too straightforward assumptions of the formation of crystals (Figure 14). First step is the creation of a droplet of dense liquid, metastable with respect to the crystalline state. During the second step inside the droplet a three-dimensional lattice structure is formed. (Lee et Myerson, 2006, Vekilov, 2010)

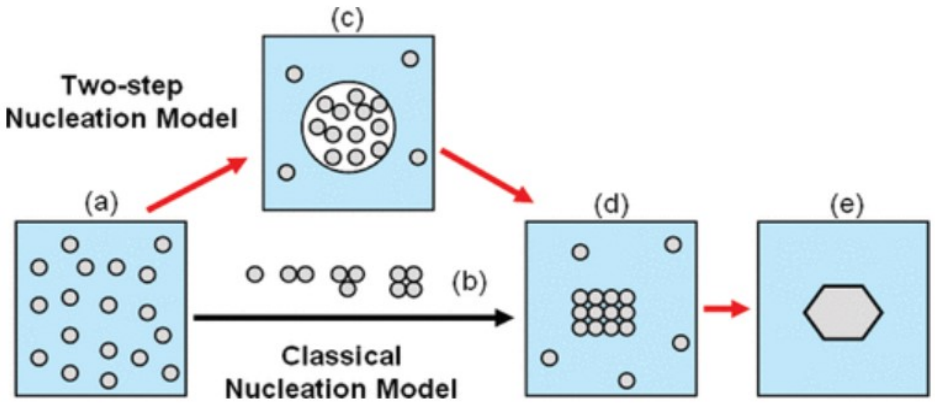

Figure 14 Crystal formation via different pathways: a) supersaturated solution b) classical nucleation theory, where the subcritical cluster of solute molecules are organised c) liquid-like cluster of solute molecules in denser or supersaturated environment d) ordered crystalline nuclei e) solid crystal (Erdemir et al, 2009)

As the two step theory expects, crystal formation starts from the denser droplet in the solution. This type of local supersaturation, where the concentration of the solute is higher

in certain areas in the solution, creates spots where the nucleation can occur. In cases where the crystal nucleation is not desirable, mixing of the solution prevents the formation of local supersaturation points. (Lee et Myerson, 2006; Vekilov, 2010)

The nucleation behaviour in the system is sometimes affected by the impurities present. Cations with high charge can have an inhibiting effect on the crystallisation, as well as there is often a threshold concentration of impurity above which the hindering effect may reduce. The primary nucleation may be suppressed by the impurities present, but often the secondary nucleation takes a place using the impurities as the seeds for nucleation. (Mullin, 2001)

5.2 Crystal growth

The characteristics of the crystal shape are a result of the regularity of the internal structure: Often the crystals have smooth surfaces developing as the crystal grows, indicating the atomic planes in the lattice, as the growing face is parallel to the lattice. Although it must be remembered that some crystals present no symmetry at all, and some may have several different axes and planes of symmetry around the centre. (Mullin, 2001)

There are many proposed mechanisms for crystal growth. Diffusion theories are common, in which the presumption is that material is deposited constantly on a crystal face at a rate dispensing on the concentration difference between the point of deposition and the bulk system. Another common type of theories are adsorption-layer theories (Figure 15), where the growth is taking place layer by layer on the crystal surface due to the adsorption and later the molecules, atoms or ions will link into the attractive centres of the lattice according to the attractive forces. Study of crystal dissolving led to the theory that crystallisation can be divided into a two-step process: bulk diffusion followed by a surface reaction at the growing crystal face (Mullin, 2001). Crystal growth happens when the cell units from the mother phase transport to the nucleus. Therefore, the crystal growth is affected by the viscosity of the mother liquid as well as the temperature and density. (Beckmann, 2013)

In the real world the lattice formed from cell units is not perfect. The crystal structure contains a variety of lattice defects having slightly different properties e.g., density. The properties of a crystal are determined via these defects, and they also influence the crystal growth. These so-called screw locations (Figure 15) are a permanent source of steps at which

growth occurs. The growth layer in the screw location creates another step on the crystal face, which will then roughen thermally and grow at low supersaturations. Often one crystal has several screw locations on its face. (Lee et Myerson, 2006; Beckmann, 2013)

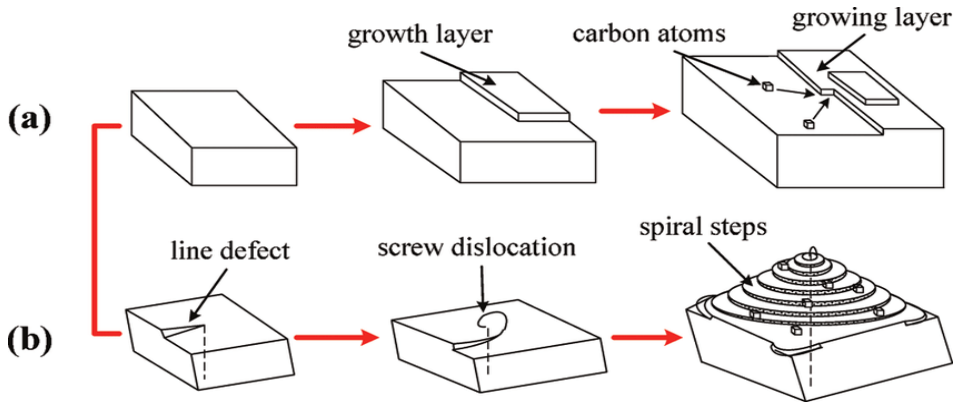

Figure 15 Possible growing routes for a crystal. A) Presents adsorption layer theory, and B) presents the screw dislocation in the growth. (Liu et al, 2011)

The growth of a crystal can be rapid or slow, and the relative size of a crystal face can vary. The variation of the faces and growth rate is called a modification of habit, and it is affected by the environmental parameters like temperature. (Mullin, 2001)

The relevant relationships between crystals and/or particles in the solution are presented in the Figure 16.

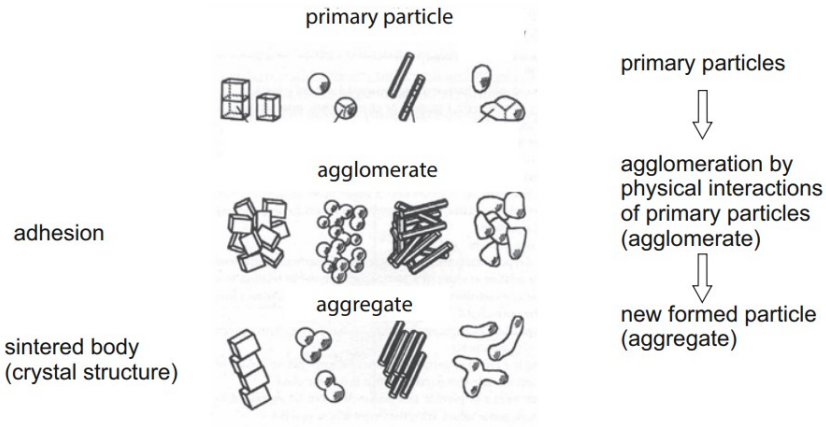

Figure 16 Relationship between individual particles, agglomerates and aggregates. (Walter, 2013)

Primary particles in the solution are agglomerating into larger units by weak physical interactions (adhesion), and therefore referred to as agglomerates. Due to the weak interactions, agglomerates are not permanent, but can differ in size and shape. The conditions in the solution affect the appearance of the agglomerates. After the particles form larger crystalline structures, they are referred to as aggregates. The formed aggregates are more stable, as the primary particles are firmly fused together. (Walter, 2013)

5.3 Crystallization of citric acid

Citric acid crystallises into two forms: anhydrous and monohydrate citric acid. In the anhydrous form, proper polymorphism is not involved but the formed crystal form is stable above 34 °C and crystallises into monoclinic prisms. This form of citric acid crystal is favourable in lower supersaturation levels and the formation of crystals is faster compared to the monohydrate crystals. The monohydrate crystalline form is stable at lower temperatures and forms rhombic prisms and is often present in higher supersaturation levels. Therefore, citric acid is following Ostwald's rule of stages, where the less stable crystalline form is formed first. (Macarigue et al, 2020)

The crystallisation of citric acid seems to be dependent on the temperature and even more of the level of supersaturation. In general terms, lower supersaturation levels show longer induction times in the solution compared to higher supersaturation levels. (Macarigue et al, 2020)

The use of citric acid and citrates has been studied in many fields. For example, in the medical industry it was discovered that citric acid prevents the crystal growth of struvite, which is a component of kidney stones. It was also noticed that the induction time increases with the amount of added citric acid, and the induction time can be shortened by more effective mixing. The preventing effect of citric acid was noted to be its adsorption to the surface of the struvite, preventing the crystal from growing. (Li et al, 2019; Viani et al, 2022)

Viani et al (2022) noticed that the gradual addition of citric acid created changes in the morphology and size of formed crystals; the size of crystals was seen to be connected to the added amount of citric acid.

In the study by Li et al (2019), it was recorded that in an aqueous solution, two or three carboxyl groups of citric acid were ionised and after that these groups formed hydrogen bonds with water molecules and then coordinated to the metal ion. The hypothesis in the study was that these carboxyl and hydroxyl groups in the middle of the CA molecule are the vital factor defining the nucleation process which involves a metal ion, particularly the formation and aggregation of clusters (Li et al, 2019). Citrates can then be formed with divalent metal ions (Krom et al, 2000).

6 Experimental work

The purpose of this chapter is to present the methods and materials used in this study. The experimental plan and choices made during the test period are presented and justified, alongside with the laboratory test equipment.

The experimental work conducted in this thesis is aiming to fulfil a knowledge gap related to the behaviour of citric acid and its citrates during the bleaching and drying procedures and their possible effect on filtration later in the process. The research plan included multiple test runs, where several factors were tested: citric acid concentration, the amount of water addition, mixing speed, and mixing time. The research experiments were carried out with purified palm oil, later with FFA addition (palmitic acid) and metal addition, alongside with two technical feedstocks from the refinery.

6.1 Materials, equipment and feedstock

Experimental research in this study focused on the behaviour of citric acid and metal citrates during the bleaching and drying procedure, and how they affect filtration. The experiments were planned to describe the effect of one parameter at a time, e.g., the amount of citric acid, mixing speed or amount of metal in the feedstock.

The basic series of experiments were carried out with refined, bleached and deodorised palm oil (RBDPO). The experimental plan can be divided into several series:

- The first experiment series was completed with only RBDPO (100 w %), called “the basic series”.
- The second set of experiments had FFA (10-30 w %) addition in the RBDPO
- The third experimental series had metal addition alongside the RBDPO (90 w %) and FFA (10 w %). The metal addition used was either Na-stearate or Ca-stearate.
- The fourth experiment series included technical feedstocks. The feedstocks used were animal fat (AF) and brown grease (BG).

Citric acid was obtained from Merck as a 50 % aqueous solution and used as such. The bleaching earth used was an industrial grade sample from one commercial supplier. Feedstock and chemicals are presented in Table 1.

Table 1 Feedstock and chemicals

Material	Information
RBDPO	(2880) RBDPO
AF	(2919) Animal Fat
BG	(2629) Trap Grease
Citric acid (CA)	Merck KGaA 50 %
Bleaching earth (BE)	Commercially available acid activated BE

The following equipment have been used in this study:

1. The Silverson L5M-A high shear mixer (Figure 17 A) unit included an oil bath for the vessel (500 mL), magnetic stirrer, a temperature sensor and the mixer itself (0-9600 rpm). The unit is batch-based setup, and its capacity is from 1 mL up to 12 L with flowrates up to 20 L/min (Silverson, 2023)

2. The bleaching and drying took place in a three-neck flask (500 ml) that was set into an oil bath (85-105 °C). The flask was connected to a pressure control unit (800-80 mbar) and equipped with a temperature sensor and magnetic stirrer (Figure 17 B).

3. The equipment used for filtration was a batch pressurised filtration equipment. This equipment included the filtration chamber (max volume 200 ml) with a filter net, oil circulation for heating (105 °C), a temperature sensor, a pressure regulator and a balance. The desired pressure was adjusted with nitrogen (1-2.5 bar). The filtration equipment was equipped with a data collection program, which collects the data from the balance as a function of time (Figure 17 C).

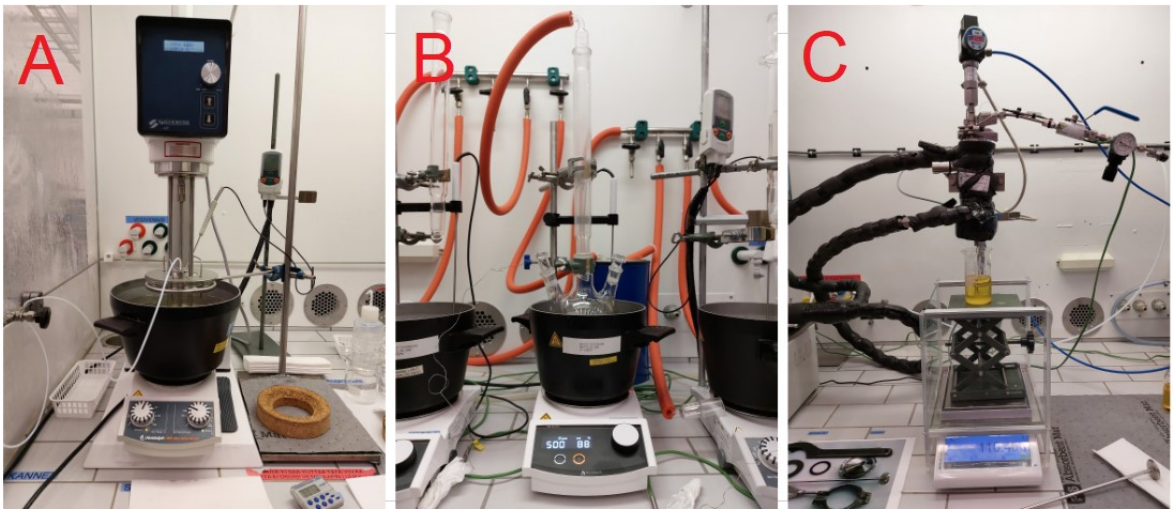

Figure 17 A) High shear mixer with oil bath and the vessel, B) Three-neck flask in the oil bath for bleaching, C) batch filtration equipment

All the equipments used are batch-based and constantly monitored by an operator.

6.1.1 Pixact

Pixact analysis is based on high-magnification imaging of liquids and suspensions by real-time computational image analysis. Pixact can be used for detecting particles, crystals, bubbles or droplets. As a measurement, it is easy to use and requires less advanced operating. The measurement can be performed online, and the data from the sample is immediately ready to be processed after the measurement is finished, or in online measurement, quickly after the measurement moment. The program connected to the equipment is highly automatized to detect particles from the solution. The Pixact measurement is based on optical imaging, more precisely dynamic image analysis presented in the chapter 4.1.4. (Pixact)

Pixact includes a Pixscope probe as an imaging unit and a computer with Pixact measurement software installed. For example, the following parameters can be recorded: particle size average and particle count as a function of measurement time, concentration, normalised arithmetic and volumetric size histograms, particle roundness and coarseness histograms and particle aspect ratio histogram. A hot plate with a magnetic stirrer was added to the systems, to ensure that the liquid is moving during the measurement. This is done to prevent the program from remeasuring the same particle multiple times. The samples were

kept at least in 60 °C during the measurement, some of the samples required even more heating than the others.

6.2 Procedure

Test runs were accomplished according to the standard bleaching and filtration procedure. In the beginning, basic conditions were determined (Table 2), as it was decided that one parameter is changed at once. Otherwise tracking down causal causes can be difficult. Some test runs used only part of the whole procedure.

Table 2 Basic condition of an experiment

Concentration of CA	Water addition	High shear mixer conditions	Bleaching and drying procedure	Filtration
1000 ppm	0.5 w %	8000 rpm for 2 min → after that slow mixing with magnetic agitator 250 rpm for 5 min	- 85 °C / 800 mbar for 20 min with BE added (1 w %) - Pressure change to 80 mbar, temperature lift 85 °C → 105 °C (10 min) - Hold in 105 °C for 15 min	- Pre-cake done with RBDPO and 1 g of BE - Filtered in 100 °C / 2.5 bar pressure

Feedstock was heated and mixed in the beginning. After that, the first Pixact measurement took place. After Pixact measurement, the feed was carried to the first step of the pretreatment process, the acid treatment. In the acid treatment, amounts of CA and RO (reverse osmosis) water were added to the oil according to the calculations made, to reach a desirable concentration of CA and water. The temperature in the acid treatment was set to 85 °C in the presence of nitrogen. After the additions, the feed was mixed with a high shear mixer first for 2 minutes using 8000 rpm, followed by 5 minutes with a magnetic stirrer (250 rpm).

After acid treatment, the acid and water dosed oil was studied with Pixact. When the Pixact measurement was ready, the bleaching and drying steps took place. First, the oil was heated to 85 °C. After reaching the desired temperature, either the bleaching earth was added or if the bleaching step was skipped, the drying procedure was started. In the bleaching procedure, 1 w% of bleaching earth was added to the oil and then mixed with a magnetic stirrer (500 rpm) for 20 min in 800 mbar. The bleaching step was followed by a drying procedure, where the temperature was increased from 85 °C to 105 °C while the pressure was decreased to 80 mbar. The temperature increase took 10 minutes, and the oil was kept at 105 °C for 15 minutes.

The last step of the pretreatment procedure was filtration. First, the pre-cake was made with 150 g of RBDPO with 1 g of bleaching earth added. The pre-cake is made according to two-step procedure: First the oil is filtered once in 1 bar, and then the product is refiltered in 2.5 bar, to make sure that all the earth remains in the cake. When the pre-cake is ready, the filtration of the feed takes place in 2.5 bar. Feed is filtered only once, and from the collected data, filterability resistance is calculated. When the filtrate was ready, it was measured with Pixact once more, before sending the sample to the analysis.

7 Results and discussion

This chapter includes the descriptions of test runs made for the thesis, and presents the main results gained from the experiments. The full version of the experiments done for this thesis can be observed in Appendix 1.

7.1 Basic series and filtrations

The effect of condition change was studied during the series of experiments called the basic series. This experiment series consisted of 17 points where one variable was changed, followed by four filtration tests. The 17 basic experiments included acid treatment and drying procedure, to study the behaviour of liquid during the variable change. Bleaching was not introduced to these points due to the blinding effect of the bleaching earth to the Pixact measurement. With the following four filtration tests, normal bleaching and filtration procedure was performed.

Before starting the experiments, RBDPO and citric acid were analysed with Pixact (Figure 18) in case there were already existing particles that could later cause problems while analysing the results. As can be seen in Figure 18, no particles were detected.

Figure 18 Crude RBDPO before pretreatment on the left, citric acid on the right

The samples were analysed with Pixact after the acid treatment and after the drying procedure. In all experiments RBDPO was used as a feedstock.

7.1.1 Variable: Citric acid

The experiments presented in this chapter are described in Table 3. Drying procedure is defined “as usual” referring to the drying procedure described in Table 2.

Table 3 Basic series - citric acid as a variable. Experimental parameters.

Exp no.	Feed	CA addition (ppm)	Water addition (w %)	Drying	HSM speed (rpm)	HSM time (min)
1	RBDPO	0	0.5	as usual	8000	2
2	RBDPO	500	0.5	as usual	8000	2
3	RBDPO	1000	0.5	as usual	8000	2
4	RBDPO	2000	0.5	as usual	8000	2
5	RBDPO	4000	0.5	as usual	8000	2

The citric acid addition tests were performed with variables 0 ppm, 500 ppm, 1000 ppm, 2000 ppm and 4000 ppm of citric acid added to the oil. The amount of citric acid was calculated with an internal calculation sheet for bleaching, in which the water content of citric acid solution was noticed. The citric acid used in the experiments was 50 % aqueous blend.

The water addition, high shear mixer setting and drying procedure were kept as constant in all experiments presented in this chapter, as they were presented in Table 2. The water addition did not include the amount of water present in the citric acid solution, but is extra water added to the solution during acid treatment.

In the experiment 1 (Figure 19), the CA addition was 0 ppm, and no extra particle formation was discovered. No visible water evaporation during the drying step was noticed. The oil itself was clean and bright.

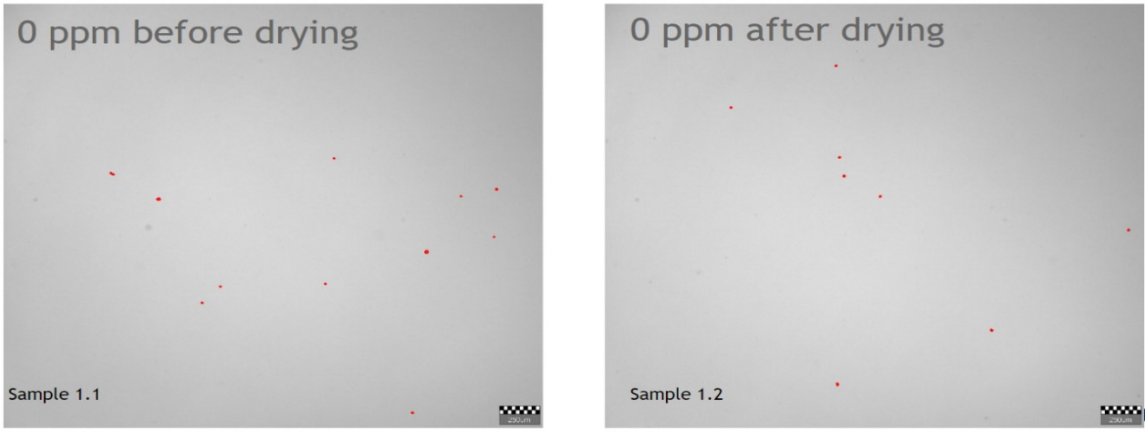

Figure 19 Exp 1, on the left there is the sample after acid treatment and on the right after drying. Feedstock in the experiment is RBDPO and the CA addition 0 ppm.

In the Exp 2, 500 ppm of CA was added during the acid treatment. The amount of particles slightly increased in the oil (Figure 20), the drying step did not seem to have any effect on the amount of particles. No visible evaporation of the water during the drying, the oil looked a bit blurrier compared to the exp 1.

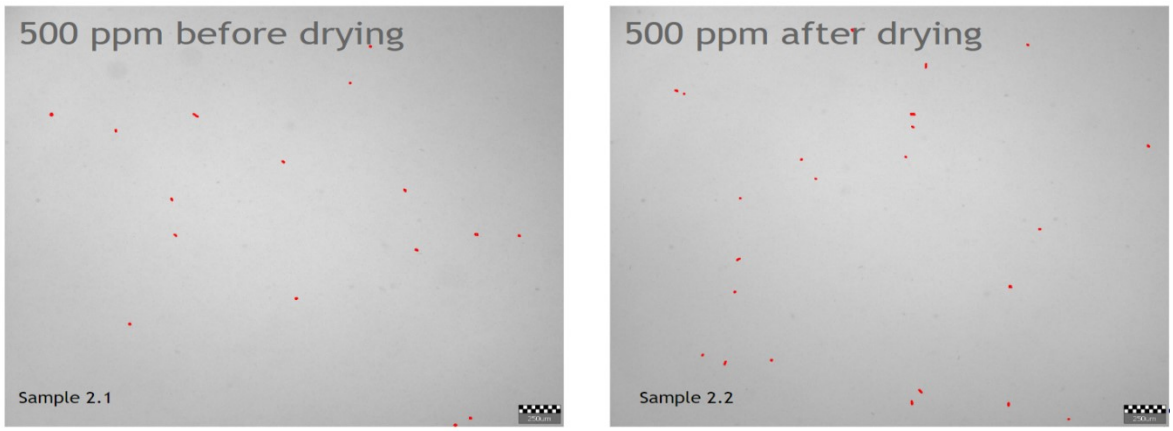

Figure 20 Exp 2, on the left there is the sample after acid treatment and on the right after drying. Feedstock in the experiment is RBDPO and the CA addition 500 ppm.

In the Exp 3, shown in the Figure 21, 1000 ppm of CA was added during the acid treatment. A notable amount of small particles were formed in the oil during acid addition. The drying seems not to have any visible effect on the particle size distribution. No visible water evaporation during the drying step.

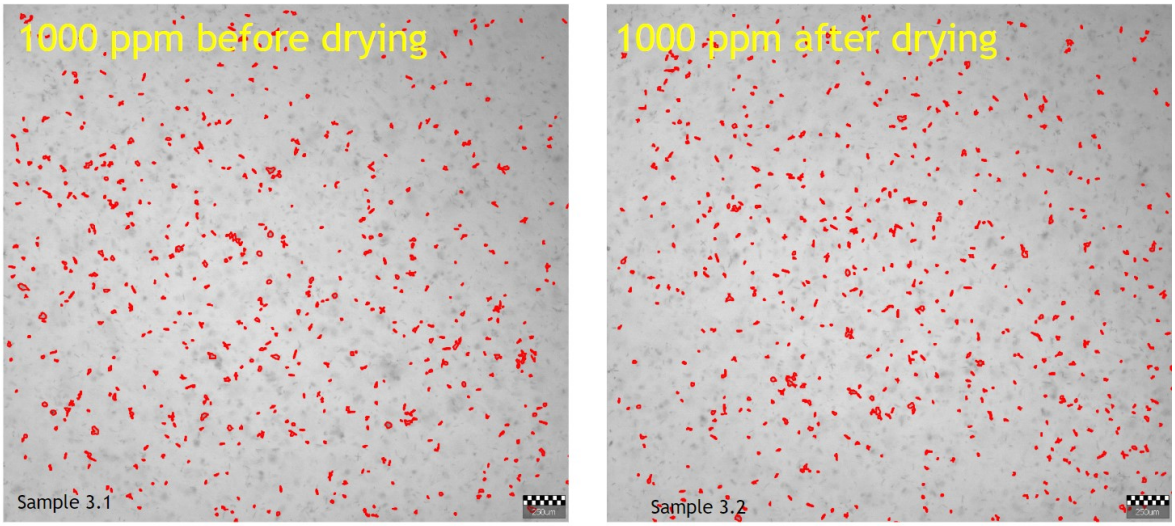

Figure 21 Exp 3, on the left there is the sample after acid treatment and on the right after drying. Feedstock in the experiment is RBDPO and the CA addition is 1000 ppm.

The Exp 4, where 2000 ppm of CA was added to the solution, showed an interesting view into the particle formation. The particles formed clusters or agglomerates during the measurement. In the beginning (Figure 22, 0 minutes), there were a notable amount of small particles, and it can be seen that the size of particles increased during the 2 minutes in analysis. The drying did not seem to impact the formed agglomerates. During the drying step, a visible evaporation of water was noted.

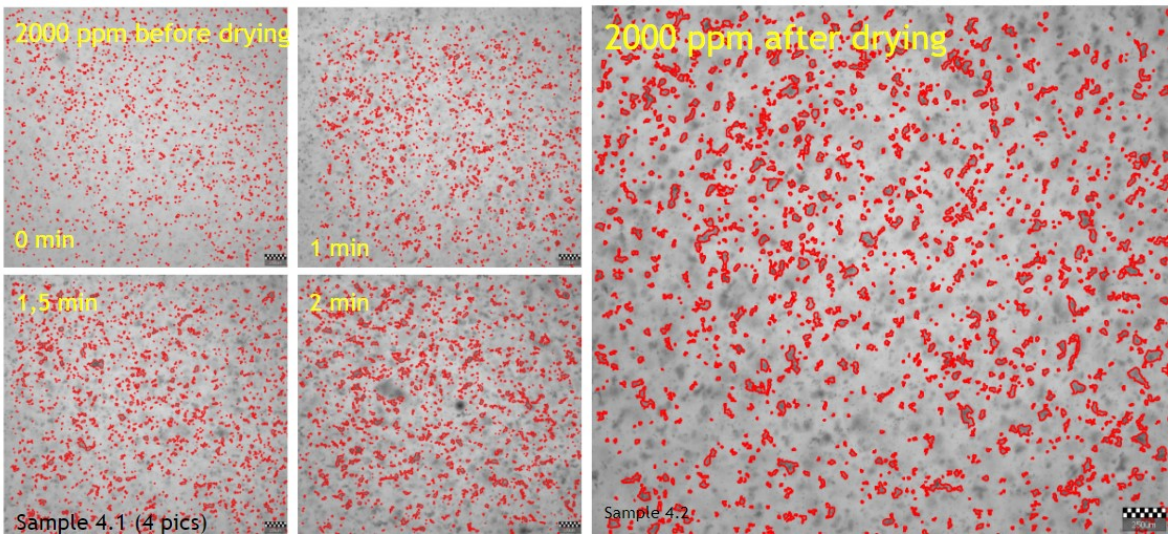

Figure 22 Exp 4, on the left is the sample after acid treatment (4 small pictures) and on the right after drying. Feedstock in the experiment is RBDPO and the CA addition is 2000 ppm.

The similar effect of time was seen in the exp 5, where 4000 ppm of CA was added to the solution. The particle formation from small units to larger agglomerated can be seen in just a few minutes (Figure 23). This experiment was repeated with a longer measurement time (Figure 24) to see if the size of agglomerates stabilized during the time.

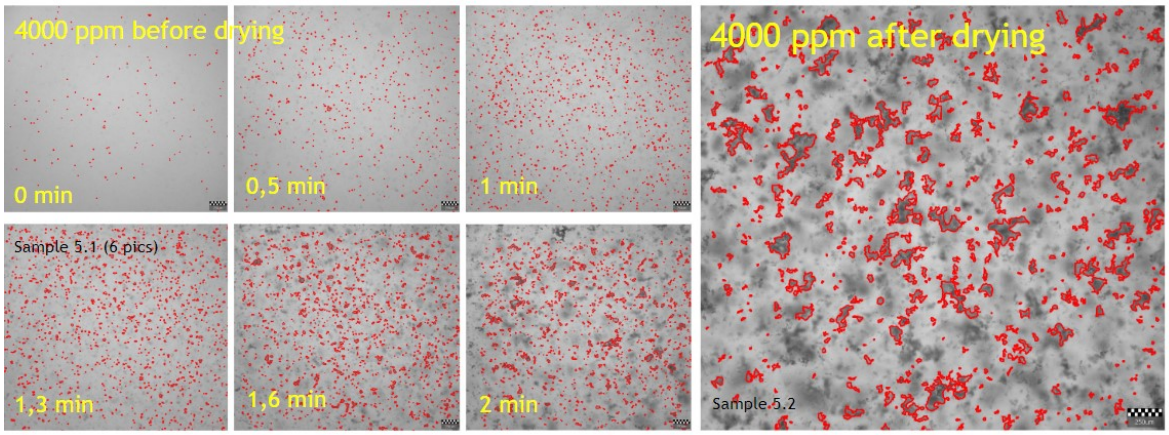

Figure 23 Exp 5, on the left is the sample after acid treatment (6 small pictures) and on the right after drying. Feedstock in the experiment is RBDPO and the CA addition is 4000 ppm.

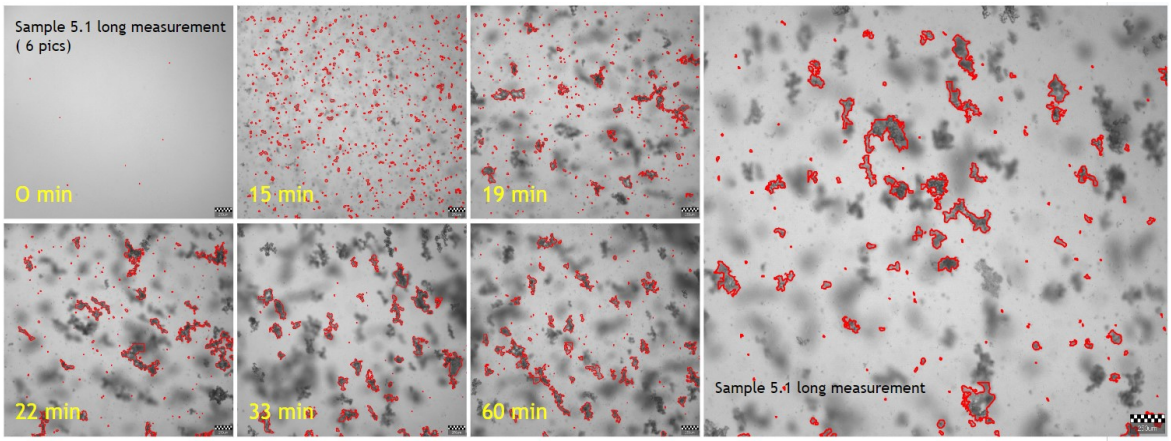

Figure 24 Exp 5 with extended measurement time. On the left after acid & water additions (6 small pictures) and on the right after drying

They were seen to reach their stable size during the measurement (Figures 25 and 26). In this experiment 8 with longer Pixact measurement time, an interesting observation was that the formation of particles did not start until almost 15 minutes. In other experiments, the particles were already visible in a couple of minutes. After 19 minutes, the amount and size of particles have reached their maximum size and no changes in these were observed later. The measurement took 60 minutes. After that the solution was dried according to the standard procedure. Pixact measurement from the dried product was prolonged to 30 minutes, but no changes were seen in the solution during that time.

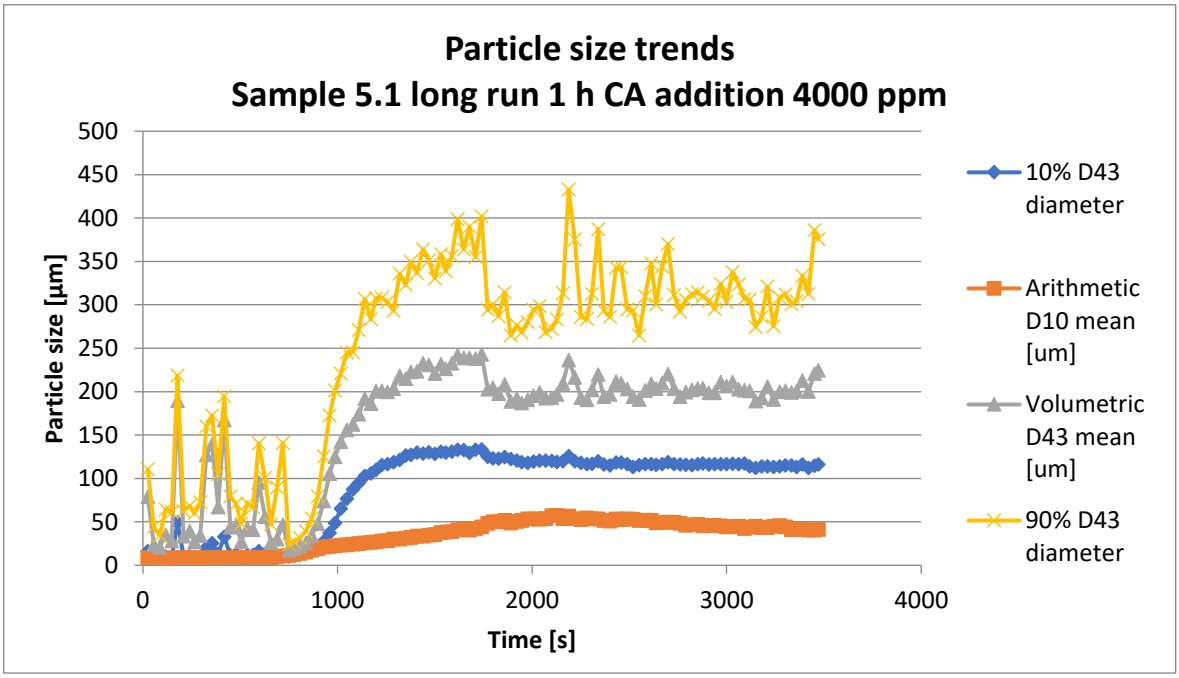

Figure 25 Increase of particle size from 0 to 50 µm during 1 h measurement time in the Pixact measurement. The size of the particles seem to stabilize after 20 minutes. 10 % and 90 % of D43 diameter are showing the minimum and maximum values for the volumetric D43 mean diameter.

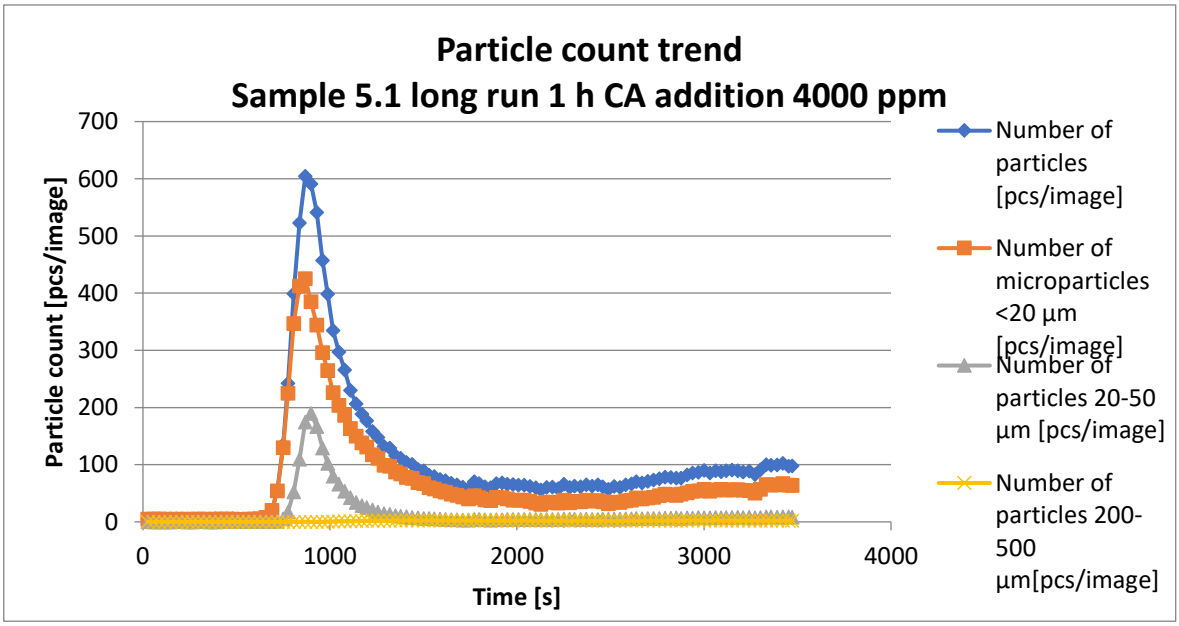

Figure 16 Particle count during the Pixact measurement. The number of counted particles (from 0 µm to 400 µm max) stabilized after 30 minutes.

The normalized arithmetic size in Figure 27 shows how the particles with different sizes are divided in each sample. It can be seen that the amount of particles with small diameter are more present in the samples with lower CA addition, whereas the samples with higher CA additions have a larger amount of bigger particles (Figures 21-24). The larger size of the particles in higher concentrations of CA could indicate the formation of agglomerates in the sample.

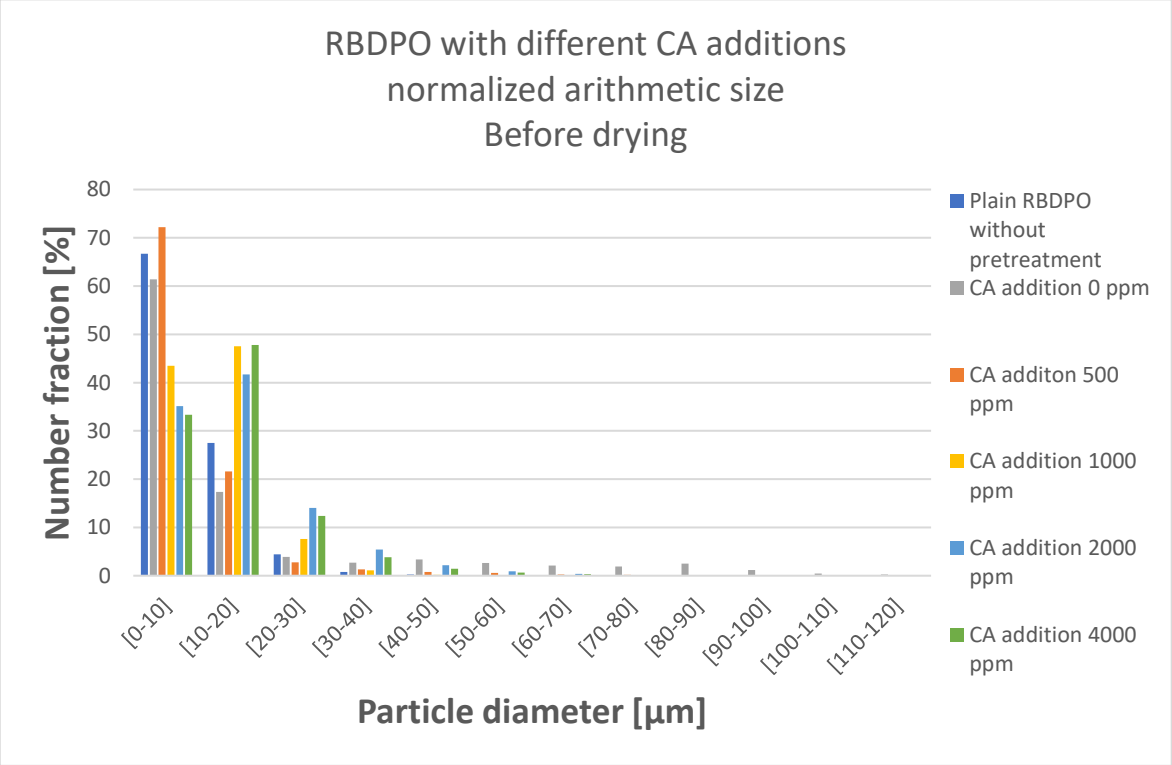

Figure 27 RBDPO with different CA additions, normalized arithmetic size data obtained from Pixact measurement. Data from the samples before the drying procedure.

Figure 28 presents the same samples after the drying procedure. When comparing Figures 27 and 28, one can notice that the size distribution before and after the drying procedure remains quite similar.

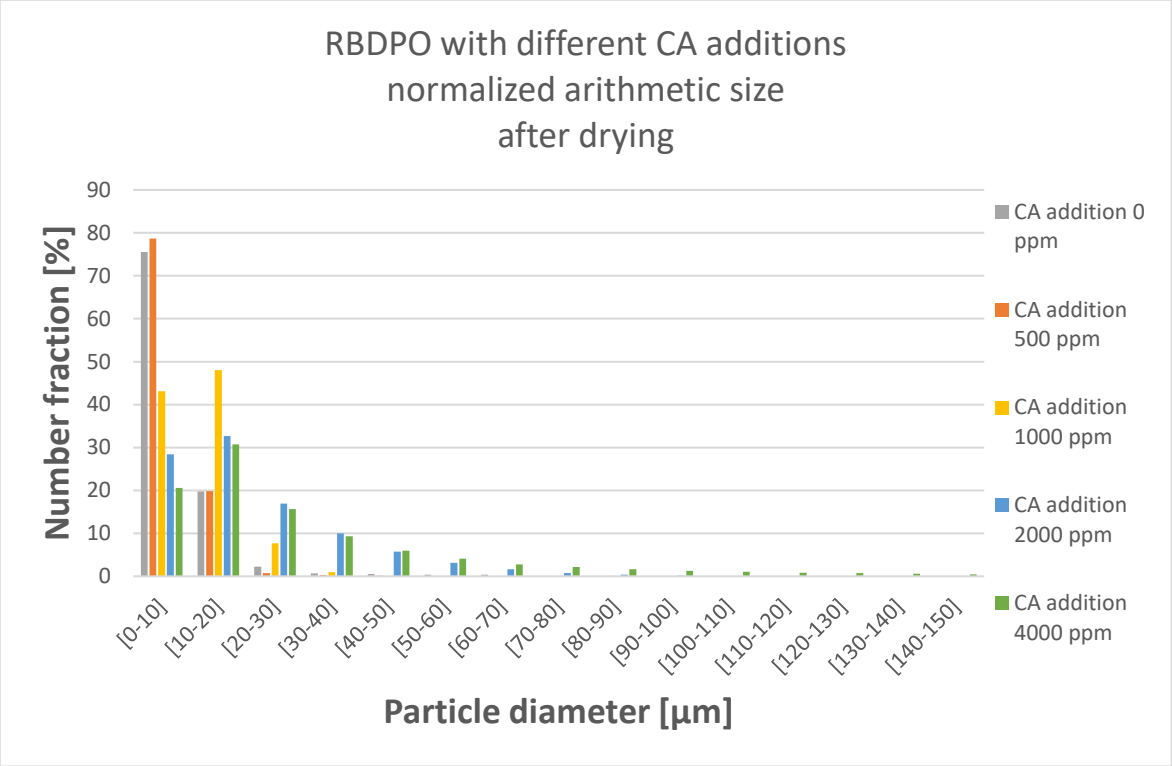

Figure 28 RBDPO with different CA additions, normalized arithmetic size data obtained from Pixact measurement. Data from the samples after the drying procedure.

The effect of the drying procedure can be observed more deeply in the Figures 29 and 30, where the normalized volumetric size distribution is presented. In Figure 29, the data is obtained before the drying procedure, and in Figure 30, after the drying. With small CA additions, the volumetric size of the particles is smaller compared to the samples with high CA addition. With higher CA additions, it is logical that the particle volume and diameter are increasing simultaneously. The sample with no CA addition has quite wide volumetric particle size distribution compared to the other low concentration samples, but this can be caused by the Pixact measurement also. As the numerical amount of particles is much smaller in this sample, one or two larger particles affect the distribution more than in other samples.

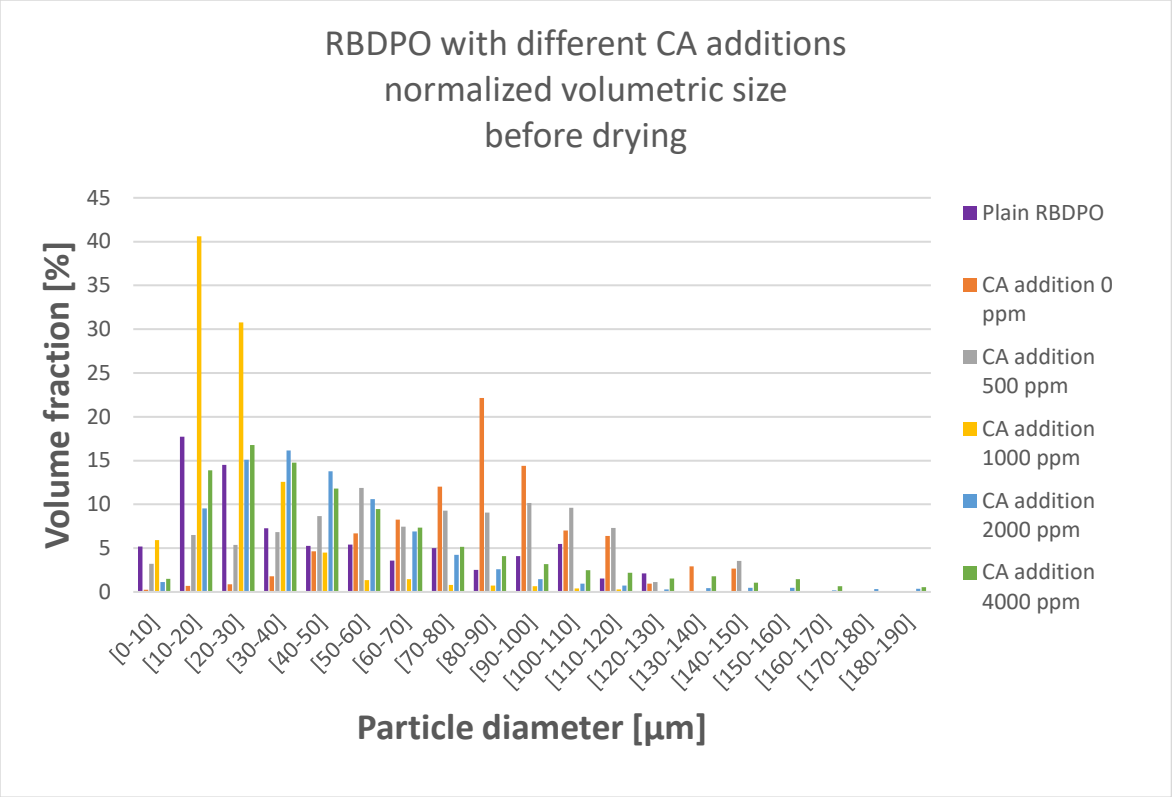

Figure 29 RBDPO with different CA additions, normalized volumetric size data obtained from Pixact measurement. Data from the samples before the drying procedure.

Figure 29 presents the situation after the drying procedure for normalized volumetric size distribution. When comparing Figures 29 and 30, one can notice that the volumes of particles present in samples having small CA addition are close to the same. The sample with no CA addition has interestingly some larger particles present after the drying procedure, which may indicate agglomeration of smaller particles to larger units. Similar behaviour can be seen in the sample with the highest CA addition. Although in this sample, the arithmetic size distribution presented in the Figure 28 indicates that the amount of particles is very small, and therefore one larger particle can affect the volumetric distribution quite much.

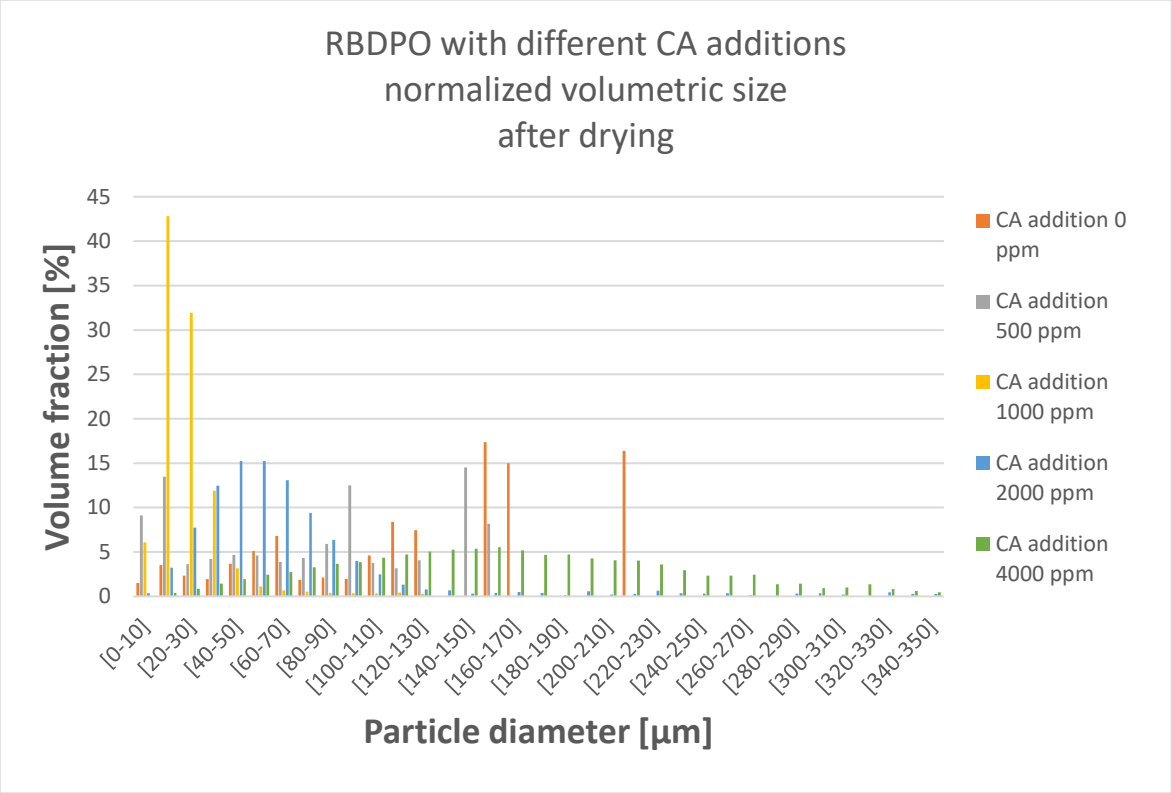

Figure 30 RBDPO with different CA additions, normalized volumetric size data obtained from Pixact measurement. Data from the samples after the drying procedure.

As a sum-up, in these experiments the amount of particles in the oil can be seen increasing while the concentration of CA is increased. The size of the particles also increased which may be caused by the agglomeration of small particles into larger clusters. The SEM (scanning electron microscope) analysis could provide more detailed information about the agglomeration. During time the growth of the particles fainted, and the size of the particles stabilised, as well as their amount in the solution. The drying step did not seem to remarkably affect the size distribution of the particles. It can be speculated that the mixing of the CA into the fat leads to the CA precipitation, so it precipitated out due to not being soluble in fat.

7.1.2 Variable: Water addition

The experiments presented in this chapter are described in Table 4. Drying procedure is defined “as usual” referring to the drying procedure described in Table 2.

Table 4 Basic series - water as a variable. Experimental parameters.

Exp no.	Feed	CA addition (ppm)	Water addition (w %)	Drying	HSM speed (rpm)	HSM time (min)
6	RBDPO	1000	0	as usual	8000	2
7	RBDPO	1000	0.5	as usual	8000	2
8	RBDPO	1000	1	as usual	8000	2
9	RBDPO	1000	2	as usual	8000	2
10	RBDPO	1000	4	as usual	8000	2

In this series of experiments, the amount of water added during the acid treatment was studied, as the other variables were kept as constant according to Table 2. The water additions were 0 w%, 0.5 w%, 1 w%, 2 w% and 4 w%, and the addition was done as a batch addition..

Experiment 6 showed similar particle formation compared to exp 3, presented in chapter 7.1.1. In the experiment 6 (Figure 31), there was no added amount of water, but it should be noticed that the CA solution used in the experiment contained 50 % of water. The similarity between exp 6 and exp 3 can depend on the similar amount of CA added to the solution. The absence of added water seems not to have any notable effect on particle formation before or after drying step.

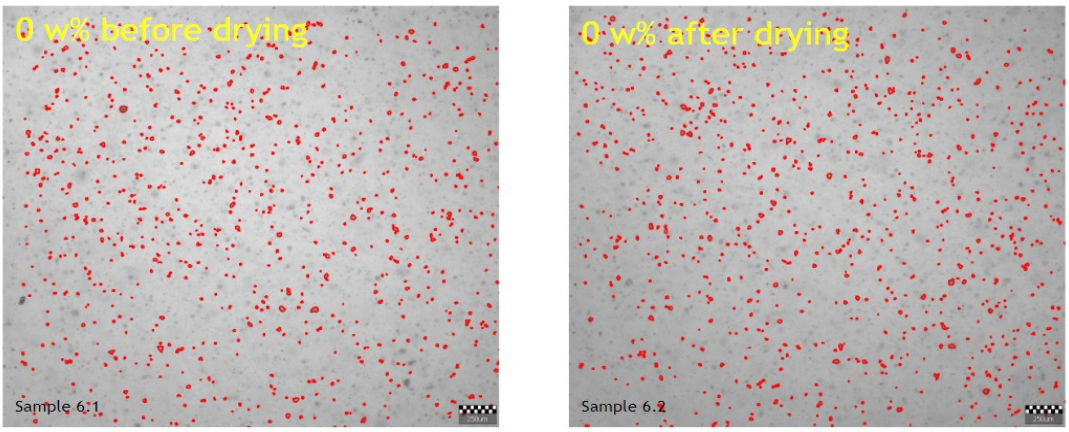

Figure 31 Exp 6, on the left there is the sample after acid treatment and on the right after drying. Feedstock in the experiment is RBDPO and the water addition 0 w%.

Exp 7, presented in the Figure 32, was a similar study point that the exp 3, with the same acid and water additions: 1000 ppm of CA and 0.5 w% of water added to the solution. The results gained are similar compared to the earlier point

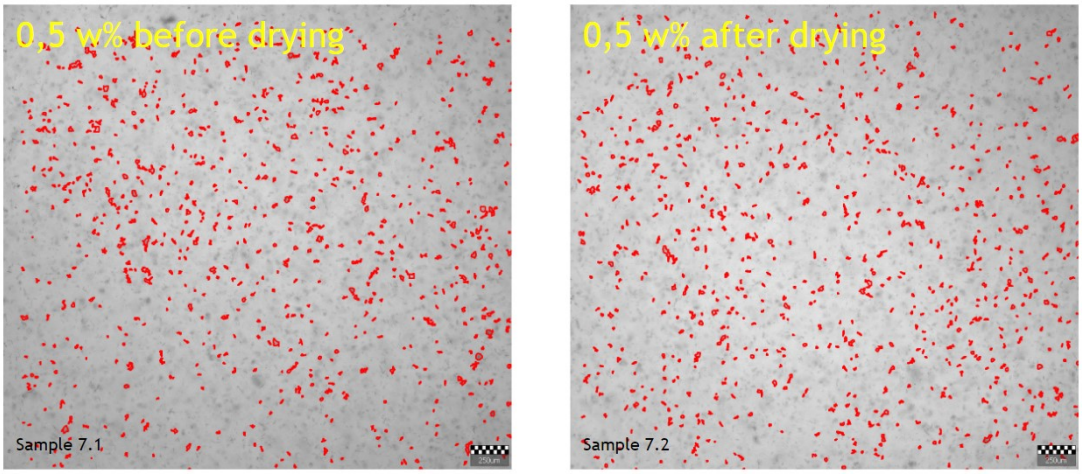

Figure 32 Exp 7, on the left there is the sample after acid treatment and on the right after drying. Feedstock in the experiment is RBDPO and the water addition 0.5 w%.

The effect of time was again seen in the exp 8 (Figure 33), where the particle formation took a few minutes. The CA addition was kept as constant but water addition (1 w %) was doubled

compared to what it usually was. The amount of water was nicely dispersed into the oil. There was no visible change in the particles after the drying.

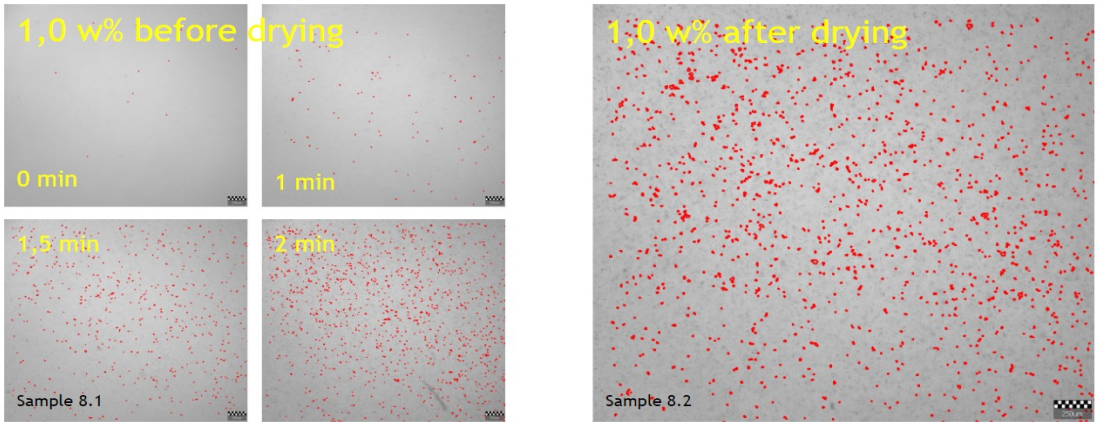

Figure 33 Exp 8, on the left there is the sample after acid treatment and on the right after drying. Feedstock in the experiment is RBDPO and the water addition is 1.0 w%.

In the Figure 34 the particle count data from Pixact measurement is presented from the experiments 6, 7 and 8, which had the water addition of 0 w%, 0.5 w% and 1 w% respectively. The Figure shows that the counted amount of particles is similar in experiments 6 and 7, but much lower in the experiment 8. The particle count trend after drying is similar for each experiment (Figure 35).

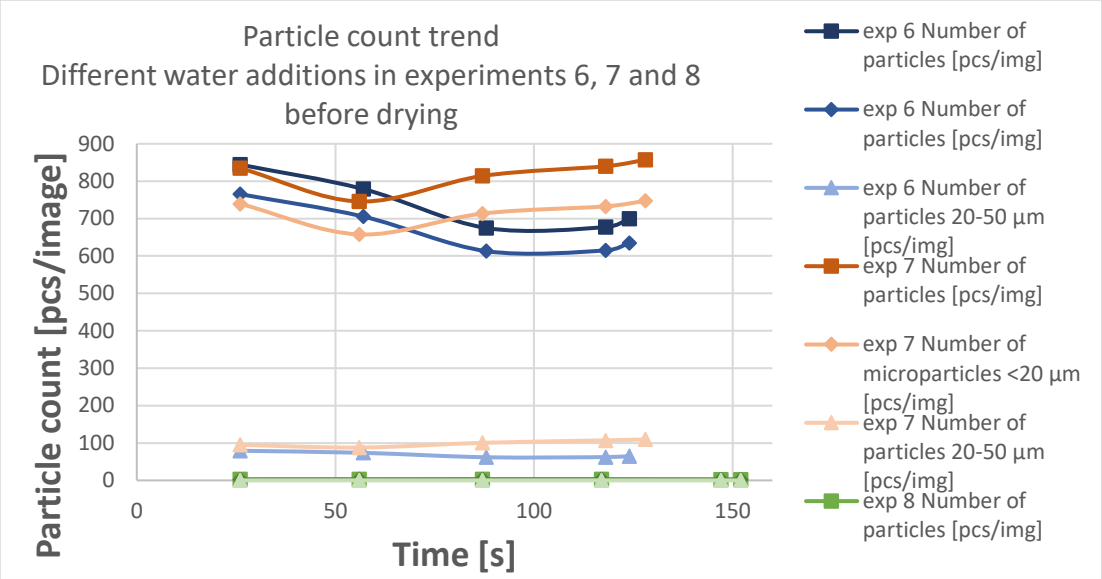

Figure 34 Particle count trends from the experiments 6, 7 and 8, with water additions 0, 0.5 and 1 w% respectively. Before the drying procedure.

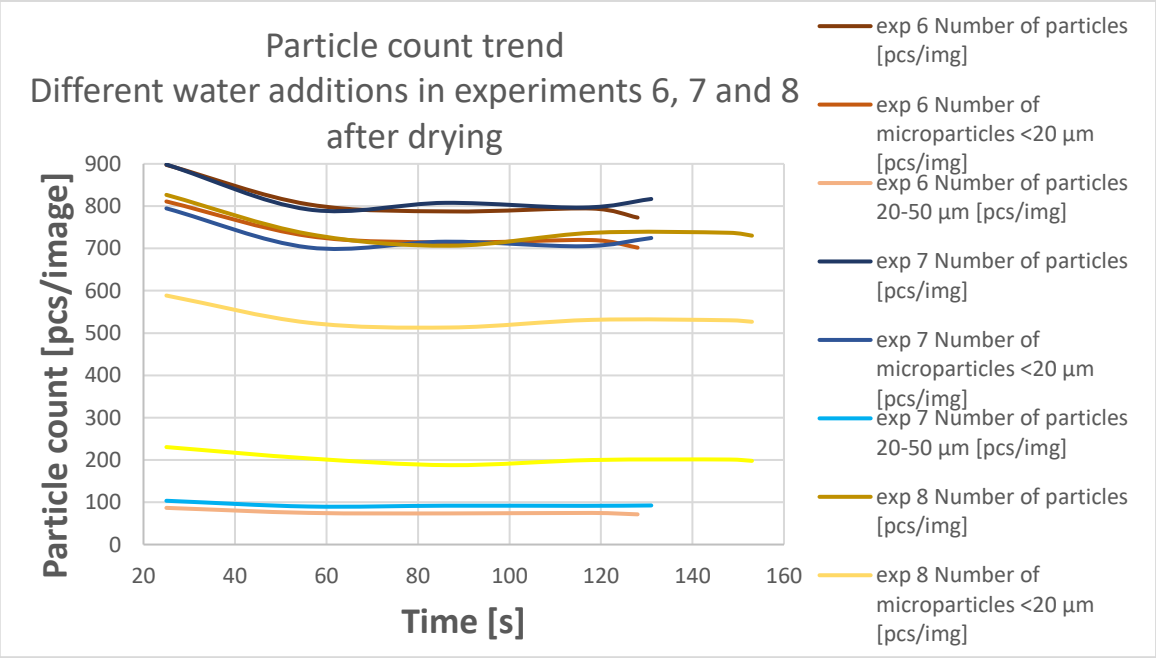

Figure 35 Particle count trends from the experiments 6, 7 and 8, with water additions 0, 0.5 and 1 w% respectively. After the drying procedure.

From exp 9 and 10 the Pixact measurement before the drying procedure was not successful anymore due to the excessive amount of water droplets in the oil (Figures 36 and 37). In

experiment 9, 2.0 w% of water was added to the solution, and in experiment 10, the added amount is 4.0 w%.

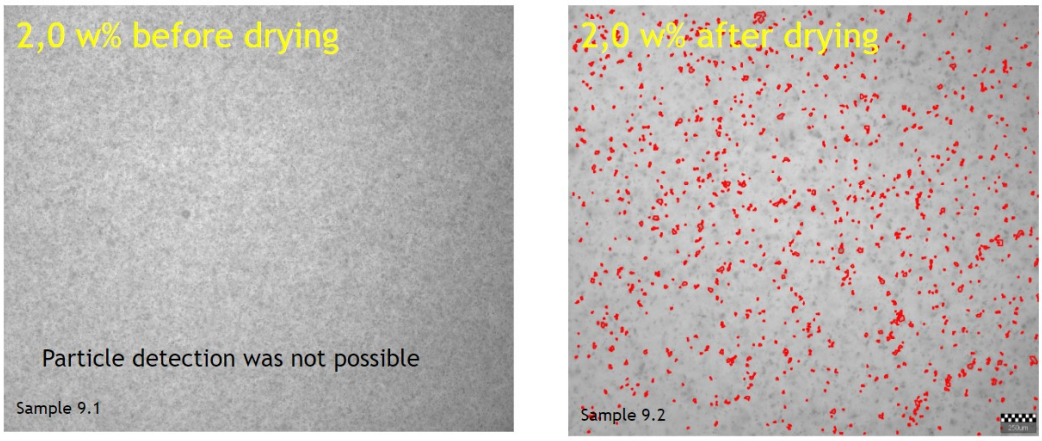

Figure 36 Exp 9, on the left there is the sample after acid treatment and on the right after drying. Feedstock in the experiment is RBDPO and the water addition 2.0 w%.

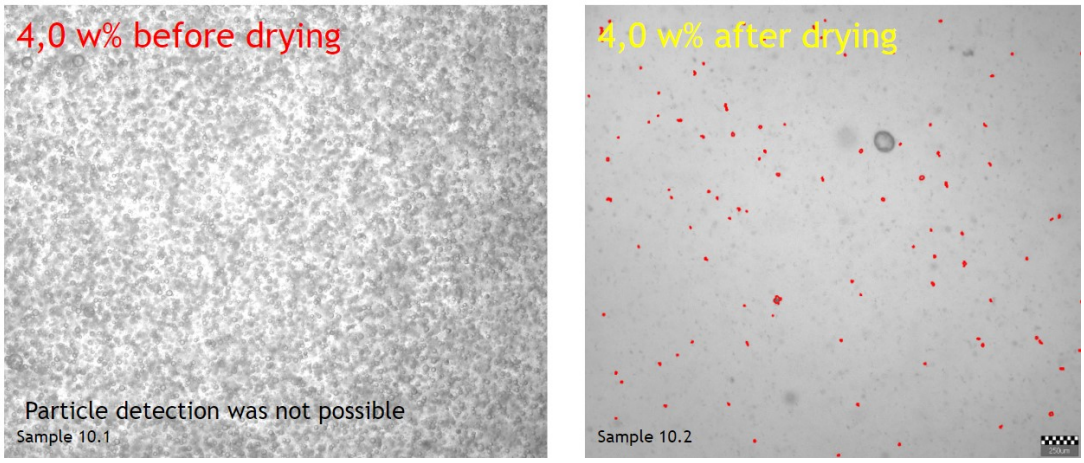

Figure 37 Exp 10, on the left there is the sample after acid treatment and on the right after drying. Feedstock in the experiment is RBDPO and the water addition is 4.0 w%.

Exp 9 was repeated with longer measurement time, and during 1 h measuring period, most of the droplets sank to the bottom of the vessel, leaving very little particles behind (Figure 38). Some water droplets remained in the solution after drying in exp 10. Mixing speed during the Pixact measurement needed to be reduced from 600 rpm to 400 rpm in order to

keep the droplets closer to the bottom. It is possible that some of the bigger particles sank to the bottoms with the water.

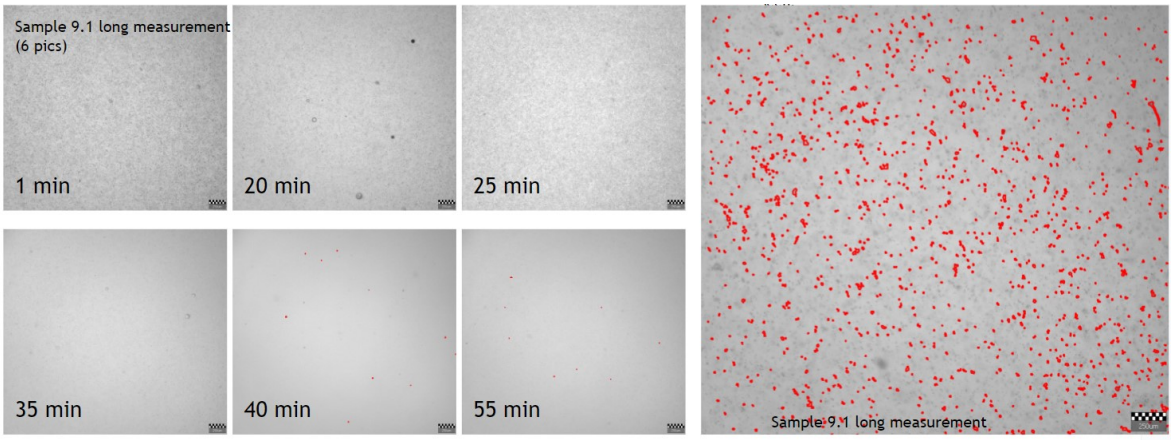

Figure 38 Exp 10 with prolonged Pixact measurement. On the left there is the sample after acid treatment (6 small pictures) and on the right after drying. Feedstock in the experiment is RBDPO and the water addition 2.0 w%. After 35 minutes Pixact measurement can recognize some small particles from the solution.

The normalized arithmetic size data obtained from the water addition experiments described in this chapter is presented in the Figure 39. From the Figure 39 one can notice that the size of particles before and after drying remains the same. The data is obtained from the experiments 6, 7 and 8. From the experiments 9 and 10 (2 and 4.0 w %), the excessive amount of water disturbed the Pixact measurement.

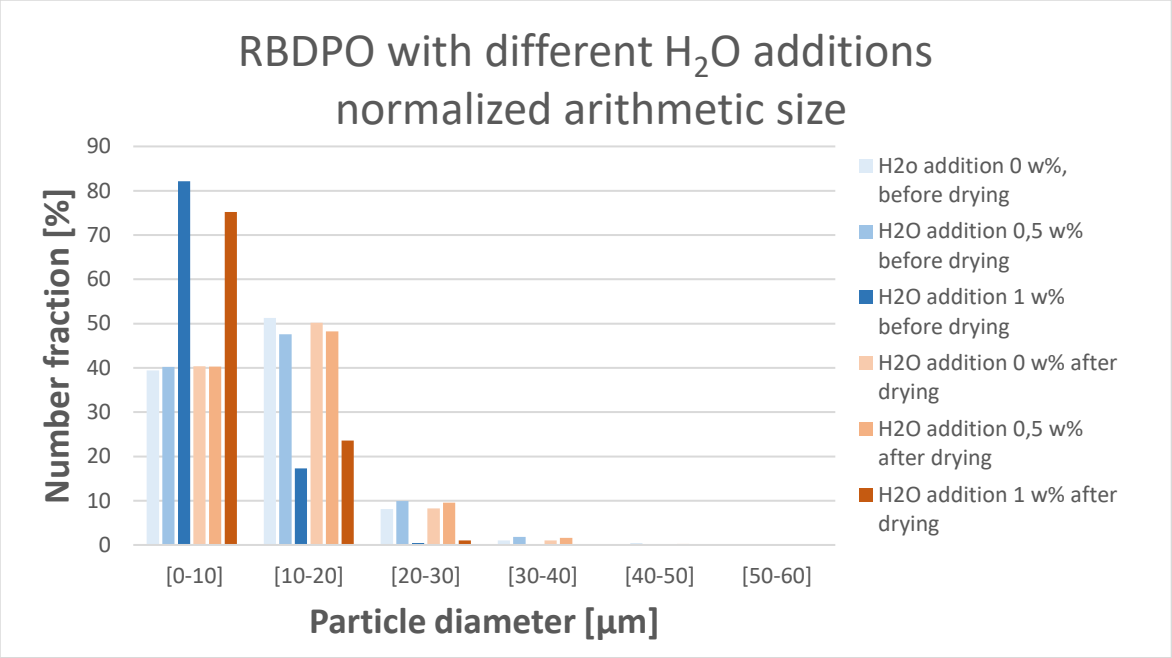

Figure 39 RBDPO with different water additions, normalized arithmetic size data obtained from Pixact measurement. Data from the samples before and after the drying procedure.

The volumetric size distribution for samples 6, 7 and 8 (0, 0.5 and 1.0 w% of water) is shown in the Figure 40. The volumetric size distribution before and after filtration remains similar for each sample, and one can assume that the particles are not swollen due to the presence of water.

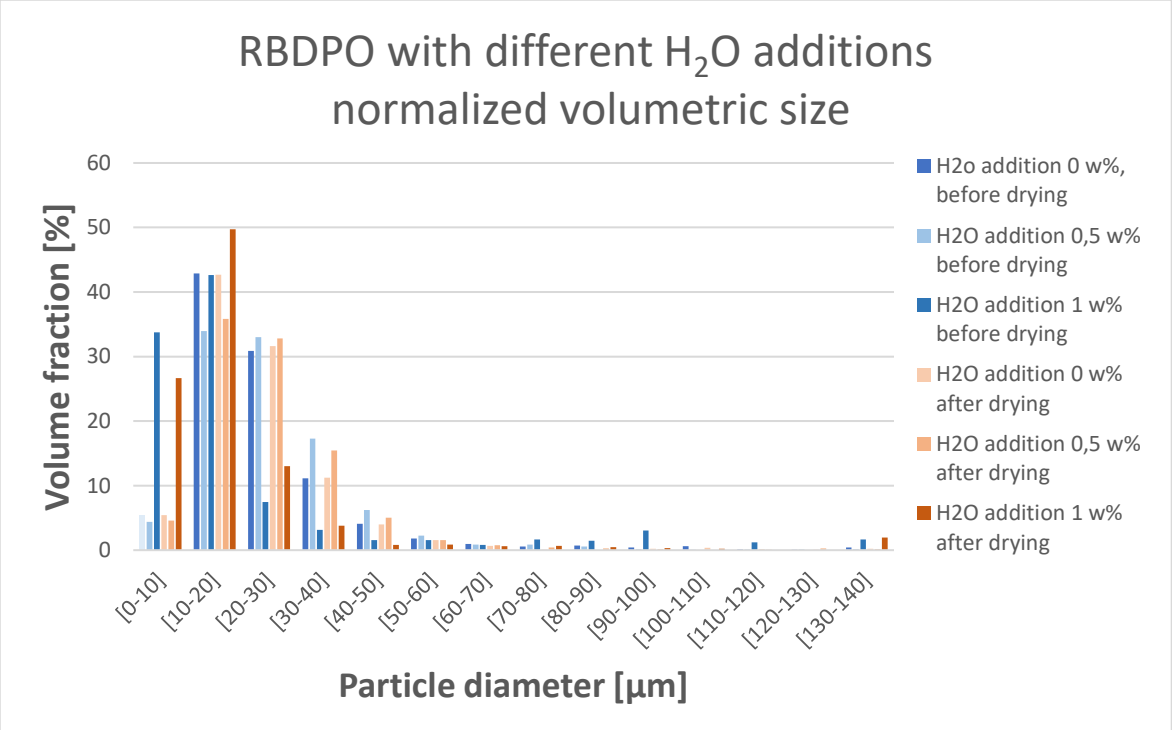

Figure 40 RBDPO with different water additions, normalized volumetric size data obtained from Pixact measurement. Data from the samples before and after the drying procedure.

As a sum-up, the amount of water seems not to have any notable effect on particle formation, but having much extra water disturbed the measurement, and therefore the effects of water could not be observed thoroughly.

7.1.3 Variable: High shear mixer speed and time

The experiments presented in this chapter are described in Table 5. Drying procedure is defined “as usual” referring to the drying procedure described in Table 2.

Table 5 Basic series - parameters of high shear mixer as variables. Experimental parameters.

Exp no.	Feed	CA addition (ppm)	Water addition (w %)	Drying	HSM speed (rpm)	HSM time (min)
11	RBDPO	1000	0.5	as usual	2000	2
12	RBDPO	1000	0.5	as usual	4000	2
13	RBDPO	1000	0.5	as usual	8000	2
14	RBDPO	1000	0.5	as usual	8000	0.5
15	RBDPO	1000	0.5	as usual	8000	1
16	RBDPO	1000	0.5	as usual	8000	4
17	RBDPO	1000	0.5	as usual	9600	1

The next experiment set ups focused on the effect of the high shear mixer used in the process. Two variables were studied: high shear mixing speed and time spent for mixing. Three speed ratios were tested (2000 rpm, 4000 rpm, 8000 rpm) and three time ratios (0.5 min, 1 min, 4 min). Each experiment was run separately. As before, other conditions were kept the same, and Pixact analysis was performed after acid treatment and after drying procedure.

In exp 11, where the HSM speed was only 2000 rpm, visible water droplets remained in the oil disturbing the Pixact measurement of the sample after acid treatment (Figure 41). Mild particle formation can be seen from the sample after drying step. The evaporation of water was visible during the drying procedure.

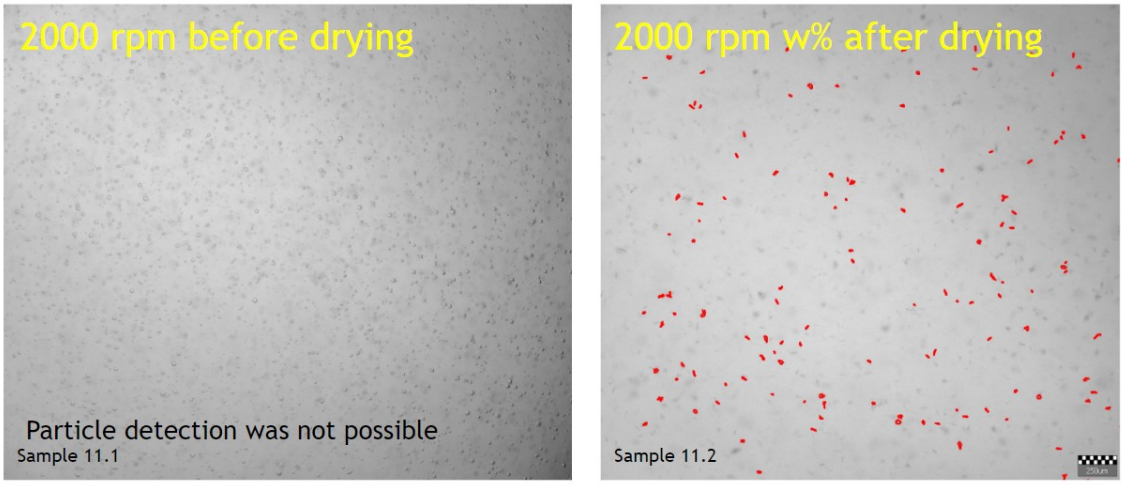

Figure 41 Exp 11, on the left there is the sample after acid treatment and on the right after drying. Feedstock in the experiment is RBDPO and the high shear mixer condition used in this experiment was 2000 rpm for 2 minutes.

In exp 12 (Figure 42), the HSM speed was 4000 rpm. The water droplets were successfully dispersed into the oil, but the particle formation is still quite modest. After the drying procedure, the amount of particles represents a similar situation than earlier experiences in these conditions.

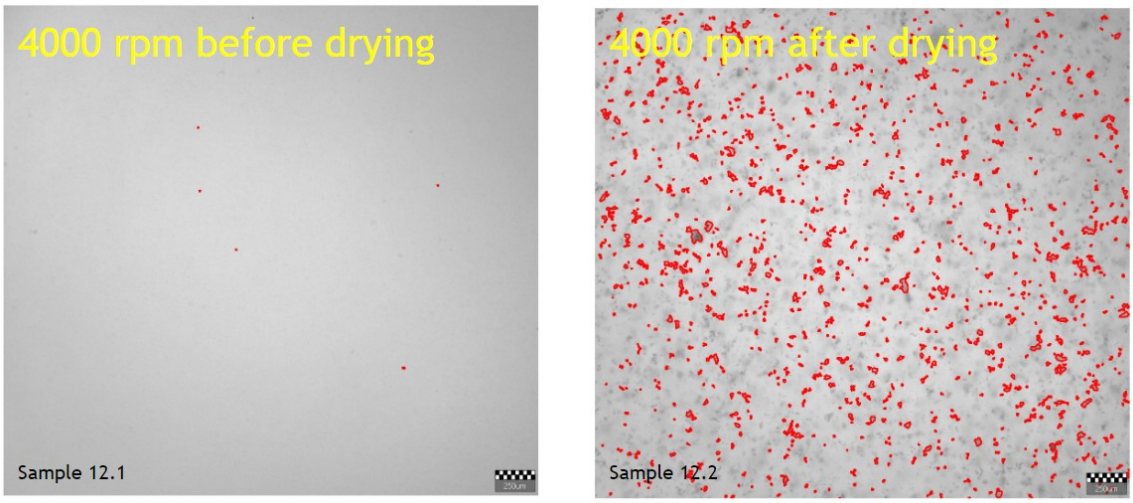

Figure 42 Exp 12, on the left there is the sample after acid treatment and on the right after drying. Feedstock in the experiment is RBDPO and the high shear mixer condition used in this experiment was 4000 rpm for 2 minutes.

Exp 13 (Figure 43), HSM speed of 8000 rpm, gave similar results compared to earlier experiments in the same conditions (exp 3 and 7).

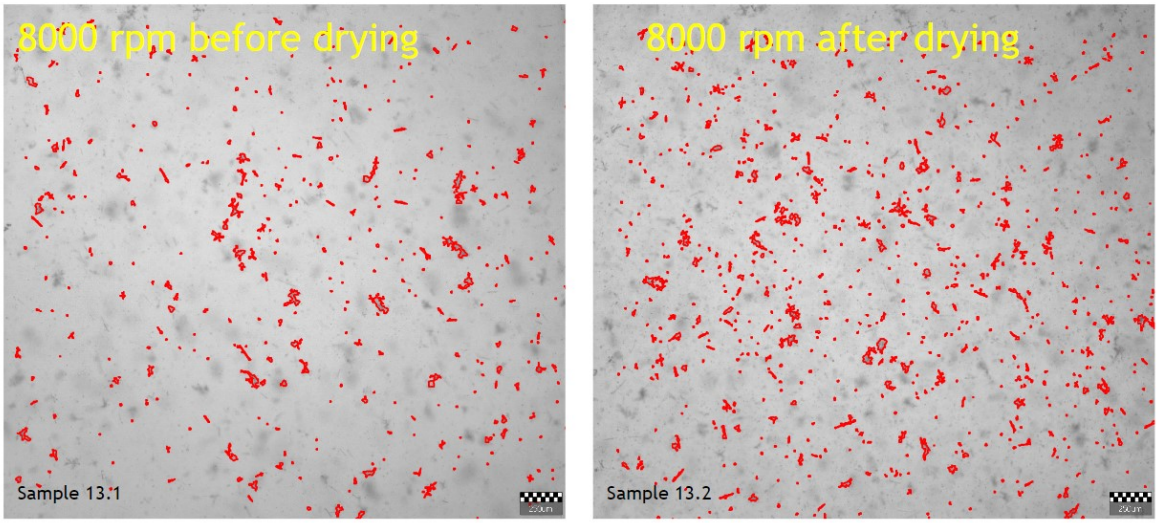

Figure 43 Exp 13, on the left there is the sample after acid treatment and on the right after drying. Feedstock in the experiment is RBDPO and the high shear mixer condition used in this experiment was 8000 rpm for 2 minutes.

When comparing experiments 3 and 13, which both had the same conditions (CA 1000 ppm, H_2O 0.5 w%, HSM 8000 for 2 minutes), the later experiment brought a bit more needle-looking particles compared to earlier experiment (Figure 44). To study the nuclei and beginning of particle formation, an XRDP (X-ray diffraction pattern) analysis could be informative. For a comparison, the same Figure includes a picture from the experiment 5, where 4000 ppm of CA was added to the solution. In Figure 45 the aspect ratio from the experiments 3, 5 and 13 can be observed. The possible reason for the difference between experiments 3 and 13 can be that the formation of particles starts from the small, needle-looking particles, growing through larger needle-shape to the big clusters seen in the experiment 5.

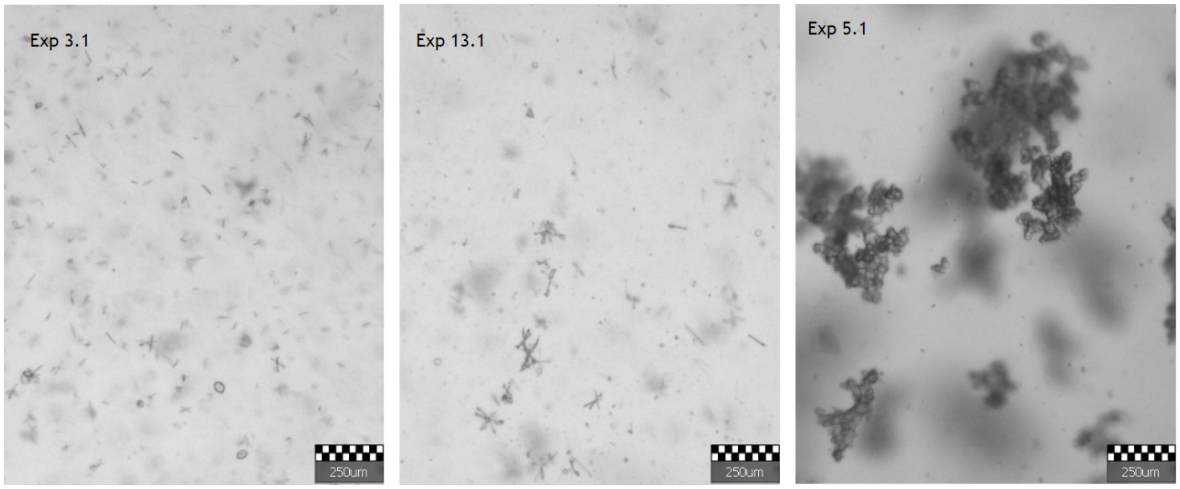

Figure 44 Pictures from Pixact measurement without the particle recognition. On the left a picture from the experiment 3, a picture from the experiment 13 on the middle (sharper needle-looking particles), and on the right a picture of experiment 5 with more CA.

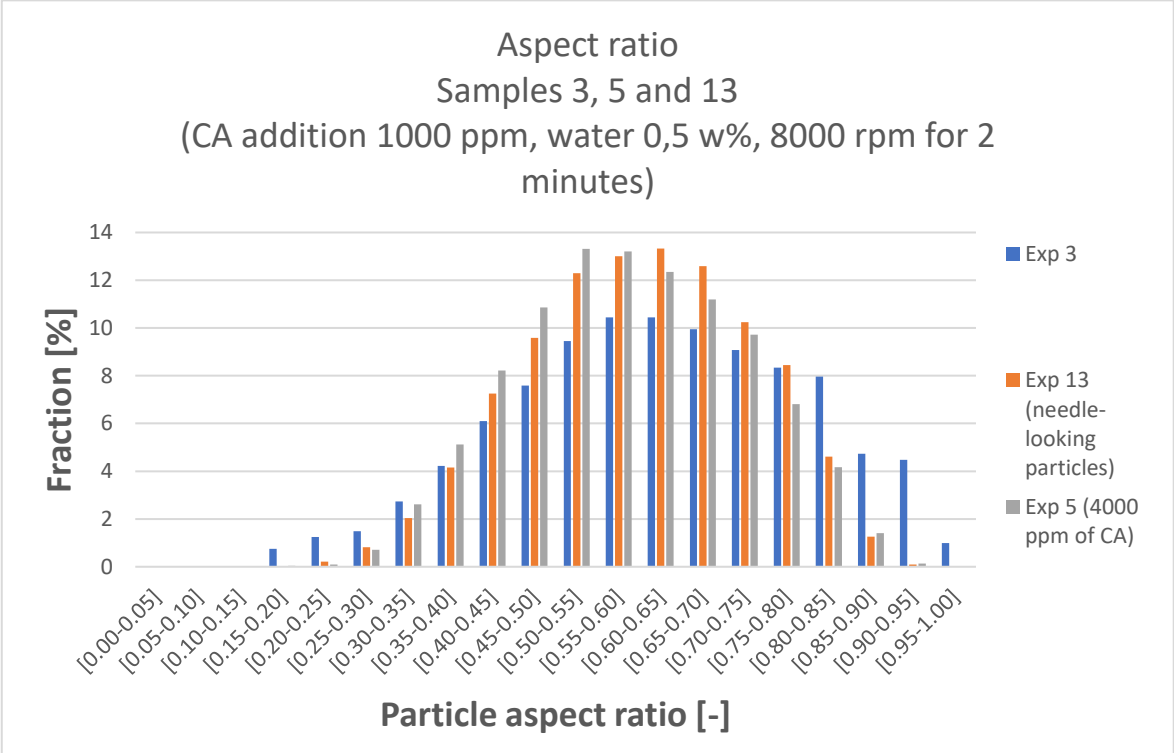

Figure 45 Aspect ratio from the experiments 3, 5 and 13. Exp 3 and 13 had similar conditions, but a bit different-looking particles. Exp 5 had a bigger amount of CA added to the solution.

The water droplets are nearly visible in the Figure 46 of exp 14, where the HSM speed was kept at 8000 rpm, but the mixing time was only 0.5 minutes. Some small particles can be seen before the drying procedure. After drying, the amount and size of particles seems to match the earlier experiments.

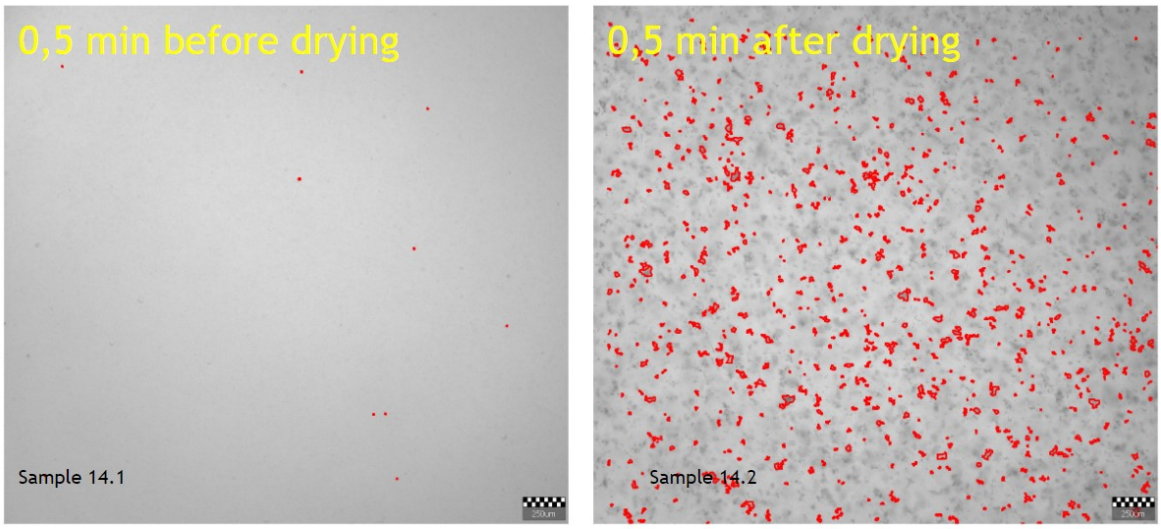

Figure 46 Exp 14, on the left there is the sample after acid treatment and on the right after drying. Feedstock in the experiment is RBDPO and the high shear mixer condition used in this experiment was 8000 rpm for 0.5 minutes.

In the exp 15, where the mixing time was 1 minute (speed 8000 rpm), the particle formation took some minutes after acid treatment, which can be observed from the Figure 47. The formed amount of particles and the size of particles are similar compared to the earlier experiments.

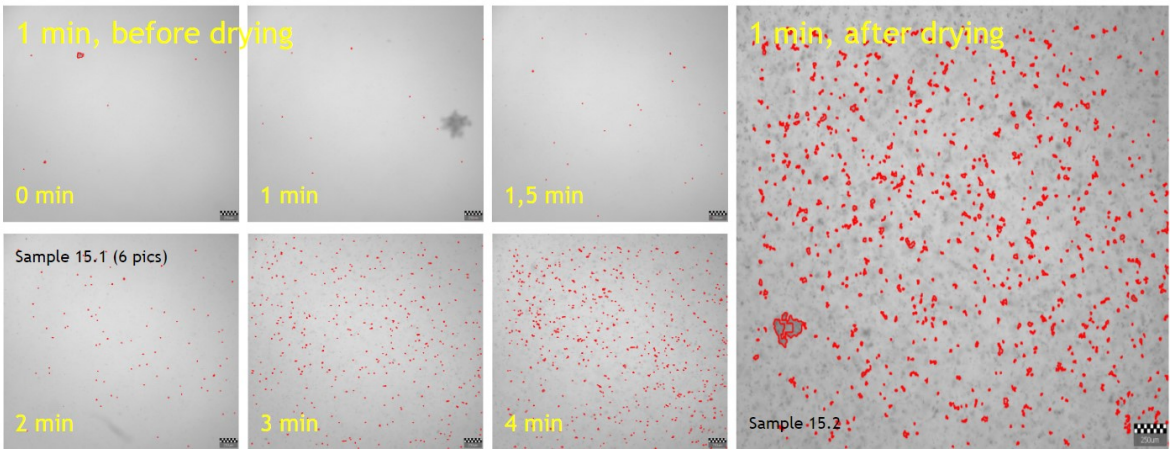

Figure 47 Exp 15, on the left there is the sample after acid treatment and on the right after drying. Feedstock in the experiment is RBDPO and the high shear mixer condition used in this experiment was 8000 rpm for 1 minute.

Exp 16, shown in the Figure 48, included a doubled mixing time (4 minutes at 8000 rpm). The obtained results for particle count are similar to the ones in exp 3, 7 and 13 (Figure 49), and therefore longer mixing time did not benefit the particle formation more than the original mixing time (2 minutes). The CA and water addition remained the same compared to the exp 3, 7, and 13 (1000 ppm of CA with 0.5 w% of water).

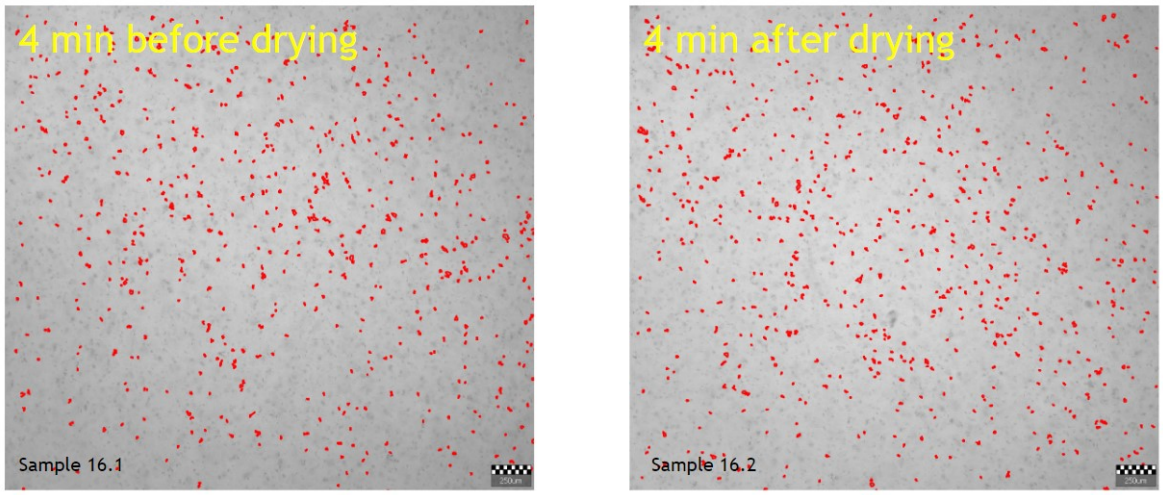

Figure 48 Exp 16, on the left there is the sample after acid treatment and on the right after drying. Feedstock in the experiment is RBDPO and the high shear mixer condition used in this experiment was 8000 rpm for 4 minutes.

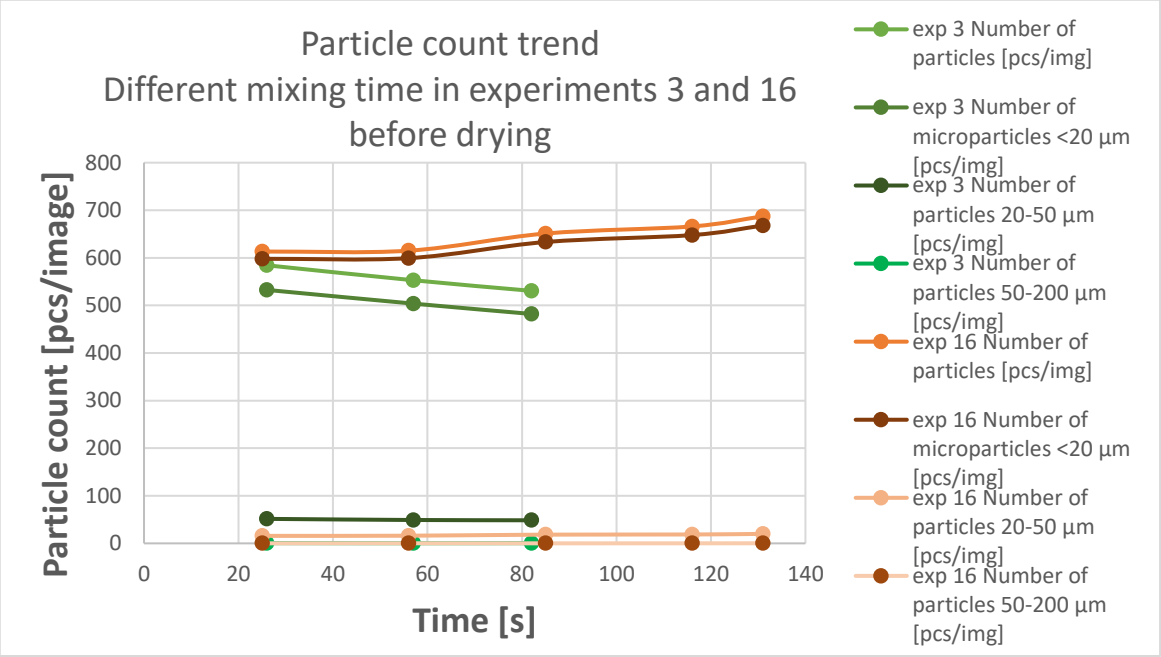

Figure 49 Particle count trend from the experiments 3 and 16. The mixing time in exp 3 was 2 minutes, and in exp 16 4 minutes.

In the experiment 17, the maximum speed of the high shear mixer was tested. From the Figure 50 it can be observed that 9600 rpm for 1 minute did not enhance the particle formation before drying. After drying a large amount of particles can be detected from the solution.

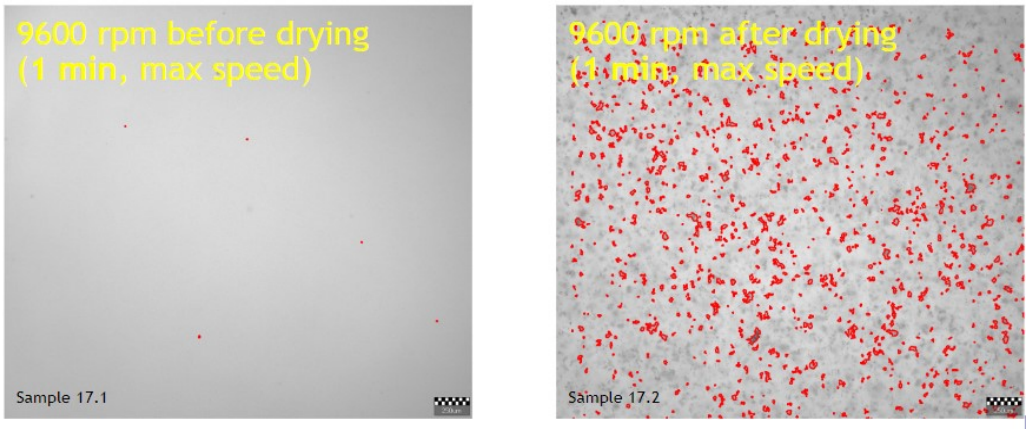

Figure 50 on the left there is the sample after acid treatment and on the right after drying. Feedstock in the experiment is RBDPO and the high shear mixer condition used in this experiment was 9600 rpm for 1 minute.

The particle size distribution for the mixing speed and mixing time can be observed from the Figures 51 and 52. With a maximum speed of 9600 rpm, the size of particles seems to be smaller before drying. During the drying procedure, the particles may form clusters. With 8000 rpm, there is only a small difference in particle size distribution before and after. With 4000 rpm it was noticed that the particle formation was modest before drying, and the mixing may have been insufficient for dispersing the water into the oil properly. The few visible particles present in the oil with lower mixing speed or shorter time are small in size.

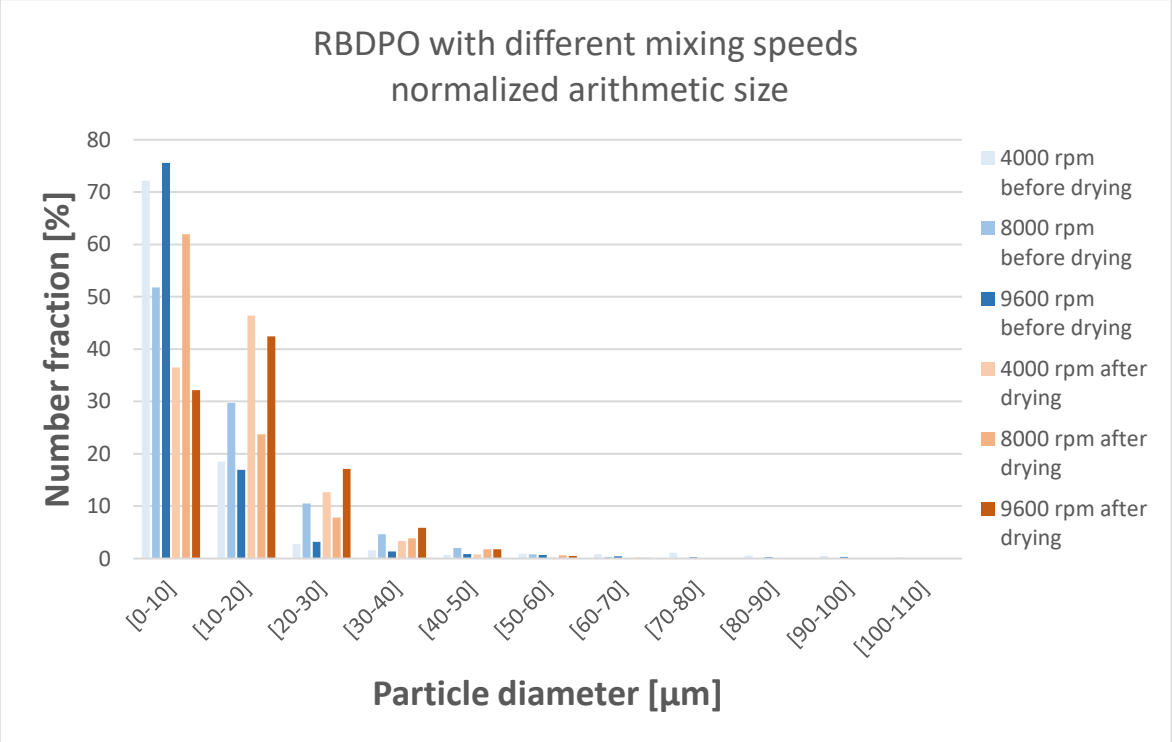

Figure 51 Different mixing speed comparison for RBDPO samples with 1000 ppm of CA and 0.5 w% of water. Larger particles are present in the samples after drying.

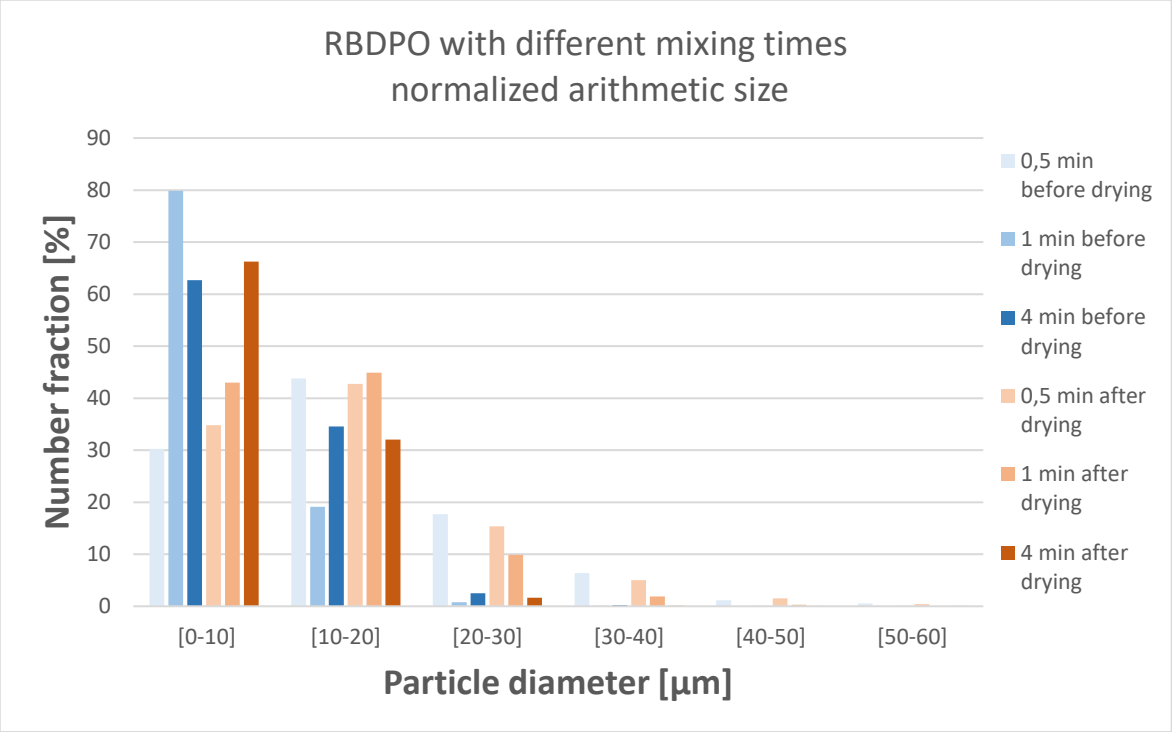

Figure 52 Different mixing time comparison for RBDPO samples with 1000 ppm of CA and 0.5 w% of water. Larger particles are present in the samples after drying.

Volumetric size distributions for the experiments presented in this chapter are presented in Figures 53 and 54. From Figure 53, it can be noticed that the volume of the particles after drying is a bit smaller. Before drying, there are only a few particles in the samples when the time or speed was shorter or lower, and one bigger particle may affect the volumetric size distribution more than in the samples after drying.

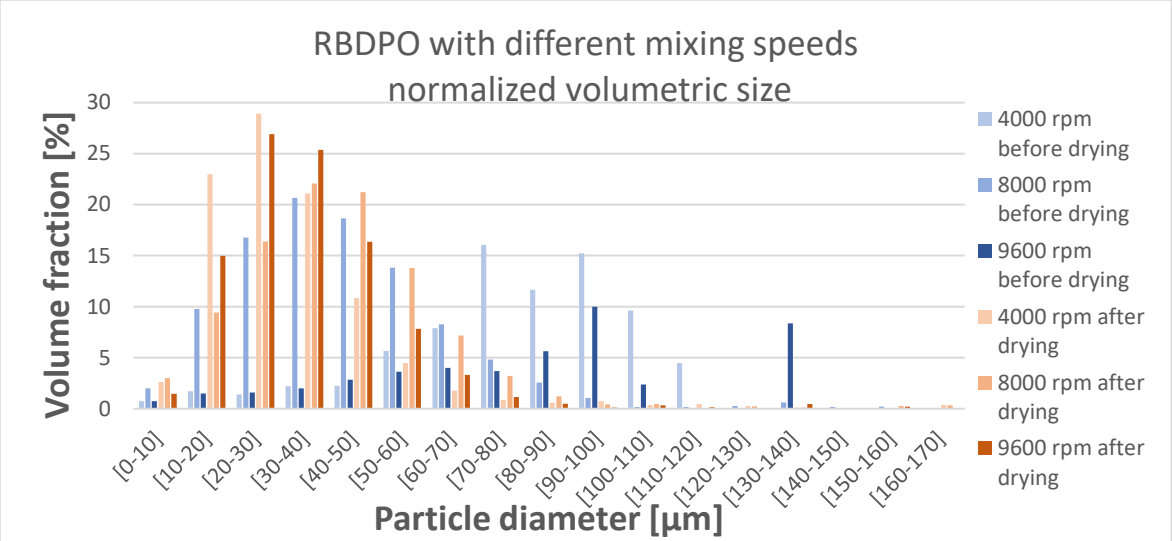

Figure 53 Volumetric size distribution for different mixing speed comparison for RBDPO samples with 1000 ppm of CA and 0.5 w% of water. Volume of the particles seems to decrease during drying.

In Figure 54, in which the volumetric size distribution for different mixing times is presented, the volumetric size of the particles is quite similar before and after.

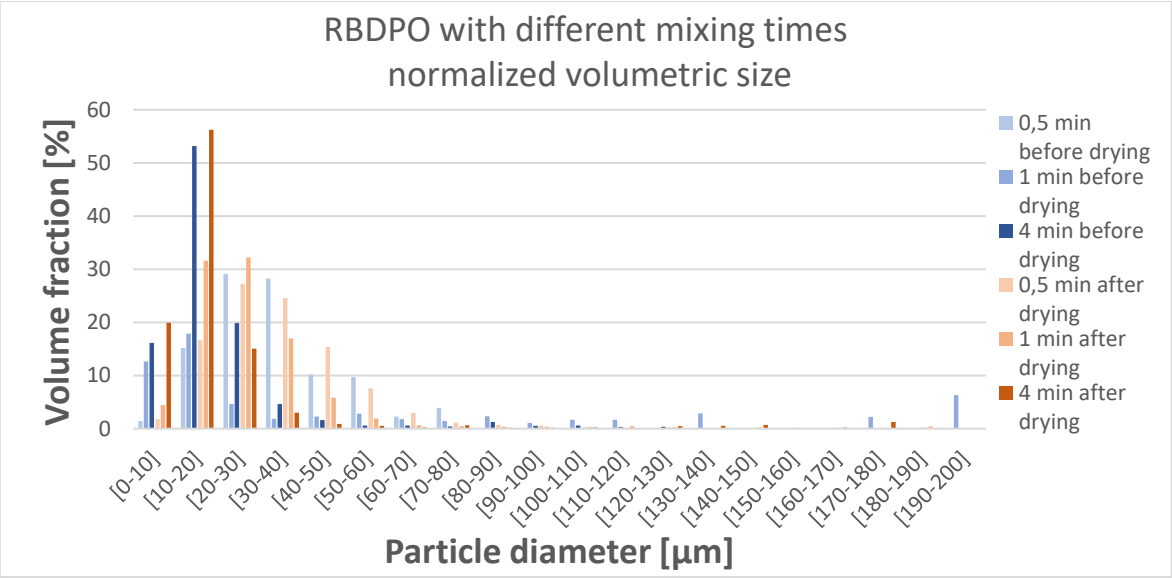

Figure 54 Volumetric size distribution for different mixing time comparison for RBDPO samples with 1000 ppm of CA and 0.5 w% of water. Volume of the particles seems to remain the same during the experiment.

From these experiments, one can notice that the mixing with too low speed or too short time led to insufficient spearing of the water into the oil, and visible droplets were observed from the solution. The particle formation was slower when the mixing time was limited, it could indicate that the formation of the particles requires a certain amount of time, as the contact between the components in the solution needs to be long enough.

Average arithmetic particle size from each experiment can be observed from Table 6.

Table 6 Average arithmetic particle size from experiments presented in the chapter 7.1. The results are collected from the dried samples.

Exp no.	Feed	CA addition (ppm)	Water addition (w %)	HSM speed (rpm)	HSM time (min)	Average arithmetic particle size (µm)
1	RBDPO	0	0.5	8000	2	9.03
2	RBDPO	500	0.5	8000	2	8.21
3	RBDPO	1000	0.5	8000	2	11.95
4	RBDPO	2000	0.5	8000	2	20.84
5	RBDPO	4000	0.5	8000	2	32.16
6	RBDPO	1000	0	8000	2	12.24
7	RBDPO	1000	0.5	8000	2	12.57
8	RBDPO	1000	1	8000	2	16.49
9	RBDPO	1000	2	8000	2	not reliable
10	RBDPO	1000	4	8000	2	not reliable
11	RBDPO	1000	0.5	2000	2	not reliable
12	RBDPO	1000	0.5	4000	2	13.81
13	RBDPO	1000	0.5	8000	2	11.85
14	RBDPO	1000	0.5	8000	0.5	14.94
15	RBDPO	1000	0.5	8000	1	12.47
16	RBDPO	1000	0.5	8000	4	9.17
17	RBDPO	1000	0.5	9600	1	15.66

Table 6 shows the increase in the average arithmetic particle size, when the amount of citric acid is increased. The water amount seems to increase the particle size a bit in larger concentrations, although the amount of water may disturb the Pixact measurement. Sufficient mixing has a decreasing effect on the particle size, as it probably prevent the formation of large agglomerates in the solution.

7.1.4 Filtrations

The experiments presented in this chapter are described in Table 7. Drying procedure is defined “as usual” referring to the drying procedure described in Table 2.

Table 7 Basic series, filtration with different CA additions. Experimental parameters.

Exp no.	Feed	CA addition (ppm)	Water addition (w %)	Drying	HSM speed (rpm)	HSM time (min)	Hold before filtration
18	RBDPO	0	0.5	as usual	8000	2	no
19	RBDPO	1000	0.5	as usual	8000	2	no
20	RBDPO	4000	0.5	as usual	8000	2	no
21	RBDPO	4000	0.5	as usual	8000	2	30 min

Based on the result achieved from the experiment presented above, the filtration was conducted with different citric acid additions (0 ppm, 1000 ppm and 4000 ppm), as it was seen as the key variable. Before filtration, the oil was bleached according to the pretreatment procedure. The other variables were kept as in Table 2. Pixact measurement was performed after acid treatment and after filtration. From the filtration data, filterability resistance was calculated for each experiment.

In the experiment 18 (Figure 55), 0 ppm of citric acid was added to the solution. A visible particle formation in the solution cannot be detected, as the experiment results before filtration are similar compared to the experiment 1 from the earlier series. After filtration some particles were detected from the solution.

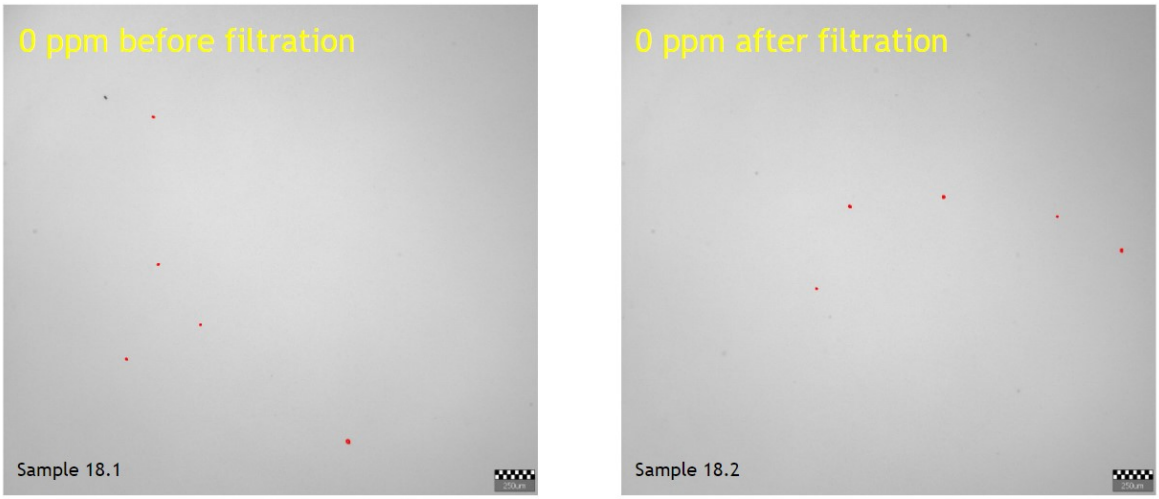

Figure 55 Exp 18, on the left there is the sample after acid treatment and on the right after filtration. Feedstock in the experiment is RBDPO and CA addition is 0 ppm.

The experiment 19 presented in the Figure 56 was conducted with 1000 ppm citric acid addition. The particle formation after acid addition is clear and similar compared to the experiments 3 and 7. After filtration some particles still remain in the solution.

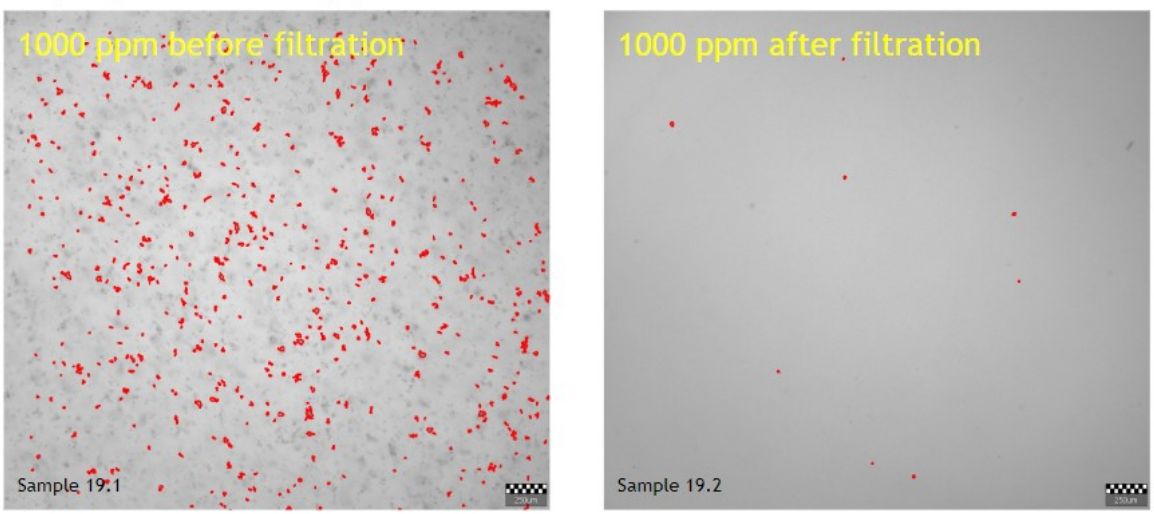

Figure 56 Exp 19, on the left there is the sample after acid treatment and on the right after filtration. Feedstock in the experiment is RBDPO and CA addition is 1000 ppm.

4000 ppm of citric acid was added in the experiment 20 (Figure 57). In this experiment, the particle formation took a bit more time than it usually did, but after 5 minutes the amount and size of the particles was seen to stabilize. The behaviour is otherwise similar compared to what was observed in the experiment 5. After the filtration, some small particles remain in the solution.

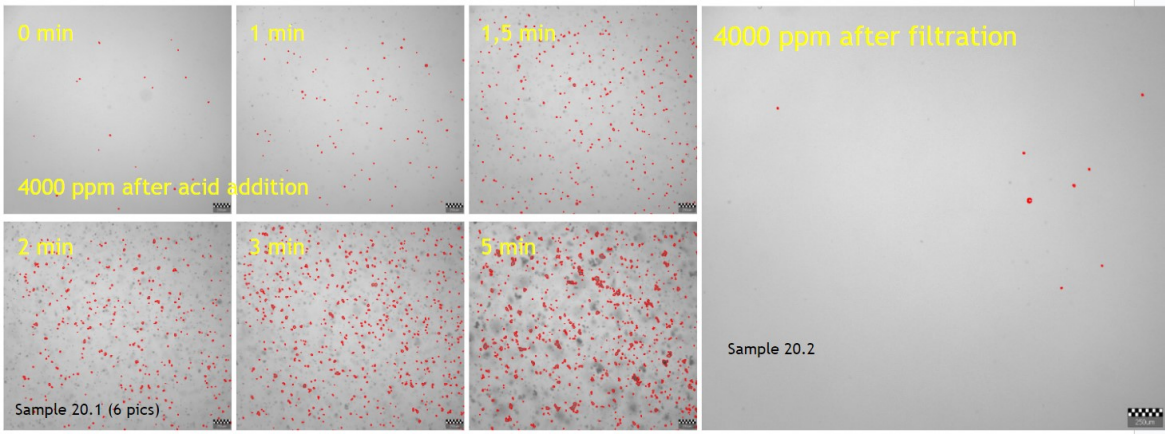

Figure 57 Exp 20, on the left there is the sample after acid treatment (6 pics) and on the right after filtration. Feedstock in the experiment is RBDPO and CA addition is 4000 ppm.

Experiment 21 (Figure 58) was otherwise similar to experiment 20 with a CA addition of 4000 ppm, but the solution was left to rest in the heating closet for 30 minutes before the filtration procedure. The appearance of the sample before this “rest” is similar compared to the earlier experiment. After the resting, filtration was performed.

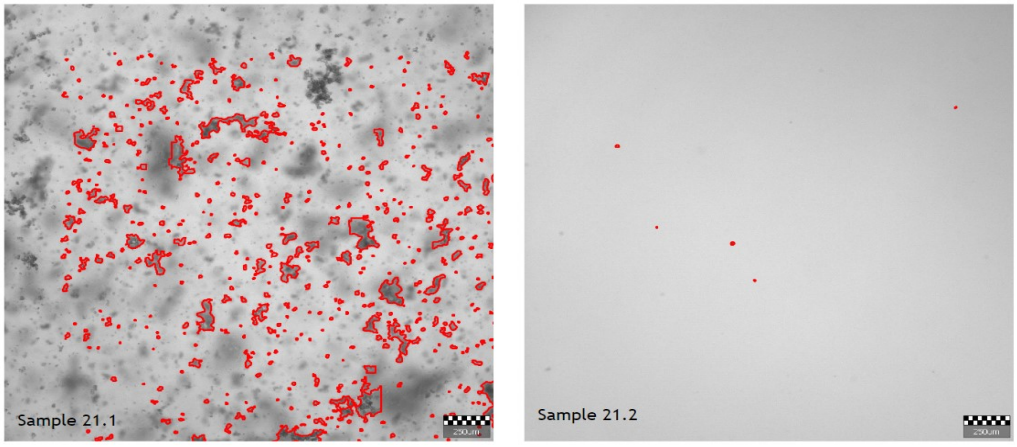

Figure 58 Exp 21, on the left there is the sample after acid treatment and on the right after filtration. Feedstock in the experiment is RBDPO and CA addition is 4000 ppm. The sample was left to rest in the heating closet 30 minutes before filtration.

In Figure 59 the particle size distribution can be observed. Please note that the Figure is showing percentages, not actual particle counts. One can notice that the size of the particles before drying and after filtration remains quite similar. The small particle size fractions are observed, meaning that the filtration did leak some of the small particles through the filter. As seen in Figures above (55-58), the leaked amount is very small.

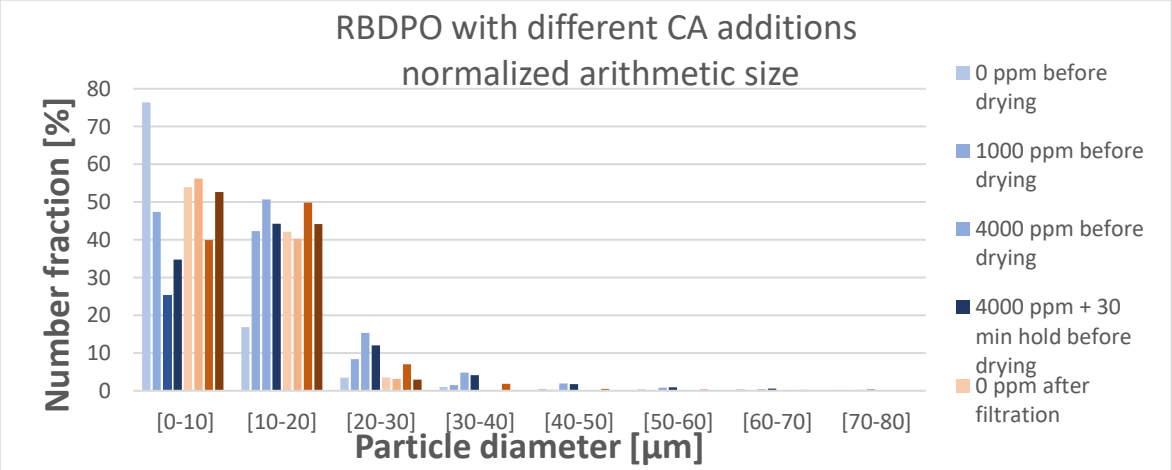

Figure 59 Normalized arithmetic size distribution for the samples with different CA additions before and after filtration. The size of the particles present in the solution remains the same before and after filtration. Please note that the Figure is showing percentages, not actual particle counts.

In Figures 60 and 61, the normalized volumetric size distributions before drying and after filtration are shown. One can observe that the 0 ppm and 1000 ppm of CA create particles with smaller volumetric size, and the samples containing 4000 ppm of CA have particles with larger volumetric size. Especially the sample that was left to rest before filtration has larger fractions of bigger particles compared to the one that was filtered right after the bleaching and drying procedure. After filtration, the volumetric size of the remaining particle in all samples is emphasized on fractions of small volumetric size.

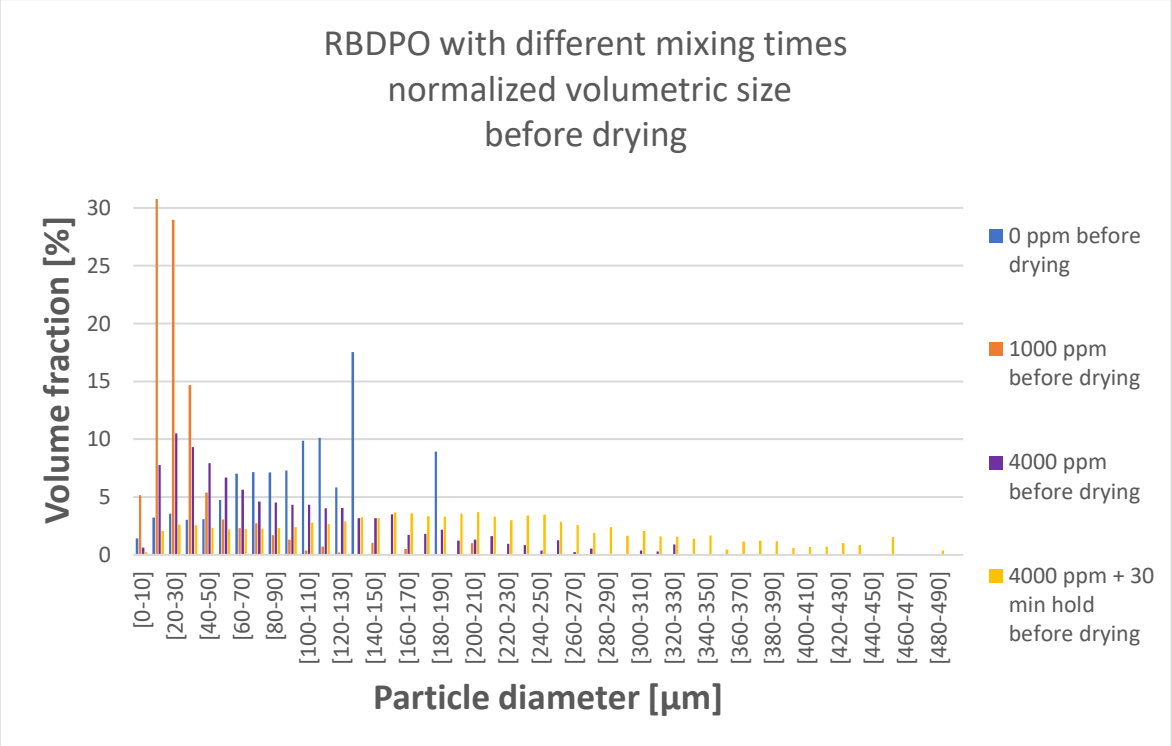

Figure 60 Normalized volumetric size distribution before drying procedure for the samples with different CA additions.

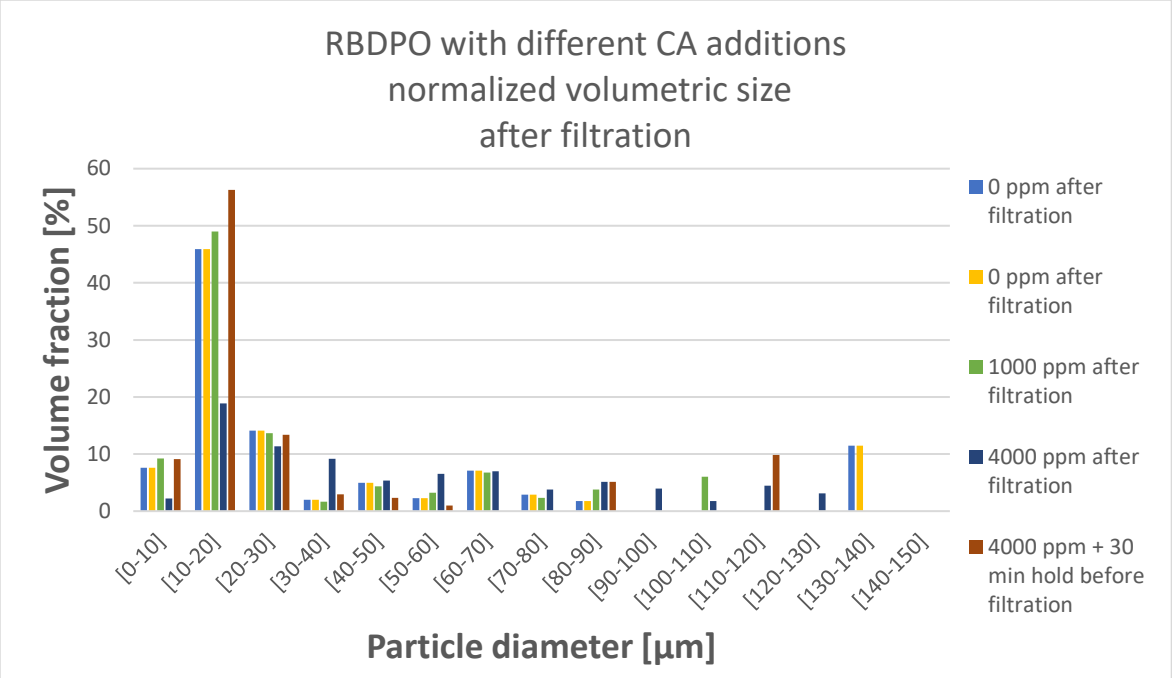

Figure 61 Normalized volumetric size distribution after filtration for the samples with different CA additions.

The filterability resistance R_c was calculated based on the filtration results according to Equations (12), (13), (14) and (15). The symbols and filtration equations have been presented earlier in the chapter 3.3.2.

Cake resistance:

$$R_c = \alpha \frac{m_c}{A} \tag{12}$$

Pressure difference:

$$\Delta p = \mu \frac{Q}{A}(R_m + R_c) \tag{13}$$

Pressure difference per filtrate flow rate:

$$\frac{\Delta p}{Q} = \mu \frac{R_m}{A} + \alpha\mu \frac{m_c}{A^2} \tag{14}$$

Pressure difference per filtrate flow rate can be plotted against mass of the cake

$$\frac{\Delta p}{Q} = a + bm_c \tag{15}$$

The plotted charts can be observed in Appendix 2. Results from these filtration experiments are collected to Table 8.

Table 8 Results from the experiments 18, 19, 20 and 21. Other related information can be found from Table 6.

Experiment	CA addition (ppm)	Filterability resistance ((GPa*s)/kg^2)	Filtration time (min)
18	0	212	5,5
19	1000	159	6,5
20	4000	139	5,5
21	4000	141	5

The filterability resistances or the filtration times were only very slightly affected by the citric acid addition: the filterability resistance was slightly decreased according to the amount of addition. It is possible that particles form bigger clusters, which were seen from the Pixact results in exp 20 and 21, and those clusters stay on the top of the cake. Smaller particles (exp 19) travel deeper into the cake and may block the cake, increasing the filtration resistance.

The correlation between the particle size and filterability resistance was briefly studied with MODDE 13 Pro design of experiments software (https://www.sartorius.com/en). Coefficients (CA, water and time) related to average particle size are described in Figure 62. From this Figure, it can be noticed that the amount of CA has a high correlation to the larger size of the particles in the solution, as the amount of water or mixing time show smaller correlation.

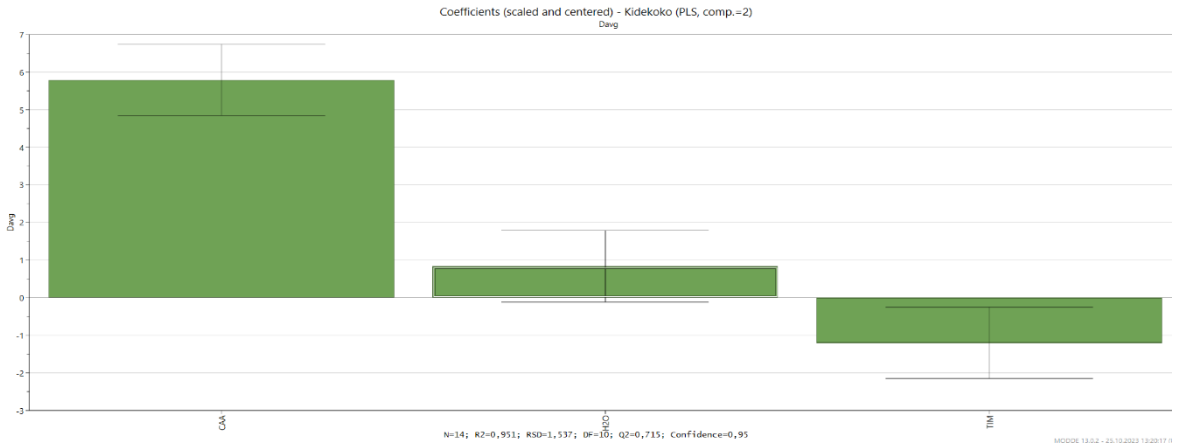

Figure 62 Coefficients (Scaled and centered) related to the particle size. The first column indicates high correlation for CA addition, the second column only small correlation for the amount of added water. The third column indicated the effect of mixing time.

Based on the results, responsive contour plots for particle size were plotted for the amount of water or for mixing time against the amount of CA. Figure 63 indicates that that together with the amount of CA, the particle size increases when the amount of water is increases, but without the CA addition, the effect of water addition is not remarkable.

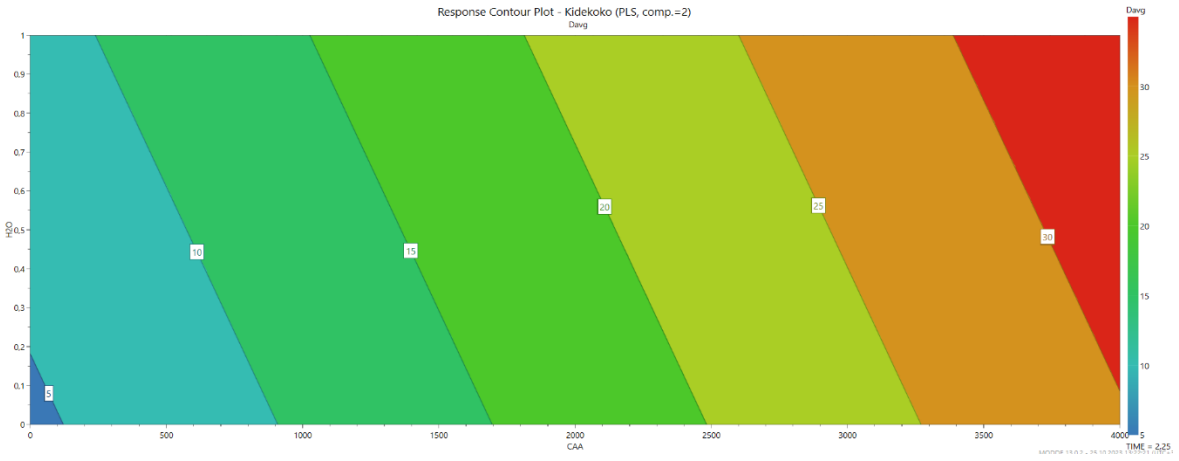

Figure 63 Responsive contour plot for particle size. The amount of water (w %) on the y-axis and the amount of CA (ppm) on the x-axis. The size of the particles can be indicated to increase when increasing the concentration of CA and the amount of water. The largest particle size could be achieved with a large water and CA additions.

Figure 64 presents the responsive contour plot for particle size when mixing time is plotted against the amount of CA. From this picture one can indicate that the prolonged mixing time can decrease the particle size, as the largest particle size could be achieved with shorter mixing times and a large amount of CA.

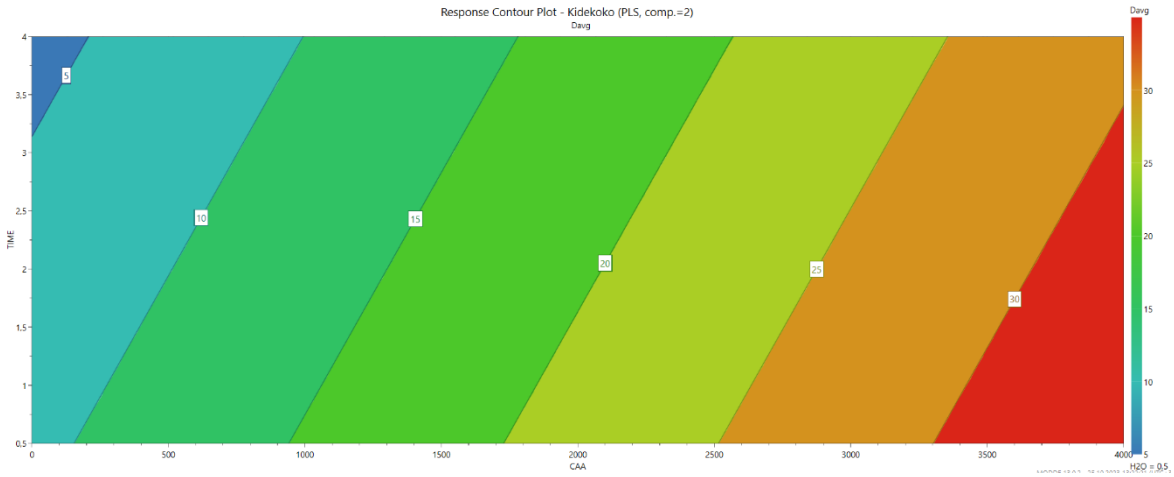

Figure 64 Responsive contour plot for particle size. The mixing time (min) on the y-axis and the amount of CA (ppm) on the x-axis. The largest particle size could be achieved with a moderate mixing time when the amount of CA is to maximum.

The model predicted the particle sizes, as can be seen in Figure 65. Larger particle size could be achieved with larger amount of CA and water in the solution.

CAA	H2O	SPEED	TIME	Davg	Lower	Upper
1000	0,5		2	13.1	12.1	14.0
4000	0,5		2	32.1	29.1	35.2
0	0,5		2	6.7	5.2	8.3
4000	1		1	35.8	31.7	39.9
6000	1		2	47.0	41.3	52.6
6000	2		2	51.2	42.3	60.1

Figure 65 Particle size prediction based on the experimental results. Davg presents the average particle size present in the solution. With larger amounts of CA and water, the particle size could increase.

Figure 66 indicated the possible effect of the particle size on filterability. The correlation in these experiments was quite weak (R2 = 0.77), but the model indicates that the filterability could be improved with larger additions of CA and water to the solution, as the average particle size increases simultaneously. The possible explanation could be that the larger particles remain in the top of the cake, instead of blocking the pores of the cake and therefore enhance the filterability.

Feed	CA addition (ppm)	Water addition (w %)	Drying	HSM speed (rpm)	HSM time (min)	Hold before filtration	**Filterability resistance**	estimated Davg
RBDPO	0	0.5	as usual	8000	2	no	**212**	7
RBDPO	1000	0.5	as usual	8000	2	no	**159**	13
RBDPO	4000	0.5	as usual	8000	2	no	**139**	32
RBDPO	4000	0.5	as usual	8000	2	30 min	**141**	32
RBDPO	6000	1	as usual	8000	2		**103**	47
RBDPO	6000	2	as usual	8000	2		**93**	51

Figure 66 Filterability resistance prediction based on the experimental results. Based on the model, increasing the amount of CA and water in the solution could enhance the filterability of the solution.

7.2 FFA addition

Before the metal addition study, it was noticed that the effect of FFA in the solution should be studied first to avoid misleading conclusions. An addition of FFA was made to increase the solubility of metal components to the RBDPO. FFA can act as a surfactant, meaning it has both hydrophilic (water-attracting) and hydrophobic (oil-attracting) regions in its molecular structure. This property can facilitate the dispersion of metal salts in oil by forming micelles or other stabilizing structures. In some cases, FFA can increase the solubility of metal salts in oil, making it easier for the salts to dissolve and remain dispersed. The increased solubility of Na-stearate and Ca-stearate to the purified oil with FFA addition was observed by Utriainen (2017). Tandon et al (2001) noticed that the solubility of Na-oleate was also increased to the oil when oleic acid was present in the solution. The presence of FFA may also affect the formation and properties of particles. Nikiforidis et al (2015)

observed that smaller aggregates were formed in the solution of Na-oleate and sunflower oil where the oleic acid was present. The solution with the added oleic acid has significantly smaller crystals.

Three different FFA additions were studied (10, 20 and 30 w %). The FFA used in these, and upcoming experiments was palmitic acid $CH_3(CH_2)_{14}COOH$, whose structure is shown in Figure 67. The amount of FFA additions were determined based on the results from Lehtinen et al (2017), as they noticed that the FFA addition to the oil increased the formation of micelles between the concentrations of 5-20 w%. All three experiments (10, 20 and 30 w %) dissolved the same amount of Na-stearate, 310 ppm. From these, the 10 w% was chosen to be used in the upcoming experiments due to consumption of the FFA.

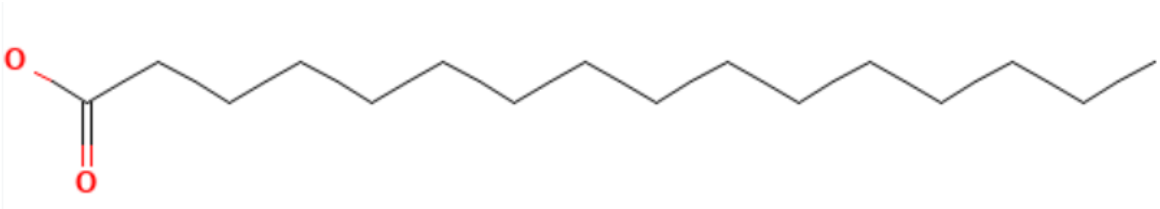

Figure 67 Structure of palmitic acid (PubChem)

The chosen FFA, palmitic acid, was diluted into the RBDPO. After that, metal addition was added to the solution. The added metal compound was Na-stearate, which is used later in the experiments. The amount of Na-stearate was calculated to correspond to the amount of citric acid addition during acid treatment, when the CA was balanced as divalent acid. Calculations will be presented later in chapter 7.3.

After choosing the amount of FFA addition, its effect with the citric acid was studied. The experiments presented in this chapter are described in Table 9. Drying procedure is defined “as usual” referring to the drying procedure described in Table 2.

Table 9 FFA in the feedstock with different CA additions. Experimental parameters.

Exp no.	Feed	CA addition (ppm)	Water addition (w %)	Drying	HSM speed (rpm)	HSM time (min)
25	RBDPO 90 w % + FFA 10 w %	0	0.5	as usual	8000	2
26	RBDPO 90 w % + FFA 10 w %	1000	0.5	as usual	8000	2
27	RBDPO 90 w % + FFA 10 w %	4000	0.5	as usual	8000	2
28	RBDPO 90 w % + FFA 10 w %	1000	0.5	as usual	8000	0.5
29	RBDPO 90 w % + FFA 10 w %	1000	0.5	as usual	8000	1
30	RBDPO 90 w % + FFA 10 w %	1000	0.5	as usual	8000	4

From the experiment 25 (Figure 68), where no CA was present in the solution, it can be seen that the FFA addition itself does not cause any visible particle formation into solution.

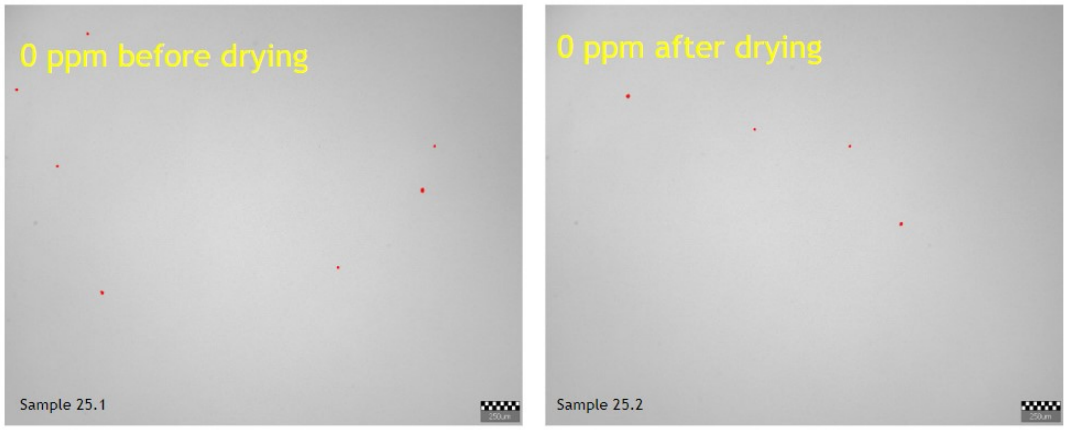

Figure 68 Exp 25, on the left there is the sample after acid treatment and on the right after drying. Feedstock in the experiment is RBDPO+FFA and CA addition is 0 ppm.

In experiment 26 (Figure 69), the CA addition of 1000 ppm increased the amount of particles in solution.

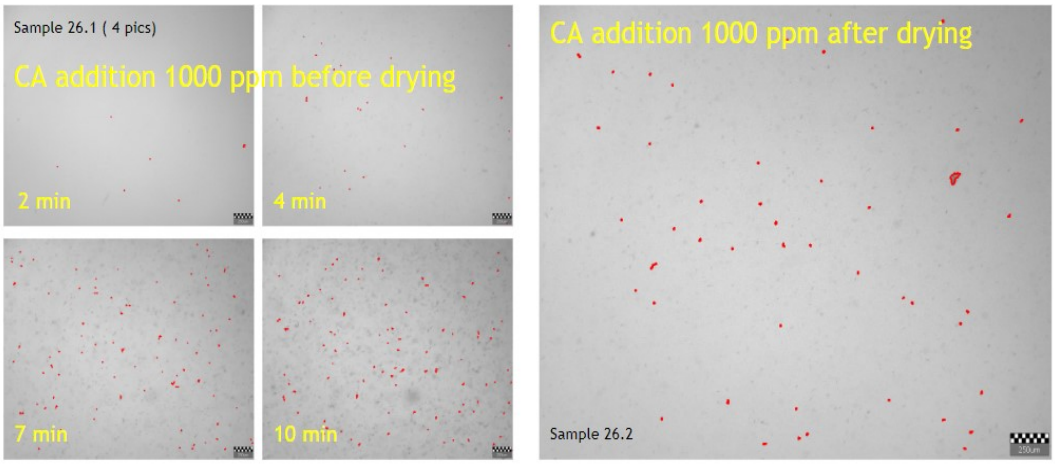

Figure 69 Exp 26, on the left there is the sample after acid treatment and on the right after drying. Feedstock in the experiment is RBDPO+FFA and CA addition is 1000 ppm.

Compared to the experiments 3, 7 and 19, where the experimental conditions were otherwise the same (CA addition 1000 ppm, H_2O addition 0.5 w%, mixing and drying according to Table 2), the amount of particles in the experiment 26 is much higher. The FFA addition also affected the timeline how fast the visible particles appeared in the solution. The particle count for the experiments 3, 7 and 19 is shown in Figure 70. The amount of counted particles varies, even though the procedure is the same in each experiment at this point, but the timeline for the appearing of particles is similar. All the samples had visible particles in the beginning of the Pixact measurement. In Figure 71 the particle count for the experiment 26 with FFA is shown. The formation of particles took several minutes, which is much slower compared to the experiments 3, 7 and 19. The amount of counted particles is also much smaller, even though the measurement time is much longer.

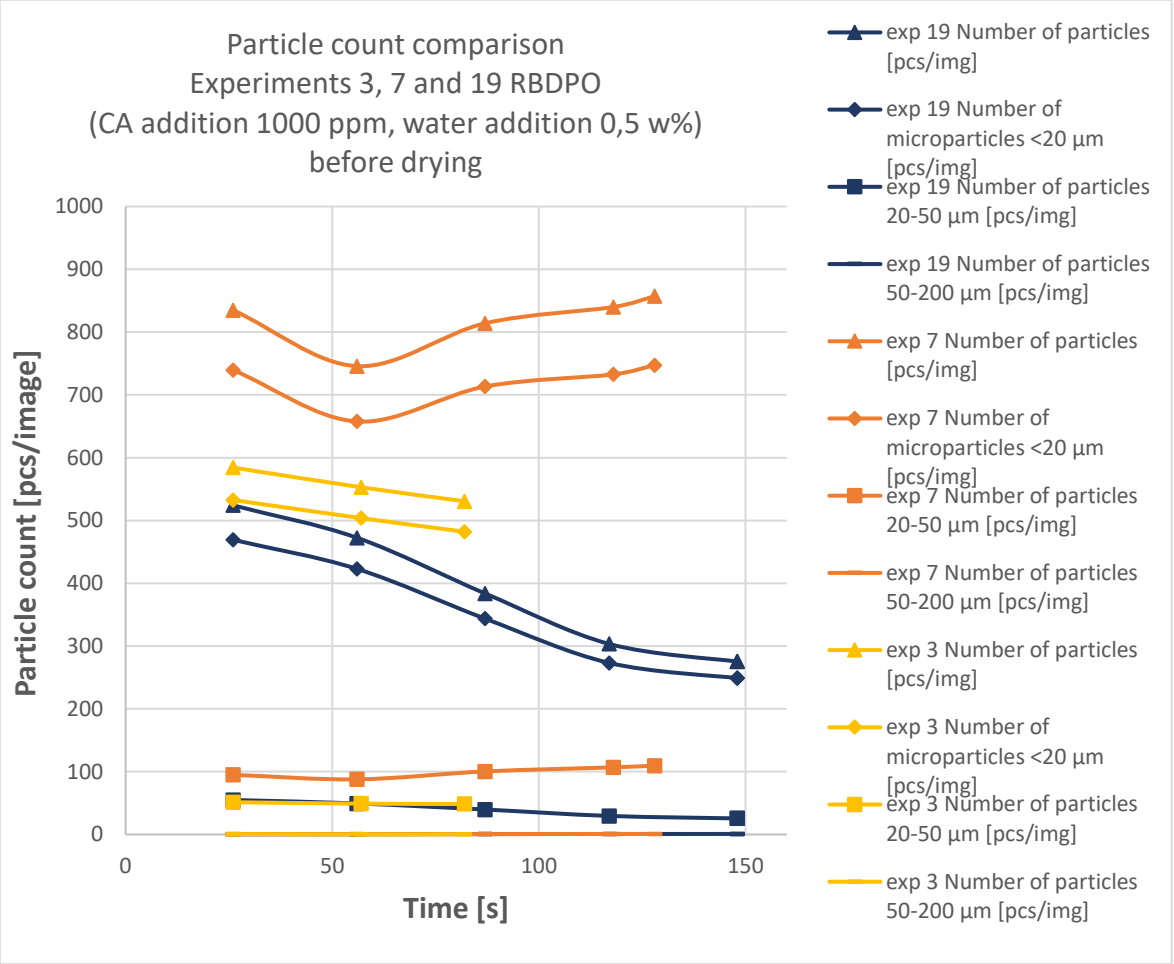

Figure 70 Particle count comparison between experiments 3, 7 and 19, where the feedstock was RBDPO and the CA addition 1000 ppm. Particle count in the experiment 7 is a bit higher compared to the other two.

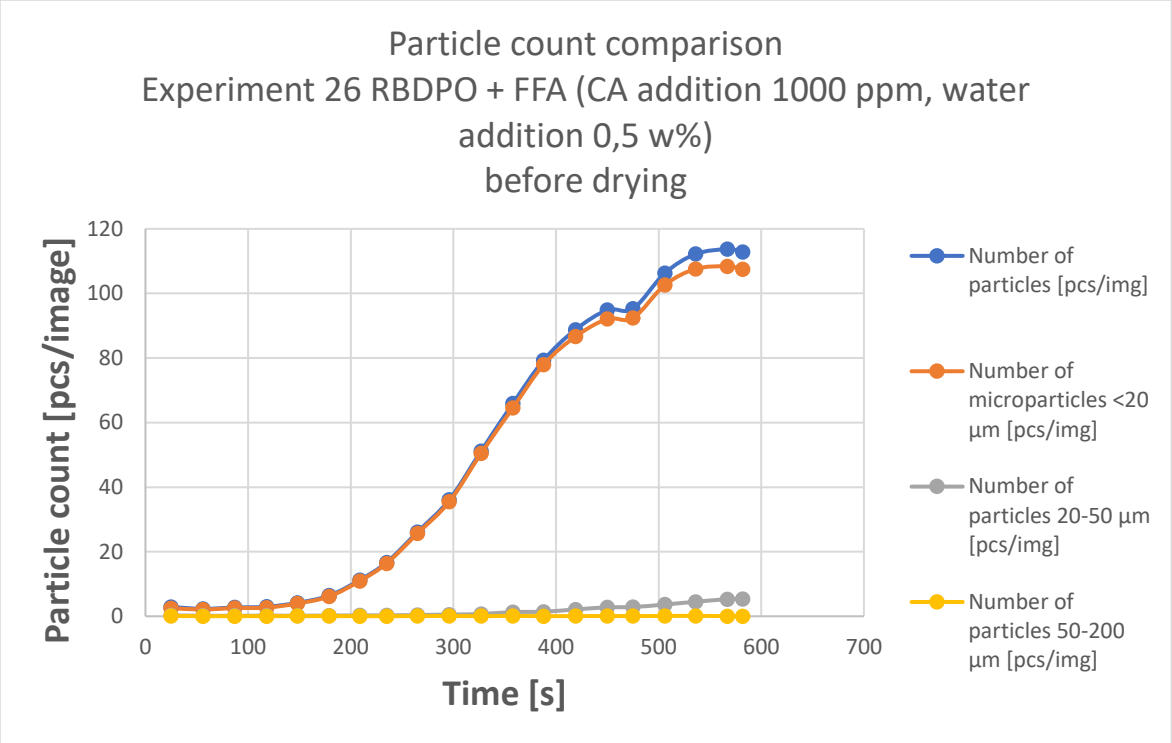

Figure 71 Particle count trend for the experiment 26, where FFA has been added to the solution.

Experiment 27 (Figure 72) with 4000 ppm of CA replicated the earlier results from the experiments 5 and 21, with one difference: the appearance of the particles was slower compared to the earlier experiments.

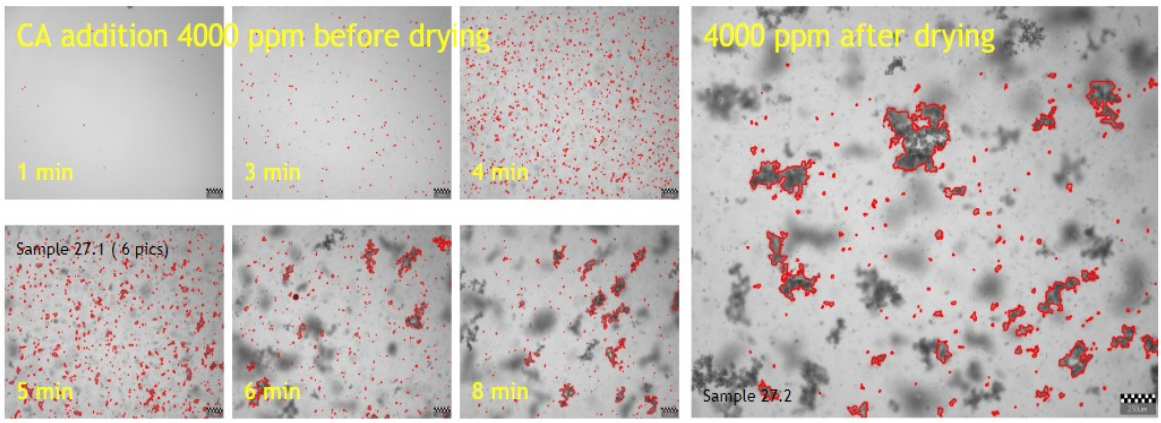

Figure 72 Exp 27, on the left there is the sample after acid treatment and on the right after drying. Feedstock is RBDPO+FFA and CA addition is 4000 ppm.

Figures 73 and 74 the particle count differences between the RBDPO based samples and the sample with FFA addition to the feedstock. In Figure 73, particle count trends from the experiments 5 and 21 can be observed. In these experiments, the feedstock is RBDPO and the CA addition is 4000 ppm. Other experiment conditions are kept according to Table 2. The particle count trends are similar in both experiments, as is the timeline for the appearance of the particles.

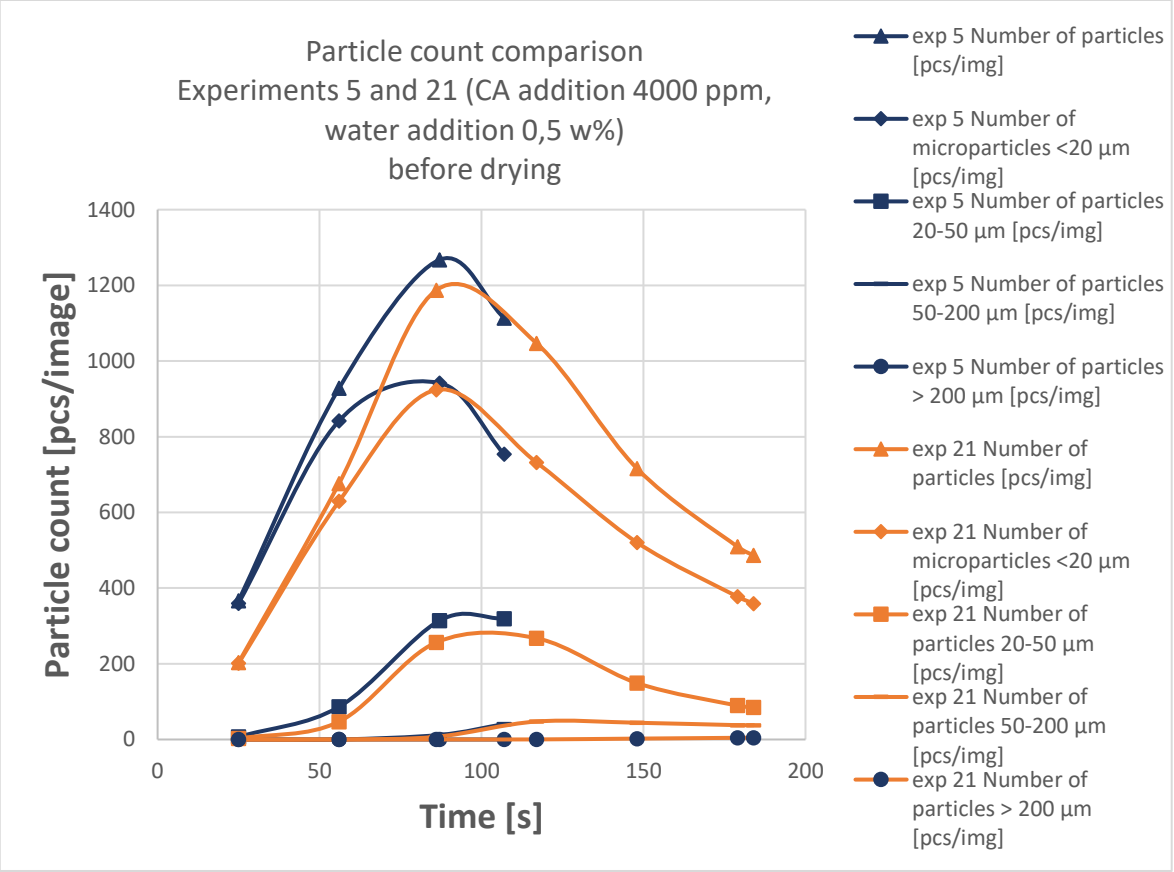

Figure 73 The particle count comparison for experiments 5 and 21, where the feedstock is RBDPO and the CA addition 4000 ppm.

In Figure 74, the FFA has been added to the feedstock of the experiment 27. Compared to Figure 73, this sample shows lower amounts of particles counted from the sample. The timeline for the particles to appear is much slower especially for the larger particles to appear in the sample.

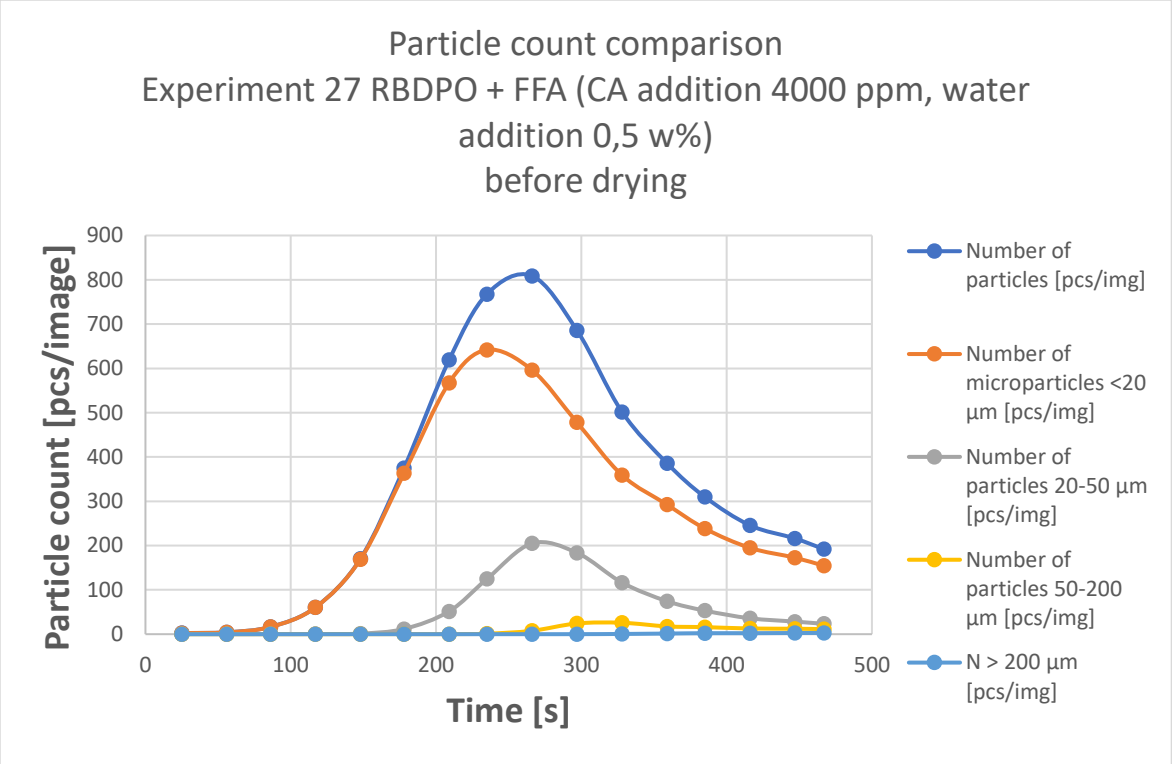

Figure 74 Particle count trend for the experiment 27, where the feedstock is RBDPO + FFA with CA addition of 4000 ppm.

In Figure 75, the normalized arithmetic particle size distribution is presented for the experiments containing FFA with different CA additions. One can observe that the size of the particles remains quite similar before and after the drying procedure, and it can be said that the drying does not affect the particle size in the samples containing FFA.

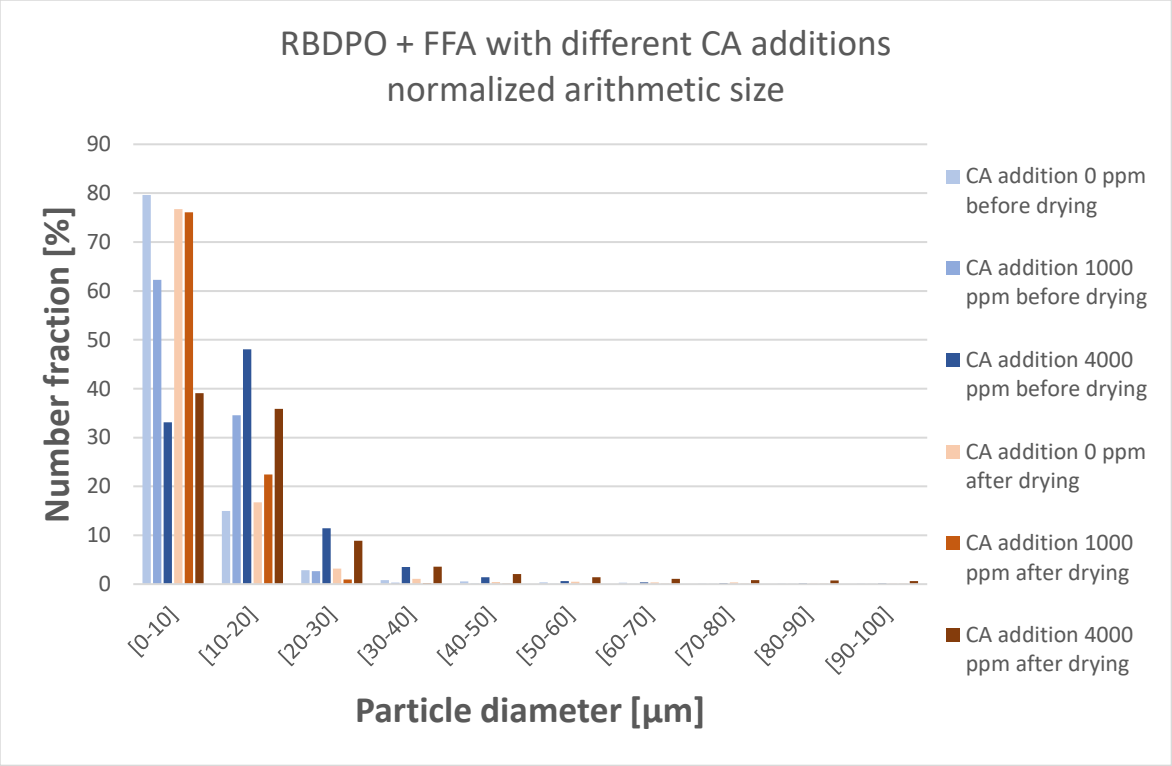

Figure 75 Normalized arithmetic size distribution for the experiments with FFA in the feedstock. The CA addition varies in these samples.

In Figures 76 and 77 the normalized volumetric particle size distribution is presented for the samples before and after drying respectively. The volumetric size distribution is similar compared to the earlier experiments with different CA additions: the 0 ppm addition leads to the smallest volume of particles, while 4000 ppm addition of CA increases the volume of the particles. After drying, the volume of the particles in the sample of 4000 ppm of CA is similar to before drying, but the smaller amounts have some bigger clusters that appeared after drying.

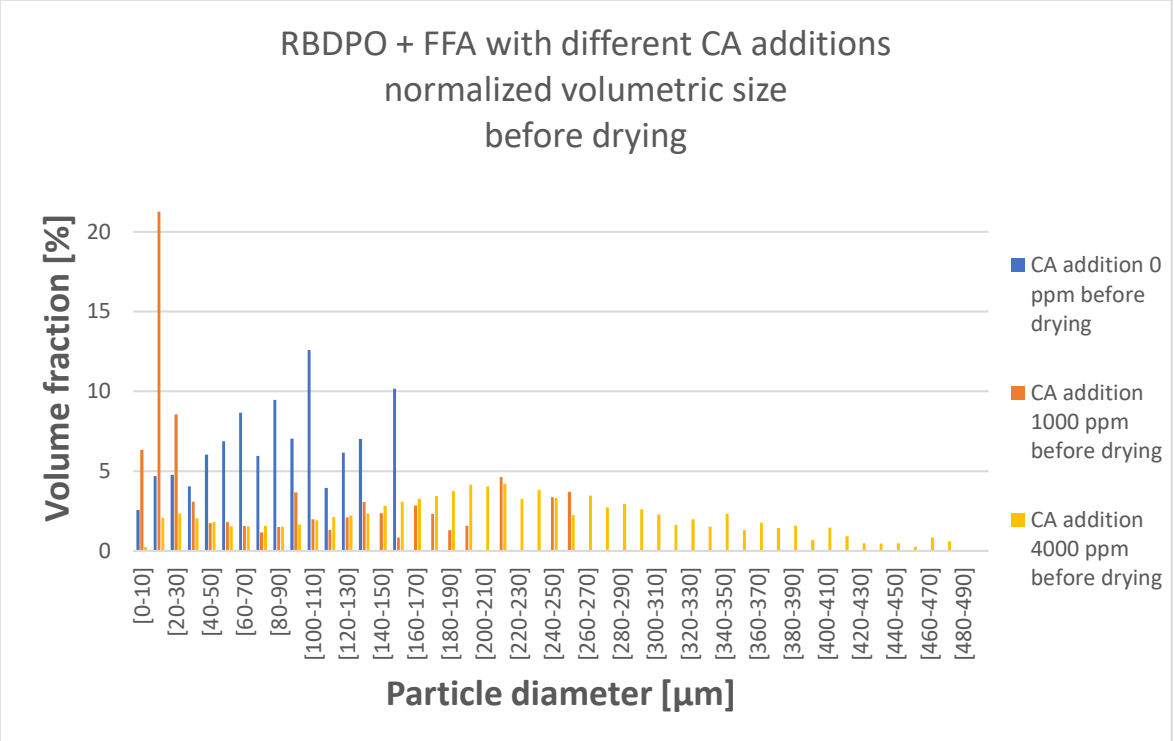

Figure 76 The normalized volumetric size distribution for the samples containing FFA with different CA additions. The samples are measured before drying.

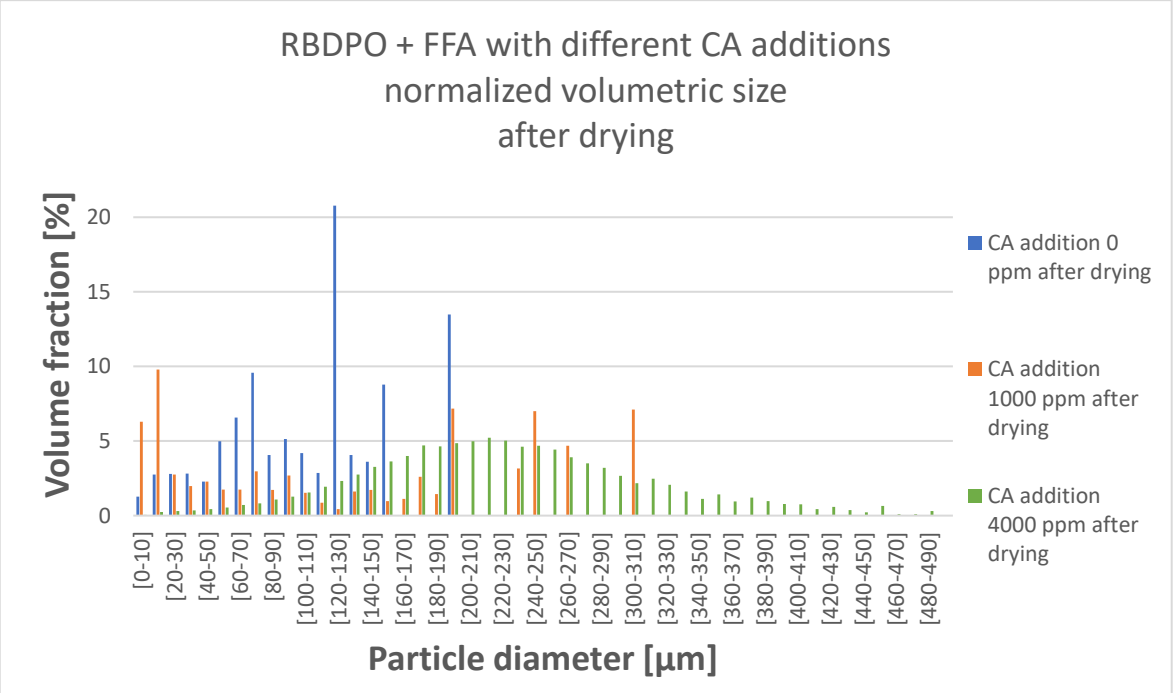

Figure 77 The normalized volumetric size distribution for the samples containing FFA with different CA additions. The samples are measured after drying.

Behaviour of solution including RBDPO and FFA was also studied with different mixing times, as it was seen earlier that the contact time needs to be long enough to form the particles in the solution. In experiments 28, 29 and 30, the mixing time was 0.5, 1 or 4 minutes respectively. The interesting result in all was that the formation of particles was not detected in the sample (Figure 78). 1000 ppm of citric acid was added to the samples.

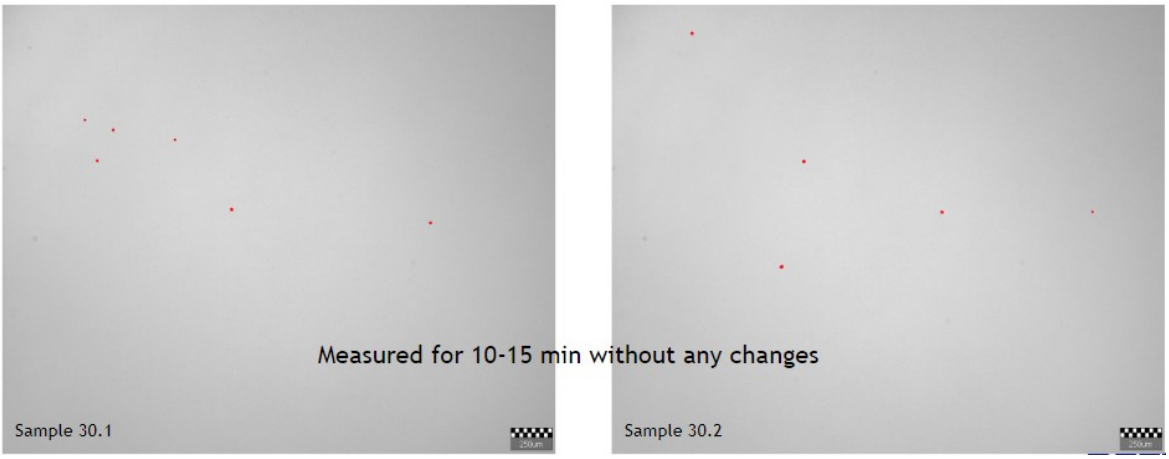

Figure 78 Exp 30, on the left there is the sample after acid treatment and on the right after drying. Feedstock in the experiment is RBDPO+FFA and the mixing time for the high shear mixer was 4 minutes.

The samples were measured for 10-15 minutes, when usually the particles appear if there is any formation. In all three experiments with different mixing times (0.5, 1 or 4 minutes) the results came out as the same. There was not any visible particle formation in any, not even during the 4 minutes of mixing. The results from experiments 28-30 differ from the other experiments, as no particle formation was discovered. Further research should be taken regarding to these experiments to figure out the root cause. Despite that the feedstock and the equipment were similar as before, possible scenarios are for example human error, small difference in experimental practicalities, unexpected reaction or small difference in the feedstock

7.3 Metal additions

After FFA addition was decided and briefly studied, the experimental work focused on the main research area, the effect of metal components in the filtration. The experimental set up remained similar as described before. In these experiments, the solution is treated by acid addition, bleaching, drying and filtration procedures. The solution is prepared 24 hours before the experiment to ensure that the components have dissolved into the oil.

The metal components used in the experiments were sodium stearate ($C_{18}H_{35}NaO_2$) and calcium stearate ($C_{36}H_{70}CaO_4$), presented in the Figure 79. Sodium and Calcium are common impurities in the real-life feedstocks (chapter 7.4).

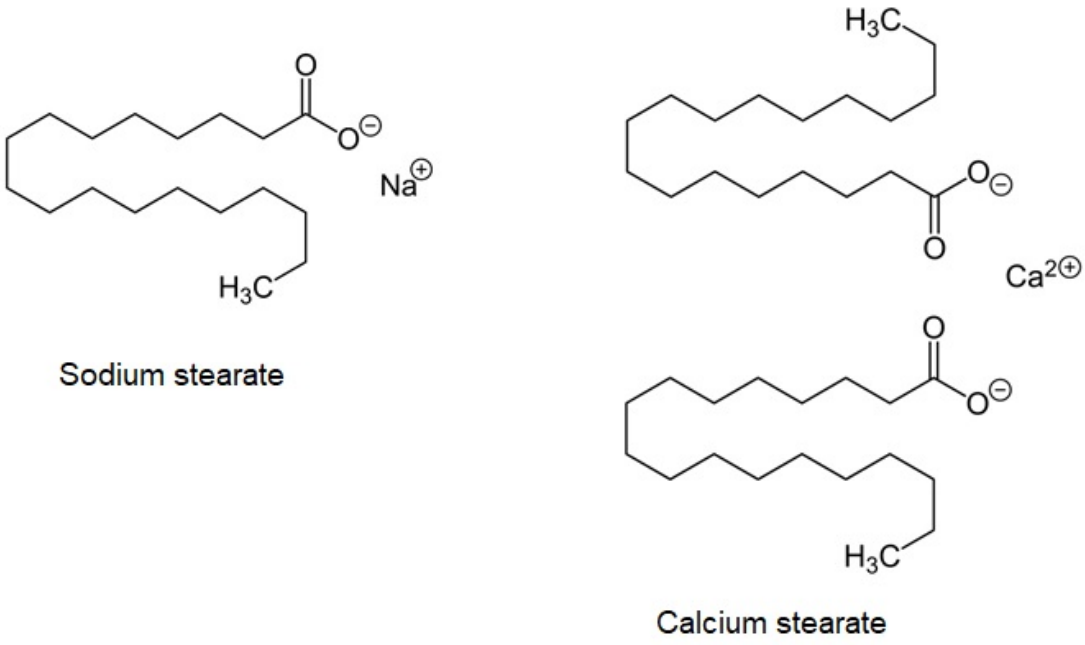

Figure 79 A structural formula of sodium stearate on the left and a structural formula of calcium stearate on the right

The amount of metal component addition to the oil was calculated and can be observed from Appendix 6.

The metal amount was calculated from the reaction equations (Figures 80 and 81). Molecule formulas for the reactions are described in Equations (16) and (17).

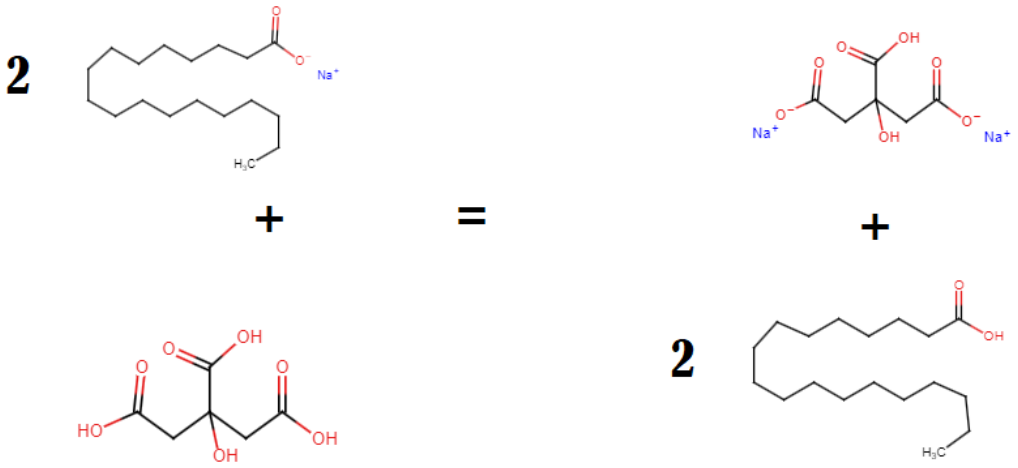

Figure 80 Reaction equation for sodium stearate and citric acid. One CA molecule can react with two Na-stearate molecules. There is a possibility for a third reaction, as the centre group remains unharmed.

$$2\ C_{18}H_{35}NaO_2 + C_6H_8O_7 = C_6H_7O_7Na + 2\ C_{18}H_{36}O_2 \quad (16)$$

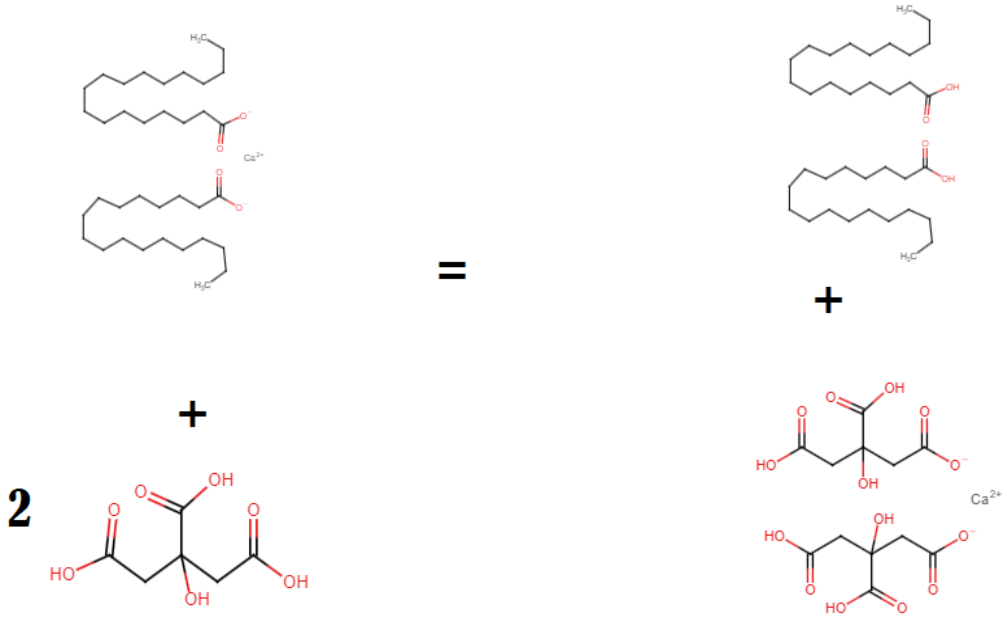

Figure 81 Reaction equation for calcium stearate and citric acid, one possible way. It is possible that the calcium ion bonds with two of three –OOH groups of CA molecule.

$$(C_{17}H_{35}COO)_2Ca + 2\ C_6H_8O_7 = (C_6H_7O_7)_2Ca + 2\ C_{17}H_{36}O_2 \quad (17)$$

When the calculations were finished, the practical work was started. The experiment included acid addition, bleaching, drying and filtration. Pixact measurement was performed after acid addition and after filtration. Samples were taken from the solution before starting the experiment (named as “feedstock”) and after filtration (named as “filtrate”).

At first, the filtration was performed on the RBDPO with FFA addition but without any metal addition. After that, metal addition experiments took place. Four experiments were performed for each sodium stearate and calcium stearate independently. First experiment in both series did not contain any citric acid addition, and the reason for the experiment is to study the effect of metal compounds on filtration. The filterability resistance for each test setup is shown in Table 8. Filtration charts related to these experiments are presented in Appendix 3.

The experiment with RBDPO + 10 w % FFA was performed with CA addition of 1000 ppm and water addition of 0.5 w %. Drying procedure is defined “as usual” referring to the drying procedure described in Table 2.

The experiment 37 (Figure 82) contained only RBDPO and FFA, continuing the interesting behaviour of the lack of particle formation after CA addition. 1000 ppm of CA was added to the solution. The filterability resistance is similar compared to the plain RBDPO filtrations presented in Table 8.

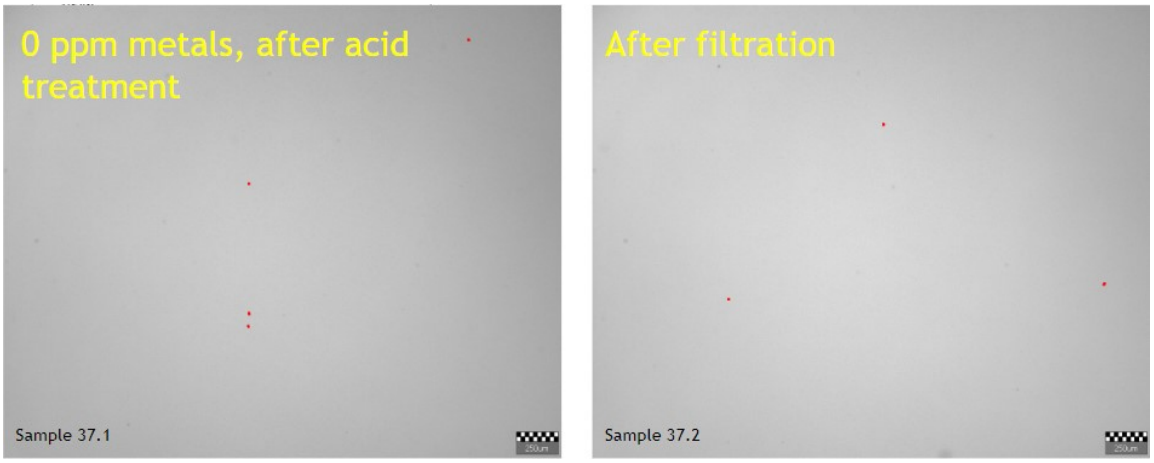

Figure 82 exp 37, on the left there is the sample after acid treatment and on the right after filtration. Feedstock in the experiment is RBDPO+FFA and CA addition was 1000 ppm.

RBDPO with FFA did not seem to affect the filterability and did not cause any practical problems during the pretreatment procedure.

7.3.1 Sodium stearate additions

The experiments presented in this chapter are described in Table 10. Drying procedure is defined “as usual” referring to the drying procedure described in Table 2.

Table 10 Metal addition in the feedstock with different CA additions. Experimental parameters.

Exp no.	Feed	Metal component addition n (mol)	CA addition (ppm)	Water addition (w %)	Drying	HSM speed (rpm)	HSM time (min)	Rest before filtration
31	RBDPO 90 w % + FFA 10 w %	Sodium stearate 0,002 mol	0	0.5	as usual	8000	2	no
32	RBDPO 90 w % + FFA 10 w %	Sodium stearate 0,002 mol	1000	0.5	as usual	8000	2	no
33, 34	RBDPO 90 w % + FFA 10 w %	Sodium stearate 0,010 mol	4000	0.5	as usual	8000	2	no
35	RBDPO 90 w % + FFA 10 w %	Sodium stearate 0,010 mol	4000	0.5	as usual	8000	2	30 min

Sodium stearate was added to the solution according to the amount of CA addition. The concentrations studied in these experiments were 0 ppm, 1000 ppm and 4000 ppm of CA and sodium stearate, with the exception that the solution with 0 ppm of CA did have the sodium stearate addition of 0,002 mol.

Figure 83 from the experiment 32 shows the feedstock on the left side. The solution with RBDPO, FFA and sodium stearate formed particles while the temperature dropped from 70 °C to 50 °C. Some particles are present in the beginning already. After acid treatment, where 0 ppm of CA and 0.5 w% of water were added, there are not many visible particles that Pixact could detect. Temperature was kept in 85 °C during the acid treatment, and the same temperature was maintained during the Pixact measurement, so likely the soap particles present in the feedstock were mostly dissolved to the oil again. Filtrate from this experiment is nice and clear.

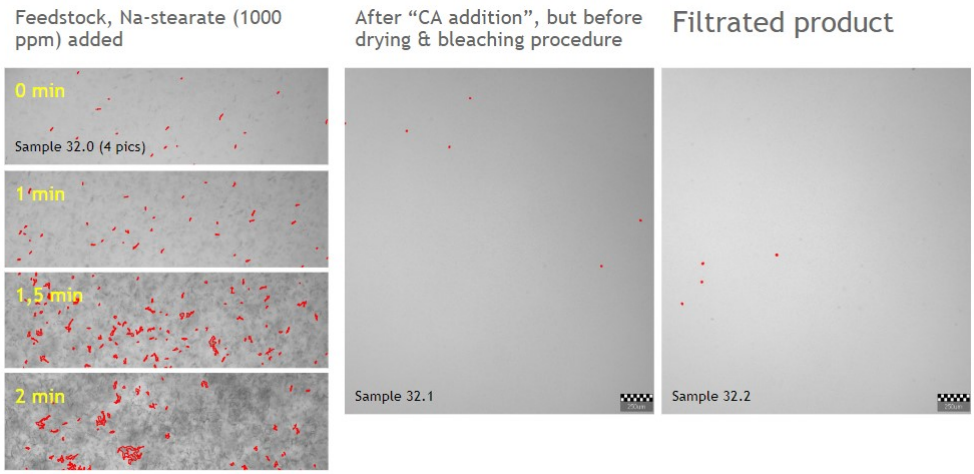

Figure 83 exp 32. Sodium stearate addition of 0,002 mol, CA addition 0 ppm. Feedstock on the left side, product after acid treatment in the middle, filtered product on the right.

In experiment 31, CA addition (1000 ppm) and sodium stearate addition were present in the solution. Feedstock was looking the same compared to the experiment 32. After CA addition, the Pixact measurement did not give a very reliable result, as the picture of the solution is looking quite blurry (Figure 84, in the middle). There are some particles present, more than in the experiment 32, but it is possible that the particles are too small for Pixact to detect them. Filtered product was clean.

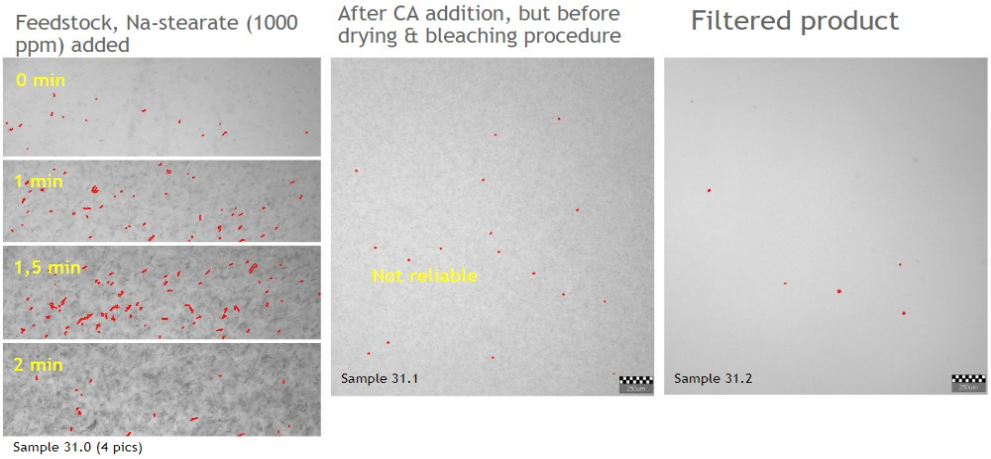

Figure 84 exp 31. Sodium stearate addition of 0,002 mol, CA addition 1000 ppm. Feedstock on the left side, product after acid treatment in the middle, filtered product on the right.

4000 ppm of CA was added to the experiment 34. The feedstock contained 0,010 mol of sodium stearate, and was hard to keep in a liquid phase. The feedstock was originally prepared at 70 °C, but it was shortly noticed that the solution will not stay in liquid form at this temperature. The temperature was raised to 90 °C, which was enough to keep the solution at liquid phase. When the temperature was 90-100 °C during the Pixact measurement, particles from the solution can be detected (Figure 85, left bottom corner). When the solution was under 90 °C, particle detection was not possible (Figure 85, left upper corner). After the effect of temperature was discovered, the solution was kept at 90 °C until the acid treatment was finished. After that the solution did not solidify at the process temperature. The particle detection from the solution after acid treatment was not very successful, as there were many small particles. The size and amount of the particles were on the limits of Pixact measurement, leading to untrustworthy detection. The same problems were seen in the experiment 35, where the product was left to rest in the heating closet for 30 minutes before filtration took place.

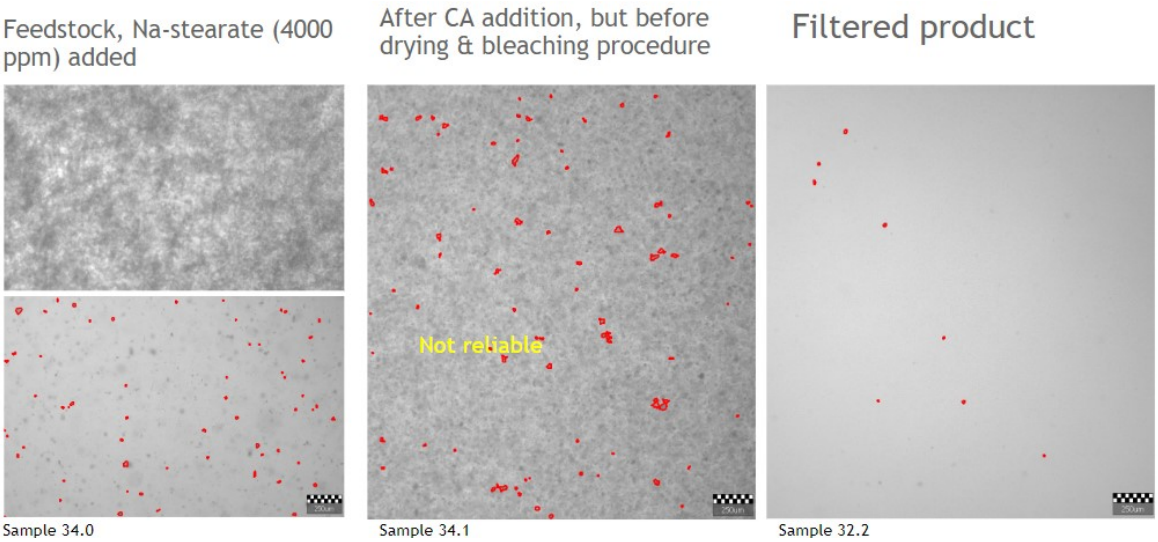

Figure 85 exp 34. Sodium stearate addition of 0,010 mol, CA addition 4000 ppm. Feedstock on the left side, product after acid treatment in the middle, filtered product on the right.

Although the before drying data obtained from the Pixact measurement is not the most reliable, the samples can be compared based on this data with a little caution. In Figure 86 one can notice that in the samples containing 0 ppm or 1000 ppm the relative amount of small particles is remarkably larger than in the samples containing 4000 ppm of CA. The size of the particle seems not to be affected by the resting, which was done to the second sample with 4000 ppm of CA addition.

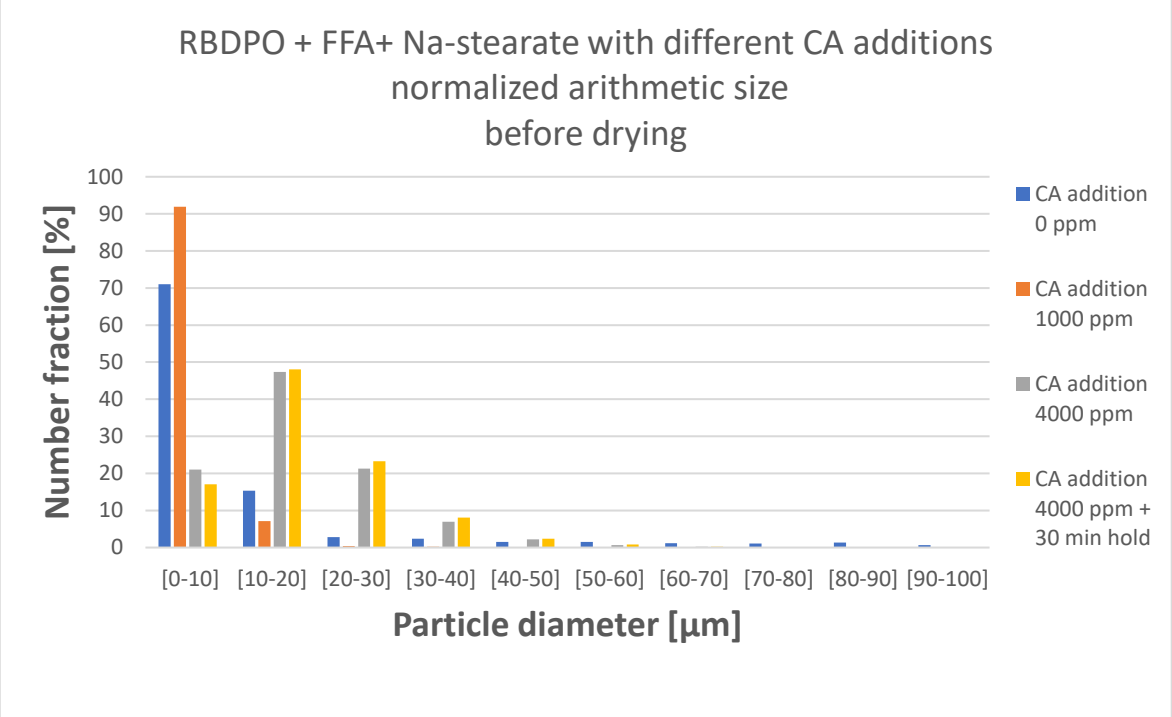

Figure 86 Normalized arithmetic size distribution with the samples containing RBDPO, FFA and Na-stearate. Samples have different CA additions, and they are measured before the drying procedure.

Some small particles leaked during the filtration to the product oil. The particle size distribution can be seen in Figure 87, where it can be noticed that the leaking concerns only very small particles. The Figure is percentage-based and therefore does not show any numerical value to how many particles have actually travelled through the filter media.

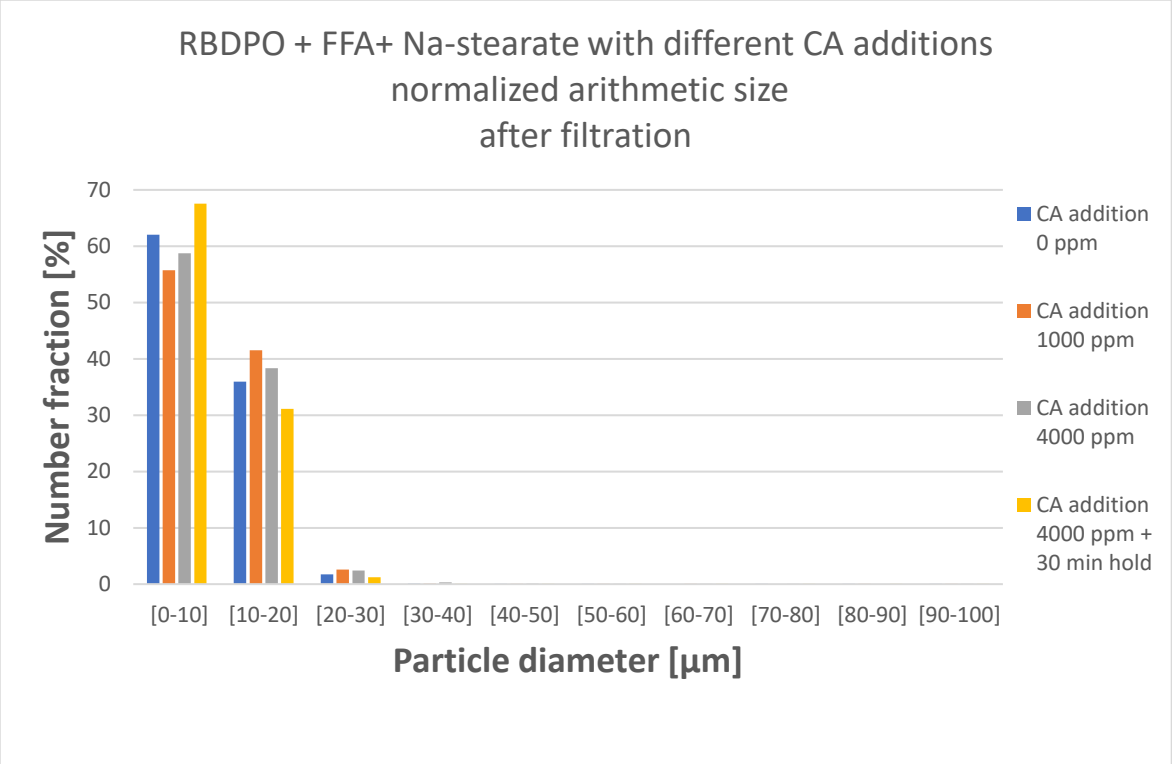

Figure 87 Normalized arithmetic size distribution with the samples containing RBDPO, FFA and Na-stearate. Samples have different CA additions, and they are measured after filtration.

The volumetric particle size distribution data from these experiments was not seen reliable enough due to the particle detecting challenges, and therefore is not presented here.

7.3.2 Calcium stearate additions

The experiments presented in this chapter are described in Table 11. Drying procedure is defined “as usual” referring to the drying procedure described in Table 2.

Table 11 Metal addition in the feedstock with different CA additions. Experimental parameters.

Exp no.	Feed	Metal component addition n (mol)	CA addition (ppm)	Water addition (w %)	Drying	HSM speed (rpm)	HSM time (min)	Rest before filtration
36	RBDPO 90 w % + FFA 10 w %	Calcium stearate 0,001 mol	0	0.5	as usual	8000	2	no
38	RBDPO 90 w % + FFA 10 w %	Calcium stearate 0,001 mol	1000	0.5	as usual	8000	2	no
39	RBDPO 90 w % + FFA 10 w %	Calcium stearate 0,005 mol	4000	0.5	as usual	8000	2	no
40	RBDPO 90 w % + FFA 10 w %	Calcium stearate 0,005 mol	4000	0.5	as usual	8000	2	30 min
41	RBDPO 90 w % + FFA 10 w %	Calcium stearate 0,001 mol	1000	0.5	as usual	8000	2	30 min

Calcium stearate was added to the solution according to the amount of CA addition. The concentrations studied in these experiments were 0 ppm, 1000 ppm and 4000 ppm of CA, with the exception that the solution with 0 ppm of CA did have the calcium stearate addition of 0,001 mol.

It was noticed in the first calcium stearate experiment (exp 36) that the solution of RBDPO, FFA and calcium stearate needed more heating to keep the solution in the liquid phase. Under 100 °C the solution tended to solidify. Even when heated, slimy clusters were present in the solution. Pixact did not recognize those as particles, and the visible appearance was more on the slimy side than the actual particle looking side. From the Figure 88, the feedstock and its

foggy nature can be seen on the left. After acid addition, there are many small particles present. The filtrate obtained from this experiment was foggy, with some particles present in the solution. The heating of the filtrate did not make any difference to the foggy look.

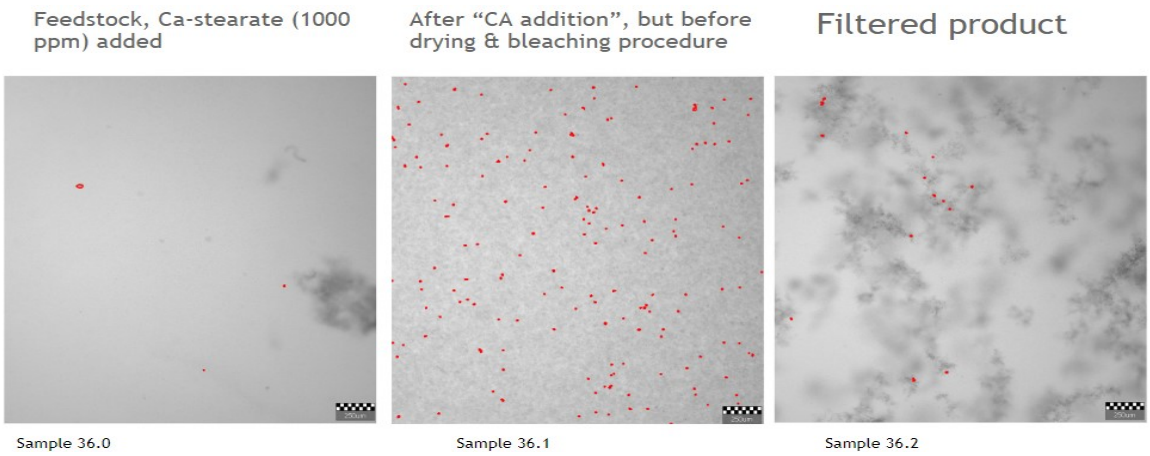

Figure 88 exp 36. Calcium stearate addition of 0,001 mol, CA addition 0 ppm. Feedstock on the left side, product after acid treatment in the middle, filtered product on the right.

Experiment 38 repeated the behaviour of the feedstock, having a tendency to solidify quite easily and including foggy clusters. The acid treatment seemed to increase the viscosity of the solution, as it was hard to get air bubbles out of the solution. The air bubbles are shown as black circles in the Pixact measurement, for example in the Figure 89 air bubbles are present in the picture.

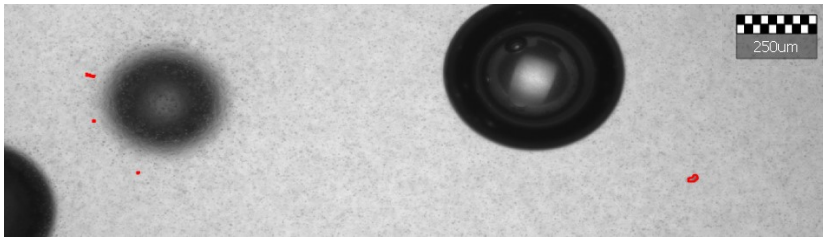

Figure 89 Air bubbles present in the solution. In the zoomed pictures small particles can be detected from the fog. Picture is taken from the experiment 36, where Ca-stearate is present.

Unlike the experiment 36, the addition of CA helped to remove foggy nature from the solution, as the filtrate came out clear (Figure 90).

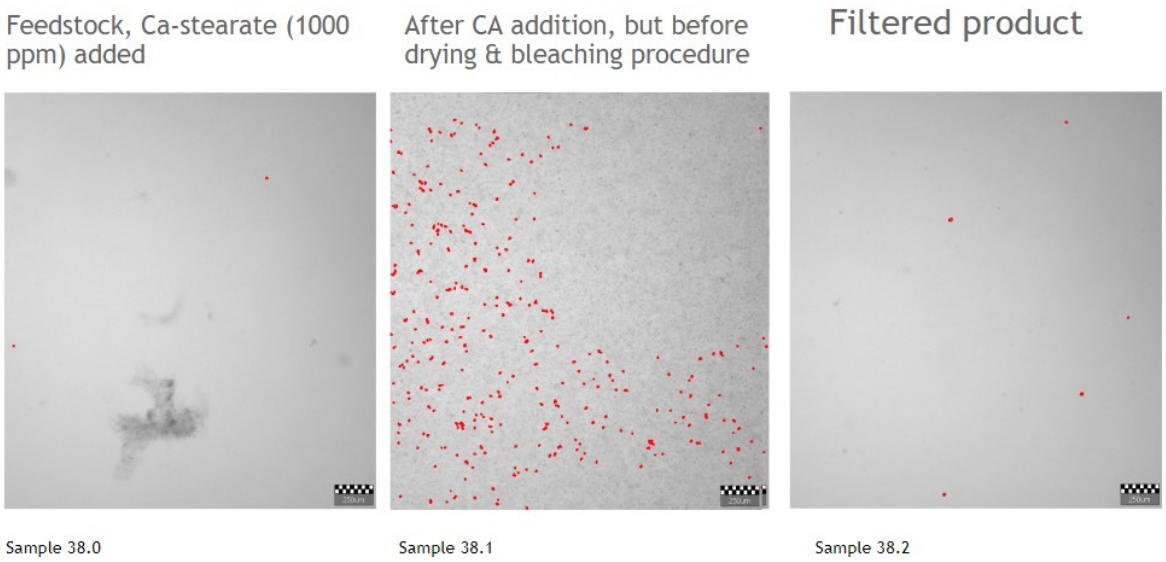

Figure 90 exp 38. Calcium stearate addition of 0,001 mol, CA addition 1000 ppm. Feedstock on the left side, product after acid treatment in the middle, filtered product on the right.

In the middle picture in Figure 90, it can be seen that the Pixact measurement was having a hard time detecting small particles from the solution. It is likely that the size and amount of particles are on the limits of Pixact measurement, as it detected particles sometimes only partly as in this picture, and sometimes its performance was improved with the same settings. The experiment 41 was otherwise a repeat of the experiment 38, but the product was held in the heating closet for 30 minutes before filtration. The resting did not affect the Pixact results, as they came out similarly.

In the experiment 39 (Figure 91), 0,005 mol of calcium stearate and CA were added to the solution. Feedstock needed at least 100 °C to stay in the liquid phase. Slimy clusters in the feedstock were not recognized as particles, and Pixact measurement could not actually detect any particles from the feedstock. After acid treatment, the amount and size of the particles are increased significantly. Viscosity of the solution was also increased and tended to hold the air bubbles in the solution. Filtrate from this experiment came out clean. The experiment

40 repeated the experiment 39 in other ways, but having the product held in the heating closet for 30 minutes before filtration. Pixact measurement did not show any difference compared to the results obtained in experiment 39.

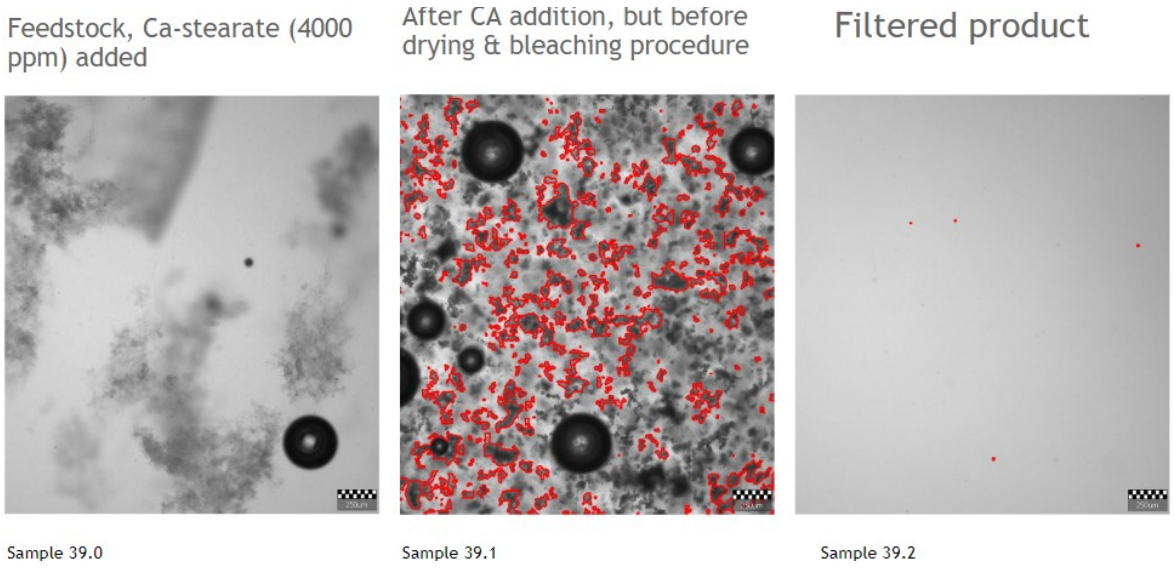

Figure 91 exp 39. Calcium stearate addition of 0,005 mol, CA addition 4000 ppm. Feedstock on the left side, product after acid treatment in the middle, filtered product on the right.

The normalized arithmetic size distribution for the experiments presented in this chapter is presented in the Figures 92 and 93. As in the earlier chapter with the experiments with Na-stearate, here with Ca-stearate the results should be read with a little caution, as there were some challenges with the Pixact measurement. The size of the particles in the samples with CA addition of 0 ppm or 1000 ppm is mostly very small. The samples with 4000 ppm, especially the samples that were left to rest before the filtration, hold larger size particles. As before, after filtration there are only very small particles left, as can be seen from the Figure 93.

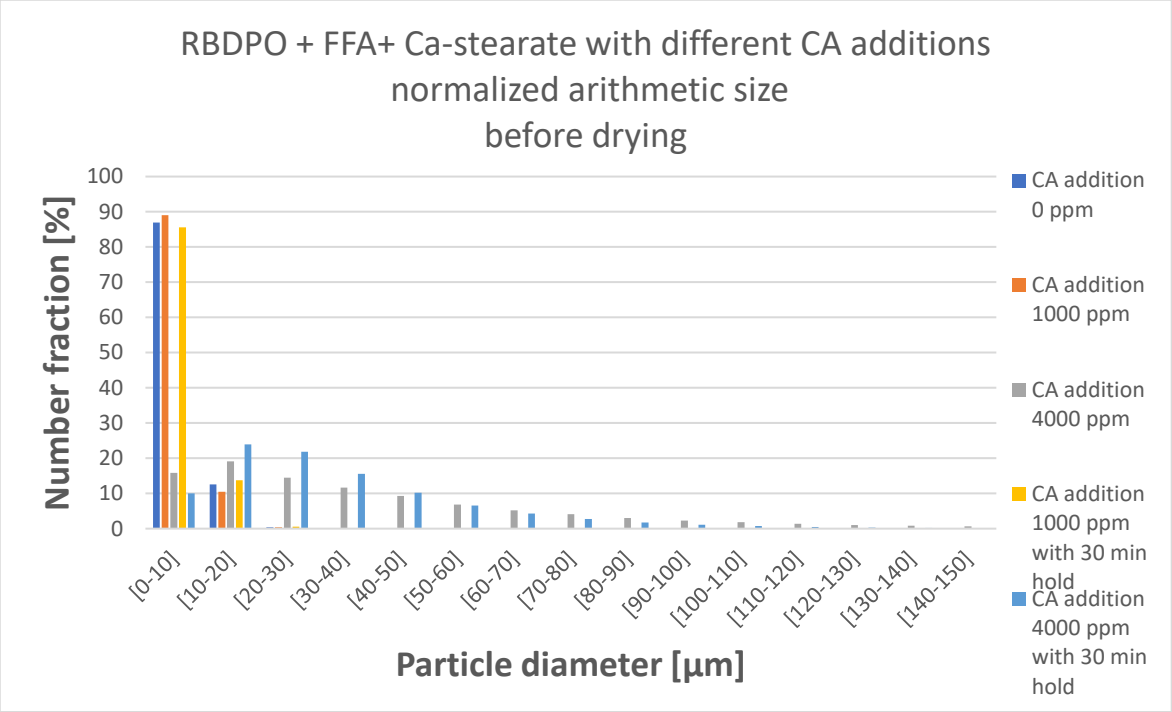

Figure 92 Normalized arithmetic size distribution for Ca-stearate experiments with different CA addition. The measurement was done before drying.

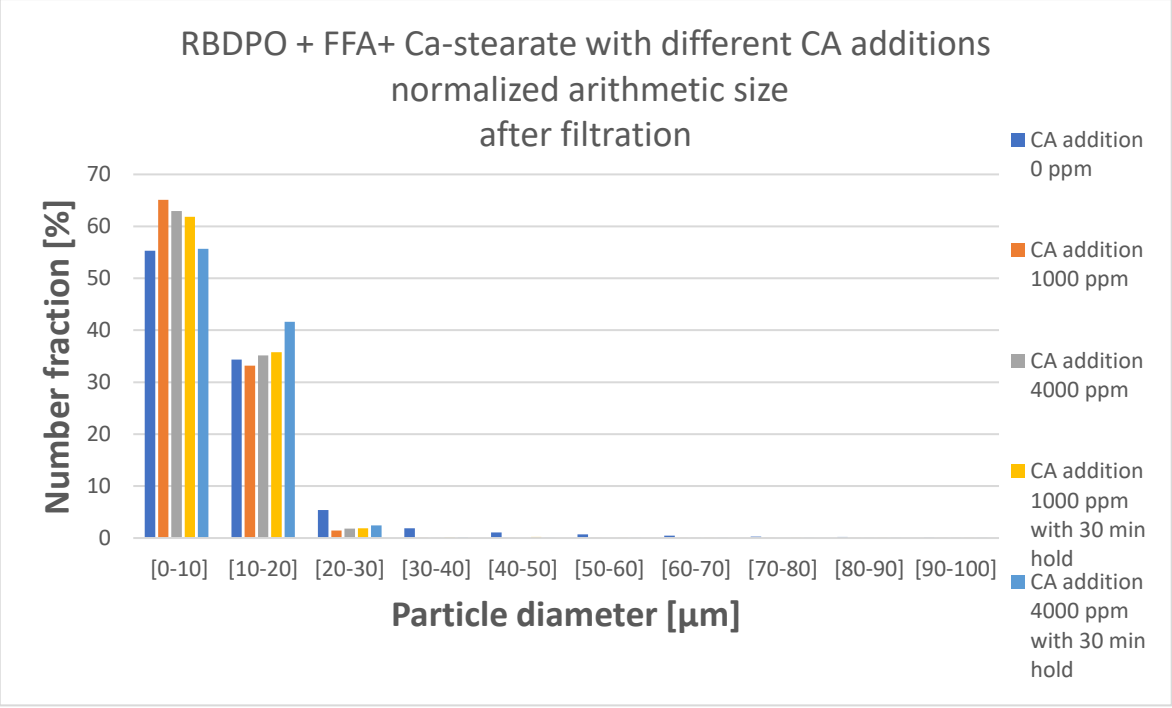

Figure 93 Normalized arithmetic size distribution for Ca-stearate experiments with different CA addition. The measurement was done after filtration.

The volumetric particle size distribution data from these experiments was not seen reliable enough due to the particle detecting challenges, and therefore is not presented here.

7.3.3 Combined results

In these metal addition experiments a certain amount of metal compound (either Na-stearate or Ca-stearate) was added to the RBDPO+FFA feedstock. Each experiment included acid treatment with additions of CA and water and mixing them with a HSM. After mixing, first Pixact measurement was completed, and the sample was brought to bleaching. The bleaching process was followed by the drying procedure, and after that the sample was either filtered or left to rest in the heating closet for 30 minutes before filtration. The Pixact analysis was performed again after filtration.

The results from the sodium stearate and calcium stearate experiment series are collected in Tables 12. Table 12 contains the filterability resistance results and includes information from the ICP metal analysis performed to the samples. In the Table 12, the metal addition given is the amount of metal component added to the solution, to meet the amount of CA addition of 1000 ppm or 4000 ppm. RBDPO and FFA are included in all experiments, but the metal addition does not give the information about the amount of soap in the solution.

Table 12 Filterability resistance results

Exp. number	Metal addition (mol)	Citric acid addition (ppm)	Filterability resistance (GPa*s)/kg^2	Duration min	Feedstock metal content (Na or Ca) mg/kg	Filtrate metal content (Na or Ca) mg/kg
37	0 mol	1000	138	5.5	Na: <0.46; Ca: <1.2	Na: <0.46; Ca: <1.2
32	Na-stearate 0,002 mol	0	293	6	310	130
31	Na-stearate 0,002 mol	1000	851	11.5	-No sample-	0.88
33, 34	Na-stearate 0,010 mol	4000	2034	22.5	1300; 1300	18; 22
35	Na-stearate 0,010 mol with resting	4000	1016	13.75	-No sample-	26
36	Ca-stearate 0,001 mol	0	299	6	260	150
38	Ca-stearate 0,001 mol	1000	6050	85	-No sample-	<1.2
39	Ca-stearate 0,005 mol	4000	799	16	1100	<1.2
40	Ca-stearate 0,005 mol with resting	4000	1192	16.75	1100	26
41	Ca-stearate 0,005 mol with resting	1000	6931	68	260	1.6

The effect of high amounts of metals is visible from the results. The filterability resistance increased immediately (although only lightly at 0 ppm of CA) when the metal compound was added to the solution.

The behaviour of sodium stearate is quite straight-forward, the filterability resistance increased while the concentration of metal compound was increased. Letting the mid-product to rest in the heating closet for 30 minutes did ease the filtration. Possible explanation is that the formed particles created bigger clusters that stayed on the top of the cake during filtration.

The behaviour of calcium stearate is a bit different but still has its own logic. Based on the pictures from Pixact, the particles formed in the experiment 38 (where metal compound and 1000 ppm of CA were present) are very small, almost on the limits of Pixact measurement. Therefore a possible explanation for the high filterability resistance laid in the cake. The small particles have probably blocked the cake almost completely. The next experiment with 4000 ppm eased the situation, as the particles were much larger. The solution of calcium stearate with high concentration was also left to rest for 30 minutes in the heating closet, but interestingly this did not bring the same result as with sodium stearate. The filterability resistance increased both with 1000 ppm and 4000 ppm. It is possible that more particles were formed during resting, but maybe larger particles did not manage to keep their structure and broke down to smaller pieces.

ICP results show that the procedure without the CA addition cannot remove large amounts of metals, only a part is removed during bleaching and filtration. CA addition enhances the removal of the metals, especially the removal of calcium is efficient. The hold did not improve but deteriorated the metal removal in any series. Sodium seems to be the harder one to be removed from the solution, although it did not affect the filtration as much. Problems caused by sodium may come up later in the process in real life situations.

Charts for arithmetic particle size distribution and volumetric particle size distribution for these experiments are available in Appendix 7. From these charts one can observe that the main fraction of the particles are very small in size. Here one needs to remember that the Pixact measurement was having troubles with the samples containing Na-stearate or Ca-stearate, so the results from Pixact analysis should be read with a little caution. When the

addition of CA was 1000 ppm, and it can be noticed that the amount of small particles is larger in the samples containing metal addition. The samples with RBDPO or RBDPO + FFA have a bit wider particle size distribution, which also might be due to the challenges with Pixact measurement.

In the sample containing 4000 ppm of CA it can be seen that the Ca-stearate added to the solution caused a significant amount of larger particles present in the solution compared to the other solutions. Na-stearate seems to form small particles similar in size than the ones present in the RBDPO or RBDPO + FFA after CA addition.

The normalized volumetric size distributions for the addition 0, 1000 and 4000 ppm with and without the resting may be affected by the challenges the Pixact measurement had with the sample, and a small caution should be taken. When the CA addition was 0 ppm, only the sample with Ca-stearate shows a bit different particle size distribution compared to the other ones. The main challenge with the Na-stearate sample was the amount of small particles that Pixact measurement could not properly measure, so the volumetric size distribution may give a bit too large volumes for the particles the measurement did see. The sample with Ca-stearate was foggy, which may or may not disturbed the measurement.

Both of the samples with metal additions and CA addition of 1000 ppm had a lot of small particles, and the volumetric size distribution may be quite correct. The amount of metal seems to widen the particle volume distribution.

When adding 4000 ppm of CA into the solution, the amount of small particles is the biggest with plain RBDPO and with Na-stearate samples, and as was seen from the Figures presented earlier, 4000 ppm of CA added to the sample with Ca-stearate caused enormous amounts of large clusters in the sample.

In these results it should be remembered that the challenges with the Pixact measurement may affect the results and small caution should be taken. Overall the results from these metal addition experiments indicate that the soap splitting is an important step in the purification process for a metal removal, although the formed particles cause problems to the filterability. Further studies regarding the amount of metal in the oil and the ratio of CA to metal/soap component should be conducted.

7.4 Technical feedstocks

Two different feedstocks were studied in this series of experiments to see how the acid addition affects the filterability of a real-life feedstock. The experimental set up remained similar as described before. In these experiments, the solution is treated by acid addition, bleaching, drying and filtration procedures. Both of the chosen feedstocks contain significant amounts of sodium and/or calcium.

7.4.1 Animal fat

The experiments presented in this chapter are described in Table 13. Drying procedure is defined “as usual” referring to the drying procedure described in Table 2.

Table 13 Animal fat feedstock with different CA additions. Experimental parameters.

Exp no.	Feed	CA addition (ppm)	Water addition (w %)	Drying	HSM speed (rpm)	HSM time (min)	Hold before filtration
42	AF	0	0.5	as usual	8000	2	no
43	AF	1000	0.5	as usual	8000	2	no
44	AF	4000	0.5	as usual	8000	2	no

The animal fat feedstock used for these experiments contains 100 ppm of sodium and 34 ppm of calcium. Three experiments were conducted with a CA additions of 0 ppm, 1000 ppm and 4000 ppm. Other variables were kept as before according to Table 2.

From the experiment 42 (Figure 94), it can be seen that the animal fat feedstock on the left in the Figure already contained quite a lot of particles in the beginning. Only the water addition was added in this experiment, and the presence of extra water seems to increase the amount of particles in the solution. After filtration the filtrate came out clear.

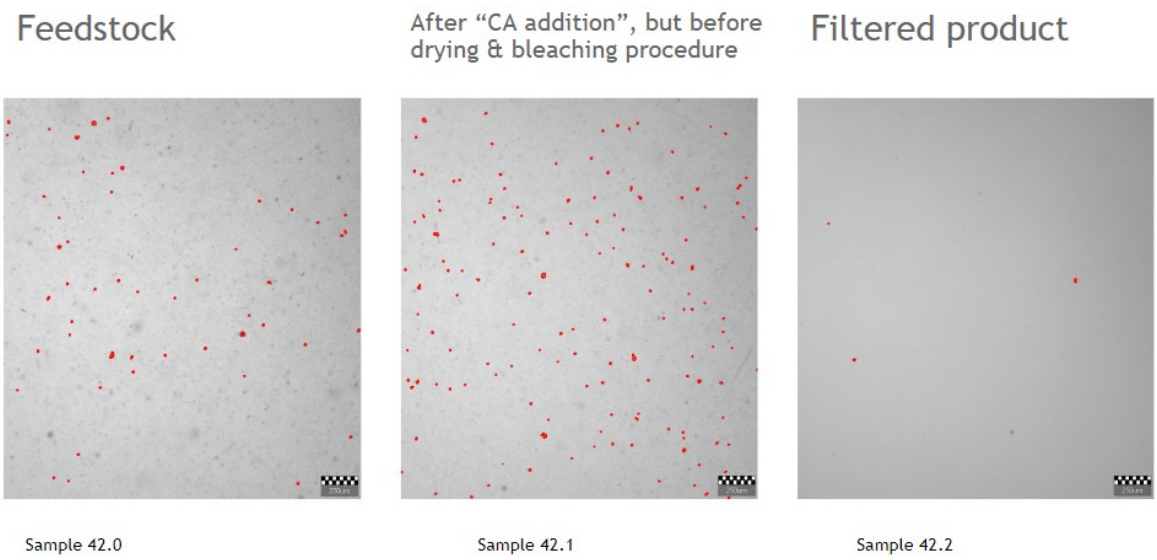

Figure 94 exp 42. Technical feedstock, CA addition 0 ppm. Feedstock on the left side, product after acid treatment in the middle, filtered product on the right.

In experiment 43, 1000 ppm of citric acid was added to the feedstock. As it can be seen from Figure 95, in the beginning animal fat contained a certain amount of particles, but the amount is visibly increased after acid treatment. The filtrate was clear.

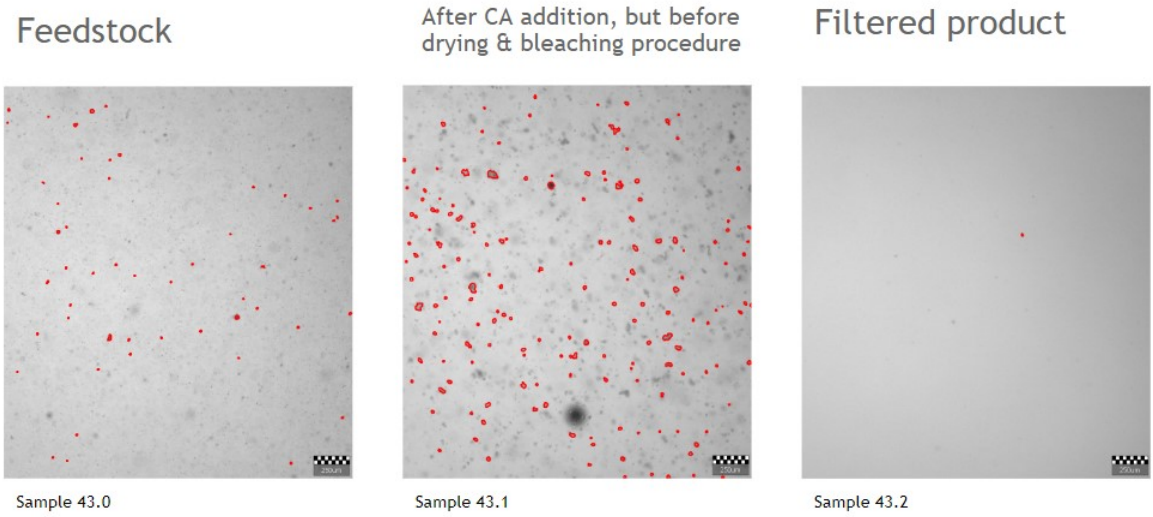

Figure 95 exp 43. Technical feedstock, CA addition 1000 ppm. Feedstock on the left side, product after acid treatment in the middle, filtered product on the right.

Experiment 44 is presented in Figure 96. The feedstock contained a certain amount of particles in the beginning. After acid treatment, Pixact measurement did not detect particles properly anymore, as there were too many of them. The difference compared to RBDPO experiments is that there are no visible clusters or agglomerates of crystallized citric acid, as seen in the earlier experiments. The presence of calcium might affect the particle formation, as the foggy outcome was present in calcium stearate experiences.

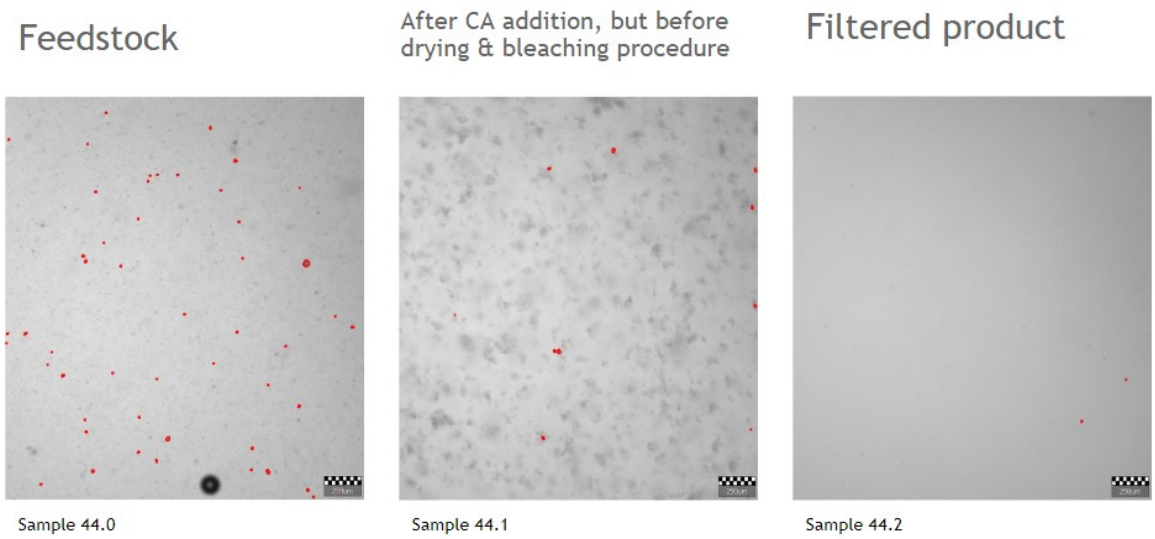

Figure 96 exp 44. Technical feedstock, CA addition 4000 ppm. Feedstock on the left side, product after acid treatment in the middle, filtered product on the right.

The normalized arithmetic size distribution of the particles can be observed from the Figure 97. The AF feedstock itself contains a certain amount of particles, which are mostly small in size based on the Pixact measurement. In 0 ppm CA addition, the water addition was done (according to Table 2) and the amount of small particles was increased in the sample. The CA additions of 1000 ppm and 4000 ppm increased the amounts of larger particles in the samples. The results from the filtered samples contained few particles that leaked through the filter media, the fractions of small particles are the main ones. The whole Figure can be observed in Appendix 5.

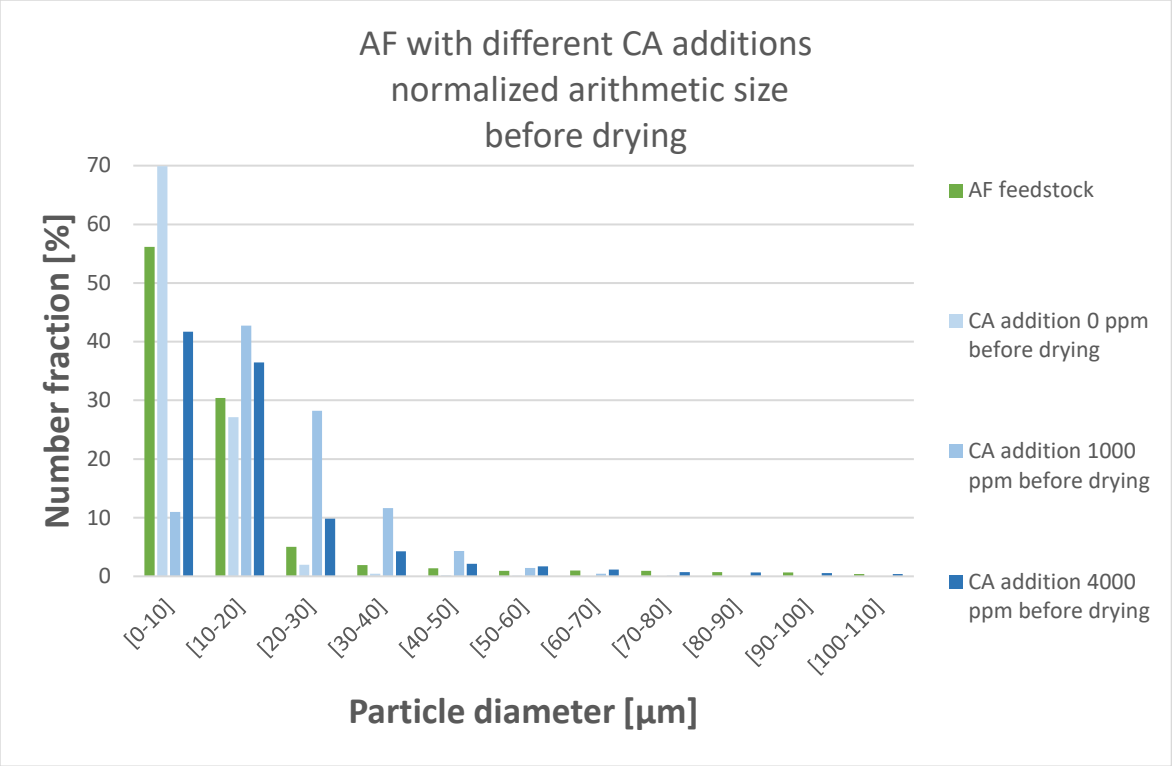

Figure 97 The normalized arithmetic size distribution for AF samples with different CA additions. The samples are measured before drying.

In Figure 98 the volumetric size distribution is shown to the samples presented in this chapter. AF itself contains a certain amount of particles, and the 0 ppm CA addition seems to move mostly on the same volumetric sizes as the AF does. As seen before, adding 1000 ppm of CA increased the amount of particles having smaller volume, and 4000 ppm of CA increased the amount of particles having larger volume.

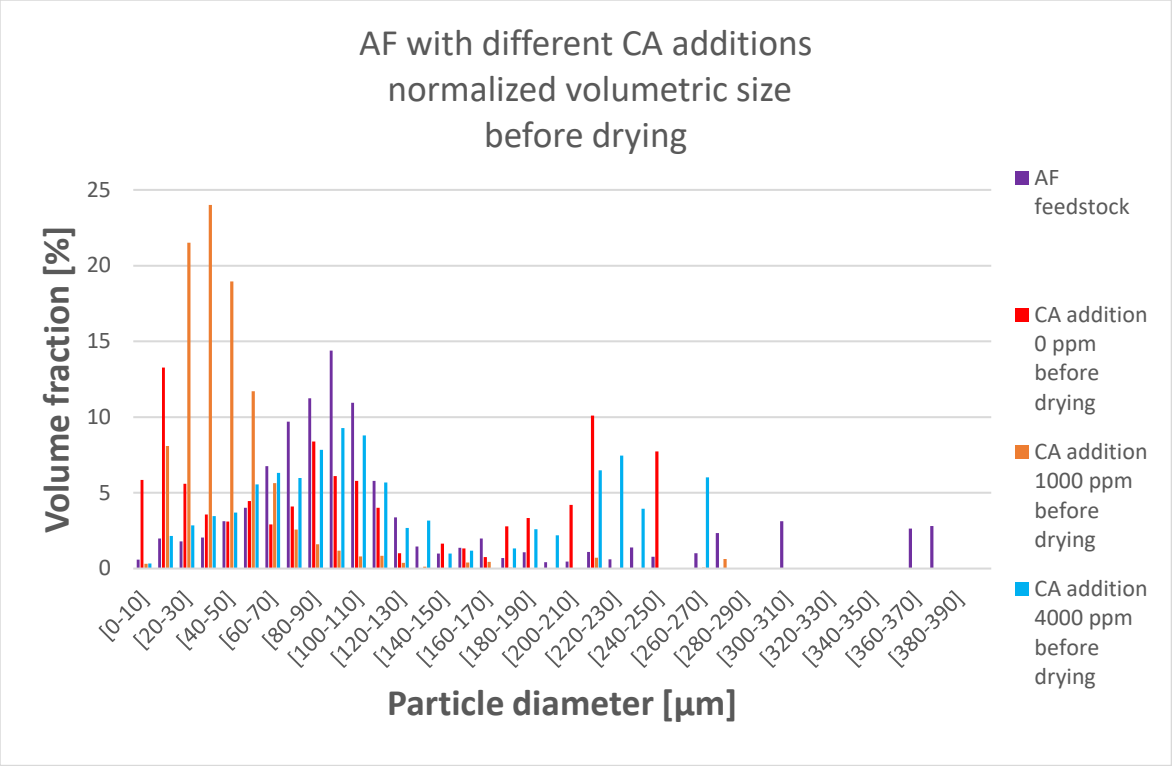

Figure 98 The normalized volumetric size distribution for AF samples with different CA additions

The Figure containing also results after filtration samples are presented in Appendix 5. From the volume fraction it can be seen that the leaked particles are having a small volume, and no extra particle or cluster formation seems to happen after the filtration step.

7.4.2 Brown grease

The experiments presented in this chapter are described in Table 14. Drying procedure is defined “as usual” referring to the drying procedure described in Table 2.

Table 14 Brown grease feedstock with different CA additions. Experimental parameters

Exp no.	Feed	CA addition (ppm)	Water addition (w %)	Drying	HSM speed (rpm)	HSM time (min)	Hold before filtration
45	BG	0	0.5	as usual	8000	2	no
46	BG	1000	0.5	as usual	8000	2	no
47	BG	4000	0.5	as usual	8000	2	no

The brown grease feedstock used for these experiments contains 240 ppm of sodium and 310 ppm of calcium. Three experiments were conducted with CA additions of 0 ppm, 1000 ppm and 4000 ppm. Other variables were according to Table 2.

In the experiment 45 (Figure 99), no citric acid addition was performed during the acid treatment. The feedstock itself contains a lot of particles, and their amount seems to stay similar during the acid treatment. The product after filtration was clear-looking.

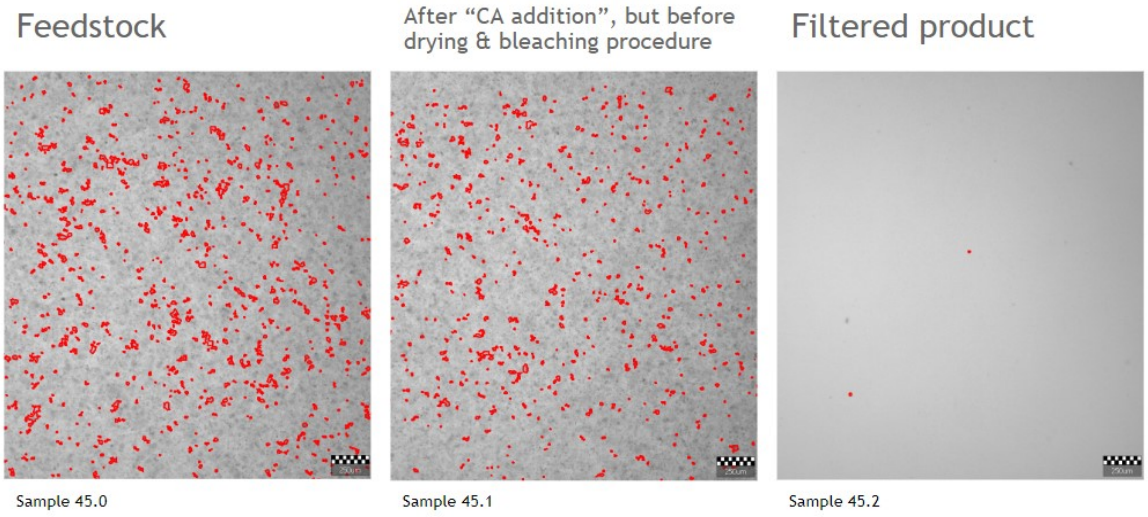

Figure 99 exp 45. Technical feedstock, CA addition 0 ppm. Feedstock on the left side, product after acid treatment in the middle, filtered product on the right.

In the experiment 46 (Figure 100), 1000 ppm of CA was added to the solution. From the Pixact measurement it can be recognized that Pixact is having troubles detecting all the particles from the acid treated sample. The high amount of calcium may disturb the

measurement, as it tends to form foggy clusters to the sample. Filtrate from this experiment was clear.

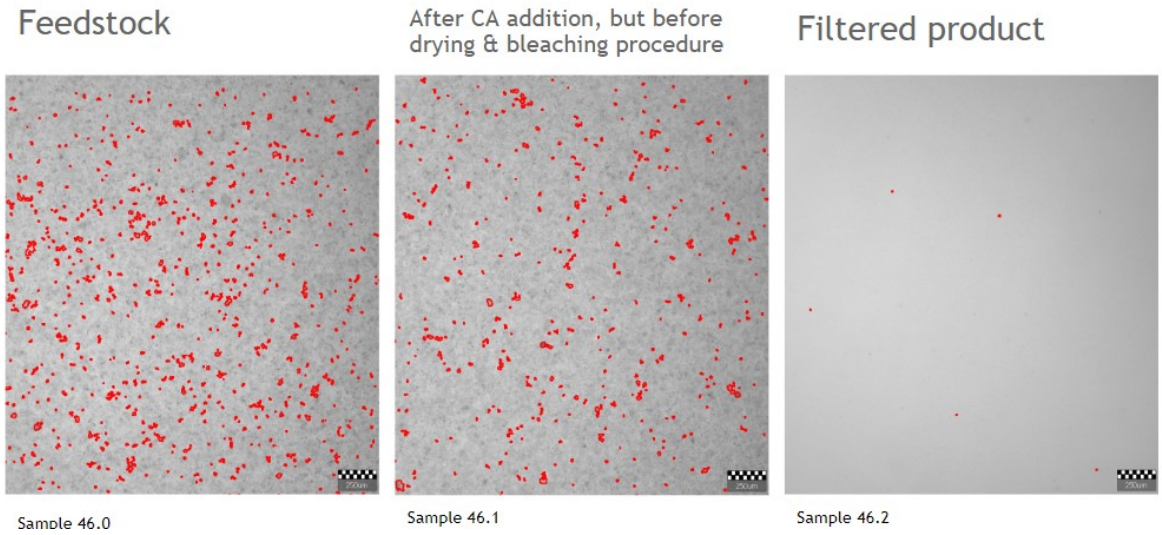

Figure 100 exp 46. Technical feedstock, CA addition 1000 ppm. Feedstock on the left side, product after acid treatment in the middle, filtered product on the right

In the last experiment, the experiment 47, 4000 ppm of citric acid was added to the solution. As can be seen from Figure 101, the feedstock contained a large amount of particles in the beginning. After acid treatment, Pixact is not able to detect most of the particles anymore. Possible reasons are the high amount of particles in the solution, the small size of the particles (sodium) and/or the foggy nature of the sample (calcium). After filtration the filtrate is clear.

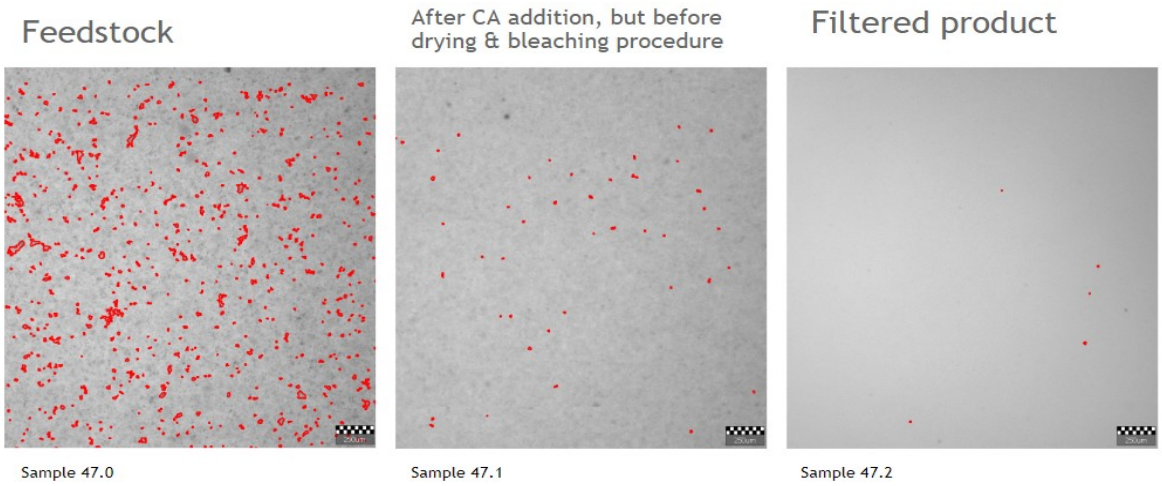

Figure 101 exp 47. Technical feedstock, CA addition 4000 ppm. Feedstock on the left side, product after acid treatment in the middle, filtered product on the right

The normalized arithmetic size distribution is shown in Figure 102. The feedstock itself contains small particles, and the CA addition in the samples did not make any notable change to the particle size distribution compared to the feedstock. The drying procedure seemed to increase the amount of small particles in the samples with all CA additions. The Figure with filtrate results can be observed in Appendix 5.

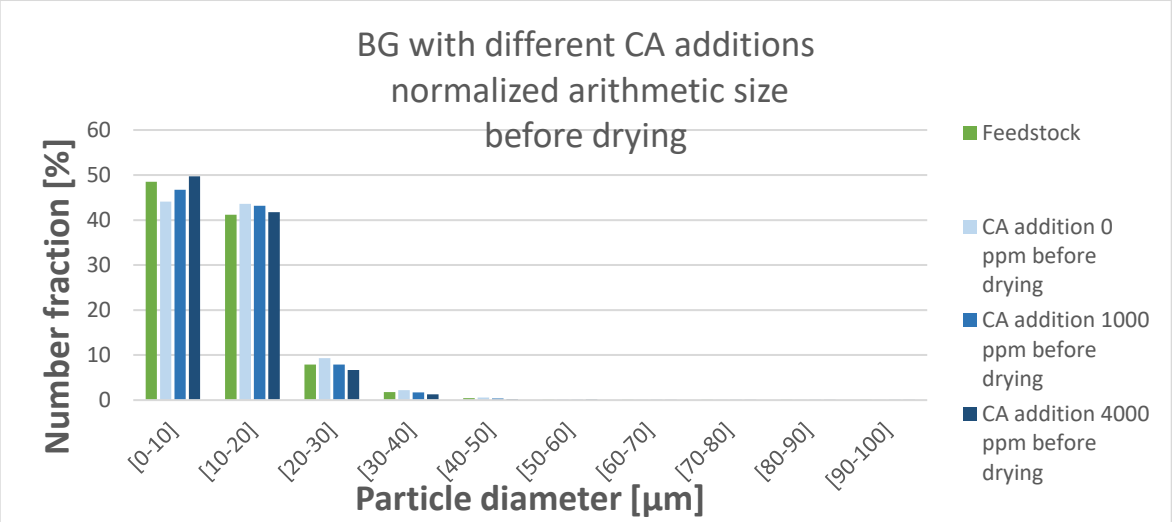

Figure 102 The normalized arithmetic size distribution of BG samples, with different CA additions.

In Figure 103 the volumetric size distribution of the particles is shown for the experiments presented in this chapter (before drying). With addition 0 ppm and 1000 ppm, most of the particles present in the solution represent small volumetric sizes. The CA addition of 4000 ppm has wider volumetric particle size distribution compared to the others.

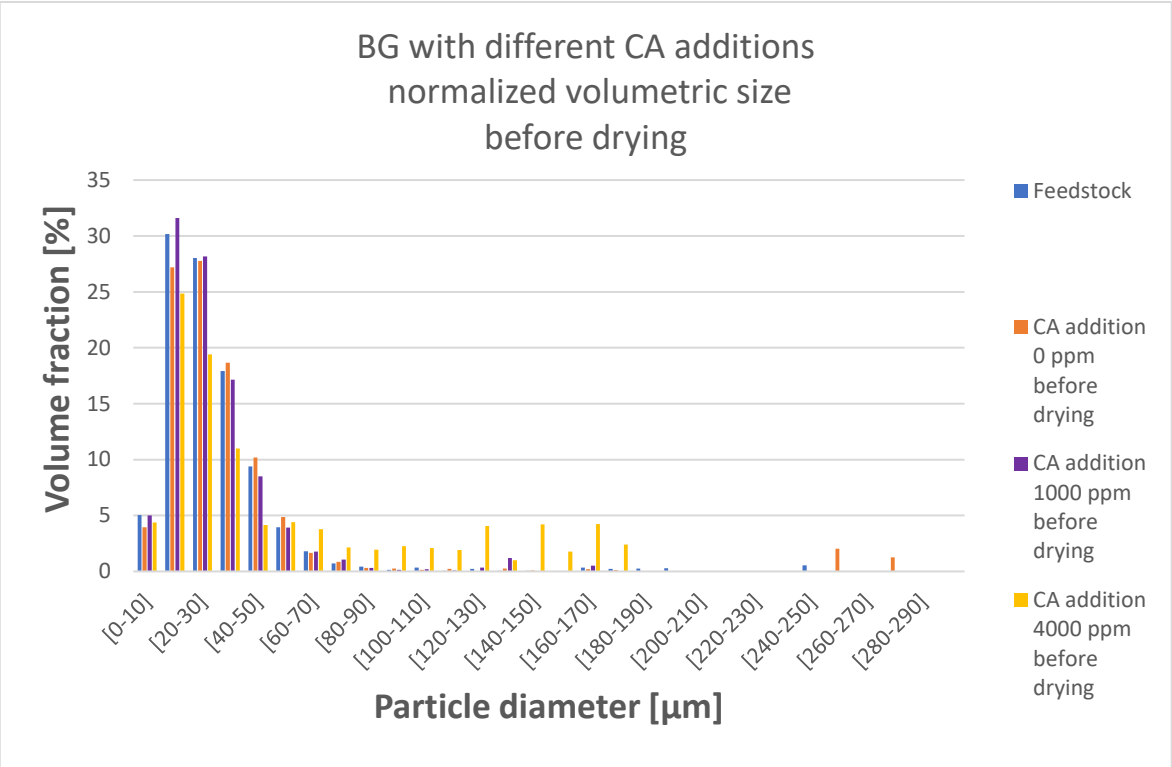

Figure 103 The volumetric size distribution of BG samples, with different CA additions.

After filtration there are interestingly some particles of larger volume present in the samples, although from the Figures it can be seen that the numerical amount of particles present is very small. The Figure including results for the filtrate can be observed in Appendix 5.

7.4.3 Combined results

The filterability resistance results and ICP analysis results are collected to Table 15. Results from the samples sent to ICP analysis are collected to Table 16. Filtration charts can be observed in Appendix 4.

Table 15 Filterability resistance results from the technical feedstock experiments

Experiment number	Feedstock	Citric acid addition ppm	Filterability resistance (GPa*s)/kg^2	Duration min
42	AF	0	1153	16.5
43	AF	1000	350	7.5
44	AF	4000	1005	19
45	BG	0	1242	15
46	BG	1000	2987	33.5
47	BG	4000	1804	18

Table 16 Results from the technical feedstock samples analysed with ICP

Experiment number	Feedstock	Citric acid addition ppm	Feedstock Na content mg/kg	Feedstock Ca content mg/kg	Filtrate Na content mg/kg	Filtrate Ca content mg/kg
42	AF	0	100	34	14	<1,2
43	AF	1000	100	34	2.3	1.4
44	AF	4000	100	34	0.84	2.6
45	BG	0	240	310	170	220
46	BG	1000	240	310	150	93
47	BG	4000	240	310	9.5	1.2

The Figure 104 includes Pixact analysis results combined from the experiments with a CA addition of 1000 ppm or 4000 ppm. The feedstock in these experiments were RBDPO, AF and BG. The RBDPO and BG seem to contain more small particles when 1000 ppm of CA was added to the solution. AF holds a bit bigger particles. Similar trends seem to be with the samples having 4000 ppm of CA added.

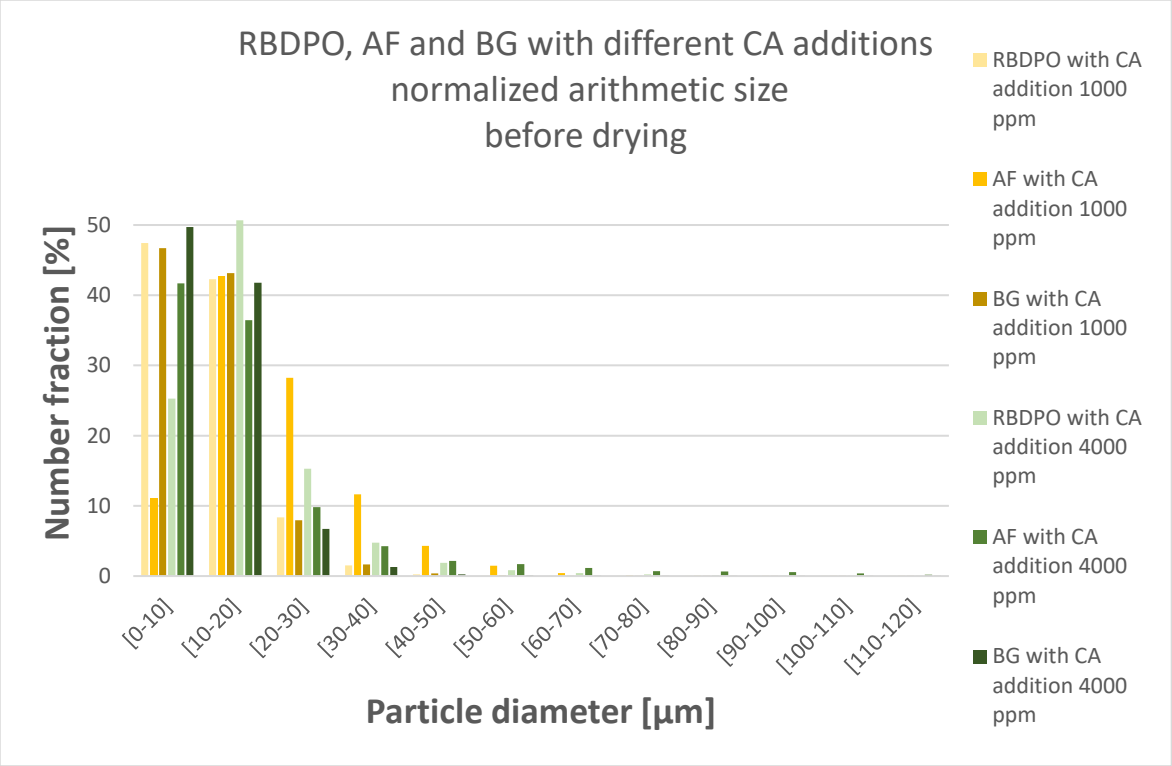

Figure 104 The normalized arithmetic size distribution for the samples of different feedstocks containing 1000 ppm or 4000 ppm of CA. The analysis has been performed before drying.

Figure 105 shows the arithmetic particle size distribution after the filtration. From the Figures delivered by Pixact, the number of particles in each sample is quite small. The particle size distribution indicated that the particles remaining in the solution are very small, and the cakes created by AF and BG seem to hold particles better compared to RBDPO, where larger size particles are present especially with 4000 ppm CA addition before filtration.

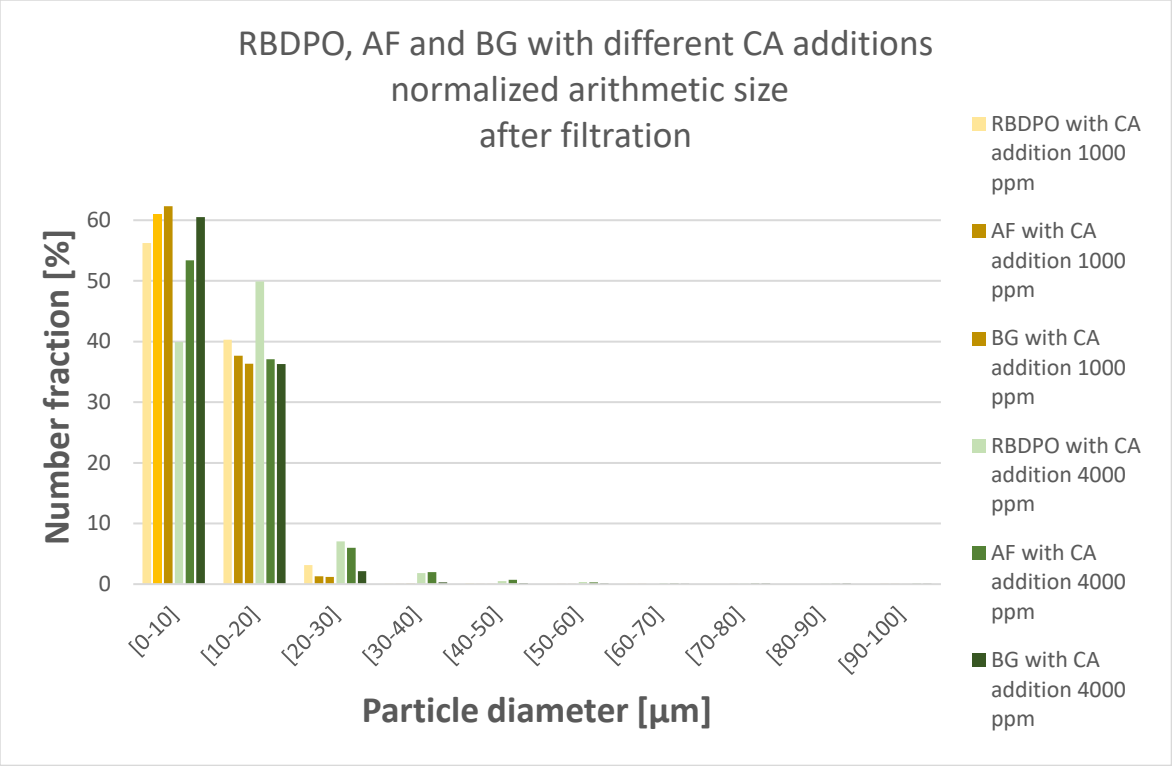

Figure 105 The normalized arithmetic size distribution for the samples of different feedstocks containing 1000 ppm or 4000 ppm of CA. The analysis has been performed after filtration.

In Figures 106 and 107 the volumetric size distribution is presented before drying and after filtration respectively. In Figure 106 one can notice that the volumetric size of particles is following the line of earlier experiments, and the samples with CA addition of 4000 ppm contain particles with larger volumetric size. With 1000 ppm CA addition, the results are quite similar for all three different feedstocks: the volumetric size of the particles present in the solution is quite small.

After filtration, Figure 107 shows that with the 4000 ppm CA addition, the volumetric size of the remaining particles is bigger compared to the remaining particles in the samples of 1000 ppm CA addition. The volumetric particle size distribution is wider with 4000 ppm of CA. Although one should remember that the numerical amount of particles after filtration is very small, and few particles with larger volume affect the measurement much more than in samples where a lot of particles are present.

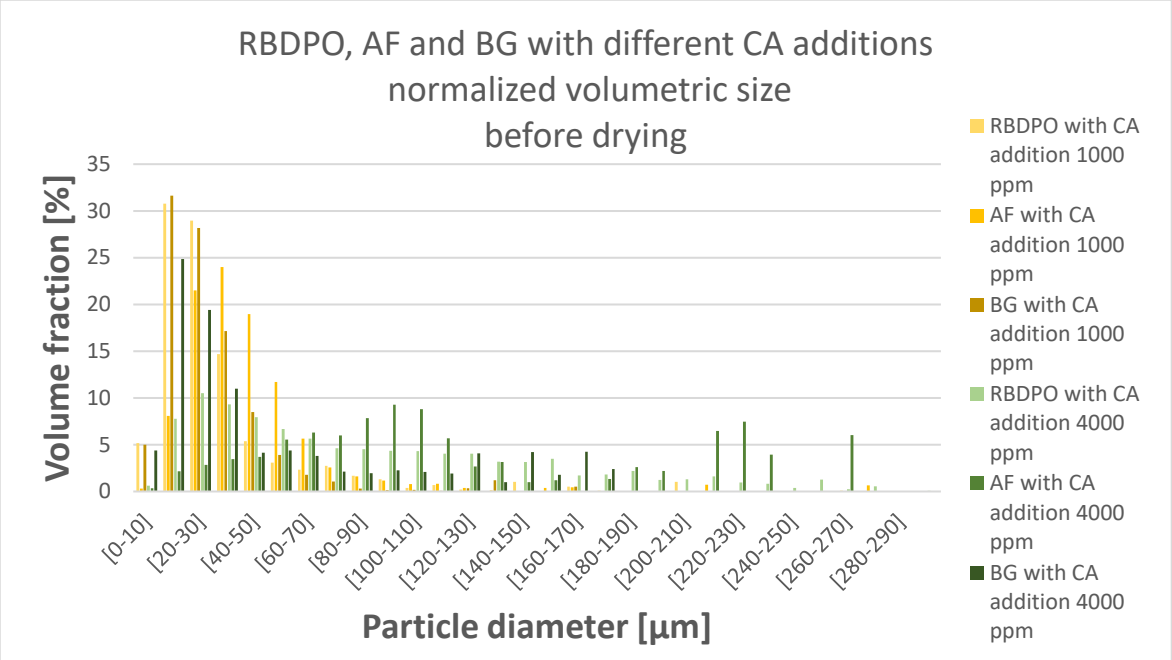

Figure 106 The normalized volumetric size distribution for the samples of different feedstocks containing 1000 ppm or 4000 ppm of CA. The analysis has been performed before filtration.

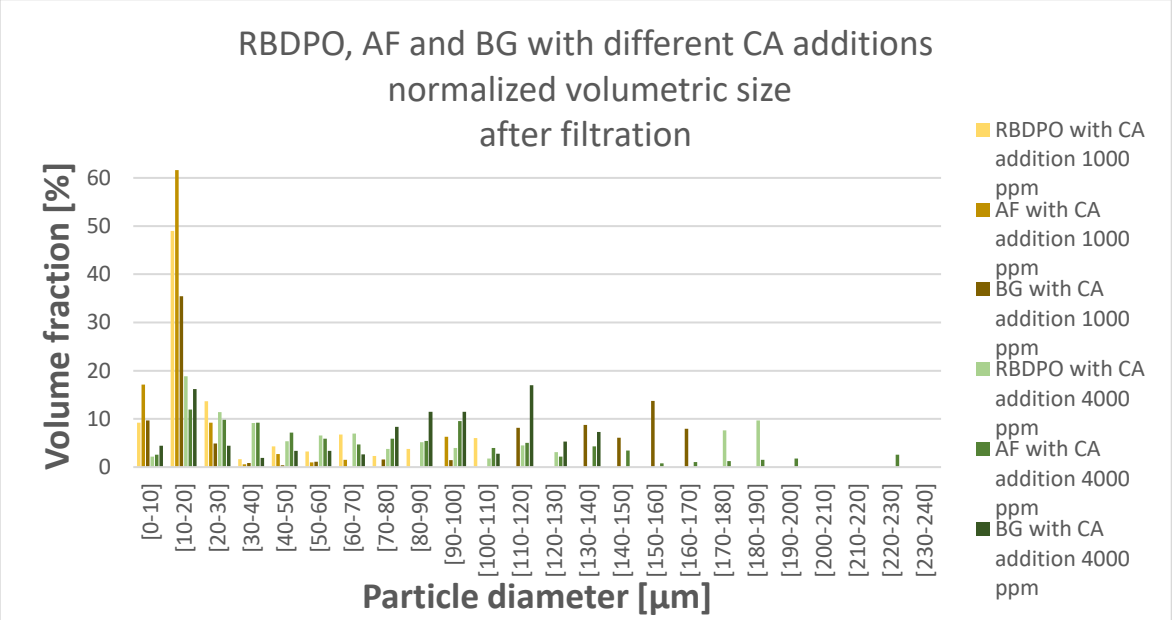

Figure 107 The normalized volumetric size distribution for the samples of different feedstocks containing 1000 ppm or 4000 ppm of CA. The analysis has been performed after filtration.

Based on the earlier experiments with sodium stearate and calcium stearate there seems to be some logic: AF contains high amounts of sodium, and some amount of calcium. The filterability resistance behaves like in the earlier experiments with sodium stearate: It increases when increasing the amount of CA. Interesting thing is that the experiment with no CA had the highest filterability resistance. It is possible that the CA creates clusters into the solution that stay on the top of the cake. With the sample similar to the AF, one can notice that the filterability is the most optimal with 1000 ppm of CA, and overdosing causes troubles to the filterability. The metal removal with a larger dose is slightly better, but not significantly.

BG for instance contains very high amounts of both sodium and calcium. Its behavior is similar compared to the calcium stearate experiments, and the foggy nature is present in these experiments, probably caused by the presence of calcium soap on the solution. It can be suspected that it is the calcium that forms very small particles in the solution, which later tend to block the cake. The filterability of BG samples was the poorest with 1000 ppm of CA addition, similarly as in the metal addition experiment with Ca-stearate. The filterability and the removal of metal components increased significantly when the CA concentration was increased in the solution. Especially with samples containing large amounts of calcium, a larger dose of CA could benefit the metal removal and improve the filterability.

8 Conclusions

The aim of this thesis was to focus on the behavior of citric acid (CA) in oil containing metal impurities. The thesis includes several experiments, where the connection between CA, its amount in the oil and the presence of metal components were observed.

The first experimental series confirms the hypothesis that increasing the amount of citric acid increased the particle formation in the oil. With larger CA additions the size of the particles was significantly increased, and the particle size distribution was wide. The amount of particles was seen to increase during time, until they stabilize to a certain level, and therefore time can be found as a valuable variable (chapter 7.1.1). During the first series, other variables were also studied. From these experiments, the amount of water in the oil did not play a significant role but disturbed the measurement when present in larger concentrations. The effect of time was also seen when different mixing times and speeds were tested. Too low mixing speed led to the situation where the water was insufficiently dispersed into the oil. Too short mixing time delayed the visible particle formation. In these experiments, the drying step did not seem to affect the particle size distribution or the amount of particles in the solution.

Filterability was first studied with RBDPO and CA, with different CA additions. The concentration of CA did not remarkably affect the filterability, and only small differences in the filterability resistance were discovered. The samples with larger CA concentration formed larger amounts of agglomerates in the solution that might ease the filtration by piling on the top of the cake during the filtration, as their filterability resistance was seen to be a slightly smaller compared to the other samples.

To study the effect of metal components in the solution, FFA was added to the original RBDPO feedstock to improve the solubility of the metal component. The effect of FFA in the solution was briefly tested, and it was seen to hinder the formation of the particles. The time for visible particles to appear increased, and their amount was smaller compared to the earlier experiments with similar CA addition. Otherwise, the FFA addition did not cause any practical issues during the experiments, and the filterability resistance was also similar compared to the RBDPO feedstock.

The results from metal addition experiments show that the filterability of the solution is immediately more challenging. The behavior of sodium stearate with CA in a RBDPO + FFA solution was seen to be quite straightforward, as the filterability resistance and filtration time increased with the concentrations of metal component and CA increased. Letting the solution rest for a while did help the filterability, as the large agglomerates formed in the solution stay on the top of the cake. Calcium stearate in the RBDPO + FFA solution had a bit different behavior, as it increased the filterability resistance and filtration time remarkably when the concentration of CA was 1000 ppm. The lower or higher concentrations did increase the filtration resistance and the filtration time as well, but the increase was not so extreme. Resting the samples before filtration increased the filterability resistance in both calcium stearate samples (additions of 1000 ppm and 4000 ppm).

The reason behind the troubles calcium stearate addition brought to the filtrations can be the shape and the size of the particles, but this would need further investigation, as in the samples with CA addition of 1000 ppm the size of the particles is so small, although the amount of particles is large, that Pixact measurement is having troubles detecting them from the sample. Hypothetically, that the particles in sodium stearate experiment with 1000 ppm of CA added to the solution are more spherical compared to the calcium stearate experiment with similar addition, as the calcium stearate solution seemed to blind the cake much more than the sodium stearate solution did. The experiments with 4000 ppm of CA are more similar when comparing the filtration results, although the sodium stearate sample tended to blind the cake mildly.

ICP results from these metal addition experiments showed that the metal content from the solution can be only partly removed from the solution by filtration, and the CA addition is necessary for the metal removal. Especially calcium can be removed almost perfectly from the solution. One can notice that the resting before filtration may improve the filterability in case of a sample containing sodium stearate, but the metal removal is poorer in all samples.

The last experiments were performed on technical feedstock samples. The samples used in these experiments were AF and BG, both containing significant amounts of sodium and calcium. AF has a large sodium content, but the amount of calcium is small. The filtration experiments are similar compared to the sodium stearate experiments, and the filterability resistance increased while the concentration of CA was increased. The interesting result was that without any CA addition, the filterability resistance is quite high. With this sample, the

formed agglomerates in the sample may enhance the filterability as the cake may retain them on the top and therefore the blinding of the cake is prevented. The particle formation continues the same logic that has been seen before in these experiments with different CA additions: the higher the concentration the higher is the amount and size of the formed particles. AF samples similar to the one used in these experiments seem to have the optimal dosage of CA set to the level of 1000 ppm, where the metal removal is sufficient, and the filterability resistance is good. Overdosing improves the metal removal, but also the filterability resistance is increased significantly.

BG feedstock used in these experiments contains large amounts of both sodium and calcium. The behavior of the samples is similar compared to the calcium stearate experiments, and the foggy nature is present in the samples. The filterability of the BG samples was at the poorest with 1000 ppm of CA addition, similar compared to the calcium stearate experiments, and may indicate that the size and shape of the particles are small needle-like, as they tend to block the cake. The filterability resistance decreased, and the metal removal increased significantly with the concentration of CA was increased in the solution. For this type of sample, the extra amount of CA could benefit the metal removal and improve the filterability.

The Pixact measurement used in these experiments seemed promising and provided a huge amount of information about the samples. In some samples, the size of the particles was on the low limit of Pixact measurement, which may have affected the results. Also, in some samples the amount of particles and formed agglomerated was so huge that detecting the particles accurately from the solution was difficult, and this may also influence the results presented in this thesis. For further development, the Pixact measurement could be developed as an analysis method, where the samples with high amounts of particles can be diluted to improve the detection of particles

Based on the results presented in this thesis, the CA addition during the pretreatment process similar to the one used in the experiments is necessary from the purification point of view for splitting the soap and removing the metal components from the oil. The CA addition may also cause challenges to the filtration process instead of improving it. The CA to metal/soap ratio in the pretreatment process is recommended to study further to improve both the metal removal and filterability.

References

Adewale, P., Dumont, M., Ngadi, M., 2015. Recent trends of biodiesel production from animal fat wastes and associated production techniques. *Renewable and Sustainable Energy Reviews*. Vol 45, Iss. 1, 574-588.

Alptekin, E., Canakci, M., Sanli, H., 2014. Biodiesel production from vegetable oil and waste animal fats in a pilot plant. *Waste Management*. Vol. 34, Iss. 11, 2146-2154.

Arancon, R., Lin, C., Chan, K., Kwan, T., Luque, R., 2013. Advances on waste valorization: new horizon for a more sustainable society. *Energy Science & Engineering; London*. Vol. 1, Iss. 2, 53-71.

AZO materials, https://www.azom.com/article.aspx?ArticleID=18136 [Accessed] 26.7.2023

Beckmann, W., 2013. Crystallization: Basic Concepts and Industrial Applications. *John Wiley & Sons, Incorporated. ProQuest Ebook Central*

Bockisch, M., 1998. Fats and Oils Handbook. *AOCS Press*.

Bondioli, P., Carelli, G., Grosso, M., 2019. Animal fats for non-food uses. A review of technology and critical points. *Rivista Italiana Delle Sostanze Grasse*. Vol 96, Iss. 1, 5-15.

Bourcier, D., Féraud, J.P., Colson, D., Mandrick, K., Ode, D., Brackx, E., Puel, F., 2016. Influence of particle size and shape properties on cake resistance and compressibility during pressure filtration. *Chemical Engineering Science*. Vol 144, Iss. 1, 176-187.

Buchori, L., Istadi, I., Purwanto, P., 2016. Advanced Chemical Reactor Technologies for Biodiesel Production from Vegetable Oils – a review. *Bulletin of Chemical Reaction Engineering and Catalysis*. Vol 11, Iss. 3, 406-430.

Carter, R., Yan, Y., 2005. Measurement of particle shape using digital imaging techniques. *Journal of Physics: Conference Series*. Vol. 15.

Chaloupková, V., Ivanova, T., Krepl, V., 2019. Particle size and shape characterization of feedstock material for biofuel production. *Agronomy Research*. Vol 17, Iss. 5, 1861–1873.

Chegg, https://www.chegg.com/learn/topic/structure-of-phospholipid [Accessed 4.8.2023]

Chen, S-Y., Teerananont, N., Sonthisawate, T., Sreesiri, P., Puemchalad, C., Mochizuki, T., Abe, Y., Toba, M., Yoshimura, Y., 2014. A cost-effective acid degumming process produces high-quality Jatropha oil in tropical monsoon climates. *European Journal of Lipid Science and Technology*. Vol 117, Iss. 7. 1079-1087.

Chiaramonti, D., Goumas, T., 2019. Impacts on industrial-scale market deployment of advanced biofuels and recycled carbon fuels from the EU Renewable Energy Directive II. *Applied Energy*. Vol. 251, 113351.

Clínica Diabetológica, https://clinidiabet.com/en/infodiabetes/cardiodiabetes/15.htm [Accessed 4.8.2023]

Cornacchia, M., Moser, G., Saturno, E., Trucco, A., Costamagna, P., 2022. Analysis of particle size distribution in municipal wastewaters. *Environmental Technology & Innovation*. Vol. 27, 102638.

Cruz-Matías, I., Ayala, D., Hiller, D., Gutsch, S., Zacharias, M., Estradé, S., Peiró, F., 2019. Sphericity and roundness computation for particles using the extreme vertices model. *Journal of Computational Science*. Vol 30, 28-40.

Di Pietro, M., Mannu, A., Mele, A., 2020. NMR Determination of Free Fatty Acids in Vegetable Oils. Processes. Vol 8, Iss. 4, 410.

Dijkstra, A. 'Introducing to Degumming', from *AOCS Lipid Library*. Read 31.03.2023 https://lipidlibrary.aocs.org/edible-oil-processing/introduction-to-degumming

Doroszkowski, A., 1999. Particle size and size measurement. Paint and Surface Coatings: Theory and Practice (Second edition). *Woodhead Publishing*, 243-285.

Ebnesajjad, S., 2011. Handbook of Adhesives and Surface Preparation. *William Andrew Publishing*.

Elena, C., Cerminati, S., Ravasi, P., Rasia, R., Peiru, S., Menzella, H., Castelli, M., 2017. B. cereus phospholipase C engineering for efficient degumming of vegetable oil. *Process Biochemistry*. Vol 54, Iss. 1, 67-72.

Elliot, D., 2007. Historical Developments in Hydroprocessing Bio-oils. *Energy Fuels*. Vol 21, Iss. 3, 1792–1815.

Endo, Y., Alonso, M., 2001. Physical Meaning of Specific Cake Resistance and Effects of Cake Properties in Compressible Cake Filtration. *Filtration & separation*. Vol. 38, Iss. 7, 42-46.

European Biofuels fact sheet: Fatty Acid Methyl Esters (FAME). https://www.etipbioenergy.eu/images/fame-fact-sheet.pdf [Accessed 31.7.2023]

European Biofuels fact sheet: Hydrogenated vegetable oil (HVO). https://www.etipbioenergy.eu/images/ETIP_B_Factsheet_HVO_feb2020.pdf [Accessed 31.7.2023]

FDPP (Factory Direct Pipeline Products), https://fdpp.com/articles/depthsurface.htm [Accessed 4.8.2023]

Fiume, M., Heldreth, B., Bergfeld, W., et al, 2014. Safety Assessment of Citric Acid, Inorganic Citrate Salts, and Alkyl Citrate Esters as Used in Cosmetics. *International Journal of Toxicology*. Vol 33, Iss. 2. 16-46.

Gharby, S. 2022. Refining Vegetable Oils: Chemical and Physical Refining. *The Scientific World Journal*. Vol. 2022.

Gupta, M., 2017. Practical Guide to Vegetable Oil Processing (2nd Edition). *AOCS Press*.

Haramkar, S., Thombre, G., Jadhav, S., Thorat, B., 2021. The influence of particle (s) size, shape and distribution on cake filtration mechanics—a short review. *Comptes Rendus. Chimie*, 24(2), 255-265.

Hirata, G., Abreu, C., Bessa, L., Ferreira, M., Batista, E., Meirelles, A., 2013. Liquid-liquid equilibrium of fatty systems: A new approach for adjusting UNIFAC interaction parameters. *Fluid Phase Equilibria*. Vol. 360, 379-391.

Hund, D., Antonyuk, S., Ripperger, S., 2017. Simulation of Bridging at the Static Surface Filtration by CFD-DEM Coupling. *EPJ Web of Conferences*. 140, 09033.

Jayasinghe, P., Hawboldt, K. 2012. A review of bio-oils from waste biomass: Focus on fish processing waste. *Renewable and Sustainable Energy Reviews*. Vol. 16, Iss. 1, 798-821.

Jiang, Y., 2019. Rice Bran and Rice Bran Oil, Chapter 4 - Bioprocessing Technology of Rice Bran Oil. AOCS Press.

Jillavenkatesa, A., Dapkunas, S., Lum, L., 2001. Particle size characterization. *National Institute of Standards and Technology*, Report no. 960-1.

Kaduk, J., Rammohan, A., 2018. Crystal structures of alkali metal (Group 1) citrate salts. *Structural Science, Crystal Engineering and Materials*. Vol 74, Iss. 2, 239-252.

Kargbo, D., 2010. Biodiesel Production from Municipal Sewage Sludges. *Energy Fuels*. Vol 24, Iss. 5, 2791–2794.

Koris, A., Marki, E., 2006. Ceramic ultrafiltration membranes for non-solvent vegetable oil degumming (phospholipid removal). *Desalination*. Vol 200, Iss. 1-3, 537-539.

Krom, B., Warner, J., Konings, W., Lolkema, J., 2000. Complementary metal ion specificity of the metal-citrate transporters CitM and CitH of Bacillus subtilis. *Journal of Bacteriology*. Vol 182, Iss. 22, 6374-81.

Lambda Scientific, website download: LEOI-30A Theory of Fraunhofer diffraction. https://lambdasys.com/uploads/info/LEOI-30A-Theory.pdf [Accessed 2.8.2023]

Lee, A., Myerson, A., 2006. Particle Engineering: Fundamentals of Particle Formation and Crystal Growth. *MRS Bulletin*. Vol 31, 881–886.

Lehtinen, O., Nugroho, R., Lehtimaa, T., Vierros, S., Hiekkataipale, P., Ruokolainen, J., Sammalkorpi, M., Österberg, M., 2017. Effect of temperature, water content and free fatty acid on reverse micelle formation of phospholipids in vegetable oil. *Colloids and Surfaces B: Biointerfaces*. Vol 160, 355-363.

Li, S., Tang, W., Li, M., Wang, L., Yang, Y., Gong, J., 2019. Understanding the Role of Citric Acid on the Crystallization Pathways of Calcium Oxalate Hydrates. *Crystal Growth & Design*. Vol 19, Iss. 6, 3139–3147.

List, G., (2009). Bleaching and Purifying Fats and Oils - Theory and Practice (2nd Edition). *AOCS Press*.

Liu, X., Jia, X., Zhuangfei, Z., Li, Y., Hu, M., Zhou, Z., Ma, H. (2011). Crystal Growth and Characterization of Diamond from Carbonyl Iron Catalyst under High Pressure and High Temperature Conditions. *Crystal Growth & Design*. Vol 11. Iss. 9.

Liu, X., Zhu, F., Zhang, R., Zhao, L., Qi, J., 2021. Recent progress on biodiesel production from municipal sewage sludge. *Renewable and Sustainable Energy Reviews*. Vol 135, Iss. 1, 110260.

Lusas, W., Riaz, M., Alam, M., Clough, R., 2017. Handbook of industrial Chemistry and Biotechnology (13th edition): Animal and Vegetable Fats, Oils, and Waxes. *Springer* p. 823-932.

Macaringue, E., Li, S., Li, M., Gong, J., Tang, W., 2020. Crystallization behavior of citric acid based on solution speciation and growth kinetics. *CrystEngComm*. Vol 22, Iss. 1, 8189-8196.

Malven Panalytical website, https://www.malvernpanalytical.com [Accessed 26.7.2023]

MedChemExpress, https://www.medchemexpress.com/Citric_acid.html [Accessed 4.8.2023]

Morales, G., Bautista, F., Melero, J., Iglesias, J., Sánchez-Vázquez, R., 2011. Low-grade oils and fats: Effect of several impurities on biodiesel production over sulfonic acid heterogeneous catalysts. *Bioresource Technology*. Vol 102, Iss. 20, 9571-9578.

Msagati, T., 2012. The Chemistry of Food Additives and Preservatives. *John Wiley & Sons, Incorporated*.

Mullin, J.W.. (2001). Crystallization (4th Edition). *Elsevier*.

Müller, F., de Oliveira, D., Michels, C., 2023. Current status, gaps and challenges of rendering industries wastewater. *Journal of Water Process Engineering*. Vol. 52, Iss. 1. 103480.

Nikiforidis, C., Gilbert, E., Scholten, E., 2015. Organogel formation via supramolecular assembly of oleic acid and sodium oleate. *RSC Advances*. Vol 5, 47455-47475.

Nisar, S., Hanif, M., Rashid, U., Hanif, A., Akhtar, M., Ngamcharussrivichai, C., 2021. Trends in Widely Used Catalysts for Fatty Acid Methyl Esters (FAME) Production: A Review. *Catalysts.* Vol 11, Iss. 9, 1085.

Picart, P., Jun-Chang, L., 2012. Digital Holography. *John Wiley & Sons, Incorporated.*

PIXACT, https://pixact.fi [Accessed 4.8.2023]

Phuah, E., Tang, T., Lee, Y., Choong, T., Chin-Ping, T., 2015. Review on the Current State of Diacylglycerol Production Using Enzymatic Approach. *Food and Bioprocess Technology*. Vol 8, Iss. 6, 1169-1186.

PubChem, https://pubchem.ncbi.nlm.nih.gov/compound/Palmitic-Acid#section=2D-Structure [Accessed 4.8.2023]

Rhodes, M., 2008. Introduction to Particle Technology (second edition). *John Wiley & Sons, Incorporated*.

Rodríguez-Machín, L., Arteaga-Pérez, L., Pala, M., Herregods-Van De Pontseele, K., Pérez-Bermúdez, R., Feys, J., Prins, W., Ronsse, F., 2019. Influence of citric acid leaching on the yield and quality of pyrolytic bio-oils from sugarcane residues. *Journal of Analytical and Applied Pyrolysis*. Vol 137, 43-53.

Santori, G., Di Nicola, G., Moglie, M., Polonara, F., 2012. A review analyzing the industrial biodiesel production practice starting from vegetable oil refining. *Applied Energy*. Vol 92, 109-132.

Scala, F., 2013. Fluidized bed technologies for near-zero emission combustion and gasification. *Woodhead Publishing.* Series in Energy, Number 59.

Shukla, P.C., Shamun, S., Gren, L., Malmborg, V., Pagels, J., Tuner, M., 2018. Investigation of Particle Number Emission Characteristics in a Heavy-Duty Compression Ignition Engine Fueled with Hydrotreated Vegetable Oil (HVO). *SAE International Journal of Fuels and Lubricants*. Vol. 11, Iss. 4, 495-505.

Silverson, https://www.silverson.com/us/resource-library/application-reports/refining-of-edible-oils [Accessed 4.8.2023]

Silverson, https://www.silverson.com/us/products/laboratory-mixers/ [Accessed 5.10.2023]

Sparks, T., Chase, G., 2016. Filters and Filtration Handbook (6th Edition). *Elsevier Science*.

Staš, M., Chudoba, J., Kubička, D., Blažek, J., Pospíšil, M., 2017. Petroleomic Characterization of Pyrolysis Bio-oils: A Review. *Energy & Fuels*. Vol 31, Iss. 10, 10283-10299.

Svarovsky, L., 2000. Solid-Liquid Separation. *Elsevier Science & Technology*.

Snowsill, W.L. (2009). ‘Particle Sizing’, in Boyes, W. (ed.) Instrumentation Reference book. 4th edition. *Elsevier*.

Sondhi, S., Kumar, P., 2020. ‘Biodiesel from Sewage Sludge: An Alternative to Diesel’, in Recent Trends in Biotechnology. *MedDocs Publishers LLC*.

Świrniak, G., Mroczka, J., 2022. Forward and inverse analysis for particle size distribution measurements of disperse samples: A review. *Measurement*. Vol. 187, 110256.

Szydłowska-Czerniak, A., Łaszewska, A., 2017. Optimization of a soft degumming process of crude rapeseed oil—Changes in its antioxidant capacity. *Food and Bioproducts Processing*. Vol 105, Iss. 1, 26-35.

Tandon, P., Raudenkolb, S., Neubert, R., Rettig, W., Wartewig, S., 2001. X-ray diffraction and spectroscopic studies of oleic acid–sodium oleate. *Chemistry and Physics of Lipids*. Vol 109, Iss. 1, 37-45.

Tien, C., Ramarao, B., 2013. Can filter cake porosity be estimated based on the Kozeny-Carman equation?. *Powder Technology*. Vol. 237, Iss. 1, 233-240.

Treviranus, I., 2011. Introduction to Particle size analyses. Available at: http://www.slideshare.net/HORIBA/essentials-of-particle-size-analysis. [Accessed 25.7.2023].

Ulusoy, U., Igathinathane, C., 2016. Particle size distribution modelling of milled coals by dynamic image analysis and mechanical sieving. *Fuel Processing Technology*, Vol 143.

University of Cambridge website: Dissemination of IT for the Promotion of Material Science, Fraunhofer diffraction. https://www.doitpoms.ac.uk/tlplib/diffraction/fraunhofer.php [Accessed 2.8.2023]

Utriainen, K., 2017. Soap micelles in nonpolar media. Master’s Thesis in Chemical engineering, Aalto University.

Varzakas, T., Tzia, C., 2016. Handbook of Food Processing: Food safety, quality, and manufacturing processes. *CRC Press.*

Wadumesthrige, K., Salley, S., Ng, S., 2009. Effects of partial hydrogenation, epoxidation, and hydroxylation on the fuel properties of fatty acid methyl esters. *Fuel Processing Technology.* Vol 90, Iss. 10, 1292-1299.

Wakeman, R. (2007). The influence of particle properties on filtration. *Separation and Purification Technology*. Vol 58, Iss. 2, 234-241.

Walter, D., 2013. Primary Particles – Agglomerates – Aggregates. Wiley Online Library by Duodecim Medical Publications. https://onlinelibrary.wiley.com/doi/pdf/10.1002/9783527673919.ch1 [Accessed 2.8.2023]

Wang, A., Wang, J., Sheti, S., Dahlin, S., Han, J., Woo, J., Xie, K., Pettersson, L., Olsson, L., 2020. A deactivation mechanism study of phosphorus-poisoned diesel oxidation catalysts: model and supplier catalysts. *Catalysis Science and Technology*. Vol 10, 5602-5617.

Vanhercke, T., Wood, C., Stymne, S., Singh, S., Green, A., 2013. Metabolic engineering of plant oils and waxes for use as industrial feedstocks. *Plant Biotechnology Journal*. Vol 11, 197-210.

Viani, I., Zárybnická, L., Ševčík, R., Mácová, P., Machotová, J., Veltruská, K., 2022. Struvite-K crystal growth inhibition by citric acid: Formation of complexes in solution and surface adsorption effects. *Journal of Crystal Growth*. Vol 598, Iss. 1, 126858.

Vekilov, P., 2010. The two-step mechanism of nucleation of crystals in solution. *Nanoscale*. Vol 2, 2346-2357.

Xia, C., Pathy, A., Paramasivan, B., Ganeshan, P., Dhamodharan, K., Juneja, A., Kumar, D., Brindhadevi, K., Kim, S.-H., Rajendran, K., 2022. Comparative study of pyrolysis and hydrothermal liquefaction of microalgal species: *Analysis of product yields with reaction temperature*. Fuel. Vol. 311.

Xu, R., Di Guida, O., 2003. Comparison of sizing small particles using different technologies. *Powder Technology*. Vol 132, Iss. 2-3, 145-153.

Xu, Z. (2014). Fundamentals of Air Cleaning Technology and Its Application in Cleanrooms. *Springer, Berlin, Heidelberg*.

Zufarov, O., Schmidt, Š., Sekretár, S. and Cvengroš, J., 2009. Ethanolamines used for degumming of rapeseed and sunflower oils as diesel fuels. *European Journal of Lipid Science and Technology*. Vol 111, Iss. 1, 985-992.

Appendix 1

					High shear mixer			
Koenro	Feedstock	CA addition	Water addition	Drying procedure	Speed	Time	Resting time?	BE addition?
1	RBDPO	**0 ppm**	0.5 w%	as usual	8000 rpm	2 min	no resting	no
2	RBDPO	**500 ppm**	0.5 w%	as usual	8000 rpm	2 min	no resting	no
3	RBDPO	**1000 ppm**	0.5 w%	as usual	8000 rpm	2 min	no resting	no
4	RBDPO	**2000 ppm**	0.5 w%	as usual	8000 rpm	2 min	no resting	no
5	RBDPO	**4000 ppm**	0.5 w%	as usual	8000 rpm	2 min	no resting	no
5, 1 h	RBDPO	**4000 ppm**	0.5 w%	as usual	8000 rpm	2 min	no resting	no
6	RBDPO	1000 ppm	**0 %**	as usual	8000 rpm	2 min	no resting	no
7	RBDPO	1000 ppm	**0.5**	as usual	8000 rpm	2 min	no resting	no
8	RBDPO	1000 ppm	**1**	as usual	8000 rpm	2 min	no resting	no
9	RBDPO	1000 ppm	**2**	as usual	8000 rpm	2 min	no resting	no
9, 1 h	RBDPO	1000 ppm	**2**	as usual	8000 rpm	2 min	no resting	no
10	RBDPO	1000 ppm	**4**	as usual	8000 rpm	2 min	no resting	no
11	RBDPO	1000 ppm	0.5 w%	as usual	**2000 rpm**	2 min	no resting	no
12	RBDPO	1000 ppm	0.5 w%	as usual	**4000 rpm**	2 min	no resting	no
13	RBDPO	1000 ppm	0.5 w%	as usual	**8000 rpm**	2 min	no resting	no
14	RBDPO	1000 ppm	0.5 w%	as usual	8000 rpm	**0,5 min**	no resting	no
15	RBDPO	1000 ppm	0.5 w%	as usual	8000 rpm	**1 min**	no resting	no

16	RBDPO	1000 ppm	0.5 w%	as usual	8000 rpm	**4 min**	no resting	no
17	RBDPO	1000 ppm	0.5 w%	as usual	**10000 rpm**	**1 min**	no resting	no
18	RBDPO	**0 ppm**	0.5 w%	as usual	8000 rpm	2 min	no resting	1 w%
19	RBDPO	**1000 ppm**	0.5 w%	as usual	8000 rpm	2 min	no resting	1 w%
20	RBDPO	**4000 ppm**	0.5 w%	as usual	8000 rpm	2 min	no resting	1 w%
21	RBDPO	**4000 ppm**	0.5 w%	as usual	8000 rpm	2 min	**30 min**	1 w%
22	RBDPO + FFA 10 w-% + Na-stearate	no addition	-	-	-	-	-	no
23	RBDPO + FFA 20 w-% + Na-stearate	no addition	-	-	-	-	-	no
24	RBDPO + FFA 30 w-% + Na-stearate	no addition		-	-	-	-	no
25	RBDPO + FFA	**0 ppm**	0.5 w%	as usual	8000 rpm	2 min	no resting	no
26	RBDPO + FFA	**1000 ppm**	0.5 w%	as usual	8000 rpm	2 min	no resting	no
27	RBDPO + FFA	**4000 ppm**	0.5 w%	as usual	8000 rpm	2 min	no resting	no
28	RBDPO + FFA	1000 ppm	0.5 w%	as usual	8000 rpm	**0,5 min**	no resting	no
29	RBDPO + FFA	1000 ppm	0.5 w%	as usual	8000 rpm	**1 min**	no resting	no
30	RBDPO + FFA	1000 ppm	0.5 w%	as usual	8000 rpm	**4 min**	no resting	no
31	RBDPO + FFA 10 w-% + Na-stearate	**1000 ppm**	0.5 w%	as usual	8000 rpm	2 min	no resting	1 w%
32	RBDPO + FFA 10 w-% + Na-stearate	**0 ppm**	0.5 w%	as usual	8000 rpm	2 min	no resting	1 w%
33	RBDPO + FFA 10 w-% + Na-stearate	**4000 ppm**	0.5 w%	as usual	8000 rpm	2 min	no resting	1 w%

34	RBDPO + FFA 10 w-% + Na-stearate	**4000 ppm**	0.5 w%	as usual	8000 rpm	2 min	no resting	1 w%
35	RBDPO + FFA 10 w-% + Na-stearate	**4000 ppm**	0.5 w%	as usual	8000 rpm	2 min	**30 min**	1 w%
36	RBDPO + FFA 10 w-% + Na-stearate	**0 ppm**	0.5 w%	as usual	8000 rpm	2 min	no resting	1 w%
37	RBDPO + FFA 10w%	**1000 ppm**	0.5 w%	as usual	8000 rpm	2 min	no resting	1 w%
38	RBDPO + FFA 10 w-% + Ca-stearate	**1000 ppm**	0.5 w%	as usual	8000 rpm	2 min	no resting	1 w%
39	RBDPO + FFA 10 w-% + Ca-stearate	**4000 ppm**	0.5 w%	as usual	8000 rpm	2 min	no resting	1 w%
40	RBDPO + FFA 10 w-% + Ca-stearate	**4000 ppm**	0.5 w%	as usual	8000 rpm	2 min	**30 min**	1 w%
41	RBDPO + FFA 10 w-% + Ca-stearate	**1000 ppm**	0.5 w%	as usual	8000 rpm	2 min	**30 min**	1 w %
42	AF	**0 ppm**	0.5 w%	as usual	8000 rpm	2 min	no resting	1 w%
43	AF	**1000 ppm**	0.5 w%	as usual	8000 rpm	2 min	no resting	1 w%
44	AF	**4000 ppm**	0.5 w%	as usual	8000 rpm	2 min	no resting	1 w%
45	BG	**0 ppm**	0.5 w%	as usual	8000 rpm	2 min	no resting	1 w%
46	BG	**1000 ppm**	0.5 w%	as usual	8000 rpm	2 min	no resting	1 w%
47	BG	**4000 ppm**	0.5 w%	as usual	8000 rpm	2 min	no resting	1 w%

Appendix 2

Filtration charts from experiments 18, 19, 20 and 21.

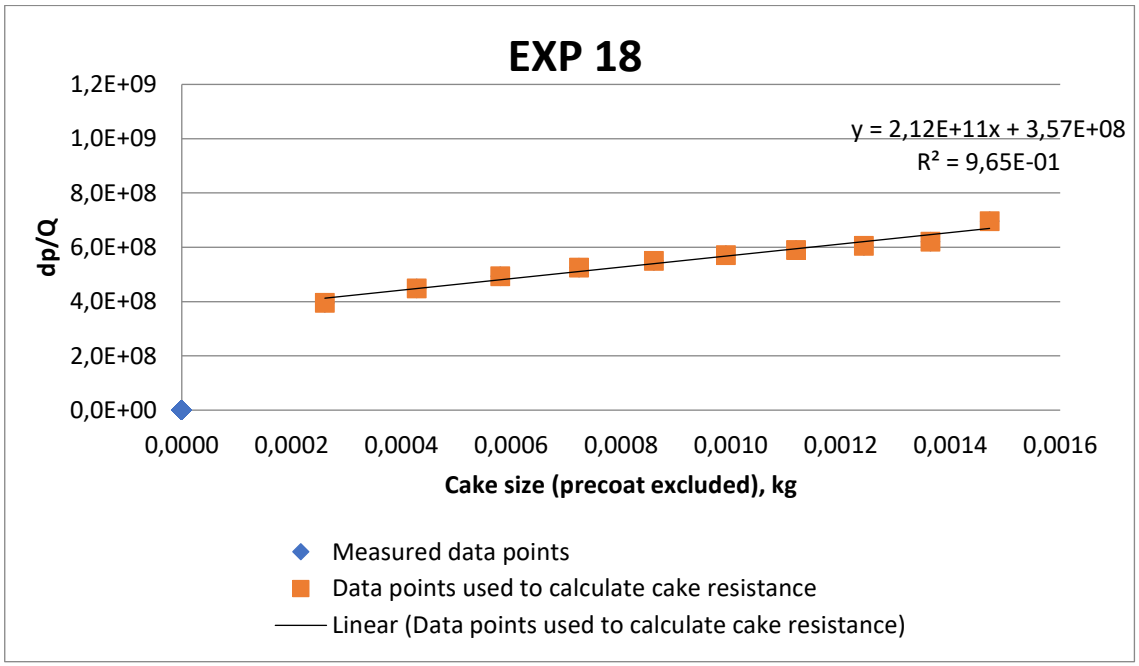

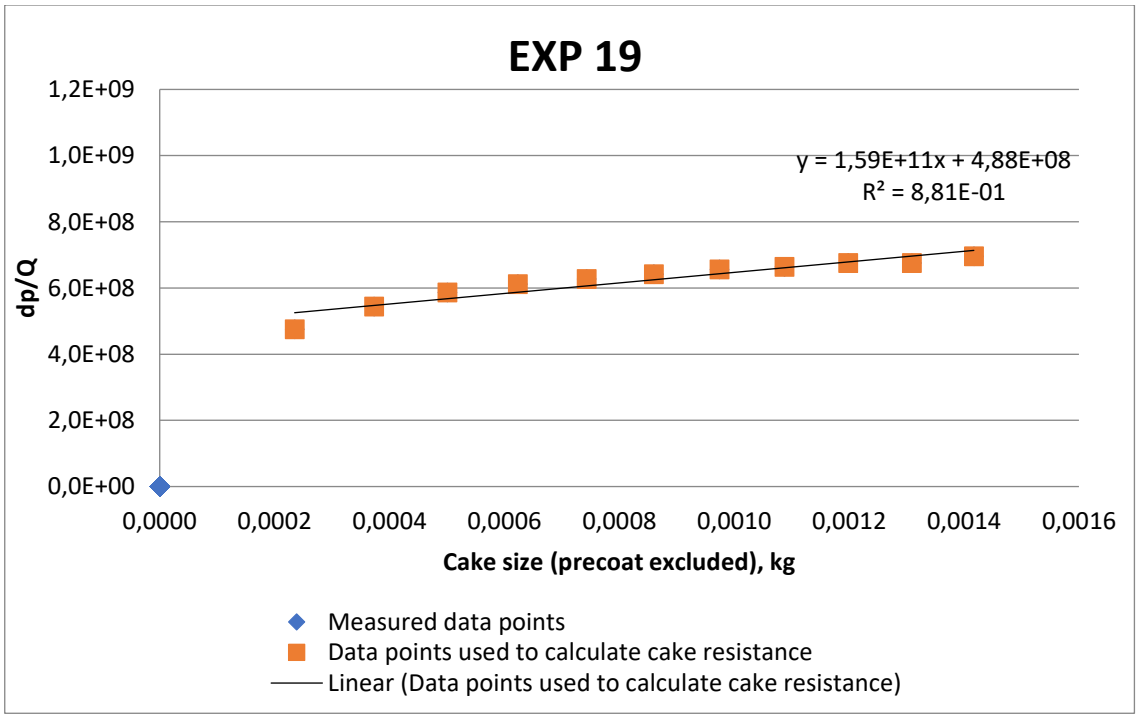

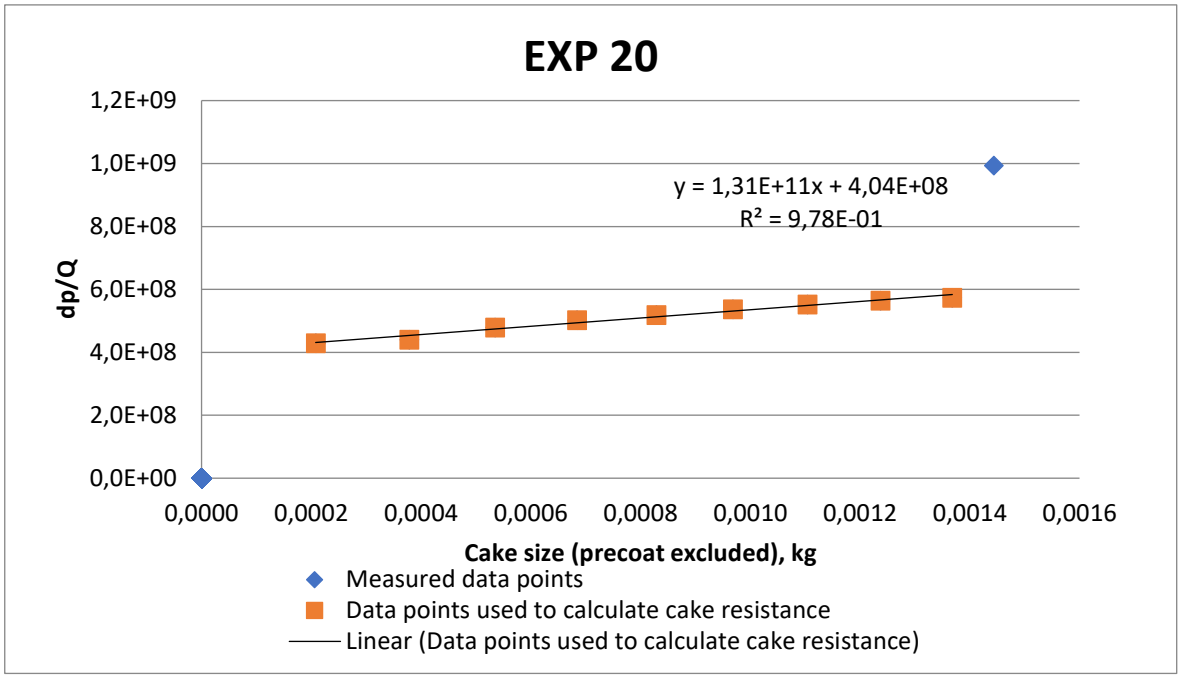
EXP 20
1,2E+09
1,0E+09
8,0E+08
6,0E+08
4,0E+08
2,0E+08
0,0E+00
dp/Q
y = 1,31E+11x + 4,04E+08
R² = 9,78E-01
0,0000
0,0002
0,0004
0,0006
0,0008
0,0010
0,0012
0,0014
0,0016
Cake size (precoat excluded), kg
Measured data points
Data points used to calculate cake resistance
Linear (Data points used to calculate cake resistance)

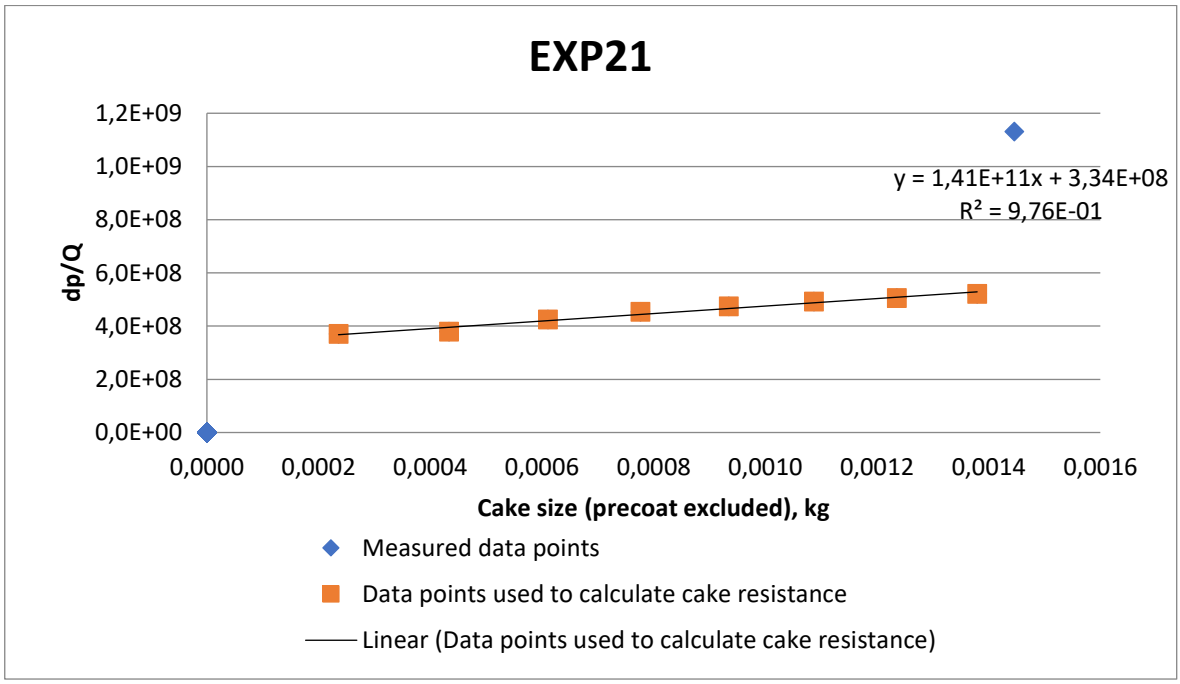
EXP21
1,2E+09
1,0E+09
8,0E+08
6,0E+08
4,0E+08
2,0E+08
0,0E+00
dp/Q
y = 1,41E+11x + 3,34E+08
R² = 9,76E-01
0,0000
0,0002
0,0004
0,0006
0,0008
0,0010
0,0012
0,0014
0,0016
Cake size (precoat excluded), kg
Measured data points
Data points used to calculate cake resistance
Linear (Data points used to calculate cake resistance)

Appendix 3

Filtration charts from the metal addition experiments.

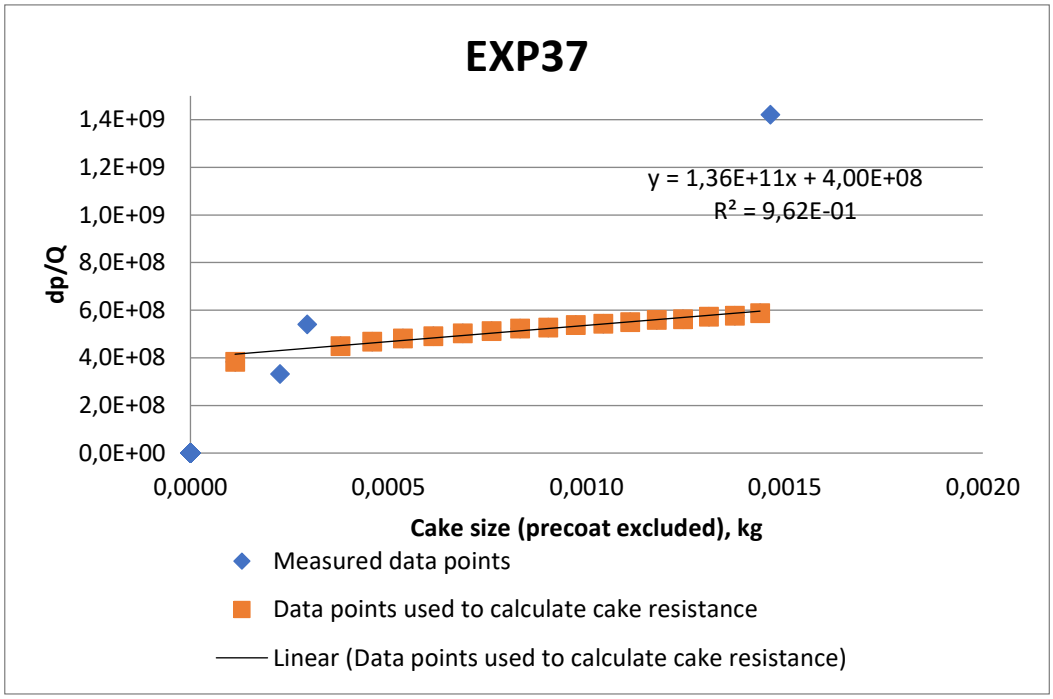

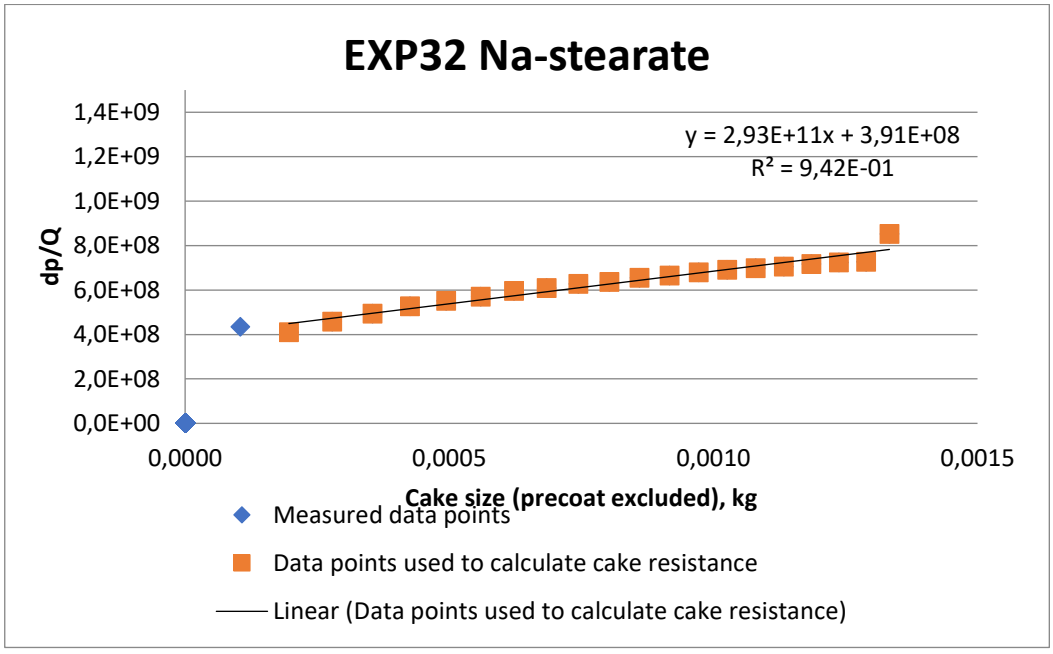

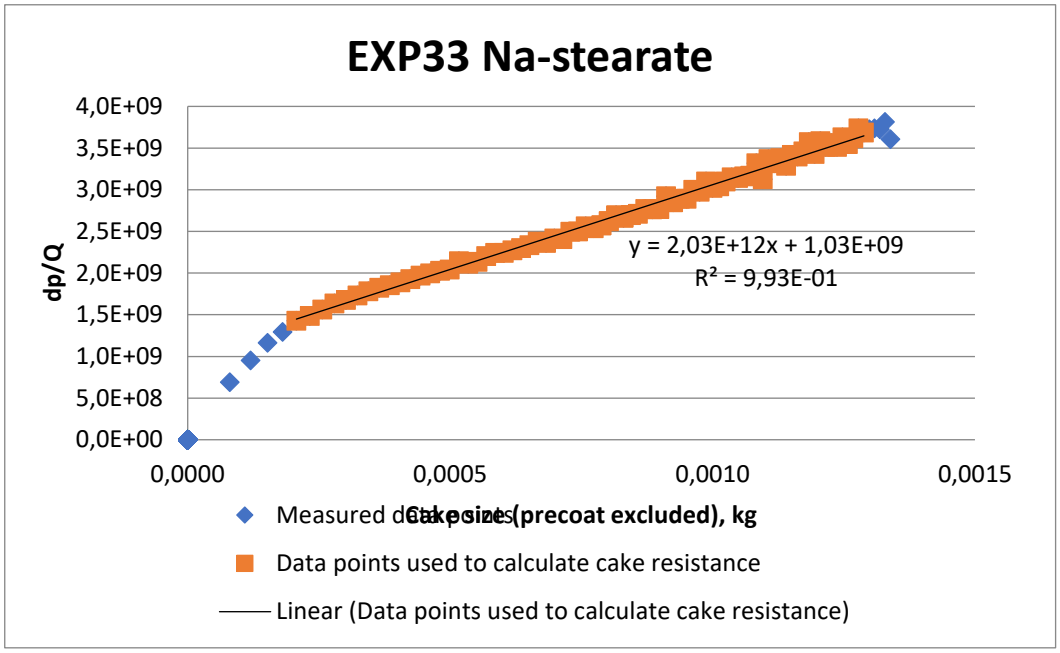
EXP33 Na-stearate
4,0E+09
3,5E+09
3,0E+09
2,5E+09
2,0E+09
1,5E+09
1,0E+09
5,0E+08
0,0E+00
dp/Q
y = 2,03E+12x + 1,03E+09
R² = 9,93E-01
0,0000
0,0005
0,0010
0,0015
Cake size (precoat excluded), kg
Measured data points
Data points used to calculate cake resistance
Linear (Data points used to calculate cake resistance)

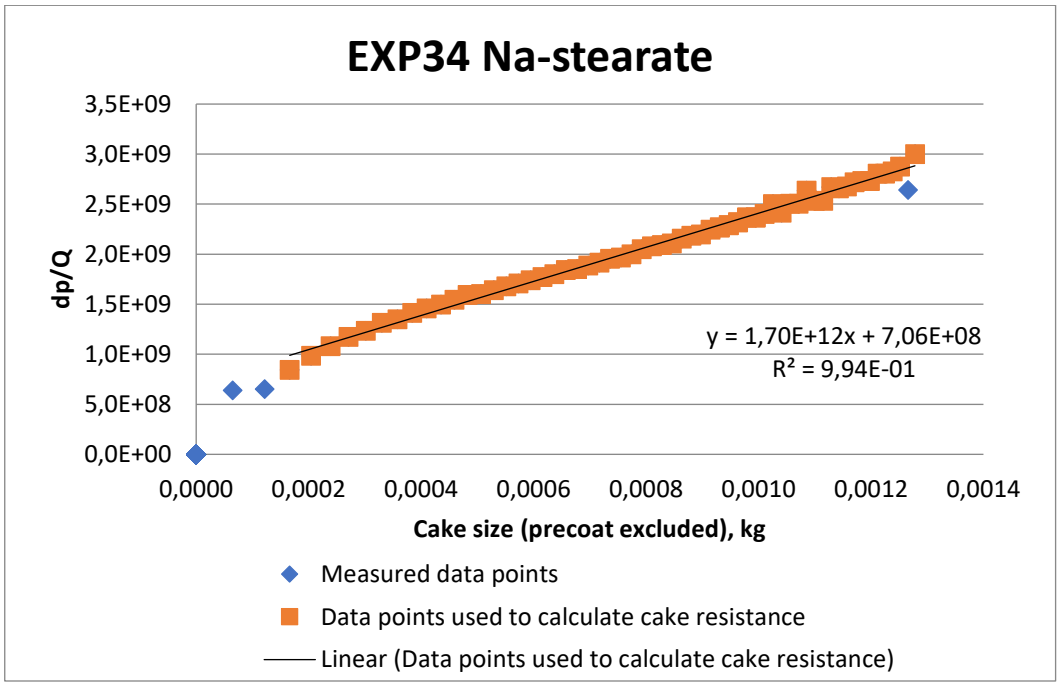
EXP34 Na-stearate
3,5E+09
3,0E+09
2,5E+09
2,0E+09
1,5E+09
1,0E+09
5,0E+08
0,0E+00
dp/Q
y = 1,70E+12x + 7,06E+08
R² = 9,94E-01
0,0000
0,0002
0,0004
0,0006
0,0008
0,0010
0,0012
0,0014
Cake size (precoat excluded), kg
Measured data points
Data points used to calculate cake resistance
Linear (Data points used to calculate cake resistance)

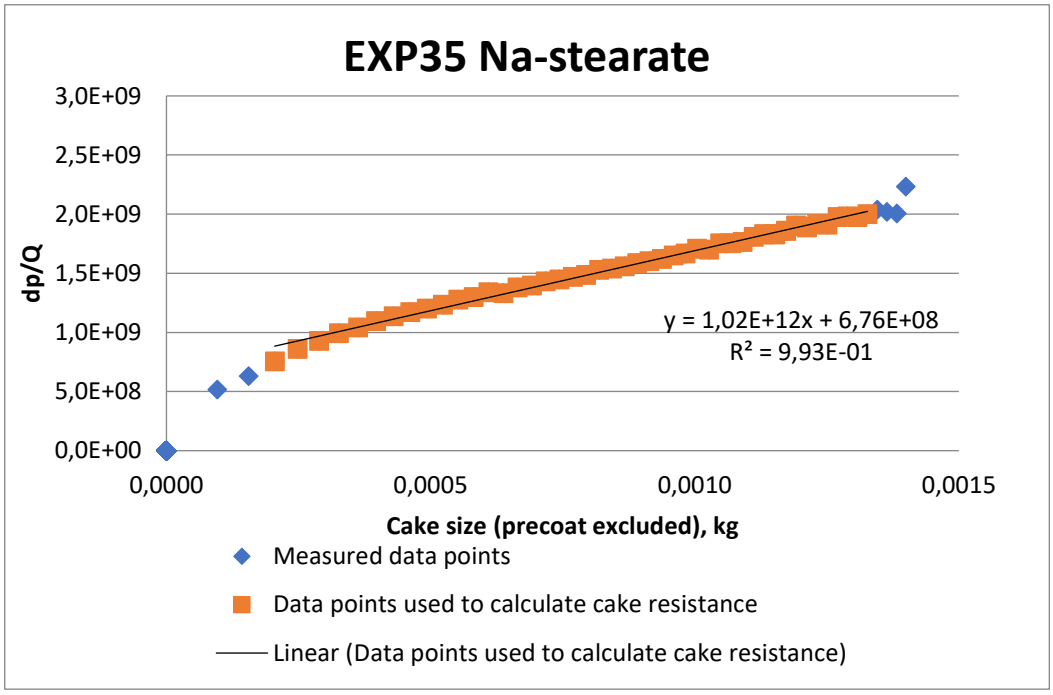
EXP35 Na-stearate
3,0E+09
2,5E+09
2,0E+09
1,5E+09
1,0E+09
5,0E+08
0,0E+00
dp/Q
0,0000
0,0005
0,0010
0,0015
y = 1,02E+12x + 6,76E+08
R² = 9,93E-01
Cake size (precoat excluded), kg
Measured data points
Data points used to calculate cake resistance
Linear (Data points used to calculate cake resistance)

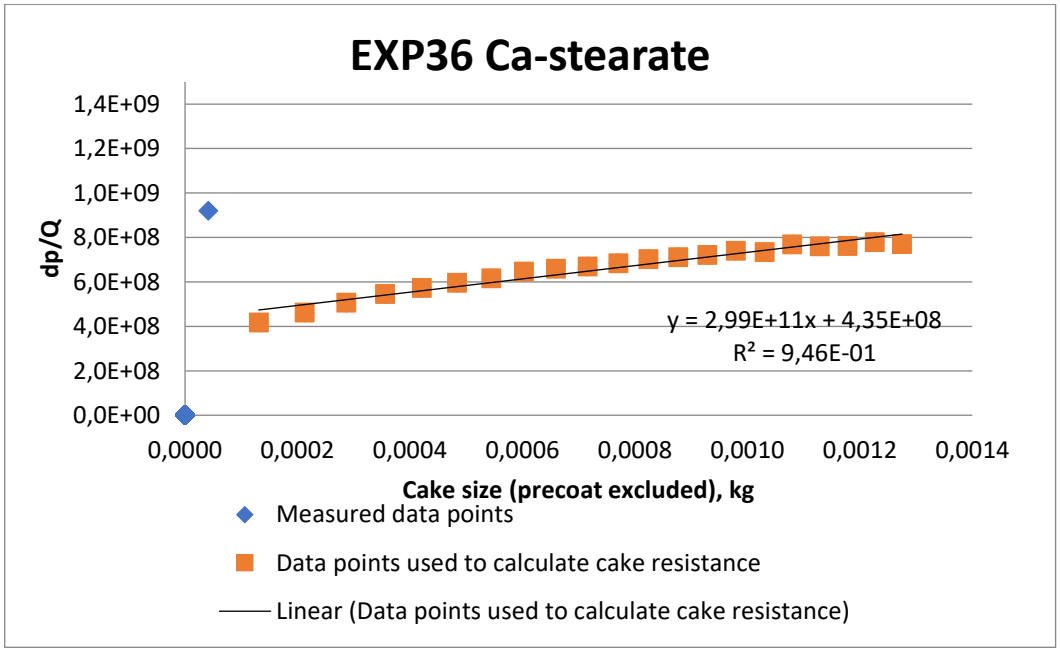
EXP36 Ca-stearate
1,4E+09
1,2E+09
1,0E+09
8,0E+08
6,0E+08
4,0E+08
2,0E+08
0,0E+00
dp/Q
0,0000
0,0002
0,0004
0,0006
0,0008
0,0010
0,0012
0,0014
y = 2,99E+11x + 4,35E+08
R² = 9,46E-01
Cake size (precoat excluded), kg
Measured data points
Data points used to calculate cake resistance
Linear (Data points used to calculate cake resistance)

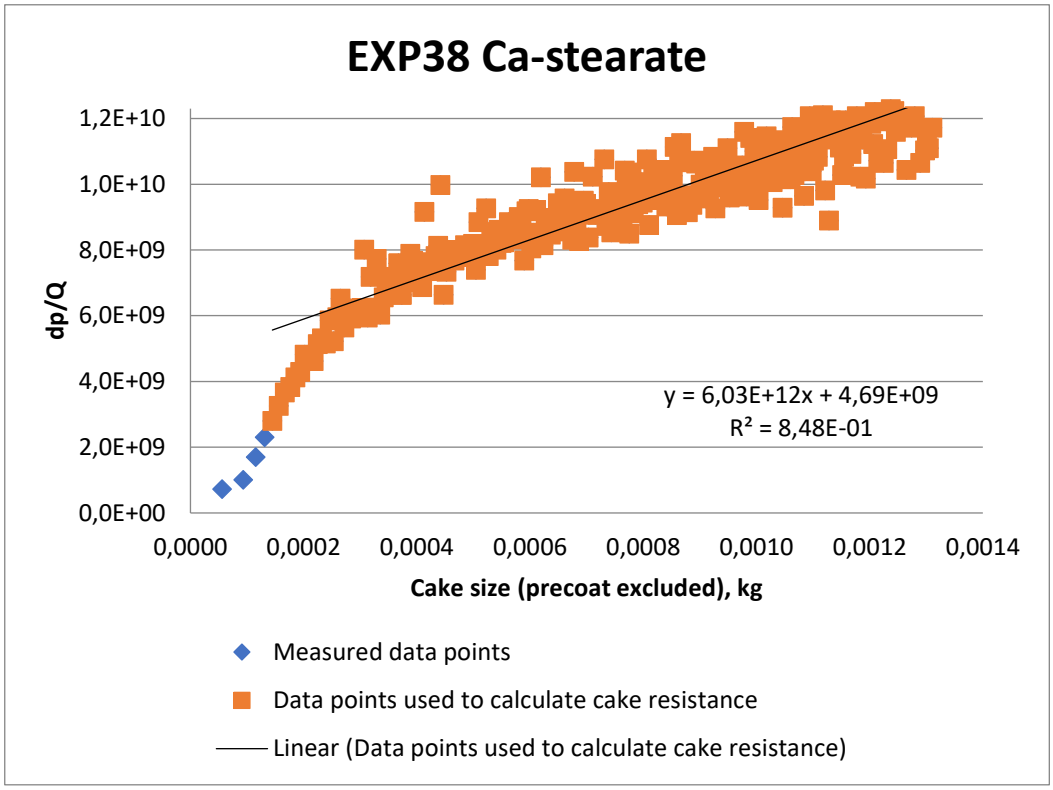
EXP38 Ca-stearate
1,2E+10
1,0E+10
8,0E+09
6,0E+09
4,0E+09
2,0E+09
0,0E+00
dp/Q
0,0000
0,0002
0,0004
0,0006
0,0008
0,0010
0,0012
0,0014
Cake size (precoat excluded), kg
y = 6,03E+12x + 4,69E+09
R² = 8,48E-01
Measured data points
Data points used to calculate cake resistance
Linear (Data points used to calculate cake resistance)

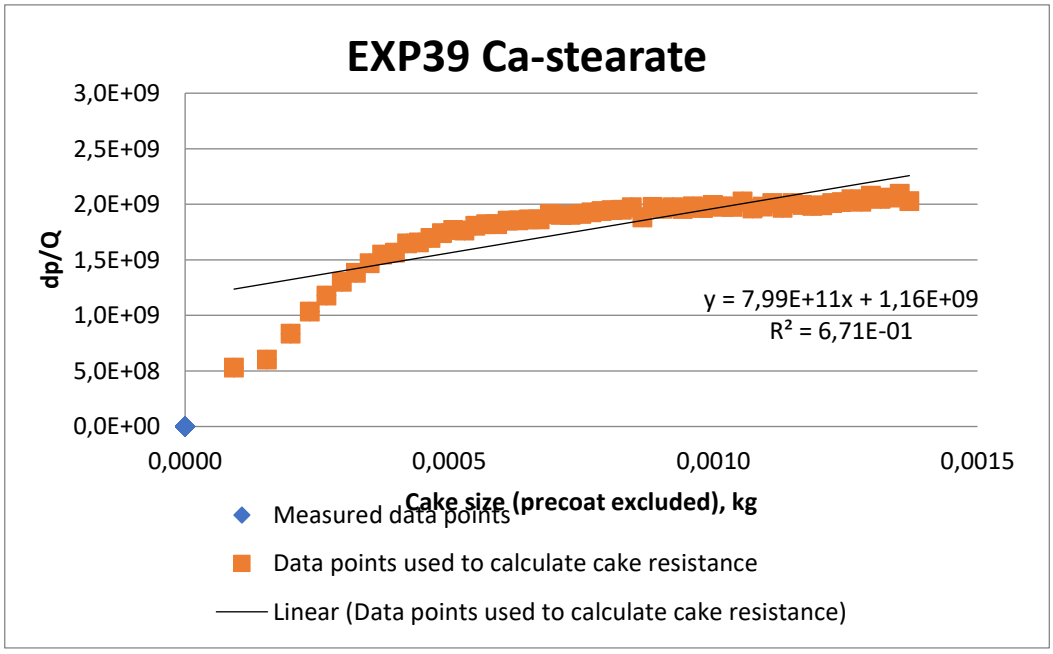
EXP39 Ca-stearate
3,0E+09
2,5E+09
2,0E+09
1,5E+09
1,0E+09
5,0E+08
0,0E+00
dp/Q
0,0000
0,0005
0,0010
0,0015
Cake size (precoat excluded), kg
y = 7,99E+11x + 1,16E+09
R² = 6,71E-01
Measured data points
Data points used to calculate cake resistance
Linear (Data points used to calculate cake resistance)

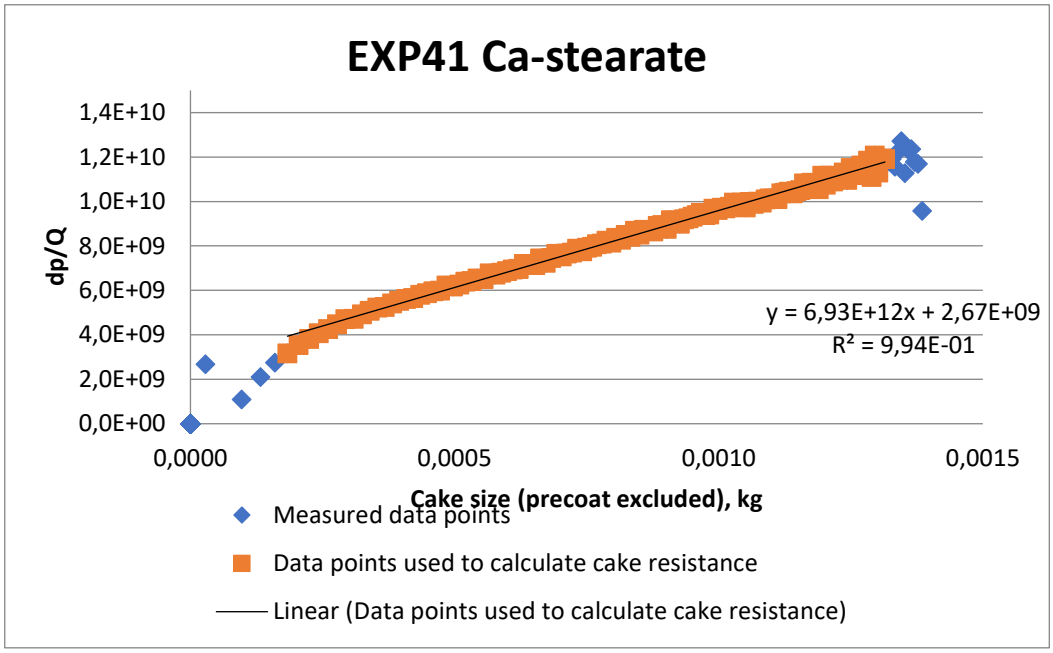
EXP41 Ca-stearate
dp/Q
1,4E+10
1,2E+10
1,0E+10
8,0E+09
6,0E+09
4,0E+09
2,0E+09
0,0E+00
0,0000
0,0005
0,0010
0,0015
y = 6,93E+12x + 2,67E+09
R² = 9,94E-01
Cake size (precoat excluded), kg
Measured data points
Data points used to calculate cake resistance
Linear (Data points used to calculate cake resistance)

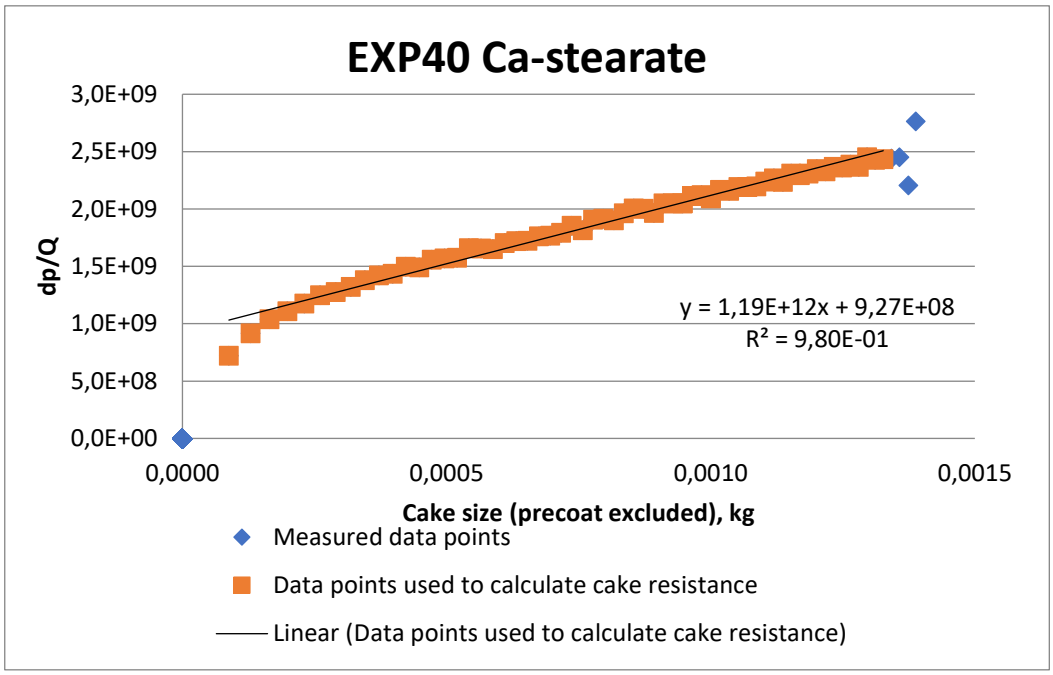
EXP40 Ca-stearate
dp/Q
3,0E+09
2,5E+09
2,0E+09
1,5E+09
1,0E+09
5,0E+08
0,0E+00
0,0000
0,0005
0,0010
0,0015
y = 1,19E+12x + 9,27E+08
R² = 9,80E-01
Cake size (precoat excluded), kg
Measured data points
Data points used to calculate cake resistance
Linear (Data points used to calculate cake resistance)

Appendix 4

Filtration charts from the technical feedstock experiments

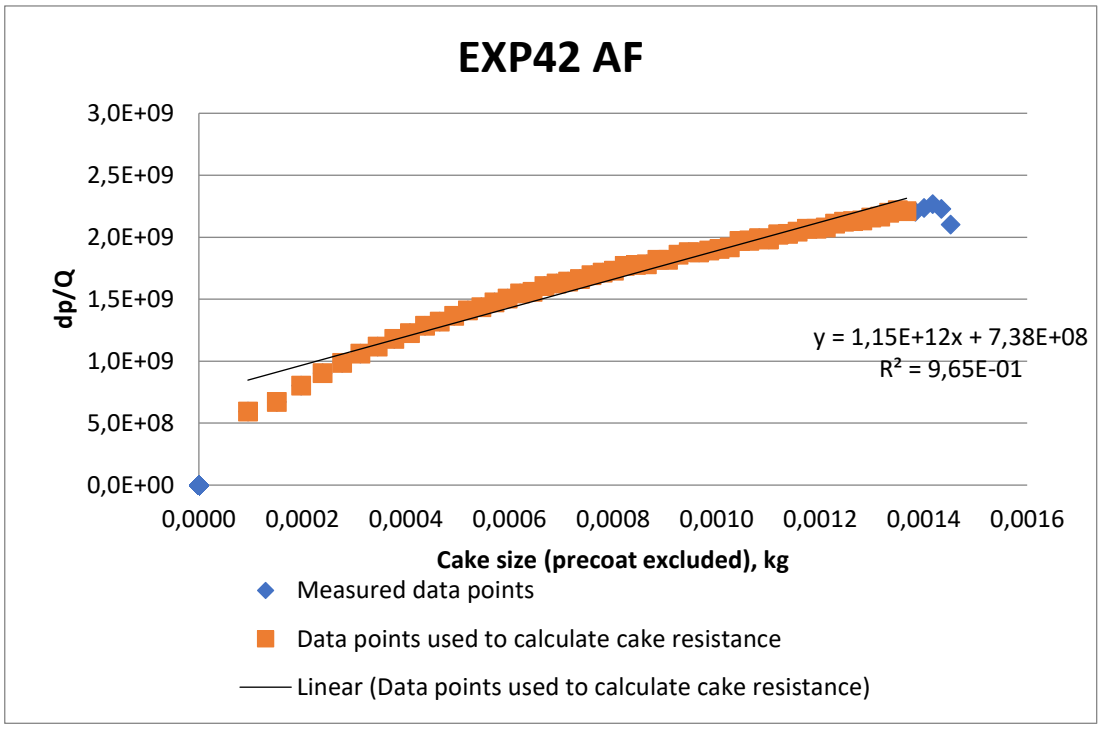

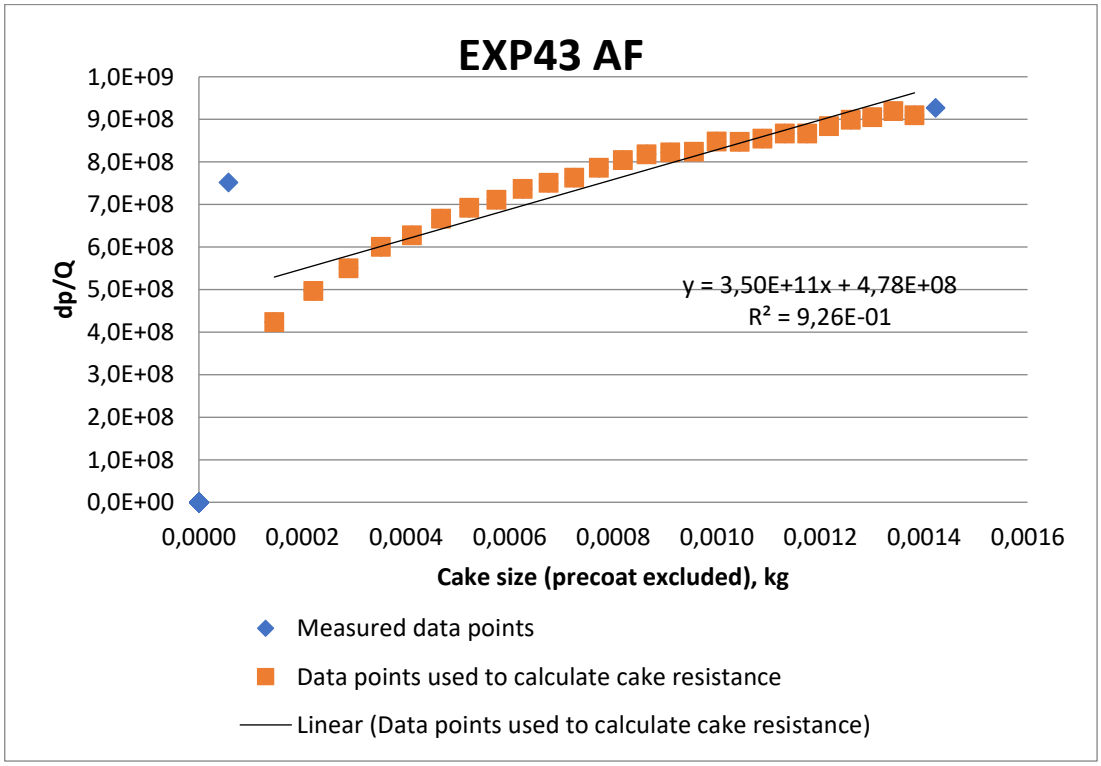

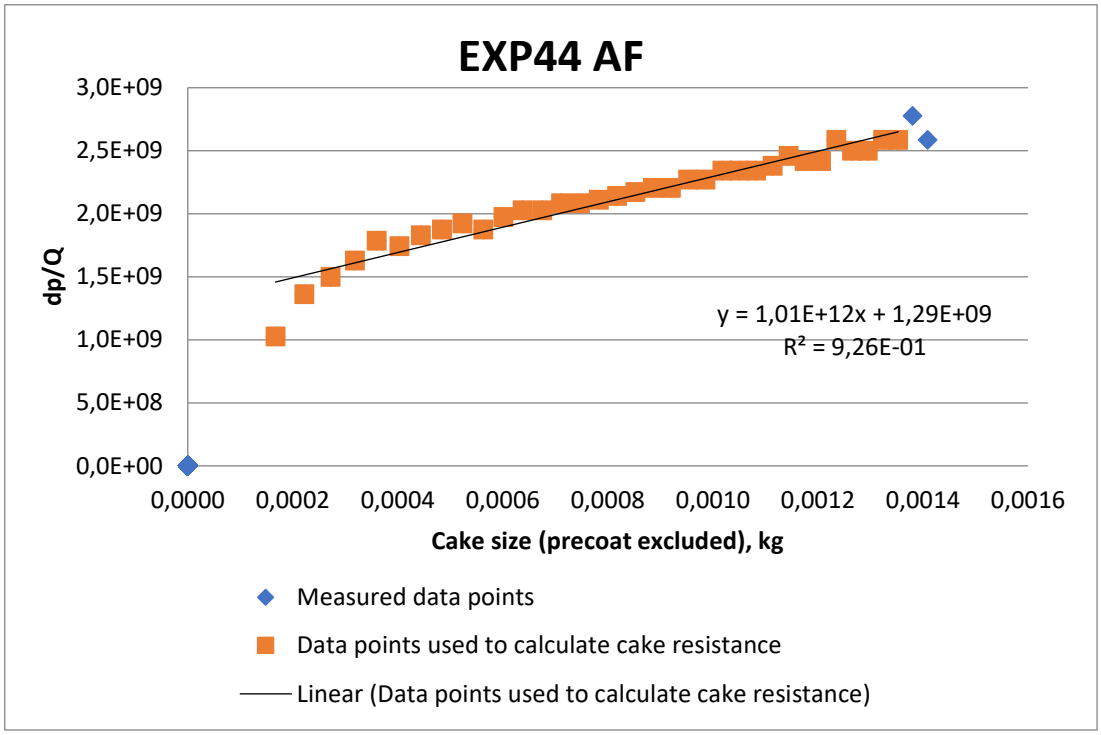
EXP44 AF
3,0E+09
2,5E+09
2,0E+09
1,5E+09
1,0E+09
5,0E+08
0,0E+00
dp/Q
0,0000
0,0002
0,0004
0,0006
0,0008
0,0010
0,0012
0,0014
0,0016
Cake size (precoat excluded), kg
y = 1,01E+12x + 1,29E+09
R² = 9,26E-01
Measured data points
Data points used to calculate cake resistance
Linear (Data points used to calculate cake resistance)

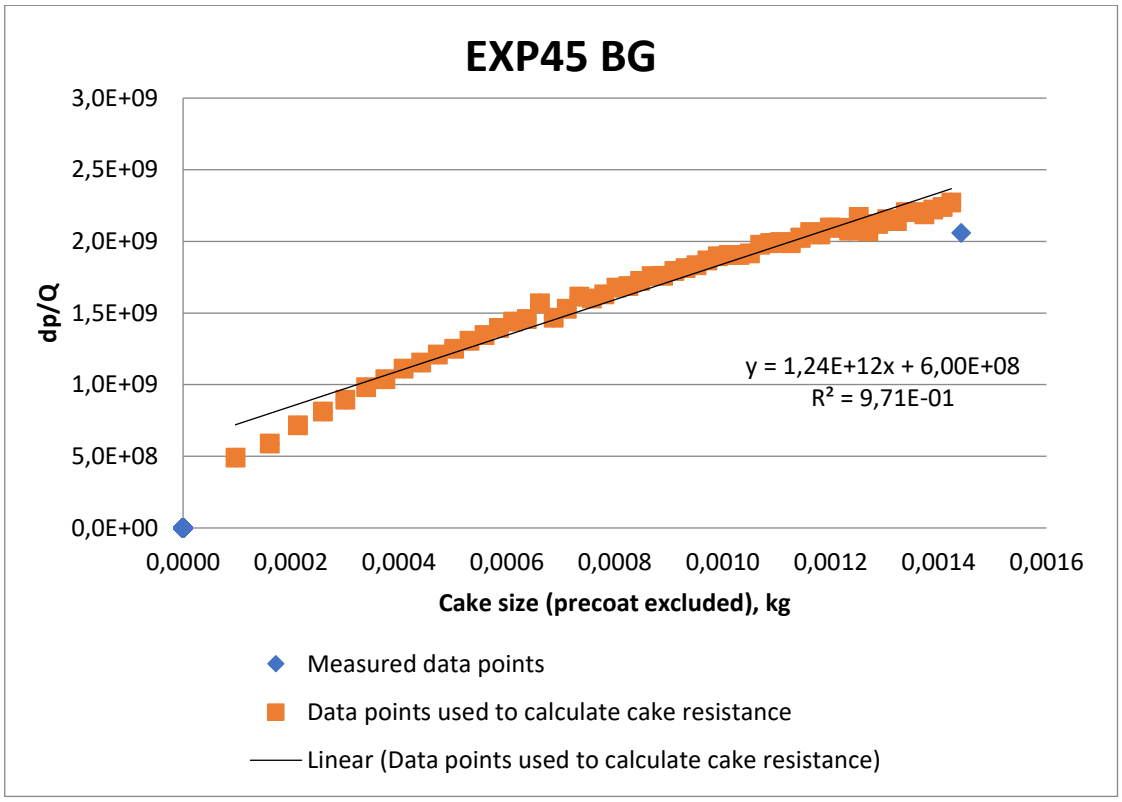
EXP45 BG
3,0E+09
2,5E+09
2,0E+09
1,5E+09
1,0E+09
5,0E+08
0,0E+00
dp/Q
0,0000
0,0002
0,0004
0,0006
0,0008
0,0010
0,0012
0,0014
0,0016
Cake size (precoat excluded), kg
y = 1,24E+12x + 6,00E+08
R² = 9,71E-01
Measured data points
Data points used to calculate cake resistance
Linear (Data points used to calculate cake resistance)

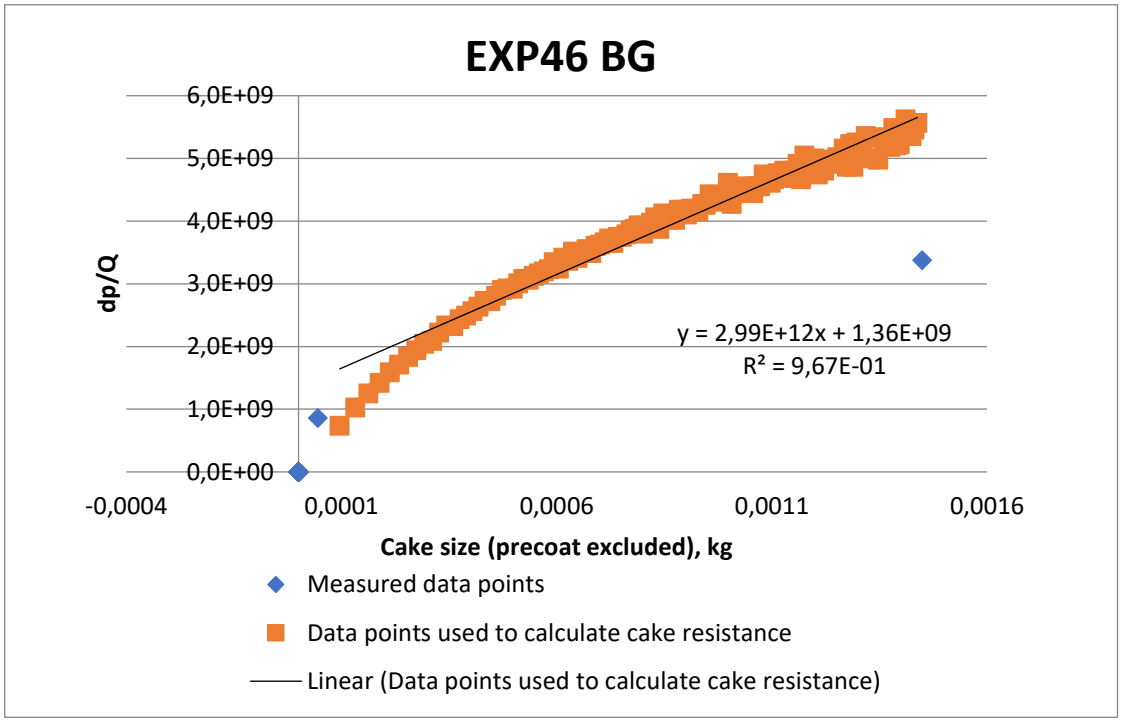
EXP46 BG
6,0E+09
5,0E+09
4,0E+09
3,0E+09
2,0E+09
1,0E+09
0,0E+00
dp/Q
-0,0004
0,0001
0,0006
0,0011
0,0016
y = 2,99E+12x + 1,36E+09
R² = 9,67E-01
Cake size (precoat excluded), kg
Measured data points
Data points used to calculate cake resistance
Linear (Data points used to calculate cake resistance)

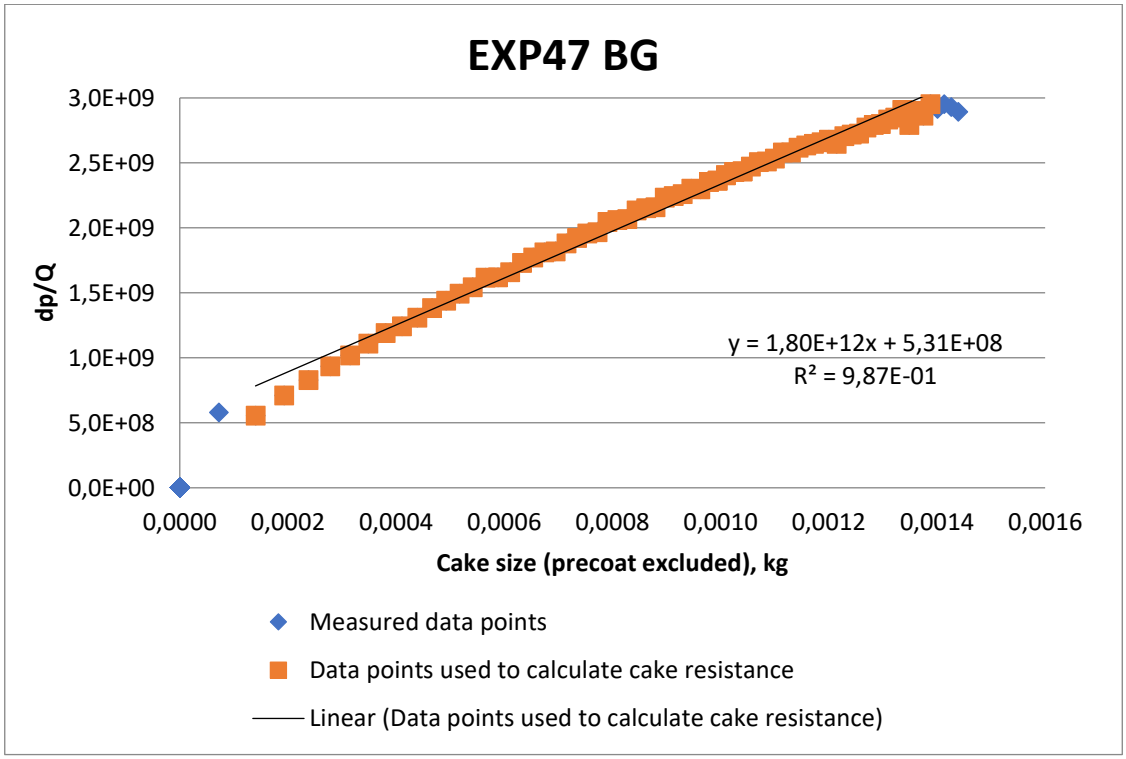
EXP47 BG
3,0E+09
2,5E+09
2,0E+09
1,5E+09
1,0E+09
5,0E+08
0,0E+00
dp/Q
0,0000
0,0002
0,0004
0,0006
0,0008
0,0010
0,0012
0,0014
0,0016
y = 1,80E+12x + 5,31E+08
R² = 9,87E-01
Cake size (precoat excluded), kg
Measured data points
Data points used to calculate cake resistance
Linear (Data points used to calculate cake resistance)

Appendix 5

Figures from the AF and BG filtrations with the filtrate particle size distribution included.

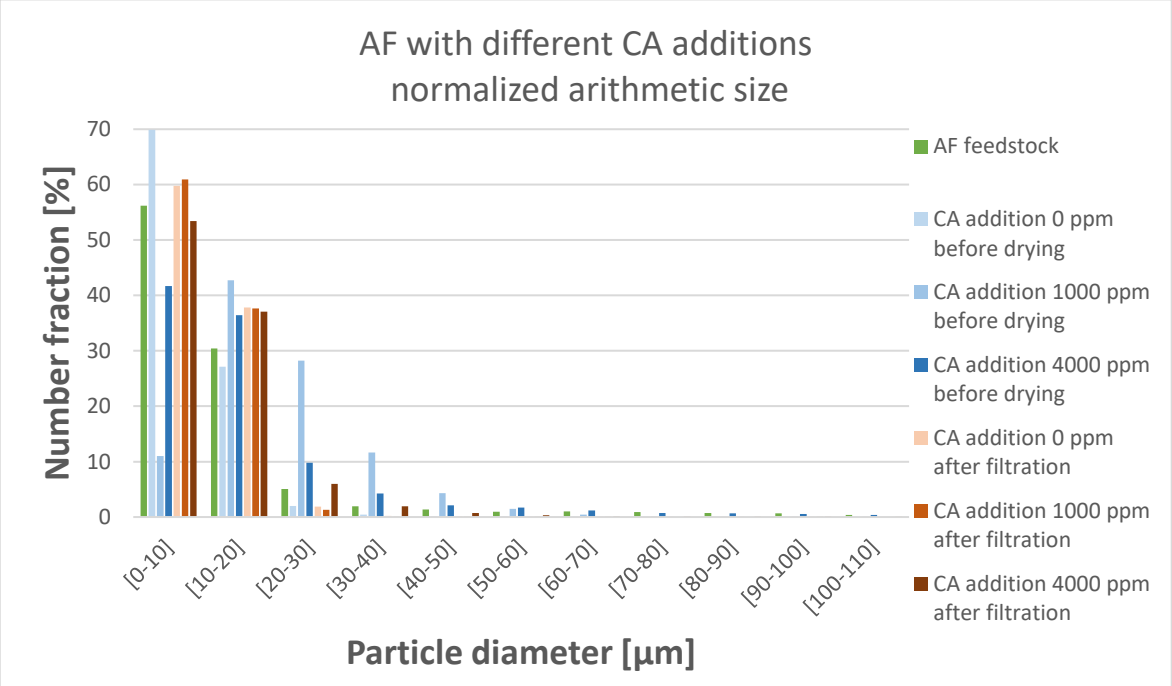

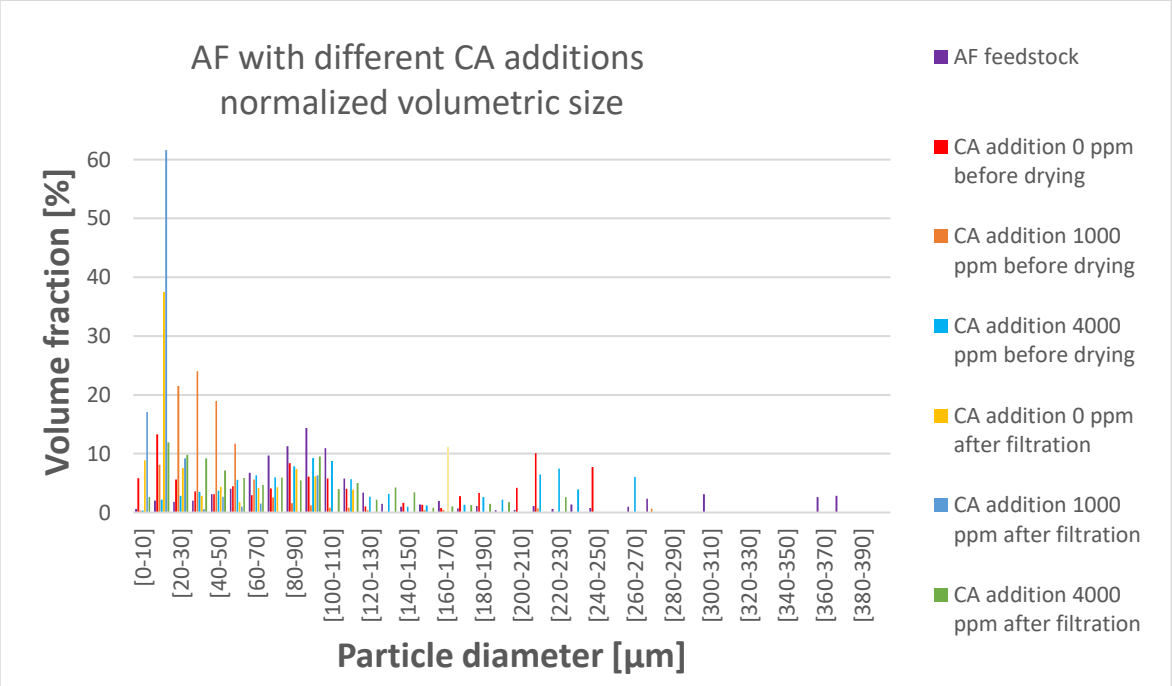

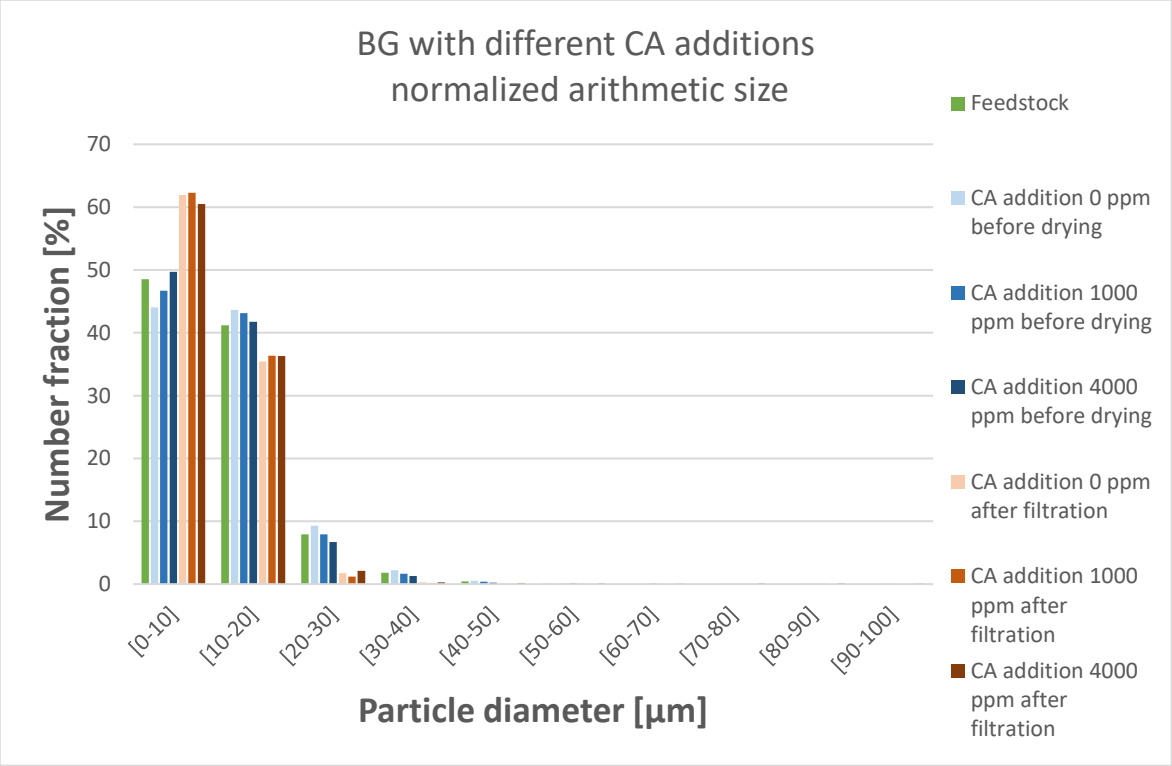
BG with different CA additions
normalized arithmetic size
Number fraction [%]
70
60
50
40
30
20
10
0
[0-10]
[10-20]
[20-30]
[30-40]
[40-50]
[50-60]
[60-70]
[70-80]
[80-90]
[90-100]
Particle diameter [µm]
Feedstock
CA addition 0 ppm before drying
CA addition 1000 ppm before drying
CA addition 4000 ppm before drying
CA addition 0 ppm after filtration
CA addition 1000 ppm after filtration
CA addition 4000 ppm after filtration

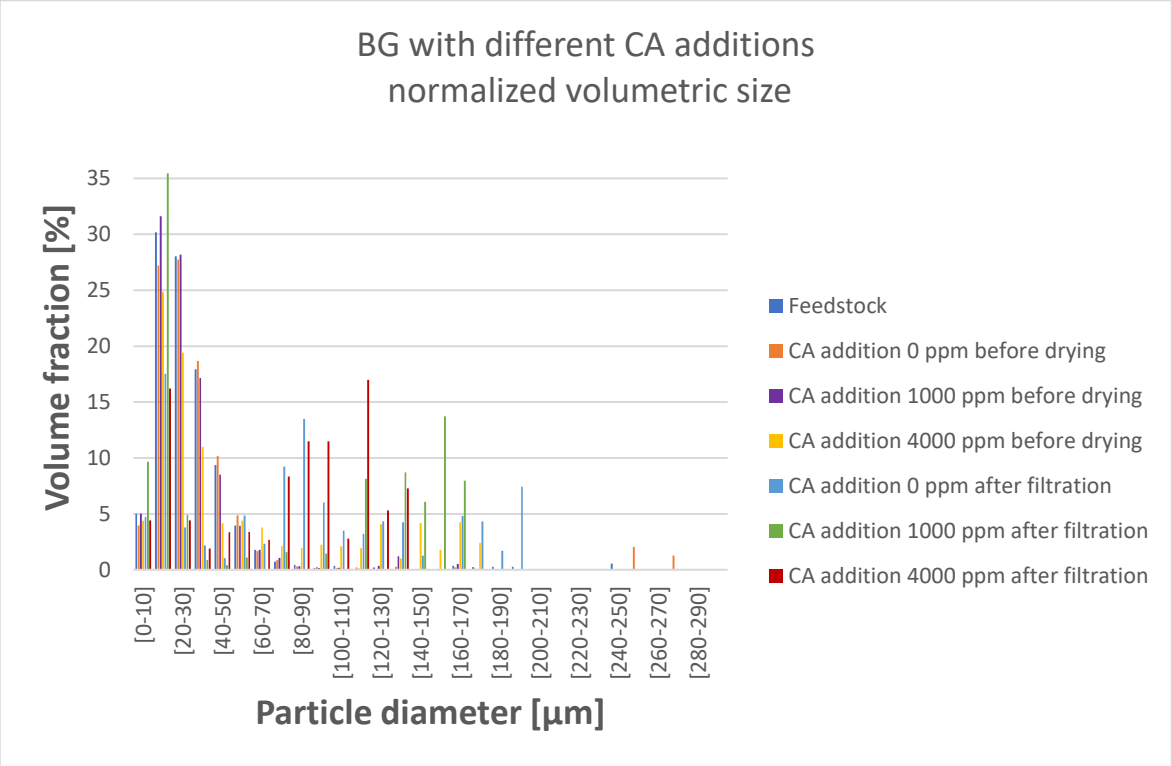
BG with different CA additions
normalized volumetric size
Volume fraction [%]
35
30
25
20
15
10
5
0
[0-10]
[20-30]
[40-50]
[60-70]
[80-90]
[100-110]
[120-130]
[140-150]
[160-170]
[180-190]
[200-210]
[220-230]
[240-250]
[260-270]
[280-290]
Particle diameter [µm]
Feedstock
CA addition 0 ppm before drying
CA addition 1000 ppm before drying
CA addition 4000 ppm before drying
CA addition 0 ppm after filtration
CA addition 1000 ppm after filtration
CA addition 4000 ppm after filtration

Appendix 6

First, the amount of substance was calculated for CA addition using the equations 18 and 19:

$$\mu(CA) = 1{,}665\,\frac{g}{ml}$$

$$M(CA) = 192{,}124\ g/mol$$

$$V(CA\ 1000) = 0{,}138\ ml$$

$$(calculated\ with\ the\ tool\ used\ for\ bleaching\ for\ 1000\ ppm)$$

$$V(CA\ 4000) = 0{,}553\ ml$$

$$(calculated\ with\ the\ tool\ used\ for\ bleaching\ for\ 4000\ ppm)$$

$$m(CA\ 1000) = \mu(CA) * V(CA) = 1{,}665\,\frac{g}{ml} * 0{,}138\ ml = 0{,}230\ g \quad (18)$$

$$n(CA\ 1000) = \frac{m(CA)}{M(CA)} = \frac{0{,}230\ g}{192{,}124\ g/mol} = 0{,}001\ mol \quad (19)$$

$$m(CA\ 4000) = \mu(CA) * V(CA) = 1{,}665\,\frac{g}{ml} * 0{,}553\ ml = 0{,}920\ g$$

$$n(CA\ 4000) = \frac{m(CA)}{M(CA)} = \frac{0{,}230\ g}{192{,}124\ g/mol} = 0{,}005\ mol$$

Where $\mu(CA)$ density of CA g/ml

$M(CA)$ molar mass of CA g/mol

$V(CA\ 1000)$ volume of CA, when the wanted concentration is 1000 ppm ml

$V(CA\ 4000)$ volume of CA, when the wanted concentration is 4000 ppm ml

$m(CA\ 1000)$ mass of the CA, when the wanted concentration is 1000 ppm g

$m(CA\ 4000)$ mass of the CA, when the wanted concentration is 4000 ppm g

$n(CA\ 1000)$ amount of substance of the CA, when the wanted concentration is 1000 ppm g

$n(CA\ 4000)$ amount of substance of the CA, when the wanted concentration is 4000 ppm g

Metal addition of sodium stearate (Na-stearate) and calcium stearate (Ca-stearate), when the CA addition to the solution is 1000 ppm:

$$n(Na-stearate\ 1000) = 2 * n(CA\ 1000) = 2 * 0{,}001\ mol = 0{,}002\ mol$$
$$M(Na-stearate) = 306{,}46\ g/mol$$
$$m(Na-stearate\ 1000) = n(Na-stearate\ 1000) * M(Na-stearate)$$
$$= 0{,}002\ mol * 306{,}46 \frac{g}{mol} = 0{,}733\ g$$

$$n(Ca-stearate\ 1000) = n(CA\ 1000) = 0{,}001\ mol$$
$$M(Ca-stearate) = 607{,}03\ g/mol$$
$$m(Ca-stearate\ 1000) = n(Ca-stearate\ 1000) * M(Ca-stearate)$$
$$= 0{,}001\ mol * 607{,}03 \frac{g}{mol} = 0{,}726\ g$$

Metal addition of Na-stearate and Ca-stearate, when the CA addition to the solution is 4000 ppm:

$$n(Na-stearate\ 4000) = 2 * n(CA\ 4000) = 2 * 0{,}005\ mol = 0{,}010\ mol$$
$$M(Na-stearate) = 306{,}46\ g/mol$$
$$m(Na-stearate\ 4000) = n(Na-stearate\ 4000) * M(Na-stearate)$$
$$= 0{,}010\ mol * 306{,}46 \frac{g}{mol} = 2{,}935\ g$$

$$n(Ca-stearate\ 4000) = n(CA\ 4000) = 0{,}005\ mol$$
$$M(Ca-stearate) = 607{,}03\ g/mol$$
$$m(Ca-stearate\ 4000) = n(Ca-stearate\ 4000) * M(Ca-stearate)$$
$$= 0{,}005\ mol * 607{,}03 \frac{g}{mol} = 2{,}907\ g$$

Appendix 7

Arithmetic size distributions and volumetric size distributions from metal addition experiments (chapter 7.3)

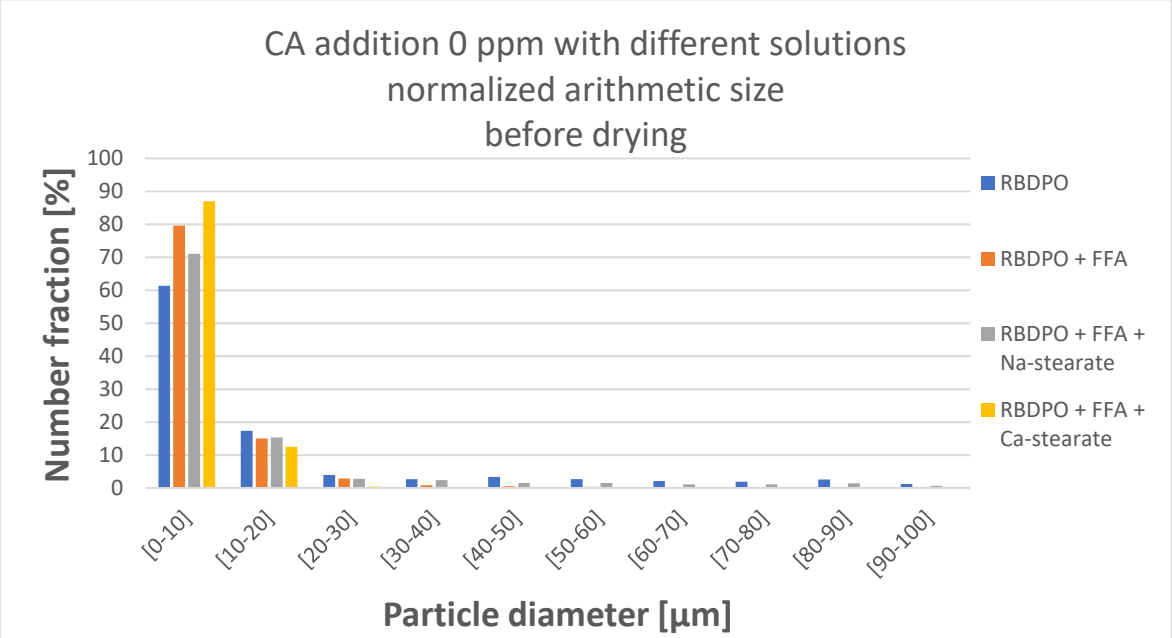

Figure 89 CA addition of 0 ppm with different feedstocks, before drying procedure.

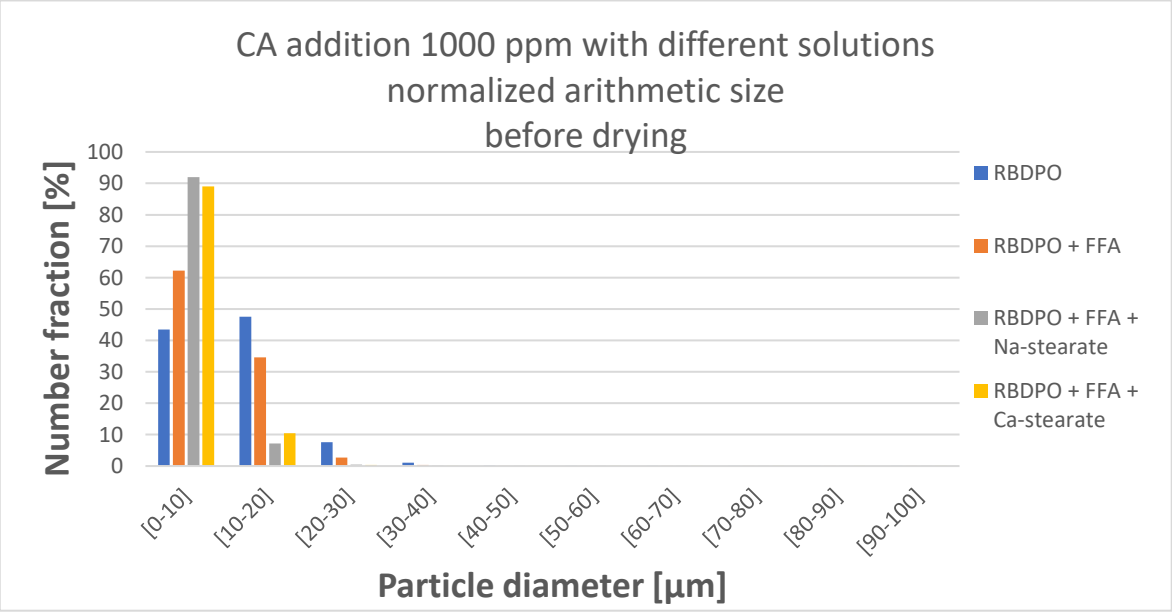

Figure 90 CA addition of 1000 ppm with different feedstocks, before drying procedure.

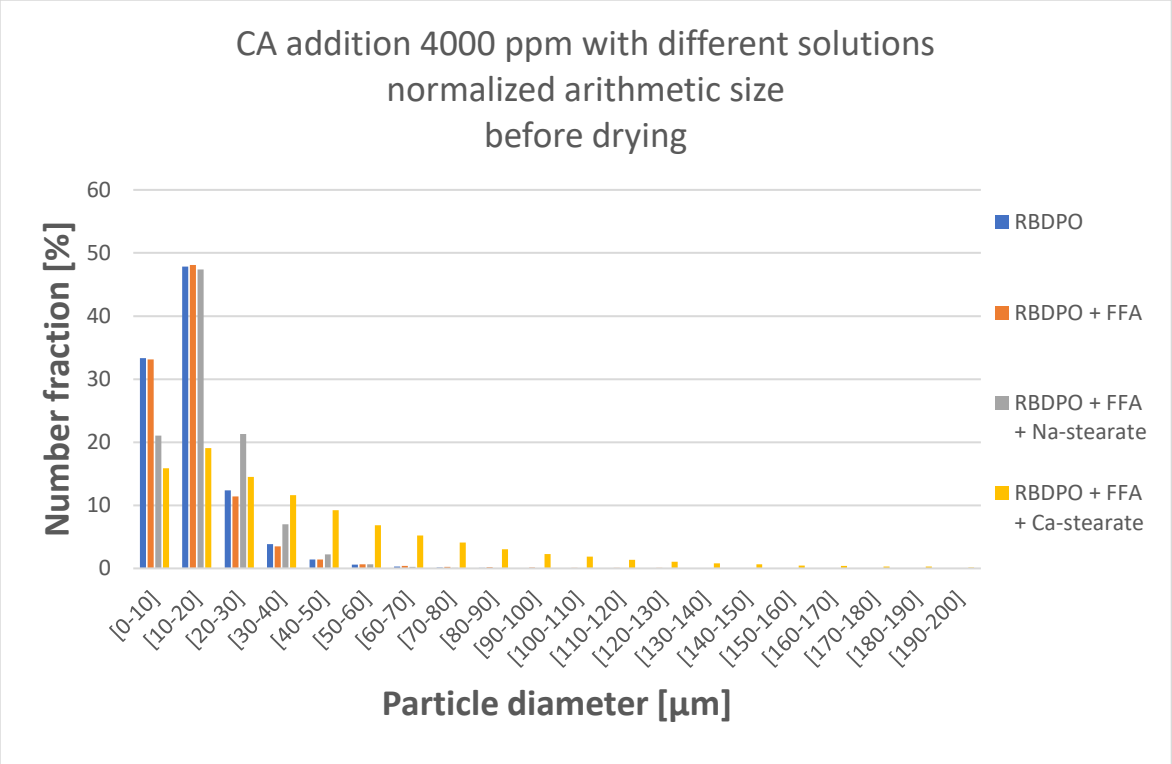

Figure 91 CA addition of 4000 ppm with different feedstocks, before drying procedure.

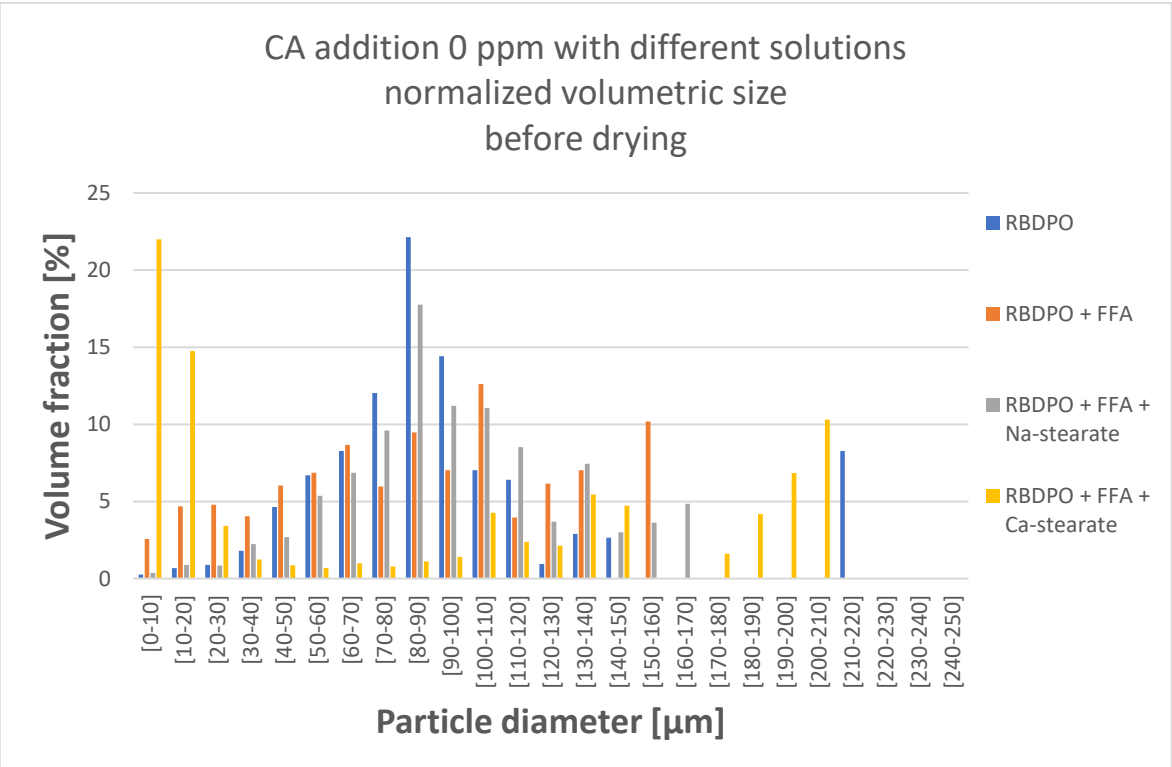

Figure 93 CA addition of 1000 ppm with different feedstocks, before drying procedure.

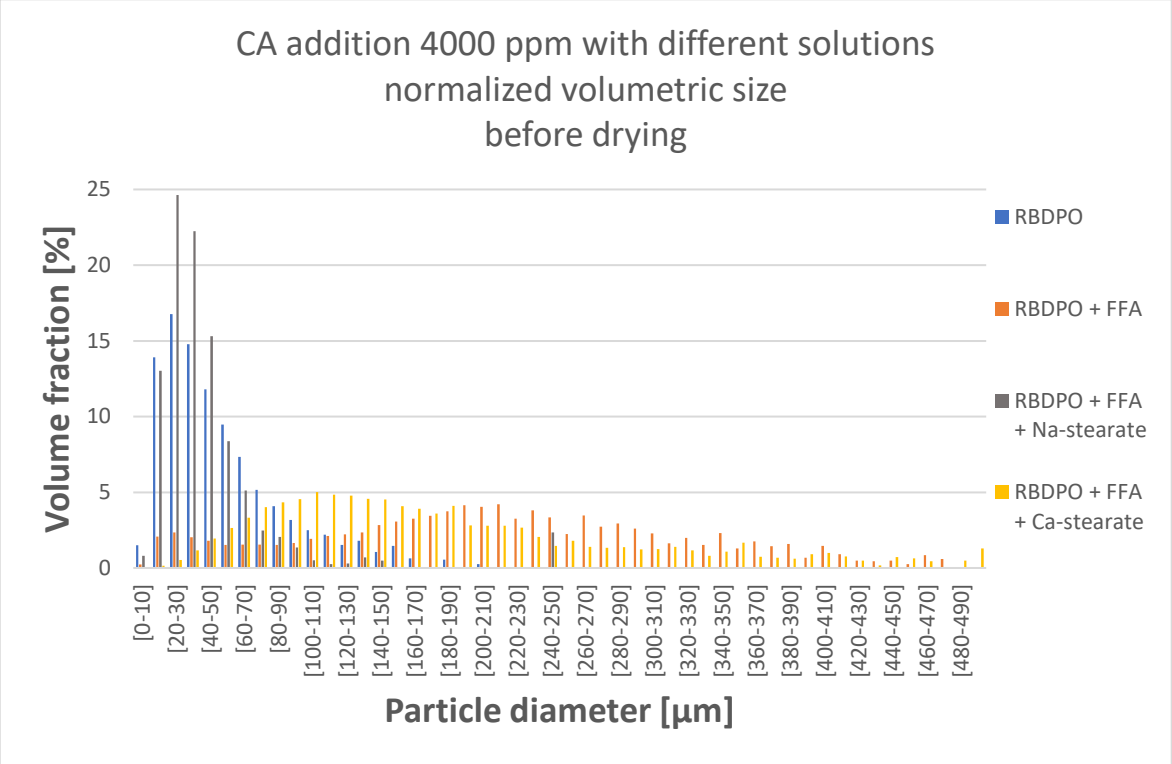

Figure 94 CA addition of 4000 ppm with different feedstocks, before drying procedure.